SMALL SCALE WIND STRUCTURE IN THE UPPER ATMOSPHERE

by

B. J. McAvaney, B.Sc. (Hons)

A Thesis

presented for the degree of

DOCTOR OF PHILOSOPHY

in the

UNIVERSITY OF ADELAIDE
(Physics Department)

August 1970

CONTENTS

SUMMARY

PREFACE

ACKNOWLEDGEMENTS

Page N

CHAPTER I - DYNAMICS OF THE ATMOSPHERE BETWEEN 30 km AND 100 km 1

1.1 Introduction 1

1.2 Sources and Sinks of Energy in the Mesosphere and Lower Thermosphere 3

1.3 Experimental Techniques: Direct Methods 5

1.3.1 Meteorological Rockets 5

1.3.2 Acoustic Grenades 6

1.3.3 Contaminant Releases 7

1.3.4 Gun-Launched Probes 7

1.4 Experimental Techniques: Indirect Methods 8

1.4.1 Ionospheric Drifts 8

1.4.2 The Radio-Meteor Method 9

1.4.3 Other Methods 12

CHAPTER II - THEORIES OF IRREGULAR STRUCTURE IN THE ATMOSPHERE 15

2.1 Description of the Problem 15

2.2 General Theory of Turbulence 17

2.2.1 Statistical Description 17

2.2.2 The Energy Balance 19

2.2.3 The Inertial Subrange 20

Page N

2.2.4 The Buoyancy Subrange 22

2.2.5 Turbulent Diffusion 25

2.3 Internal Acoustic-Gravity Waves 26

2.3.1 General Characteristics 27

2.3.2 Ducting of Internal Gravity Waves 31

2.3.3 Critical Layers 33

2.3.4 Sources and Effects of Internal Gravity Waves 34

2.4 Application of Theories to the Mesosphere and Thermosphere 35

CHAPTER III - OBSERVATIONS OF IRREGULAR, SMALL SCALE WIND VARIATIONS IN THE MESOSPHERE AND LOWER THERMOSPHERE 37

3.1 The General Wind Field and Observational Techniques 37

3.2 Radio-Meteor Measurements 40

3.2.1 Measurements of Wind Shear 40

3.2.2 Gross Random Fluctuations 42

3.3 Observations of Contaminant Release Trails 45

3.3.1 Structure Inferred from Wind Measurements 46

3.3.2 Diffusion Measurements 48

3.4 Summary of Observations and a Possible Model of Irregular Winds 51

CHAPTER IV - THE REFLECTION OF RADIO WAVES FROM METEOR TRAILS 56

4.1 Introduction 56

4.2 The Formation and Decay of the Trail 57

4.3 Scattering of Radio Waves by Meteor Trails 57

4.3.1 Stationary Trail 58

4.3.2 Trail in Presence of a Wind 61

Page N

4.4 The Effect of a Wind on the Measurement of Relative Positions of t_o Points and the Velocity of the Meteoroid 63

4.5 Summary 64

CHAPTER V - THE ADELAIDE RADIO METEOR SYSTEM 65

5.1 System Development 65

5.2 Measurement Technique 66

5.2.1 Location of One Reflection Point and the Determination of the line-of-sight Wind 67

5.2.2 Orientation of the Meteoroid Flight Path and the Separation of Reflection Points 69

5.3 Description of Equipment 70

5.3.1 Main Transmitters 70

5.3.2 27 MHz Receivers 71

5.3.3 The Outstations and Telemetry Links 72

5.3.4 Recording 75

5.4 Film Records 84

5.5 Summary of System Parameters 86

CHAPTER VI - METHODS OF DATA REDUCTION 88

6.1 Film Reading 88

6.2 Determination of Reflection Point Separation 90

6.3 Data Statistics 93

6.4 Determination of the Mean Wind 97

6.5 Determination of the Irregular Velocity Field 100

CHAPTER VII - OBSERVATIONS OF THE PREVAILING AND TIDAL WINDS DURING 1968-1969 104

7.1 Introduction 104

7.2 The Prevailing Wind 105

7.3 Periodogram Analysis 108

7.4 Tidal Winds 112

7.4.1 The Data 113

7.4.2 Comparison with Theory 120

CHAPTER VIII - MEASUREMENTS OF WIND SHEAR IN THE LOWER THERMOSPHERE 123

8.1 Introduction 123

8.2 Statistical Wind Shear Relationships 124

8.3 The Observations 125

8.4 Comparison with Previous Observations at Adelaide 131

8.5 Discussion of Present Observations 133

CHAPTER IX - A DIRECT COMPARISON OF WIND AND SHEAR MEASUREMENTS MADE WITH RADIO-METEOR AND CHEMILUMINESCENT TRAIL TECHNIQUES 136

9.1 Details of the Experiment 136

9.2 Wind Profiles 138

9.2.1 TMA Release Observations 138

9.2.2 The Radio-Meteor Observations 140

9.3 Wind Shear and Turbulence Measurements 143

9.4 Summary 147

		Page No
CHAPTER X - ROCKET MEASUREMENTS OF WIND AND DENSITY IN THE MESOSPHERE AND STRATOSPHERE		150
10.1	Introduction	150
10.2	Experimental Methods	151
10.3	Data Analysis	152
10.4	Errors in Measurement	154
10.4.1	Errors in Wind I - Mean Radar Errors	154
10.4.2	Errors in Wind II - Individual Radar Errors	157
10.4.3	Error in Density	159
10.5	Other Methods for Determining the Errors	161
10.6	Conclusions	161
CHAPTER XI - CONCLUSIONS AND FUTURE WORK		163
11.1	Small Scale Wind Structure	163
11.2	The Prevailing and Tidal Winds	165
11.2.1	General	165
11.2.2	The October 1969 Comparison	167
11.3	Wind and Density Measurements by Radar Tracking of Falling Spheres and Parachutes	169
11.4	Suggestions for Future Work	169
11.4.1	Equipment Improvement	169
11.4.2	Future Experiments	170
BIBLIOGRAPHY		172

SUMMARY

This thesis is concerned with an experimental investigation of small scale wind structure in the mesosphere and lower thermosphere. Emphasis is placed on the observations made with a multi-station radio-meteor system in the height range 75 - 105 km. Observations were made of the line-of-sight wind at a minimum of three and a maximum of five reflection points on a single meteor trail. Occasional separations of up to 14 km were possible but reliable statistical measurements were only made for separatio up to about 5 km.

Previous observations of wind shear have been collated and it has been found that the small scale wind structure in the region 70 - 110 km can be regarded as due to anisotropic turbulence with horizontal scales of up to a least 10 km and a vertical scale of about 2 km. The energy for this turbulent regime is considered to originate from the background wind field of internal gravity waves and tidal waves. The statistical measurements of wind shear described in this thesis show that this concept may be too simple. While turbulence certainly is responsible for the rapid diffusion of a chemical release below about 110 km, there still remains an uncertaint in the extension of turbulence theory to measurements of wind shear by the radio-meteor technique even though the results from the two methods are consistent.

Two wind profiles determined by tracking contaminant release trails ar compared with simultaneous radio-meteor wind observations. Both similariti

and differences are evident in the wind profiles and the latter are not fully explained, but a number of possible causes have been examined. The turbulent phenomena which appeared on the trails are discussed briefly and compared with the multi-station wind shear measurements.

The variation in the diurnal and semidiurnal tidal winds over the two year period 1968-1969 has also been determined. It appears that the theory of atmospheric tides is still incomplete as many discrepancies between observation and theory are found. The consistency of the seasonal changes in the prevailing wind is emphasised by the results for the years 1966-1969.

The possibility of measuring wind shears over scales of the order of 2 km with the falling sphere technique has been examined and shown to be limited by observational errors to heights below 60 km.

PREFACE

To the best of the author's knowledge and belief this thesis contains no material previously published or written by another person, except where due reference is made in the text. This thesis contains no material which has been accepted for the award of any other degree or diploma in any University.

(B. J. McAvaney)

University of Adelaide
14/8/70

ACKNOWLEDGEMENTS

The work described in this thesis was carried out in the Physics Department of the University of Adelaide under the supervision of Dr. W. G. Elford. The author is grateful to Dr. Elford for many helpful discussions and general encouragement throughout the course of the work. Also the author would like to thank Dr. R. G. Roper for many helpful suggestions.

The operation and maintenance of the radio meteor system required much cooperative effort. Many of the authors colleagues in the Radiophysics Group have given invaluable assistance from time to time. In particular the author would like to thank Mr. J. W. Smith for his many helpful suggestions at the design stage and also to thank Mr. E. J. Welsby for his most capable construction of the equipment and careful maintenance of the transmitters. The author is also indebted to his colleague, Mr. G. Gartrell who assisted in the design of part of the tape delay unit and shared the responsibility for operating the equipment and reading the films.

The processing and part of the reading of the films, involving much tedious work, was ably carried out by Misses Janice Gordon, Judy Hearse, Rille Walshe and Suzanne Spain. Part of the necessary computer programming was the work of a former colleague Dr. E. M. Doyle who also provided some of the wind data used in this thesis.

The experiment described in Chapter IX was carried out in collaboration with University College, London and the Upper Atmosphere Research Group, Weapons Research Establishment, Salisbury. The data pertaining to the contaminant releases was provided by Dr. D. Rees of University College and Mr. K. H. Lloyd of Weapons Research Establishment. The author is grateful for the many helpful discussions held with Messrs K. H. Lloyd and C. H. Low concerning the results of this experiment.

The error analysis described in Chapter X was performed at the instigation of Flight Projects Group, Weapons Research Establishment. The assistance of Mr. R. Curnow with some of the programming for the IBM 7090 was much appreciated.

Finance for the radio-meteor project was provided by the National Aeronautics and Space Administration, U.S.A. (Grant NGR 52-042-004), Australian Research Grants Committee (Grant No. B66-16370), Radio Research Board, Australia and the University of Adelaide. The author is grateful to the CSIRO for the award of a Senior Post-graduate Research Studentship and to the University for a grant which has enabled completion of this thesis.

CHAPTER I

DYNAMICS OF THE ATMOSPHERE BETWEEN 30 km AND 120 km

1.1 INTRODUCTION

The structure and circulation of the atmosphere above the levels accessible by meteorological balloons has been a subject of considerable interest during the last two decades. The rapid development in radio, rocket and satellite techniques over this period has enabled relatively sophisticated sounding methods to be devised. The accumulation of experimental data has in turn stimulated much theoretical interest in the dynamics of the region.

The ultimate source of energy for the motion observed in the atmosphere is of course the sun. The manner in which solar energy is absorbed in and transmitted through various levels in the atmosphere is of prime importance An indirect method of heating the atmosphere is the eventual dissipation by turbulence of the kinetic energy of various types of wave motion. This contribution is of importance in the energy budget of the mesosphere and lower thermosphere. The relative amounts of energy dissipated by turbulence internal gravity waves and tidal waves are not well established in this region. Hence simultaneous observations of tides and small scale structure may enable a better understanding of the distribution of energy among these forms of motion.

In order to separate the tidal and small scale wind motion from the total wind field continuous observations are required. A radio-meteor system is ideal for this purpose over a limited region in the mesosphere and lower thermosphere. This thesis describes observations of tides and small scale structure made with such a system.

Throughout the thesis, emphasis is put on small scale wind structure in the mesosphere and lower thermosphere. After a theoretical consideration of small scale phenomena due to turbulence and internal acoustic-gravity waves, previous observations are discussed. Observations of the prevailing and tidal wind components determined with a radio-meteor system are presented. Measurements of wind shear made with a multi-station system are also discussed. A direct comparison with observations of chemiluminescent trails is also made. The possibility of using balloon and parachute sensors for small scale wind measurements is also examined.

In the remainder of this chapter the present knowledge of the energy budget of the mesosphere and lower thermosphere is summarised and a brief description is given of the various experimental methods which have been used to determine both large and small scale structure in the atmosphere. These techniques can be broadly classified into two types; direct methods which depend on sensors to be injected directly into the region of interes and indirect measurements which rely on ground based observation of some naturally occurring sensor. Some of the techniques used are described in §1.3 and §1.4.

1.2 SOURCES AND SINKS OF ENERGY IN THE MESOSPHERE AND LOWER THERMOSPHERE

The thermal structure of the mesosphere and lower thermosphere (50 - 120 km) is determined by the local sources and sinks for solar energy. In addition adiabatic expansion and compression associated with vertical motion in the circulation systems can modify temperature structure significantly.

The meridional temperature structure for summer and winter are shown in Figure 1.1 (after Newell, 1968). The most surprising feature is the extremely low temperature at 85 km observed over the summer pole which is continuously sunlit and heated by radiative effects, while at 60°N at this height in winter high temperatures occur in the presence of radiative cooling. A satisfactory explanation of the temperature patterns has been proposed in terms of the adiabatic heating associated with the atmospheric circulation. The main features of the patterns below 90 km are a summer maximum at 50 km over the pole and equator and a winter maximum over the equator at 50 km.

Leovy (1964) and Newell (1968) have proposed successful dynamical models driven by radiative heating which can maintain cold mesopause temperatures over the summer pole. The winter temperature structure is only partially understood but it appears that the effects of large scale eddies must be included.

Below about 80 km most regions of the atmosphere can be considered to be in a state of radiative equilibrium, the absorption of solar

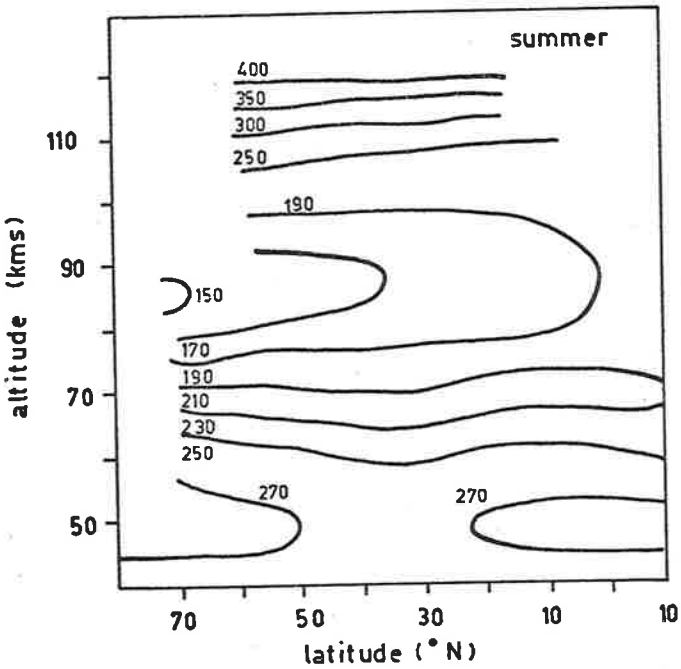

(a) MERIDIONAL TEMPERATURE (°K) CROSS-SECTION IN SUMMER.

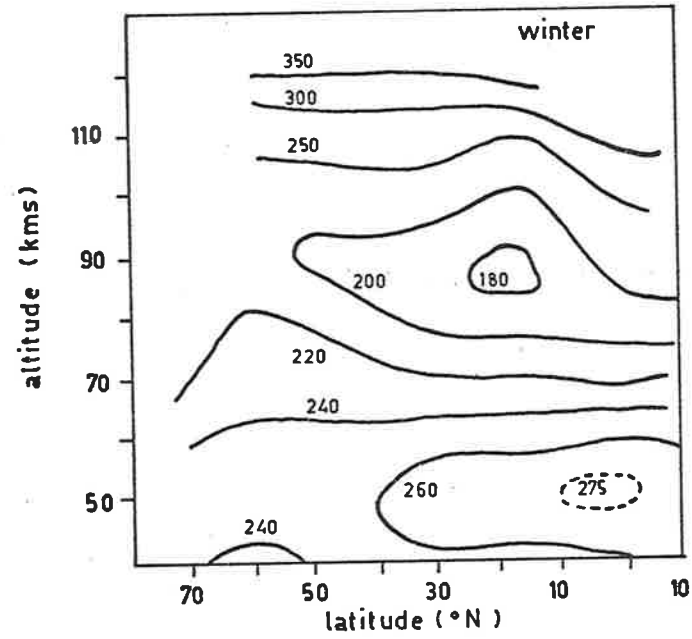

(b) MERIDIONAL TEMPERATURE (°K) CROSS-SECTION IN WINTER.

Figure 1.1: Meridional mean temperature distribution for Summer and Winter (after Newell, 1968).

ultraviolet by ozone being balanced to a large extent by emission of infrared radiation by carbon dioxide. Leovy (1969) has discussed the various sources and sinks of energy that are consistent with the gross features of the wind field in this region.

Above 80 km the atmosphere departs significantly from radiative equilibrium as a number of non-radiative processes begin to influence the distribution of heat sources and sinks. Thus the following sources of energy must be considered in the region 80 - 110 km:

(i) absorption of solar radiation by molecular oxygen ($\sim$ 14 ergs/cm^2 - sec),

(ii) transport of energy by thermal conduction and turbulent heat transfer from higher in the thermosphere ($\sim$ 5 ergs/cm^2 - sec),

(iii) release of chemical energy by recombination of atomic oxygen transported from higher levels ($\sim$ 1 ergs/cm^2 - sec),

(iv) dissipation of turbulent energy generated by wave motions such as gravity waves and tidal waves ($\sim$ 10 ergs/cm^2 - sec).

These sources must be balanced by infrared emission by carbon dioxide ($\sim$ 28 ergs/cm^2 - sec) and nightglow emission by the hydroxyl radical ($\sim$ 2 ergs/cm^2 - sec). Both large and small scale motions can have a significant effect on the heat sources and sinks, so that an understanding of these motions is essential if reliable circulation models are to be developed.

Because of the variable nature of heat sources and sinks, it is not surprising that the temperature structure of the atmosphere has the

variations shown in Figure 1.1. These temperature differences must produce large pressure gradients that give rise to the mean winds observed. Superimposed on these mean winds are meteorological disturbances (e.g. Newell and Dickinson, 1968) and above 70 km tidal and gravity waves of various modes become important.

1.3 EXPERIMENTAL TECHNIQUES: DIRECT METHODS

Figure 1.2 illustrates the height range encompassed by some of the experimental techniques used. In general direct methods cannot be used on a routine basis because of the high cost of each sounding. However they do make possible controlled experiments and, in general, give essentially an instantaneous vertical sample of the parameters being measured. Current methods being used most extensively are described below.

1.3.1 Meteorological Rockets

Small and relatively inexpensive meteorological rockets capable of reaching an altitude of about 65 km are being used in increasing numbers to measure the main meteorological parameters of wind, temperature and density. The wind sensors which have been employed include radar chaff dipoles, inflatable spheres and parachutes. These sensors are tracked with an accurate radar so that winds can be determined from the measured displacements. In the case of the falling sphere the atmospheric density can also be found from the drag acceleratio

The falling sphere technique was developed by Bartman et al. (1956) and has been in operation since 1952 using both inflatable balloon

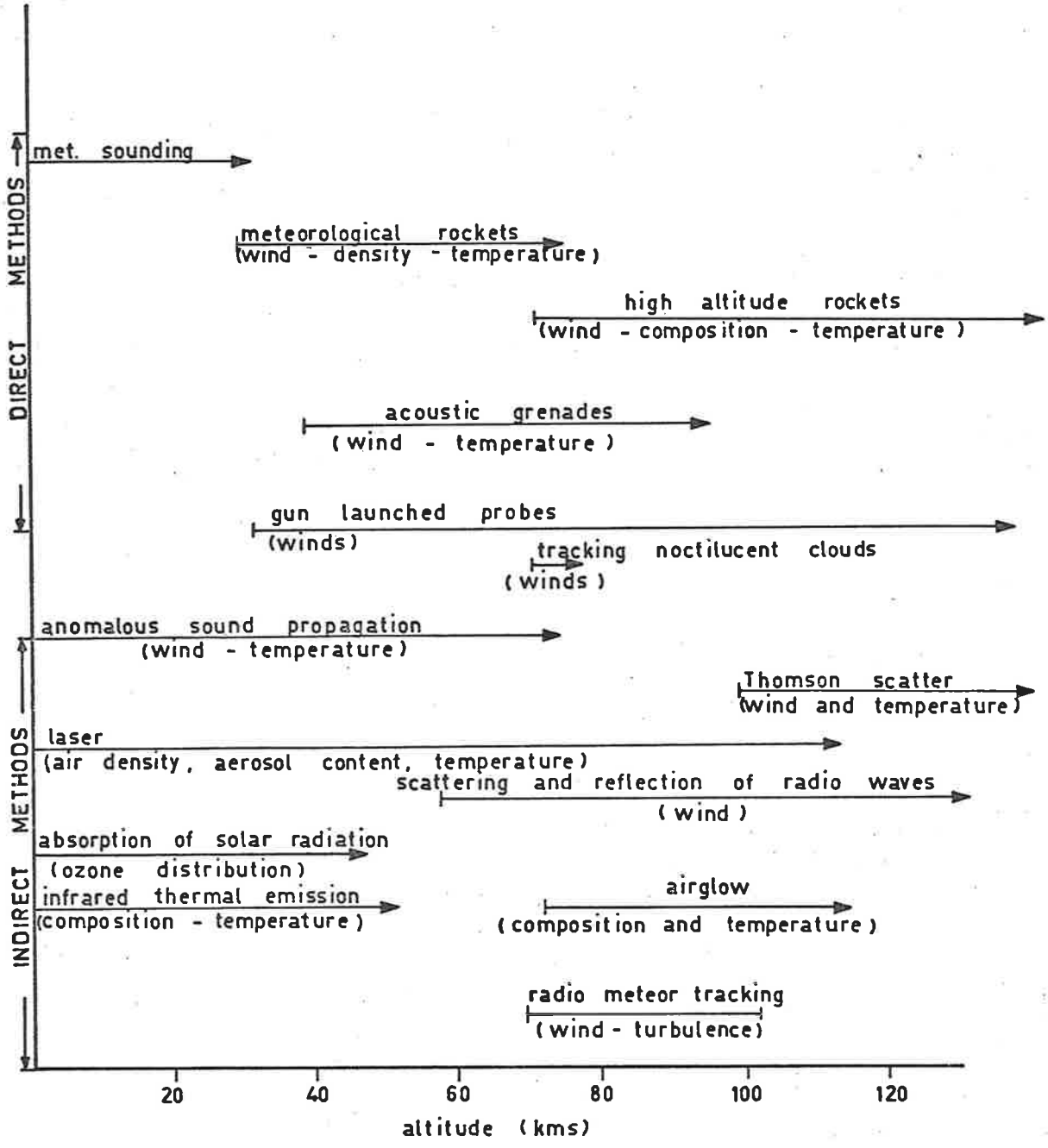

FIG. 1·2 EXPERIMENTAL METHODS IN EXPLORING THE ATMOSPHERE (AFTER FEDELE, 1968).

and rigid spheres. Essentially this technique measures the mean wind and density and its extension to measurement of small scale structure involves careful assessment of the accuracy of the system. This aspect is discussed in Chapter X.

The most general technique employed at the present time is to lower an active package through the region by a parachute. The fall rates obtained with this type of system are generally acceptable for accurate radar tracking. A bead thermistor is normally used to measure the temperature. This system is currently used by the Meteorological Rocket Network (Webb et al., 1961).

1.3.2 Acoustic Grenades

This technique is applicable to the upper stratosphere and mesosphere (30 - 100 km) and is capable of determining both temperature and wind. A sequence of grenades are fired from an ascending rocket at intervals of a few kilometres. The exact time and location of each explosion is determined by photographic and photoelectric techniques and the time and direction of arrival of the acoustic wave at the ground is recorded by an array of microphones. Each wave front is traced back through a model atmosphere to find the "virtual" position of the explosion and by gradually modifying the wind and temperature structure of the model a closer and closer approximation to the true distribution of wind and temperature can be achieved (Stroud et al., 1956). Groves (1960) has considerably modified the technique to give greater accuracy and information on vertical wind strengths.

1.3.3 Contaminant Releases

The most convenient method for determining winds above 70 km is to employ some form of artificial tracer. The usual technique has been to eject selected chemicals from high altitude rockets. Alkali vapours, particularly sodium, have often been used since these resonantly scatter sunlight and hence can be tracked photographically provided the background sky illumination is sufficiently small. This latter requirement restricts the use of these chemicals to a 20 - 40 minute period at twilight when the trail is sunlit and the background is dark. Observations of these trails are usually made by several cameras on the ground and the winds are deduced by triangulation of particular features in the trail (Manring et al., 1959).

By using materials which undergo photochemical reactions with atomic oxygen, trails can be made luminous at night. Rosenberg et al. (1963) have developed a technique for producing trails of trimethylaluminium which is now used by many experimenters for wind measurement over the height range 85 to about 160 km. Further details and some results found using this technique are discussed in Chapter IX.

1.3.4 Gun-Launched Probes

Gun-launched probes are being used to inject sensors up to an altitude of 150 km. Because of the extreme accelerations involved, typically 40000 g, active payloads which telemeter information back to ground have not yet been successfully developed for general use. The normal payloads used to date have been packages of radar chaff which are expelled and tracked by radar, and tanks of chemicals which can lay vapour trails (Bull, 1964). Murphy et al., (1966) have used this techniqu

to lay trimethylaluminium trails throughout several nights. This experiment is attractive because of the considerable reduction in cost compared to an equivalent rocket programme.

1.4 EXPERIMENTAL TECHNIQUES: INDIRECT METHODS

Ground based observations of wind and temperature at altitudes above 30 km have been made using many different techniques. The main advantage over direct methods is the possibility of routine measurements which cannot be carried out with rockets because of the high cost. One disadvantage of many ground based observations is the limited height resolution often available.

Some of the indirect methods shown in Figure 1.1 are now seldom used because of the difficulty of interpreting the basic measurements. Other techniques, in particular radio-meteor systems, are being used more frequently to obtain routine measurements at many sites distributed widely in latitude and longitude.

1.4.1 Ionospheric Drifts

When radio waves are reflected from the ionosphere a diffraction pattern is formed on the ground. By sampling with three or more close-spaced receivers, parameters which describe the behaviour of this pattern can be found. These enable a measure of the drift velocity in the ionosphere to be determined.

The technique has mainly been applied to the E-region at heights near 110 km. Kent and Wright (1968) have reviewed many of the observations made and pointed out the various assumptions necessary at

various stages during the analysis. Some of these assumptions have only recently been experimentally tested with the aid of a large aerial array near Adelaide (Felgate, 1970; Golley and Rossiter, 1970). The main difficulty in interpreting the results is the uncertainty as to when the drift of the charged particles is the same as that of the neutral air.

A most interesting development of this technique has been in its application to the weak partial reflections from the D region (Fraser, 1965 and 1968; Rossiter, 1970). Depending on ionospheric conditions, drifts can be obtained at about 5 km intervals over the height range 70 to 100 km for two or three hours around noon each day.

1.4.2 The Radio-Meteor Method

The first measurements of winds by tracking a meteor trail by radio techniques were made by Manning, Villard and Peterson (1950) although detection of meteors by radar was accomplished much earlier. Since meteoroids enter the earth's atmosphere throughout the day the tracking of meteor trails is an extremely useful method of wind measurement in the height region 75 km to 110 km. Details of the scattering of radio waves from a meteor trail are described in Chapter IV.

The basic measurements required are the location of the reflection point in space and the radial velocity of the meteor trail at this point. Many techniques have been developed for this purpose but they can be classified into two main types: phase-coherent pulse

methods with narrow beam antennae and with simple direction finding techniques or continuous wave methods with more sophisticated direction finding systems.

The first continuous wave system was developed by Manning, Villard and Peterson (1950) at Stanford, U.S.A. The angle of arrival of the signal reflected from a meteor trail was determined using a special direction finding system while the Doppler shift in frequency of the reflected wave relative to the transmitted wave (frequency 23 MHz) gave a measure of the radial drift velocity. The sense of the drift (toward or away from the observing site) was found by beating the sky wave with a phase-shifted ground wave.

A slightly more sophisticated CW system was developed at Adelaide by Robertson, Liddy and Elford (1953). This system is described in more detail in Chapter V. The direction of arrival of the reflected signal is determined by comparing the phase of the signal at an array of aerials. The range of the echo is found using a separate pulse transmitting system. Thus echoes are obtained at accurately known heights (± 1.5 km) in the height range 70 - 110 km. The maximum usable echo rate achieved with the present transmitting power (1.5 kw at 27 MHz) is about 60 echoes/hour.

Spizzichino et al. (1965) have developed a different CW technique at Garchy, France using three transmitting frequencies (f_1 = 29.972 MHz, $f_2 = f_1 + 4.8$ kHz, $f_3 = f_1 + 5.4$ kHz). A direction finding system similar to that in use at Adelaide is employed except that phase

comparisons are made at the radio-frequency itself instead of the low frequency Doppler heat. The direction of arrival is found to an accuracy of $\pm 0.5^{\circ}$. By phase comparison between the three frequencies received, the slant range of an echo is determined to an accuracy of about 300 metres. A usable echo rate of about 100 echoes per hour is achieved with this equipment but only one component of the wind (east-west) is measured*.

The phase-coherent pulse method was developed by Greenhow (1952a) and has been used at a large number of installations since. Perhaps the main reasons for the popularity of this system are that it can be operated from a single site and the relative ease of discriminating against reflections from aircraft. Narrow beam antennae are normally used; range is determined by standard radar techniques, direction of arrival is determined either by simply relying on the antennae beam or else by simple phase comparisons between aerials with different vertical radiation patterns. The original system of Greenhow and Neufeld relied upon the measured decay rates to determine the heights and only had an accuracy of ± 5 km. Many stations in the USSR do not attempt height measurement. High rates can be achieved with this type of system owing to the gain possible in the aerial beam but at the expense of an accentuated diurnal rate, and accuracy.

Southworth (1968) at Havana, Illinois has developed a highly accurate phase-coherent pulse system for observing a limited region

---

* As from April 1970 the north-south component is also determined.

of the atmosphere. A very high power transmitter (3 megawatt) is used in conjunction with a series of eight receiving sites. By comparing Fresnel diffraction patterns of the echoes received at each of these sites the orientation and height of the trail can be determined. In its final form this system should be able to measure the complete vector winds in a volume 50 km × 30 km × 16 km.

The radio-systems currently known to be operating taking routine wind observations are shown in Table 1.1. Information on the systems operating in USSR is not as recent as for other countries but is based on the latest available publications. The minimum hourly rates given where possible are estimates of the minimum number of useful echoes obtained during the least favourable time of the day (usually near 1800 hours local time). Other stations planned, with equivalent system orientation, are

Georgia Tech., Atlanta, Georgia, U.S.A. (Adelaide, Alaska)
Washington State U., U.S.A. (Stanford)
British met. stations (2), U.K. (Sheffield)
Jamaica, W.I. (Sheffield)
University of Kyoto, Japan (Stanford)
University of Saskatchenan, Canada (probably CW)
University of Western Ontario, Canada, (probably pulse)

(Roper, 1970; private communication).

1.4.3 Other Methods

The occasional appearance of noctilucent clouds at a height of 80 km observed at high latitudes enables a quite detailed study of the

Station	Power	Frequency (MHz)	Location	Minimum Hourly Rate	Height Accuracy (km)
Adelaide, South Aust.	1.5 kW (CW) 65 kW (pulse)	26.8 27.5	35°S, 139°E	10	± 2
Havana, Ill., U.S.A.	3 MW (pulse)	40.9	40°N, 90°W	(500)	± 3
Garchy, France	5 kW (CW)	29.8 (3 frequencies)	47°N, 3°E	15	± 2
Durham, N.H., U.S.A.	30 kW (pulse)	36.8	43°N, 71°W	15	± 3
Stanford, Calif., U.S.A.	5 kW (pulse)	30.1	37°N, 122°W	20	± 2.5
Fairbanks, Alaska, U.S.A.	1.5 kW (CW)	30.2 (2 frequencies)	65°N, 148°W	10	± 5
White Sands, M.M., U.S.A.	30 kW (pulse)	32.8	33°N, 106°W	(still testing)	
Englin AFB, F/a, U.S.A.	5 kW (pulse)	36.8	30°N, 87°W	20	± 2.5
Sheffield, England	75 kW (pulse)	25	53°N, 1°W	30	± 3
Kharkov, U.S.S.R.	100 kW (pulse)	36.9	50°N, 36°E	50	± 4
Kazan, U.S.S.R.	100 kW (pulse)	72	56°N, 49°E		± 4
Moscow, U.S.S.R.	100 kW (pulse)	33	59°N, 37°E		± 4
Hayes Isld., U.S.S.R.	75 kW (pilse)	33.5	79°N, 58°E		(decay)
Tomsk, U.S.S.R.	50 kW (pulse)	30.0	55°N, 85°E		(decay)
Obninsk, U.S.S.R.	75 kW (pulse)	24.0	56°N, 35°E		(decay)
Kiev, U.S.S.R.	10 kW (pulse)	34.5	52°N, 30°E		(decay)
Frunze, U.S.S.R.	45 kW (pulse)	38.3	43°N, 72°E		(decay)
Duschanbe, U.S.S.R.	80 kW (pulse)	37.4	38°N, 68°E		(decay)

TABLE 1.1: RADIO-METEOR SYSTEMS KNOWN TO BE OPERATING AS AT DECEMBER 1969; THERE IS SOME DOUBT AS TO THE STATUS OF RUSSIAN METEOR WIND MEASUREMENTS

horizontal wind field to be accomplished (Witt, 1962). However since these clouds occur infrequently routine measurements cannot be made.

An interesting possibility of measuring winds in the height range 100 - 120 km is by the use of the incoherent backscatter (Thomson scattering) technique. By observing the spectrum of a return pulse the Doppler shift due to the ions moving along the field lines can be determined (Carru et al., 1967). Over the height range 100 - 120 km the collision frequency is high enough so that the ions should move with the neutral air. Thus in principle the wind can be measured.

CHAPTER II

THEORIES OF IRREGULAR STRUCTURE IN THE ATMOSPHERE

2.1 DESCRIPTION OF THE PROBLEM

Any attempt to explain the movements and structure of the atmosphere below 120 km would be incomplete without some discussion of turbulence and internal gravity waves. In particular the observations to be discussed in Chapter III indicate that the irregular winds of the mesosphere and lower thermosphere contain a significant fraction of the energy in this region. Both the theory of atmospheric turbulence and the theory of internal gravity waves must be used to explain the observations. For example the fine-scale motion observed within a particular globule of a chemical trail can be explained by the application of turbulence theory whereas the larger-scale background fluctuations of the trail may often be explained in terms of motion due to internal gravity waves.

The purpose of this Chapter is to present an outline of the theories of atmospheric turbulence and internal gravity waves. Rather than presenting mathematical detail, physical ideas and interpretation will be emphasised.

A common problem in a discussion of turbulence in the atmosphere is in the definition of turbulence itself. Pasquill (1963) states that "in all its physical essentials a turbulence condition is adequately described as one of irregular motion in which mixing of fluid properties occurs at a rate many orders of magnitude greater than that occurring by molecular motion".

A more formal definition has been used by Lumley (1964); "turbulence is any random, three dimensional velocity field with a continuous spectrum, displaying spectral transfer and dissipation at high wave numbers". This definition of Lumley's, which includes a velocity field due to random internal gravity waves is most useful in its application to the mesosphere and lower thermosphere.

Gravity waves are basically natural modes of oscillation of the atmosphere which can be excited by some external driving forces. In general coupling between various modes is not important and hence the distribution of energy is determined mainly by the driving forces. In the case of turbulence, interaction between various modes has become so strong that in an equilibrium state the distribution of energy is determined primarily by internal energy transfer. The driving mechanism merely determines the total amount of energy available and ultimately the region of viscous dissipation.

For both theories presented here the governing equations of motion are the same as for most classes of problem in Atmospheric Physics. The equations are those for the conservation of momentum, mass and energy for a viscous, compressible, Newtonian fluid in a uniform gravitational field (see, for example, Landau and Lifshitz, 1959). Both theories are concerned with the deviation of meteorological parameters from their mean values and hence perturbation techniques are applied to the basic equations.

2.2 GENERAL THEORY OF TURBULENCE

The structure of a turbulent field can be discussed under three classifications:

(i) A description of the continuous character in the structure and the effects of turbulence through the use of the concept of an energy spectrum;

(ii) the energy balance involved in the generation, transport and decay of the turbulence;

(iii) the diffusive nature of turbulence.

The present discussion will mainly be concerned with the first two classifications above.

Useful texts which cover turbulence as a problem in fluid dynamics are those of Batchelor (1953) and Hinze (1959). The problem of turbulence in the atmosphere is well covered by Lumley and Panofsky (1964) to which frequent reference will be made in the following discussion.

2.2.1 Statistical Description

Any experimental investigation of turbulence requires observations of some fluctuating quantity either as a function of time or space and sometimes both. These fluctuations are normally described by the auto-correlation function. In the case of a wind field with velocities $\underline{u}'$ expressed as a deviation from a mean wind speed $\bar{\underline{u}}$ the correlation function for the point at $\underline{r}$ and at time t is given by

$$\rho(\tau) = \overline{\underline{u}'(\underline{r}, t)\underline{u}'(\underline{r}, t + \tau)} / \overline{\underline{u}'(\underline{r}, t)^2} \qquad 2.1$$

where τ is the temporal lag. An alternative description which avoids some of the complications when the data is non-stationary is by means of the structure function, defined as the variance of the differences

$$D(\tau) = \overline{|\underline{u}'(t) - \underline{u}'(t + \tau)|^2} \quad . \qquad 2.2$$

In both (2.1) and (2.2) the independent variable τ could equally well be replaced by a spatial displacement ξ. Thus a velocity field $\underline{V}(\underline{r})$ can be characterised by a set of nine similar structure functions,

$$D_{lk}(\underline{\xi}) = \overline{|V_l(\underline{\xi} + \underline{r}) - V_l(\underline{r})| \; |V_k(\underline{\xi} + \underline{r}) - V_k(\underline{r})|} \quad l, k = 1, 2, 3 \qquad 2.3$$

A description of a fluctuating quantity by means of the structure function alone would not be particularly useful. Usually the distribution of energy in time and space is of most interest. The spectral energy density $\Phi(\underline{\kappa})$ can be calculated from either the structure function or the correlation function using the appropriate relation,

$$\underline{\Phi}(\underline{\kappa}) = \frac{\underline{\kappa}}{16\pi^2\kappa^2} \iiint_{-\infty}^{\infty} \sin\,(\underline{\kappa}\cdot\underline{r})\underline{V}D(\underline{r})d\underline{r} \qquad 2.4$$

or

$$\underline{\Phi}(\underline{\kappa}) = \frac{1}{(2\pi)^3} \iiint_{-\infty}^{\infty} \rho(\underline{r}) \exp\,(-i\underline{\kappa}\cdot\underline{r})d\underline{r} \qquad 2.5$$

where $\underline{\kappa}$ is the wave-number.

The spectral energy density tensor has many statistical and geometrical implications but by itself does not express anything about the physical processes involved. The distribution of the available kinetic energy among eddies of various sizes, the generation of this energy and its

ultimate dissipation have all to be investigated if the basic physical processes are to be understood. The methods of production of turbulence in the atmosphere are not fully understood but probably depend on instability mechanisms. The energy budget in fully developed turbulence is discussed in §2.2.2 below.

2.2.2 The Energy Balance

Two methods for the production of turbulence are

(i) breakdown of the mean flow in the presence of shear, and

(ii) vertical motion associated with thermal effects in the medium.

As yet is it impossible to predict precisely the characteristics of a turbulent field directly from the characteristics of a particular energy source. However once the turbulence has been established it is possible to describe the energy balance of the turbulent field.

Lumley and Panofsky (1964, p67) derive an expression for the rate of change of kinetic energy which can be described term by term as follows:

(i) an "eddy stress" term which describes the transfer of energy from the mean motion to the eddy motion superimposed on this mean;

(ii) vertical energy exchange due to the action of buoyancy forces;

(iii) transfer of energy among components by pressure forces with no dissipation occuring;

(iv) transfer of kinetic energy among components by viscous stresses which ultimately are responsible for the dissipation of the energy;

(v) convection and viscous transport (no net gain or loss of energy).

The relative importance of these terms in the energy budget depends on the particular model of turbulence considered.

2.2.3 The Inertial Subrange

The ultimate sink for turbulent energy is conversion to heat by viscous action. This dissipative mechanism occurs by progressive transfer of kinetic energy from large eddies to smaller eddies until eventually the eddies are sufficiently small that viscous forces can extract energy from these eddies. Consideration of these terms in the energy budget led Kolmogorov (1941) to develop the highly successful "similarity" theory of turbulence . The basis of this theory is that in the transfer of energy from larger to smaller eddies, a range of wave numbers should be reached in which energy transfer is isotropic. This equilibrium range is self-adjusting through the operation of inertia forces and must depend only on the parameters which describe external effects. These effects are simply the insertion of energy at low wave numbers and the removal of energy at high numbers by viscous dissipation. The two parameters concerned are the rate of energy dissipation ε and the kinematic viscosity ν. If further an extensive range of wave-numbers exists in which no production or dissipation occurs (an inertial sub-range) then motion associated with this subrange is independent of both the energy containing eddies and the

eddies responsible for the dissipation (and hence independent of the viscosity). In such an inertial subrange the energy spectrum for wave-numbers, κ, must be of the form

$$E(\kappa) = \alpha\varepsilon^{2/3}\kappa^{-5/3} \qquad 2.6$$

where α is a universal constant (Kolmogorov, 1941). The corresponding structure function also has a characteristic power law for the inertial subrange, for example

$$D_{11}(\xi) = \overline{(u_1(x_1 + \xi, x_2, x_3) - u_1(x_1, x_2, x_3))^2}$$

$$= \beta\varepsilon^{2/3}\xi^{2/3} \qquad 2.7$$

where β is an absolute constant (see also Lumley and Panofsky, 1964).

The value of the exponent in the power law for an inertial subrange has been confirmed in the atmosphere (e.g. by MacCready, 1962; Pond et al., 1963), in the ocean (Grant et al., 1962) and in the laboratory (Gibson, 1962 and 1963). The numerical value of the universal constant in the expression (2.6) above has been the subject of some debate and is discussed further below.

For the longitudinal component of the wave-number expression (2.6) is written as

$$S(k) = a\varepsilon^{2/3}k^{-5/3} \qquad 2.8$$

where S(k) is now a one-dimensional energy spectrum. As measurements are frequently made of only one component of the motion this form of the power

law for an inertial subrange is generally used. A similar expression exists for the lateral component viz.

$$S_2(k) = \frac{4}{3} a\varepsilon^{2/3} k^{-5/3} .$$

Various estimates of the numerical value of the constant a in expression (2.8) above have been discussed by Panofsky and Pasquill (1963); the more recent determinations suggest that the value lies between 0.45 and 0.50 (spectral measurements in a tidal current, Grant et al., 1962 spectral measurements of wind speed, Pond et al., 1963 and 1966; laboratory measurements, Gibson, 1962). The relation between the constant β in expression (2.7) and the constant a in expression (2.8) is $\beta = 4.82a$ (Batchelor, 1953).

It is apparent that if measurements of, say, wind speed can be made in an inertial subrange and the spectrum determined then the value of ε, the rate of dissipation of energy, can be determined from the measured spectrum on substitution of the appropriate constants.

2.2.4 The Buoyancy Subrange

In general the Kolmogorov spectrum should only apply to an atmosphere with neutral stratification because of the neglect of buoyancy effects. Most parts of the atmosphere can have some degree of stable stratification and hence the effects of buoyancy should be considered in a complete analysis of turbulent motion. This problem has been discussed by a number of authors for the case of small mean shearing motion (Bolgiano, 1959 and 1962; Shur, 1962; Monin, 1962; Lumley, 1964). The form of the energy spectrum predicted is

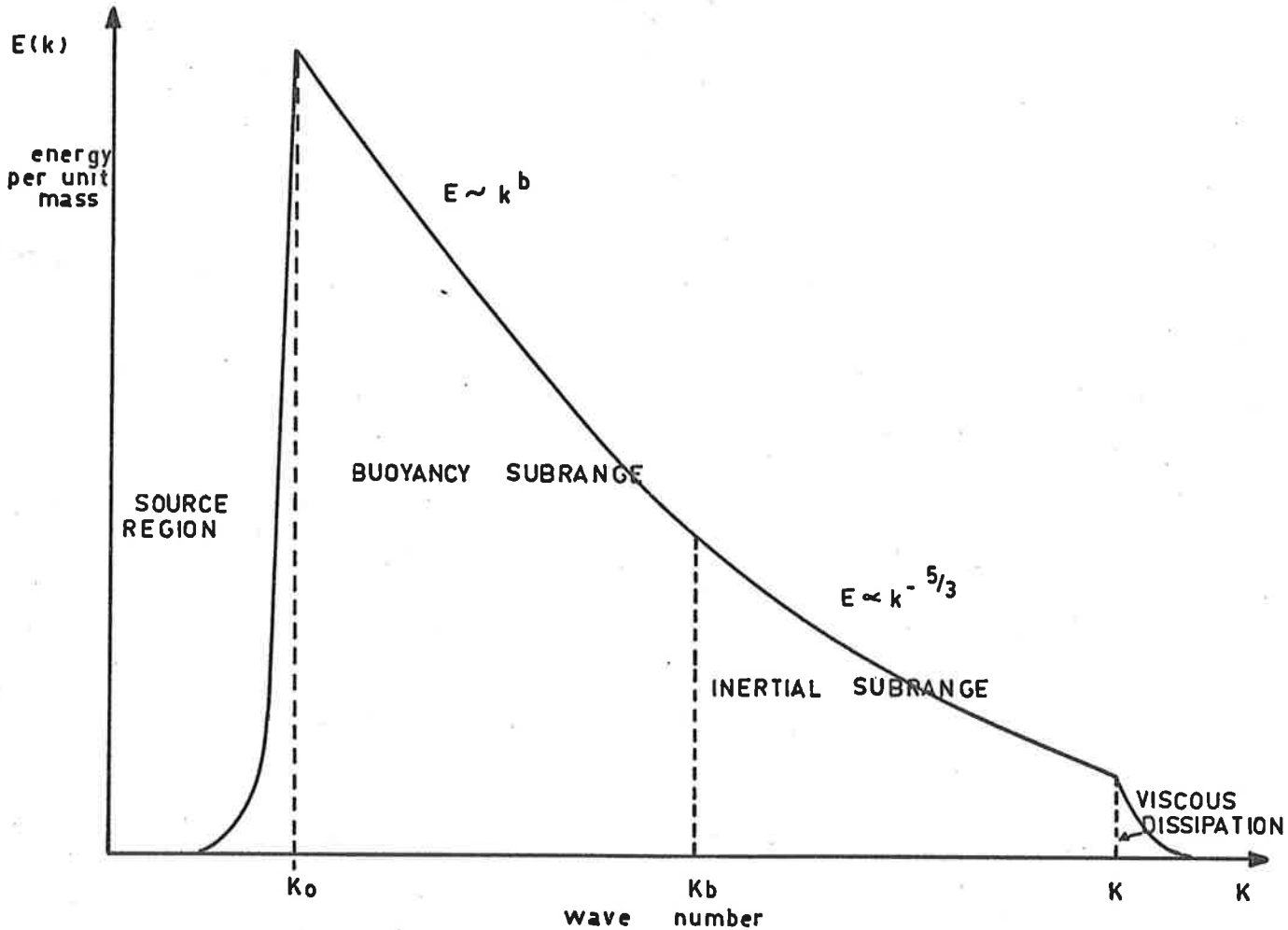

FIG. 2·1 SCHEMATIC GRAPH OF ENERGY SPECTRUM FUNCTION FOR A STABLY STRATIFIED REGION.

$$E(\kappa) \propto \kappa^{b} \qquad 2.9$$

where the value of the exponent b lies between - 5/3 and - 3 depending on the assumptions made.

The underlying concept which gives rise to power laws of the form of expression (2.9) is that of a "buoyancy subrange". This term applies to that region of the spectrum in which the energy of the turbulent field is suppressed by the action of negative buoyancy forces associated with a stable atmospheric environment. The range of eddies in the buoyancy subrange is determined by the condition that the eddies should be small enough that any mean shear present has no influence but large enough that buoyancy forces are important.

Provided that the turbulence in the buoyancy subrange remains approximately isotropic in spite of the anisotropic influence of the environment, then the one dimensional energy spectrum should also have the form

$$S(k) \propto k^{b}$$

since a relatively small amount of the turbulent energy cascading from large to small wavelengths is being removed by buoyancy at a given wave-number in the buoyancy subrange. The values of the exponent b predicted by various theories are given in Table 2.1.

When the buoyancy effects are included, the energy spectrum is divided into four regions as shown in Figure 2.1:

(i) large scale fluctuations for wave-numbers k such that $0 \leq k \leq k_o$, these fluctuations carry the turbulent energy extracted from the mean flow,

Theory	Value of Exponent (b)
Bolgiano (1962)	- 11/5
Shur (1962)	- 3
Lumley (1964)	- 3
Monin (1962)	$-5/3 < b < -11/5$

TABLE 2.1 POWER LAWS PREDICTED BY VARIOUS BUOYANCY SUB-RANGE THEORIES

Theory	Diffusion Law
Bolgiano (1962)	$d^2 = \beta\omega_g^2 \varepsilon t^5$ (buoyancy subrange)
Lin (1960)	$d^2 = \frac{4}{3} B(\varepsilon) t^3$ (inertial subrange)
Batchelor (1950)	$d^2 = \frac{16}{3} \varepsilon t^3$ " "
Tchen (1961)	$d^2 \sim t^2$ high shear $d^2 \sim t^3$ low shear

TABLE 2.2 DIFFUSION LAWS PREDICTED BY VARIOUS THEORIES

(ii) the buoyancy subrange, $k_o \leq k \leq k_B$ for which the spectrum has the form $E \propto k^b$

(iii) the inertial subrange, $k_B \leq k \leq k^*$ in which the energy is simply passing from larger to smaller eddies with $E \propto k^{5/3}$

(iv) the viscous dissipation region, $k^* \leq k < \infty$ where the kinetic energy of the smaller eddies is dissipated by viscous forces.

2.2.5 Turbulent Diffusion

In general mass, momentum and heat are transported much more effectively by turbulence than by molecular motion. The two forms of transport are similar in the type of motion involved but the temporal and spatial scales of each are greatly different. The scales of turbulent motion are of the same order as the temporal and spatial scales characterising the distribution of the scalar being transported. The fluid consequently interacts with itself over a wider area than purely local properties can describe.

Coté (1965) discusses several theories of turbulent diffusion and finds that some of the relations concerned can be written in the form

$$d^2 \alpha v_o^{6-2n} \varepsilon^{n-2} t^n \qquad 2.10$$

where d is the diameter of the diffusing cloud at time t after formation and v_o is the rms turbulent velocity. The value of the exponent n in the expression (2.10) depends on the form assumed for the turbulent energy spectrum. Table 2.2 gives the form of the diffusion law predicted by various theories.

If observations of actual turbulent diffusion yield a time exponent compatible with expression (2.10) then the value of ε can be calculated.

2.3 INTERNAL ACOUSTIC-GRAVITY WAVES

Possible solutions to the equations of motion for the atmosphere include a set of waves. In principle a complete set of natural modes can be determined; however the properties of a particular class of waves are usually investigated by making certain assumptions in the equations of motion. Waves with periods of the order of days and scales of the order of the circumference of the earth are termed planetary waves and are associated with large scale meteorological disturbances and continental-scale orographic perturbations. Thermal and gravitational tides form a second rather special class of waves since the periods and driving forces are well known. Waves with periods of a few minutes to a few hours and horizontal scales of the order of a few hundred kilometres form a third class normally termed internal acoustic-gravity waves. The present section is only concerned with this latter type of wave.

Internal acoustic-gravity waves follow naturally from the consideration of sound wave propagation in a gravitational field. In a sound wave there is a continuous exchange of energy between the kinetic energy of the wave-motion and the compressional energy of the medium (the stored energy). In the presence of a gravitational field potential energy is stored by raising the fluid mass. If there is also a variation with height in the density of the medium then there may be an exchange of less dense fluid with fluid

of greater density hence storing energy. It is this latter internal energy storage which is important in the consideration of internal acoustic-gravity waves.

Gravity waves in an incompressible fluid were first discussed by Rayleigh (1883). Lamb (1910) extended the theory to compressible fluids. More recently interest has been renewed mainly due to the work of Hines (1960) in application of the theory to the irregular winds observed in the mesosphere and thermosphere.

2.3.1 General Characteristics

The essential features of internal acoustic-gravity waves can be illustrated by considering an isothermal atmosphere with no mean wind. With these simplifications a dispersion relation can be determined from the linearised governing equations(Hines, 1960). Although this dispersion relation is extremely useful in describing many of the properties of these waves a more realistic atmospheric model must be considered if useful quantitative results are to be obtained.

The dispersion relation (equation 14 of Hines, 1960) is presented in diagramatic form in Figure 2.2(a). This is a plot of curves of constant angular frequency, ω, in the two-dimensional k_x, k_z space (k_x and k_z being the components of the wave number vector in the horizontal and vertical directions respectively). These curves show only propagating waves for which k_x and k_z are real; evanescent waves with imaginary vertical wave-number can also exist. Two frequencies are important on this diagram:

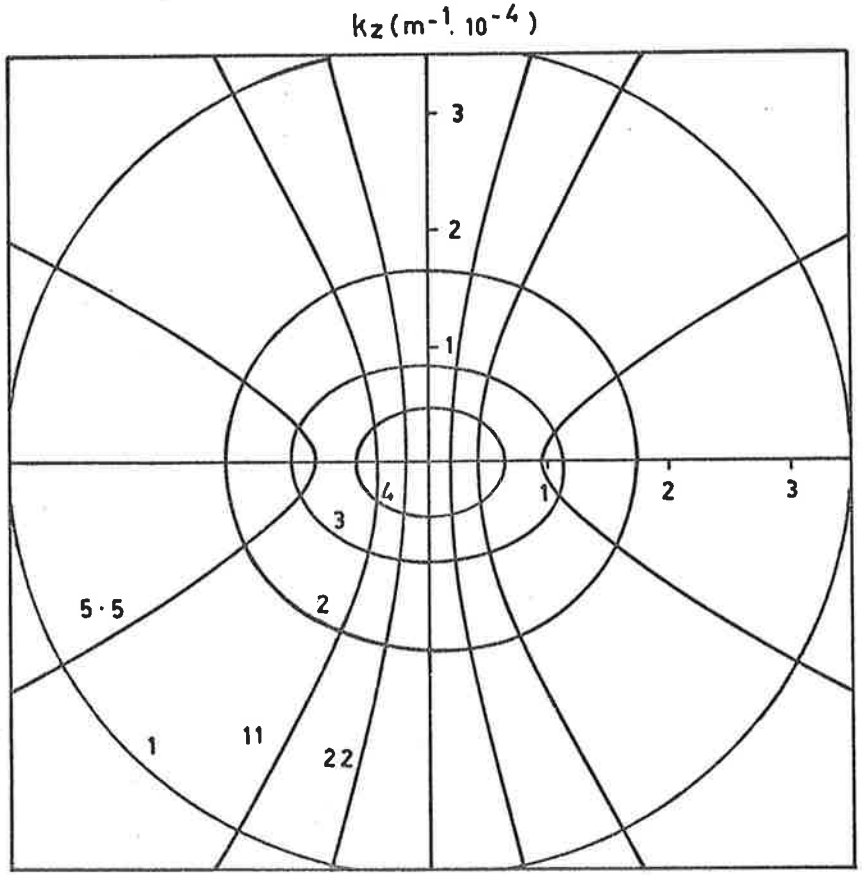

(a) CONTOURS OF CONSTANT PERIOD IN THE kx - kz SPACE. THE ACOUSTIC WAVE BRANCH IS REPRESENTED BY THE FAMILY OF ELLIPSES. PERIODS ARE SHOWN IN MINUTES.

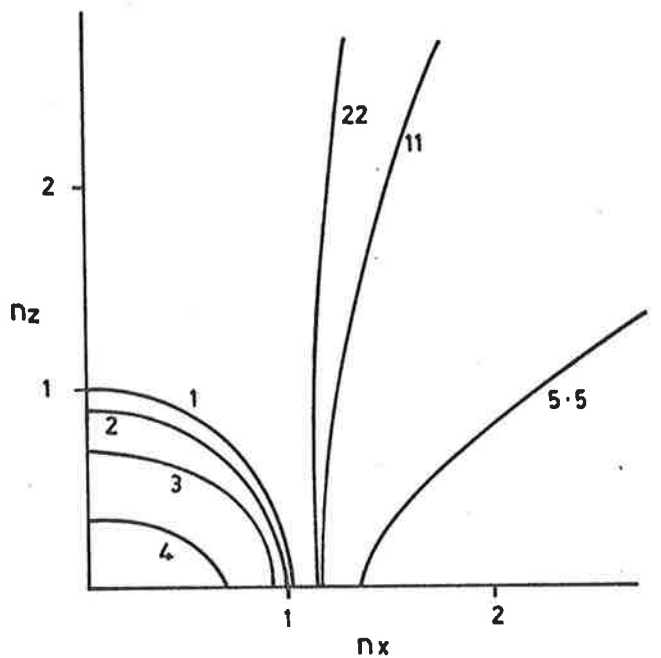

(b) CONTOURS OF CONSTANT PERIOD IN THE nx - nz SPACE. PERIODS ARE SHOWN IN MINUTES.

Figure 2.2: Two methods of representing the dispersion relationship for internal acoustic, gravity waves.

(i) $\omega = \omega_a = \frac{\gamma g}{4c}$

where γ = ratio of specific heats;

g = gravitational acceleration;

c = speed of sound,

this is the acoustic cut-off frequency and represents the lower frequency limit at which "sound" waves will propagate in the atmosphere.

(ii) $\omega = \omega_g = (\gamma - 1)^{\frac{1}{2}} \frac{g}{c}$,

this is the Brunt-Vaisälä frequency and is the natural frequency of oscillation of the atmosphere.

The high frequency ($\omega > \omega_a$) waves are termed acoustic waves since energy storage is predominantly due to the compressibility of the atmosphere. Waves with frequencies $\omega < \omega_g$ are termed internal gravity waves since energy storage is predominantly due to gravitational effects. The frequency region $\omega_g < \omega < \omega_a$ is prohibited if only propagating waves are to be considered. Table 2.3 gives values of the acoustic cut-off period and Brunt-Vaisälä period for various heights in the atmosphere. The two series of waves are distinguished clearly in Figure 2.2(a), the family of ellipses in this diagram represents the sequence of acoustic waves, while the superimposed family of hyperbolae represents internal gravity waves.

If the coordinates in Figure 2.2(a) are normalised to $n_x = k_x c/\omega$ and $n_z = k_z c/\omega$ where c is the phase velocity of the wave, then Figure 2.2(b) results (only one quadrant of the plot in n_x, n_z space is shown).

HT (km)	T_a (seconds) Acoustic cut-off	T_b (seconds) Brunt-Vaissälä
60	310	340
70	300	330
80	280	310
90	250	280
100	250	280
110	280	300
120	350	400

TABLE 2.3 VARIATION OF BRUNT-VAISSALA PERIOD (T_b) AND T_a (ACOUSTIC CUT-OFF PERIOD) WITH ALTITUDE IN MESOSPHERE AND LOWER THERMOSPHERE

These curves can be considered as propagation surfaces and have been discussed by Hines (1960), Eckart (1960) and Tolstoy (1963). The circle ($n^2 = 1$) represents waves which propagate with the speed of sound while acoustic waves ($n = (n_x^2 + n_y^2)^{\frac{1}{2}} < 1$) have phase speeds faster than the speed of sound and internal gravity waves travel slower.

A number of interesting facts emerge from consideration of these curves. A particular combination of k_x and k_z (or n_x and n_z) implies a particular direction of phase propagation. If waves with frequencies much less than the Brunt-Väisälä frequency are considered then it is apparent that the ratio $\frac{k_x}{k_z} = \frac{n_x}{n_z}$ is nearly constant over most of the hyperbolae. Thus waves with these frequencies can only propagate in certain directions. In particular, for internal gravity waves of low frequency, the wave fronts are slightly tilted from the horizontal moving upward or downward. Furthermore the particle motion associated with such a wave is nearly a straight line oscillation normal to the wave front. It is well known that the direction of energy propagation for a wave packet is the same as that of the group velocity. Thus the direction of energy propagation for internal acoustic-gravity waves can readily be found from the direction of the normals to the propagation surfaces shown in Figure 2.2(b). It is apparent that downward phase progression for an internal gravity wave can be accompanied by upward energy propagation.

Another interesting characteristic of internal gravity waves is the fact that the amplitude of these waves increases with altitude inversely as the square root of the density. This increase compensates for

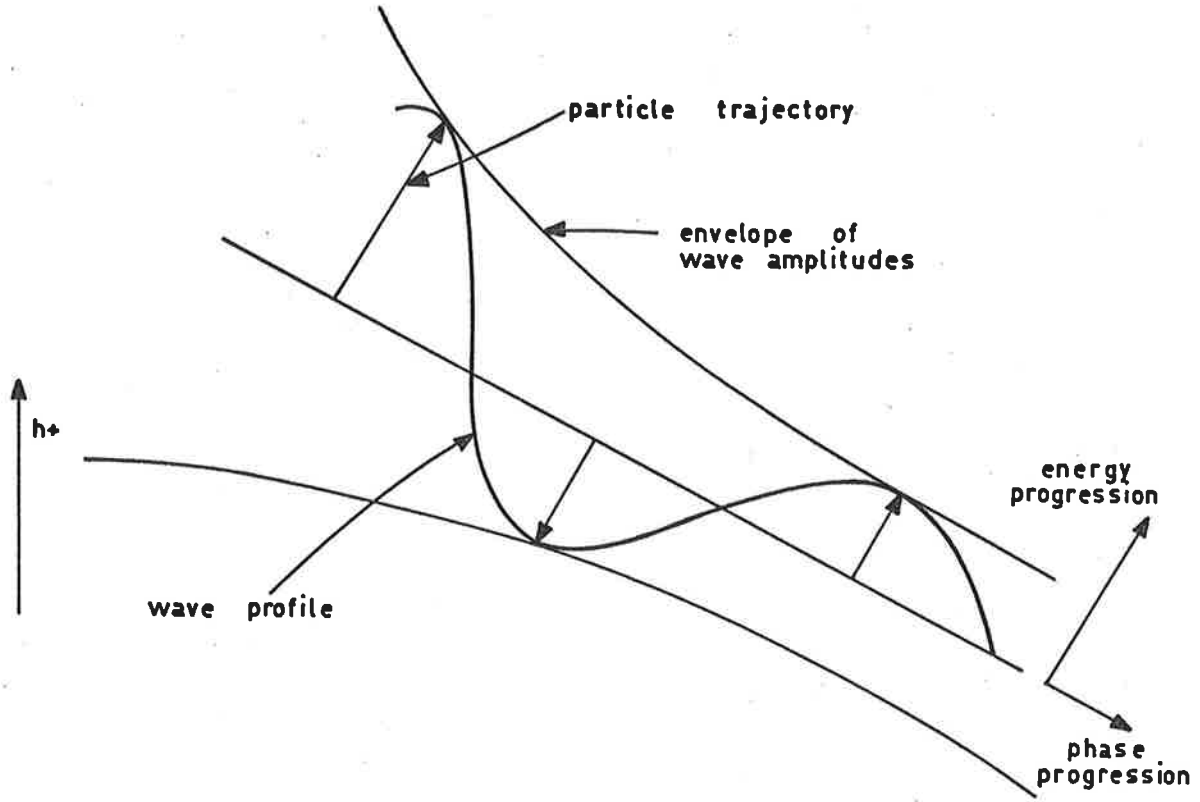

FIG. 2·3 PICTORIAL REPRESENTATION OF AN INTERNAL GRAVITY WAVE.

the upward decrease of atmospheric density and hence maintains a constant energy flux upward. Disturbances that are quite small in the troposphere may be quite significant in the mesosphere (providing they can propagate that far); a wave with an amplitude of 3 cm/sec near the ground would have an amplitude of 3 m/sec at 68 km and 30 m/sec at 95 km.

A pictorial representation of an internal gravity wave indicating the main features discussed above is shown in Figure 2.3. Many of the features of internal gravity waves have been demonstrated experimentally by Mowbray and Rarity (1967).

2.3.2 Ducting of Internal Gravity Waves

When more realistic model atmospheres are used with the equations of motion then new phenomena appear with the introduction of a variable temperature and wind profiles. These phenomena include ducting or trapping of waves and reflection of waves at so called 'critical levels'.

The principles involved in the ducting of these waves can be discussed using a simple three layer model consisting of the ground (the lower boundary), an isothermal layer (in which the allowed wave modes are transmitted vertically) and an upper layer at a different temperature from which reflection can occur. Certain combinations of horizontal wavelength and frequency can undergo repeated reflections between the upper layer and the ground and hence can be trapped in this duct. The process is analogous to the behaviour of light which undergoes repeated total internal reflection in "light pipe" fibres.

Pfeffer and Zarichny (1962) and (1963), Press and Harkrider (1962) have used multilayer approximations to the atmosphere and have computed the expected behaviour of the various modes allowed. Pierce (1966) has shown that this multilayer approximation is valid provided that the step size used is sufficiently small. Weston (1962) has used the alternative procedure of using layers of continually varying but analytic temperature profiles.

In some cases the reflecting layer may be of limited thickness and weakly reflecting allowing some energy flux through this region and into upper layers. In such cases the duct can be considered "leaky" since a wave can propagate along the duct but with gradually decreasing amplitude. Freidman (1966) has shown that the thermal incline in the thermosphere is important in establishing a duct and that in fact waves can propagate for many hundreds of kilometres without suffering severe attenuation.

The background wind structure of the atmosphere can also be important in ducting of gravity waves primarily for waves with slower phase velocities. The mean wind is most easily included in the basic equations of motion by translating the coordinate system into a frame of reference moving with the mean wind. The intrinsic frequency of the wave in this moving frame of reference then becomes the important frequency parameter. There is the possibility that ducting may occur due to a layer of low intrinsic frequency being sandwiched between layers of high intrinsic frequency. The parameter which is important in determining whether the wave is reflected is the ratio of intrinsic frequency to the Brunt-Vaisälä frequency (Bretherton, 1966).

2.3.3 Critical Layers

Another interesting phenomenon of internal gravity waves occurs at a level (a 'critical' level) where the intrinsic frequency is zero. The singularity of the mathematical equations at such a level gives rise to some complexity. An argument based on the concept of a wave group leads to the realisation that the waves do not penetrate such a level. The vertical component of the group velocity in the vicinity of the critical level is proportional to the square of the vertical distance from it. Thus an upward propagating group would take an infinite time to reach it so that nothing can be transmitted (Bretherton, 1966). This is analogous to the behaviour of quantum-mechanical waves in the presence of infinite potential barriers; no "tunneling" is possible regardless of the thinness of the barrier.

Booker and Bretherton (1967) have concluded from a more rigorous study of critical levels that transmission will be finite but negligibly small in most cases of interest. If the atmosphere near the critical level supports dissipation by viscous or thermal effects then the absorption of energy may be intense. Such a limited height region is a possible area in which extensive turbulence might be expected.

Hines and Reddy (1967) have considered various atmospheric models in discussing the general problem of internal gravity waves propagating through regions of variable wind and temperature. They conclude that in general the waves with small horizontal phase velocity are most affected. Wind induced reflections impose a directional filter on the

gravity-wave spectrum. Waves propagating in the direction of the background wind may be strongly reflected whereas there may only be weak reflections in other directions. Houghton and Jones (1969) have designed more sophisticated models in an attempt to describe the time-dependent properties of internal gravity waves.

2.3.4 Sources and Effects of Internal Gravity Waves

Unlike tidal oscillations the sources of internal gravity waves are uncertain. Because of the exponential growth factor it seems reasonable to expect generation at lower levels or at least in situ rather than to propose a source at a higher altitude. Possible mechanisms suggested include airflow over mountains, tropospheric fronts, extreme wind shears such as found in the jet stream (Hines, 1960), and turbulent mixing (Townsend, 1966). The efficiency of nuclear explosions as gravity wave generators has been discussed by Baker and Davis (1968), Row (1968) and Hines (1967). Row (1966) has also considered the possibility of earthquake generation of acoustic-gravity waves. Lindzen (1968) has suggested that non-linearities in the atmospheric tides might generate higher harmonics which would behave in the same manner as internal gravity waves.

Whether or not a gravity wave can propagate from lower levels into the thermosphere is still an open question. As discussed earlier the underlying temperature and wind structure may cause reflection at a lower level. The energy of the wave may also be dissipated by the effects of eddy viscosity and of thermal conductivity since these become gradually more important as the wave propagates upward. The heating effect produced

by these dissipative effects in the thermosphere may be quite important in the general dynamics of the region (Hines, 1965).

Hodges (1967) has suggested that the lapse rate associated with internal gravity waves may become super-adiabatic somewhere in the lower thermosphere. This would be a possible source of turbulence in a region where normally stable conditions might be expected. The observed eddy diffusion coefficients (Colegrove et al., 1966) can be explained using only this mechanism for the production of turbulence (Hodges, 1969).

2.4 APPLICATION OF THEORIES TO THE MESOSPHERE AND THERMOSPHERE

As yet insufficient temporal and spatial resolution in the wind field has been achieved to enable unambiguous identification of turbulence or gravity wave phenomena. The following chapter (Chapter III) outlines some of the observations that have been made. The general problem is one of measuring energy spectra and then deciding whether the spectra can be described in terms of turbulence or gravity waves or possibly both.

Lindzen (1969) has discussed some of the requirements for the detection and delineation of gravity waves. In particular Lindzen states that: "one will need data with time resolution of the order of 20 min ..... vertical resolution of the order of 1 km and horizontal resolution of the order of 10 - 100 km". No observing system currently being used can meet both of these requirements but a combination of a meteor-radar system (time resolution of the order of 15 mins, spatial resolution of the order of 2 km) with a contaminant release system (spatial resolution of the order of 50 m, time resolution limited by cost of rocket firing) may prove extremely useful.

Some of the characteristic properties of a turbulent regime have been outlined in §2.2. The main properties include a cascade of energy through eddies of diminishing size and transport of mass, momentum and heat. The properties of internal gravity waves discussed in §2.3 indicate that, in principle, it should be possible to distinguish between motion due to these waves and motion due to turbulence. However as the lower thermosphere is generally stably stratified there is the possibility of having the two types of motion intermingled in this region. Some of the difficulties associated with the interpretation of the results to be discussed in Chapter III are due to the inability to distinguish between these two types of motion when the scales involved are of the same order.

A common difficulty in even a preliminary interpretation of the observations is the lack of sufficient temporal and spatial resolution. With the observational techniques currently available a promising method of investigation might be an interplay between theory and observation (Lindzen, 1969). Knowing something of the mean wind and temperature structu of the atmosphere it might be possible to predict the nature of the wind (amplitude and vertical structure) at a given time and height resulting from say the transmission of an internal gravity wave. A single observation would then suffice to decide the applicability of a particular theory.

CHAPTER III

OBSERVATIONS OF IRREGULAR, SMALL SCALE WIND VARIATIONS IN THE MESOSPHERE AND LOWER THERMOSPHERE

3.1 THE GENERAL WIND FIELD AND OBSERVATIONAL TECHNIQUES

Various experimental techniques for determining the wind field in the region 70 to 140 km have been outlined in Chapter 1. The important techniques for the determination of small scale structure in the wind field include photographic observation of contaminant release trails and radio-meteor studies. Further details of these latter techniques are given in following sections.

The wind field determined either by the radio-meteor or contaminant release technique can often be described in terms of a superposition of a number of different simple wind patterns. For continuous observations (for example by the radio-meteor technique) Fourier analysis is frequently used to separate the data into various time scales (Elford, 1959; Greenhow and Neufeld, 1961; Spizzichino, 1968; Doyle, 1968). Observations made with poor time resolution but good height resolution (for example contaminant releases) are usually discussed in terms of the vertical wavelength of the phenomena (Kochanski, 1964; Rosenberg, 1968; Woodrum and Justus, 1968).

The usual classification scheme distinguishes the following components

(i) the prevailing wind, which is normally presented as the constant component of the wind but can also include variations with quasi-periods of many days (Doyle, 1968).

(ii) Gravitational and thermal tides, principally solar in origin and with periods of 24 hour, 12 hour, 8 hour etc.

(iii) Small-scale variations, which produce a continuous spectrum of periods varying from a few minutes to a few hours. These have been variously attributed to turbulence and internal gravity waves.

Observations made with a radio-meteor system are restricted in that only the line-of-sight component of the drift of a meteor trail can be measured directly. Horizontal wind velocity components can only be obtained by combining several line-of-sight observations. The largest spatial scales that can be determined are limited either by the beam width of the aerial system used (for single station measurements) or by station geometry (if multi-station measurements are made). The largest time scales are virtually unlimited, since continuous operation is possible. The minimum time scale is determined by the time required to obtain a meaningful average and this in turn depends on the echo rate (see later §3.2.2). The smallest distance over which wind measurements can be made is determined by the size of the reflecting region (about 700 m, see Chapter 4)*.

As discussed in Chapter 1 photographic tracking of contaminant release trails yields atmospheric wind profiles with good height resolution. If the time dependent motion of individual features on a trail is also

---

* But see also the discussion in §6.4

followed then the horizontal and vertical components of the fluctuating wind can be determined (Justus, 1966). The maximum temporal and spatial scales are determined by the duration (10 to 15 minutes) and physical dimensions of the contaminant cloud (typically 10 km). The minimum scales are determined by the time interval between successive photographs and the resolving power of the optical systems used.

Measurements of the growth rate of contaminant release trails can also yield useful information about small-scale structure of the atmosphere (Blamont and de Jager, 1961; Blamont, 1963; Justus, 1967a; Rees et al., 1970). Similarly the rate of diffusion of photographic meteor trails can also be used to infer parameters of the small-scale structure (Millman, 1959).

With the experimental techniques currently available the determination of small-scale structure in the mesosphere and lower thermosphere has been limited to observations of the irregular component of the wind field and the diffusion rate of contaminant release trails. Other meteorological parameters such as temperature are not yet available with sufficient resolution. The observations presently available are discussed in the following sections. Interpretation of these observations will be attempted in the final section, in which a possible model for the small scales will be introduced.

3.2 RADIO-METEOR MEASUREMENTS

3.2.1 Measurements of Wind Shear

When radio reflections from meteor trails were first detected it was found that the echoes from long enduring trails exhibited large amplitude fluctuations. Greenhow (1952b) and Manning (1959), amongst others, have satisfactorily explained this fading in terms of interference between waves reflected from two or more reflection points. These extra reflection points occur on a meteor trail due to the distorting effects of a wind shear. By comparing the observed fading rates with those expected from various model wind profiles some information on the nature of the wind shear can be found. Revah et al., (1963) and Phillips (1969) have proposed various models which show reasonable agreement with experimental observations. In particular Revah and Spizzichino (1964), using a forward scatter link, have deduced seasonal and height variations in the frequency of occurrence of wind shears (maximum in winter and near 100 km). Since the actual values of wind shear determined from this method depend on the particular model chosen, quantitative measurements may be unreliable.

The wind shear can be determined more directly by measuring the rate of change in the Doppler frequency as the reflection point moves along the meteor trail (see §4.3.2 for details of the reflection process). This technique is most useful for small displacements along the trail (less than 1 km). Müller (1968), using the Sheffield radio-meteor system, has determined root mean square radial velocity differences for specific

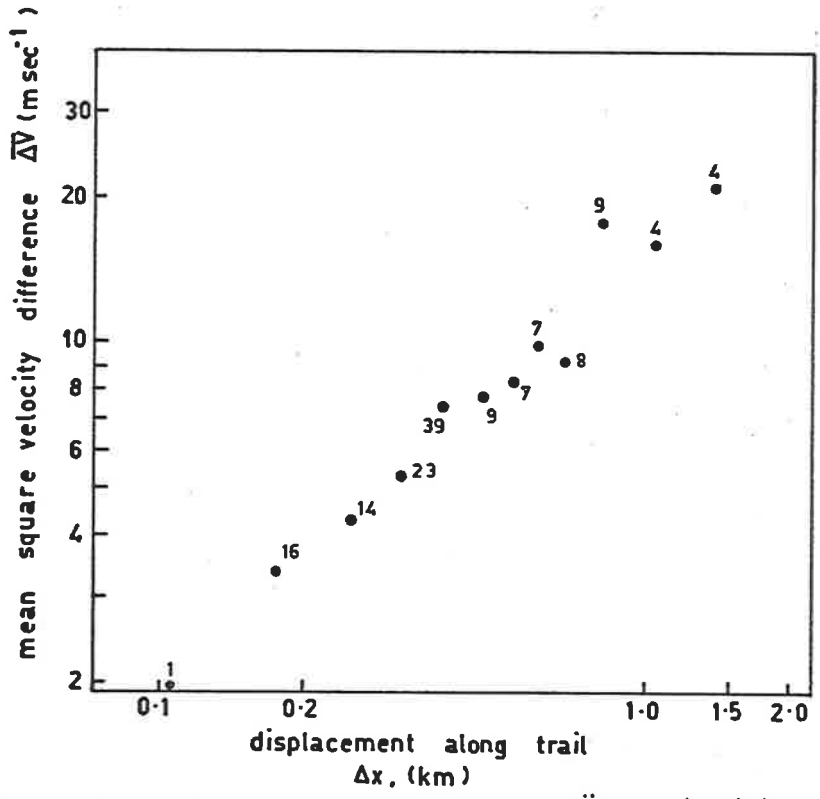

Figure 3.1: Wind shear measured by Müller (1968).

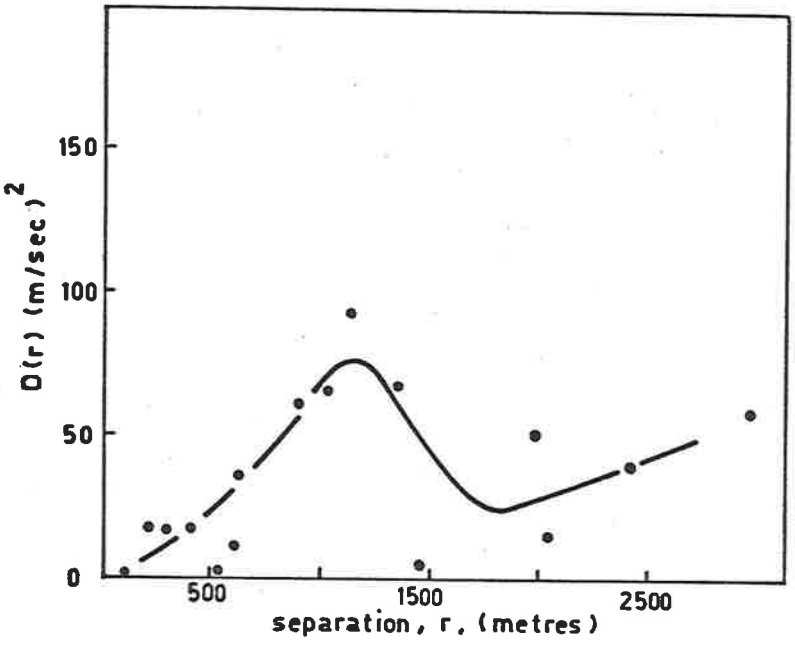

Figure 3.8: Structure function obtained with high resolution photographs of a sodium cloud, December 1961. (After Blamont, 1963.)

values of reflection point separation. Figure 3.1 shows the result of such an analysis over a period of 4.5 hours. The wind shear is slightly non-linear since the slope of the best fit straight line is 0.9. Müller has further argued that the Doppler frequency will decrease with time if the meteor trail is moved by a wind with non-linear shear. However even with a linear wind profile the Doppler frequency can increase or decrease with time depending on whether the trail is moving towards or away from the receiving station (Roper, 1966). Thus some of the results presented by Müller must be viewed with caution.

Multi-station observations, which enable simultaneous measurements of line-of-sight wind velocities at two or more points along a meteor trail, have been made by Greenhow and Neufeld (1959b) and Roper (1966). As the orientation of the trail can be found from the time of commencement of the echoes at each reflection point (see §6.2 for details), both horizontal and vertical wind shears can be measured. Data is generally presented in the form of correlation functions or structure functions (as defined in §2.2).

Greenhow and Neufeld used two additional receiving stations with the Jodrell Bank radio-meteor system and were able to measure the line-of-sight component of the wind at three points on a meteor trail. Figure 3.2 shows the correlation functions obtained for separations measured both along the trail and in height. The behaviour of the spatial separation curve in Figure 3.2(a) can be explained if the fall off in correlation with horizontal separation is less rapid than with vertical

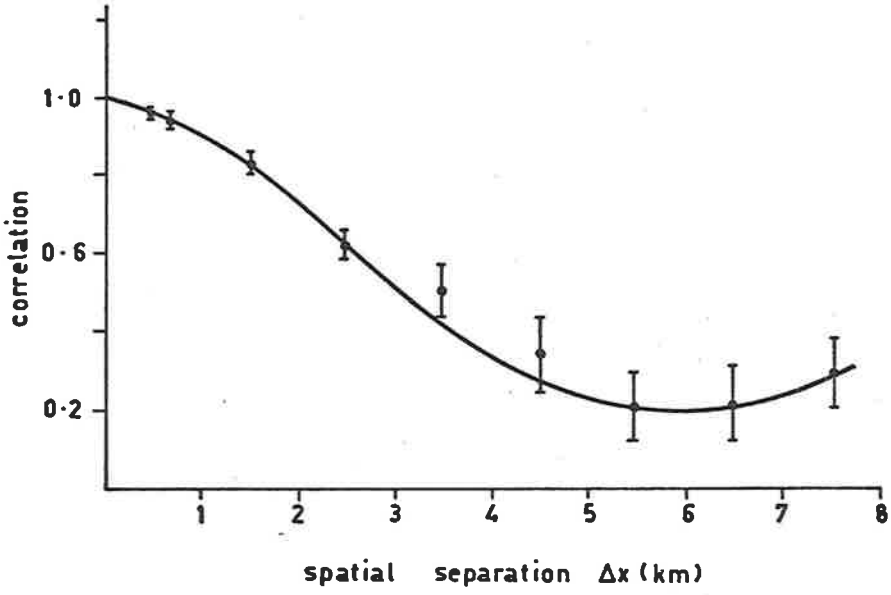

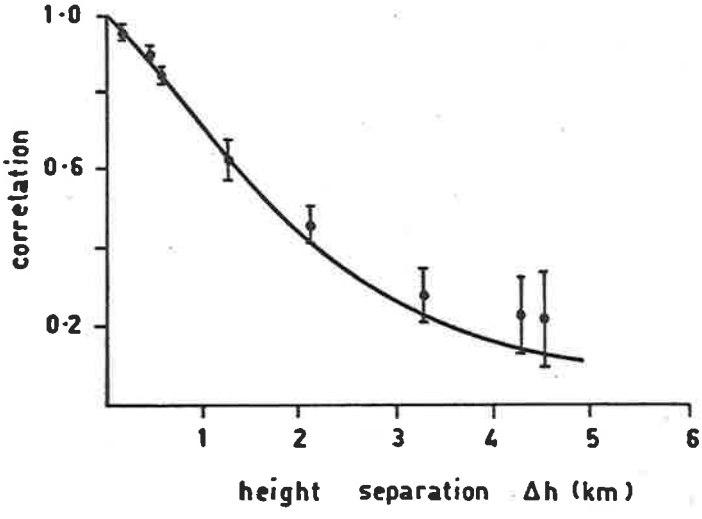

Figure 3.2: Variation of correlation coefficient with
(a) spatial separation
(b) height separation
of reflection points. (After Greenhow and Neufeld, 1959.)

separation. Greenhow and Neufeld deduced that the irregularities being measured had a vertical extent of 6 km and a horizontal extent of the order of 100 - 200 km.

In an earlier survey with the Adelaide radio-meteor system, Roper (1962) obtained measurements of the wind at three reflection points along a trail up to a maximum separation of 3.5 km. Figure 3.3 and Figure 3.4 show structure functions for height differences and for distances measured along the trail for 169 meteors recorded in May 1961. The two best fit straight lines to this data have different slopes indicating a possible anisotropy. There is no significant departure from a linear trend in these log-log plots up to the limit of measurement and hence it is interesting to extrapolate the best fit straight lines to the observed mean square velocity fluctuation for all the data. This procedure gives 8 km as an estimate of the vertical scale of the irregularities and 150 km for the horizontal scale. An extreme extrapolation such as this must obviously be viewed with caution but it is interesting to note that the values so obtained are not in disagreement with other independent observations (Greenhow and Neufeld, 1960; Justus and Roper, 1968).

3.2.2 Gross Random Fluctuations

One quite simple observation that can be made with a single station radio-meteor system is to investigate fluctuations in the wind over relatively small time intervals (5 - 10 mins) and in a relatively small volume. Greenhow and Neufeld (1960) and Zadorina et al., (1967) have subtracted the prevailing and 24 and 12 hour periodic components from

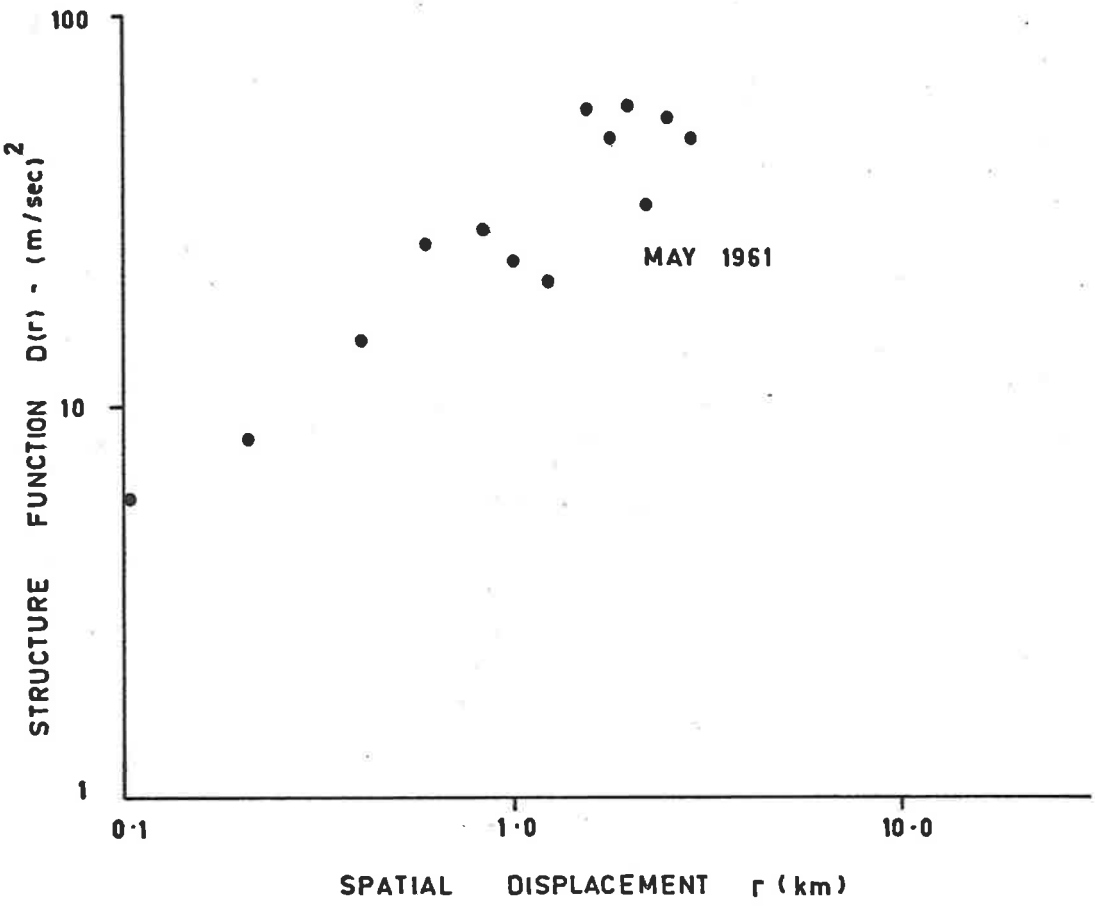

Figure 3.3: Variation of structure function with reflection point separation for May 1961 at Adelaide - 169 meteors.

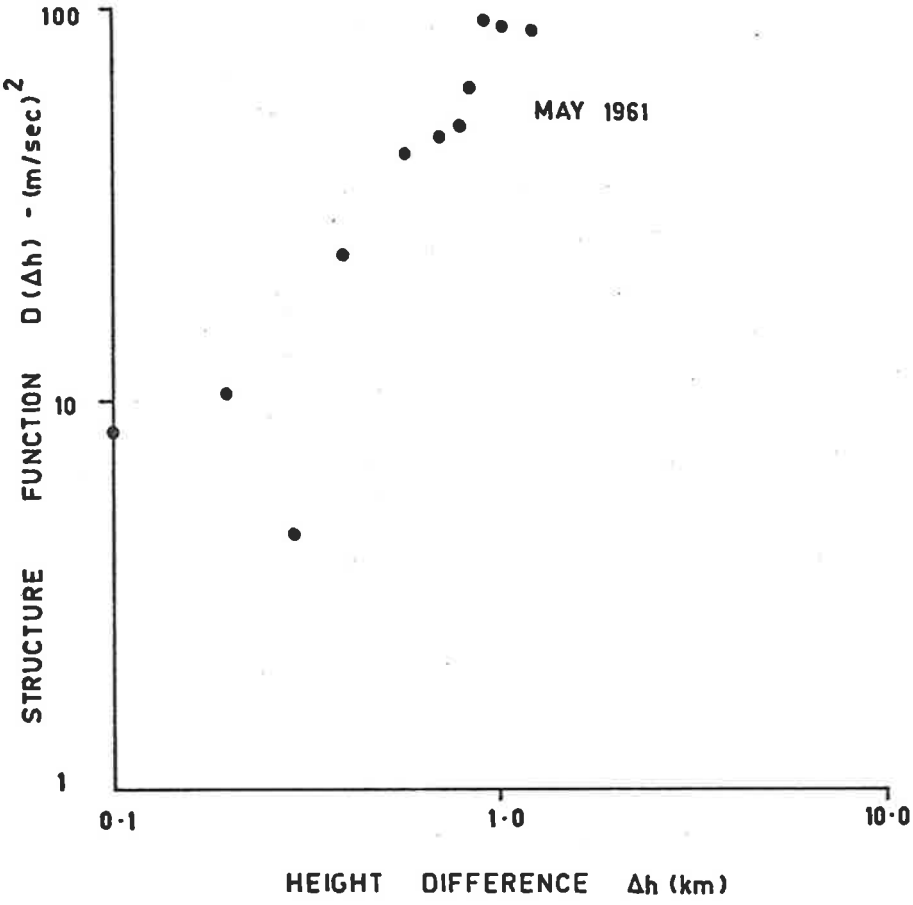

Figure 3.4: Variation of structure function with height separation for May 1961 at Adelaide.

the wind measured at times of high meteor rate. Statistically reliable estimates of the time constants of the residual wind were obtained by averaging the results over several recording intervals of 48 hours duration. The time constants found are about 100 min with a r.m.s. velocity fluctuation of about 25 m/sec so that scales of 100 km - 200 km can be deduced. It is useful to plot the auto-correlation functions (g) in the form 1 - g as suggested by Elford and Roper (1967), Figure 3.5 shows the results of Greenhow and Neufeld, and Zadorina et al., plotted in this form. The two sets of results are in extremely good agreement which itself is surprising for a geophysical measurement. The volume of space over which the wind measurements were made was determined by the beam-width of the aerial and was similar for both observers (50 km to 150 km along the horizontal and 20 km vertically).

Zadorina et al., performed a further experiment to measure the wind in a much smaller volume (4 km in height and 12 km along the horizontal) by selecting a time when the echo plane of the Ursid shower was perpendicular to the direction of the prevailing wind. The results of this further experiment are also shown on Figure 3.5, the time constant deduced from this curve is 15 min with a corresponding horizontal scale of 20 km. At the same time data obtained using the full aerial beam-width gave a time constant near the 100 min value found previously. These results can be understood if a whole range of scales is assumed to exist at this height. Then those scales of the order of the dimensions of the sampling volume will determine the shape of the auto-correlation function.

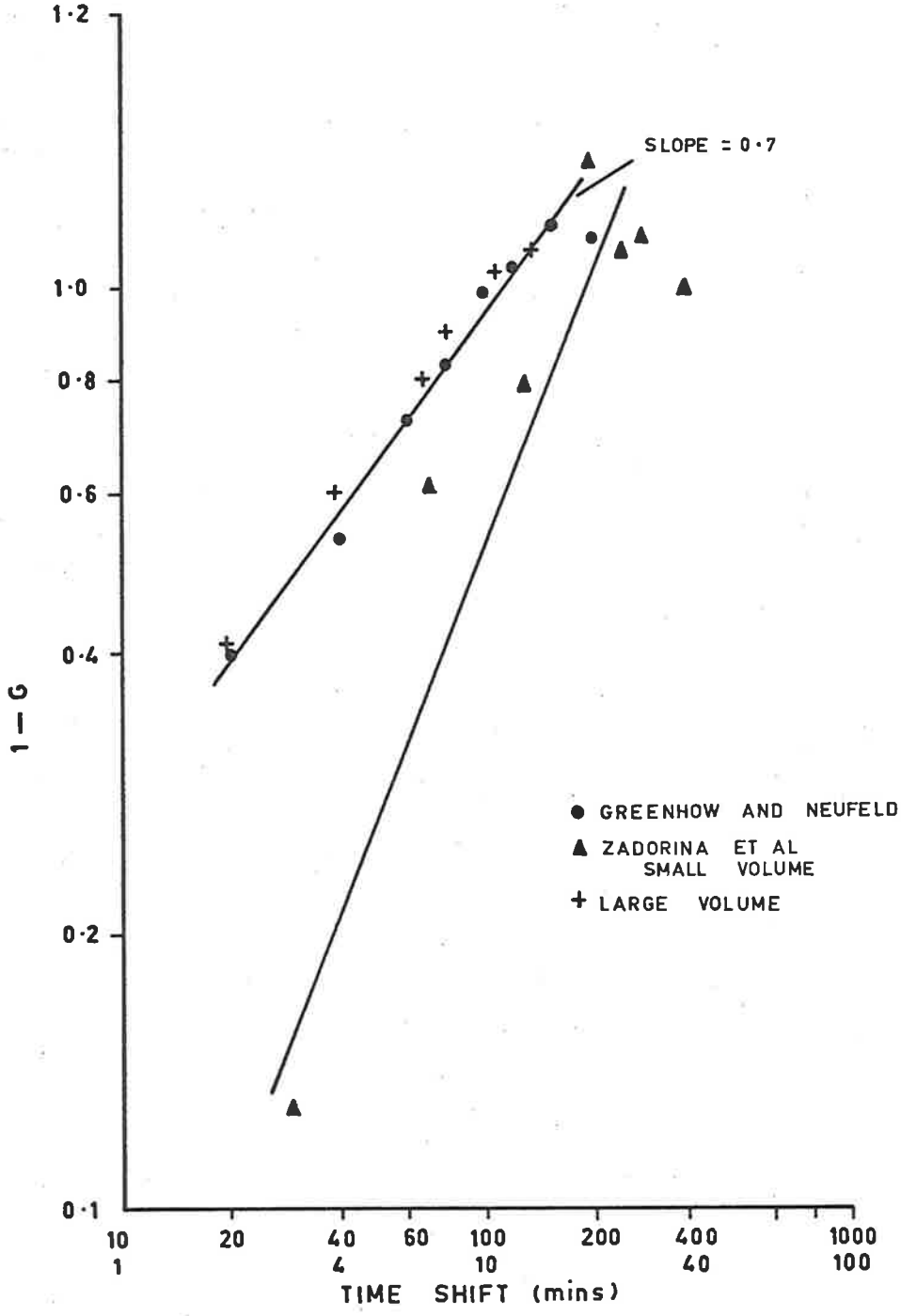

Figure 3.5: The autocorrelation functions of Greenhow and Neufeld (1960), and Zadorina et al. (1967) replotted to show power law behaviour. The lower time shift scale refers to the small volume data of Zadorina et al..

It is apparent that some of the conclusions drawn from this type of observation must be viewed with caution.

Revah (1969), using the radio-meteor system at Garchy has been able to determine the zonal wind component with an average height resolution of ± 2 km and an average temporal resolution of 10 mins, provided that the meteor rate is sufficient.* When these results are presented in the form of contour diagrams as in Figure 3.6 there is strong evidence of a dominant semi-diurnal tide with downward phase progression. During the time interval encompassed by Figure 3.6 the meteor rate varied from 75 meteors/hour to 18 meteors/hour so that the apparent variation in small scale structure in the diagram is most probably due to this variation in rate.

The average auto-correlation function found by Revah for a mean height of 103 km for December 1965 is shown in Figure 3.7. The importance of the semi-diurnal tide is obvious from inspection of Figure 3.7(a). If the semi-diurnal component is removed from the data and the auto-correlation function recomputed then the results shown in Figure 3.7(b) are obtained. This latter diagram indicates the presence of a periodic component with a vertical wavelength of 23 km, a period of 2 hours and a downward phase progression of 10 km/hour. This component is similar to that found by Greenhow and Neufeld (1959b) and Roper (1966).

---

*At least two meteors at each height within a 10 min. time interval.

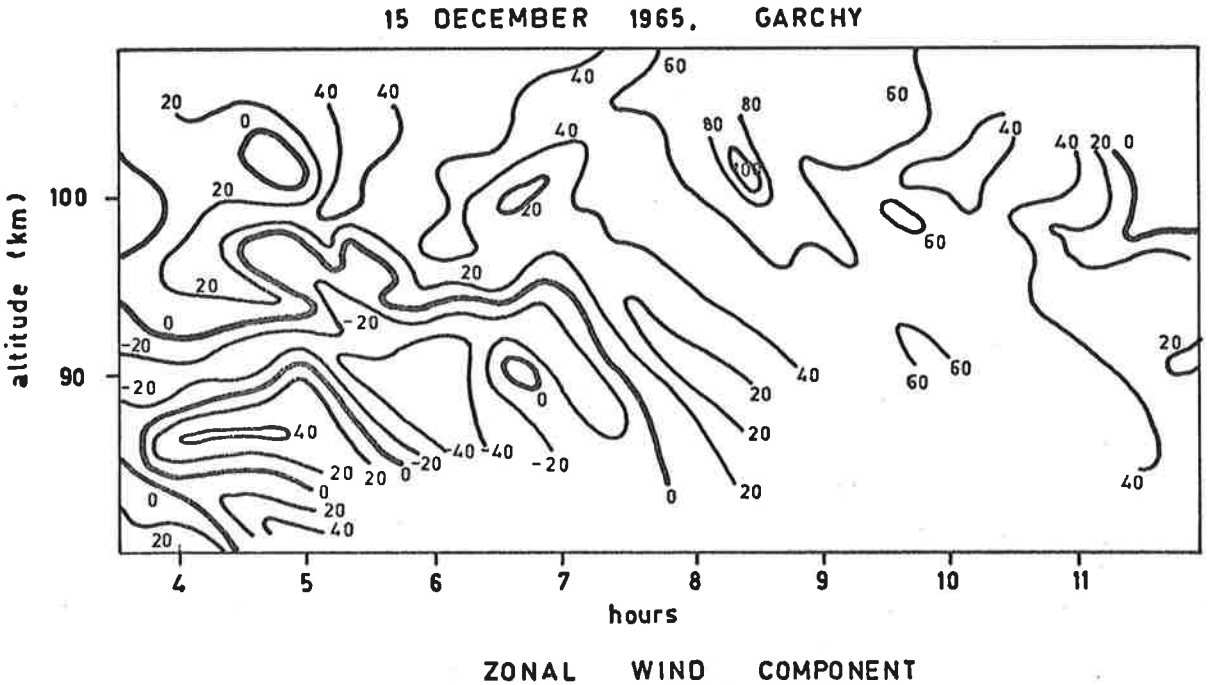

Figure 3.6: Zonal wind component found at Garchy, 15th December 1965. The basic data has been interpolated to ensure data points at intervals of 1 km in height and 10 mins in time. (After Revah, 1969.)

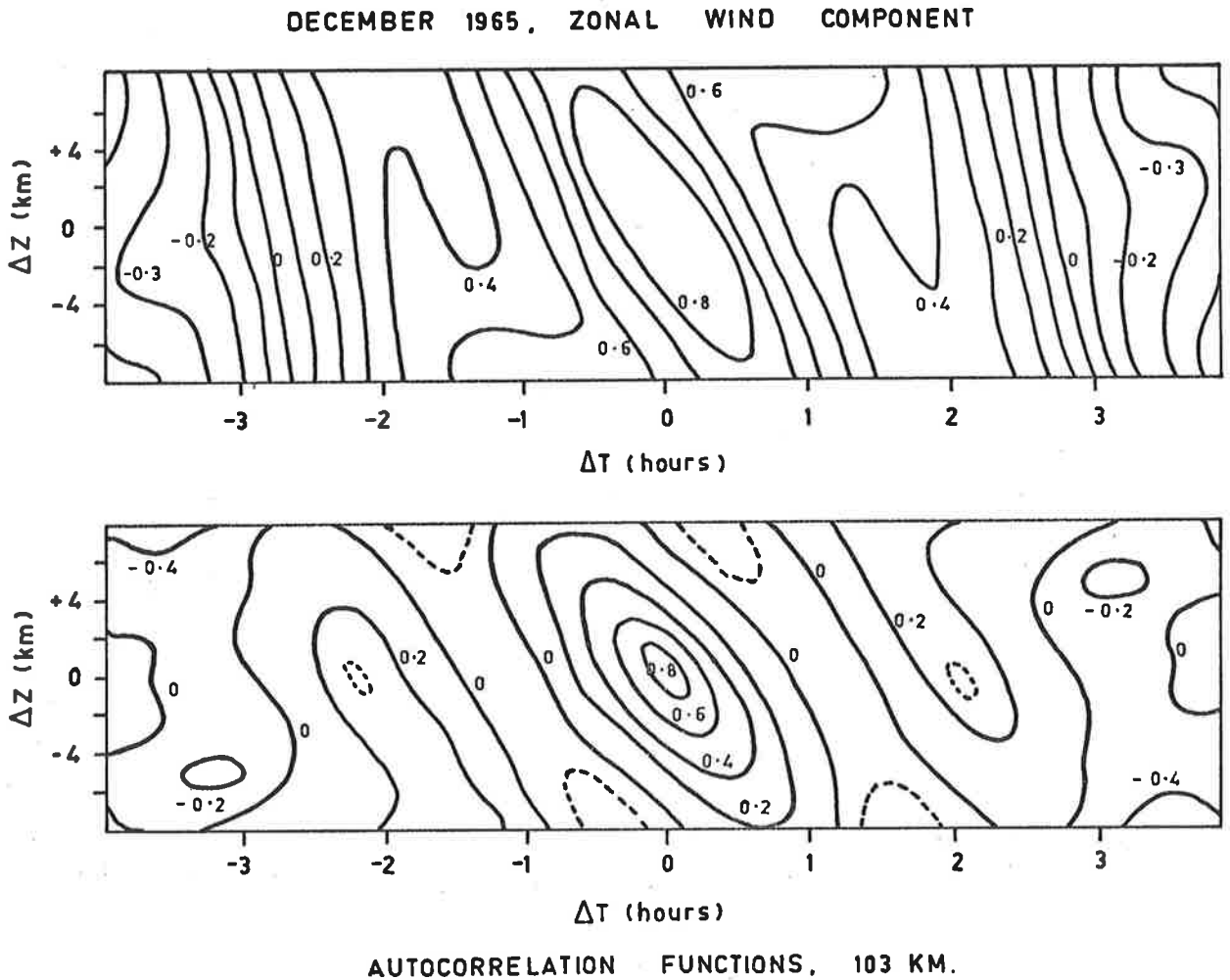

Figure 3.7: Autocorrelation functions, at a mean altitude of 103 km, for the zonal wind component at Garchy for December 1965. The upper diagram includes all data and is dominated by the semi-diurnal tide. The lower diagram illustrates the effect of suppressing the semi-diurnal tide. (After Revah, 1969.)

As a result of a power spectrum analysis of the Garchy data Revah (1969) finds evidence for other periodic components which he attributes to internal gravity waves propagating through the region. However the components found all have frequencies close to harmonics of the diurnal tide, vertical wavelengths of 4 to 15 km and remain phase coherent for about two days.* These facts suggest that the waves found are probably generated in situ due to non-linear effects in the diurnal tide (Lindzen, 1968). Spizzichino (1969) has suggested an alternative explanation in terms of interaction between the diurnal tide and internal gravity waves.

3.3 OBSERVATIONS OF CONTAMINANT RELEASE TRAILS

At least two simultaneous photographs from separate sites with accurately known positions are required to locate the positions of a contaminant release feature in space. Typical exposure times used are one to ten seconds. Absolute accuracies of 0.1 to 0.3 km at 100 km are claimed, while relative measurements involving the separation of two points in a trail may be made with higher precision. The largest source of error in position is usually due to a fluctuating background intensity which makes the dimensions of the cloud uncertain.

---

*The data was collected and analysed in groups of two or three days.

3.3.1 Structure Inferred from Wind Measurements

The most obvious features in a photograph of a contaminant release trail are a very irregular or rough appearance below about 110 km and a relatively smooth trail at higher altitudes. The wind profiles obtained by photographic tracking of a release show irregular variations below 110 km with a dominating maximum wind speed between 100 km and 120 km. The discussion in this section is centred around the variations in the motion of the cloud, the following section is mainly concerned with the development and growth of the could itself.

The resolution in most photographs of contaminant release trails is such that the smallest identifiable feature on the trail has a scale of the order of 500 metres. The wind profiles obtained with this low resolution photography are usually considered to be due to the superposition of three types of motion; a prevailing wind, tidal wind components and a residual component which includes internal gravity waves and turbulence. Because of the limited time resolution available due to the relatively short duration of the trail (10 - 20 mins) these three components cannot usually be separated. However by averaging a large number of such wind profiles, a number of authors have investigated the statistical properties of these three components [Kochanski (1964), general; Rosenberg and Justus (1966), tides; Rosenberg (1968a), prevailing and tides; Rosenberg (1968b), residual; Woodrum and Justus (1968a), tides; Woodrum and Justus (1968b), residual]. In general these studies show that the average value of the dominant vertical wavelength is 20 km. The

profiles also describe a circular helix progressing clockwise with increasing height (for the Northern hemisphere). These facts are consistent with the diurnal (1,1) mode of the thermal atmospheric tide (Lindzen, 1967). The r.m.s. irregular wind found is about 50 m/sec with the r.m.s. wind shear in the range 0.001 - 0.02 sec^{-1} with maxima between 100 and 110 km.

A few workers have carried out high resolution (scales $\geq$ 6 metres) studies of trails and have shown that considerable detailed information can be obtained on the nature of the irregular component in the wind profiles. Blamont (1963) has computed structure functions for the winds measured over very small height ranges; Figure 3.8 shows the structure function computed for a sodium cloud at 95 km. A maximum appears for a separation around 1 km. In contrast the structure functions computed from low resolution studies are unable to distinguish any features at separations of the order of 1 km and generally have maxima at vertical separation of 6 to 8 km. Blamont has suggested that the motion in the small scale region (of the order of 1 km) is due to isotropic turbulence with the larger scale (of the order of 10 km) wind shears being a possible energy source.

Further high resolution studies by Blamont and Barat (1967), a (1968) indicate that at the transition region between the rough and smooth portion of the trail near 110 km a change in the character of the wind profile also occurs. These authors conclude that the rough nature of the trail is due to turbulent phenomena. Even in the region below 110 km

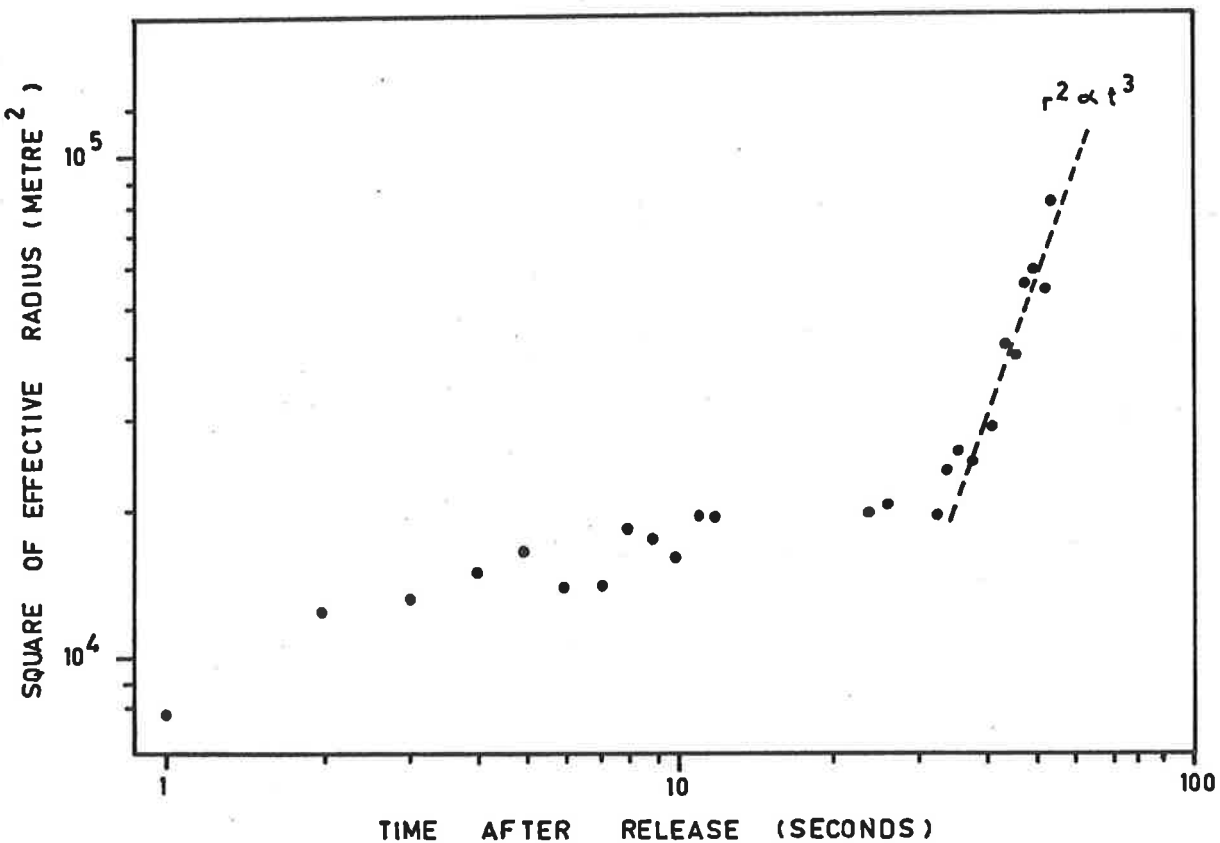

FIG. 3·9 VARIATION OF RADIUS WITH TIME AFTER RELEASE FOR TMA TRAIL AT 105 KM, MAY 1968.

individual trails sometimes show an abrupt transition from smooth to irregular (turbulent) flow at several heights (Blamont and Barat, 1967; Rees, 1968).

Another method of studying the small scale structure in a contaminant release cloud has been developed by Justus (1966). By tracking individual features within a cloud or trail he has determined irregular winds with a resolution of the order of 400 metres.* These irregular winds can be attributed to turbulence because the structure functions computed from them have the form expected from turbulence theory (see §2.2.3).

3.3.2 Diffusion Measurements

In principle the measurement of the growth rate of a contaminant release cloud or trail is simple and should lead directly to a measure of the parameters which describe the diffusive process. However in practice a variable background illumination, particularly for experiments performed at twilight, means that considerable care in measurement is required if a reliable estimate of the size of a globule or diameter of a trail is to be made. Further if the cloud is optically thick, particular care must be taken in deciding the position of the edges.

One method of approaching this difficulty is to make careful densitometric measurements of the cloud. It is then possible to determine a parameter such as the Gaussian half-width (or the effective radius) of

---

*Features less than 200 metres in size could not be resolved.

the trail which can be used as a measure of the size of the cloud (Lloyd and Sheppard, 1966; Golomb and MacLeod, 1966). An example of the variation of the effective radius of a TMA trail with time after release is shown in Figure 3.9, these measurements were made from plates taken with a Baker-Nunn camera with exposures of 0.2 sec and a frame rate of 1 per second. Measurements of effective radius were only made up to a time of 55 seconds after release since the chaotic nature of the trail after this time made it impossible to determine a meaningful estimate of the effective radius (Rees et al., 1970). The anomalous high growth rate up to 8 seconds after release can be regarded as the release phase in which the behaviour is definitely non-ambient. The growth rate between 8 and 32 seconds after release could be due to molecular diffusion but the inaccuracies in the determination of the effective radius prevent a reliable estimate of diffusion coefficient being made. At 33 seconds the trail has begun to break up and growth proceeds as $r_e^2 \propto t^3$ until the maximum observing time of 55 seconds. This form of the growth curve is expected for diffusion in an inertial subrange of a turbulent field.

Other densitometric observations of the growth rate of trails at altitudes below 110 km and up to 100 seconds after release show that laws of turbulent diffusion are usually followed (Blamont and Barat, 1967 and 1968; Golomb and MacLeod, 1966; Rees et al., 1970). In addition, other observations of the growth rate of trails or globules based on the observable diameter of the trail (e.g. Justus, 1966) indicate that the laws of turbulent diffusion are still obeyed for times much greater than

100 seconds after release. However detailed interpretation of these latter results are still in doubt (Zimmerman, 1968). Recent measurements of the variation of interglobular distances with time (Justus, 1969) can also be interpreted in terms of turbulent diffusion with some degree of success.

Above about 120 km the observed growth rates can be satisfactorily explained using molecular diffusion. Although a trail usually appears smooth above 110 km the growth rates at all heights up to 120 km are generally greater than would be expected for molecular diffusion alone. Below 110 km the observed growth rates are almost invariably greater than would be expected for molecular diffusion alone and can more readily be explained using the laws of turbulent diffusion. (Manring et al., 1961; Zimmerman and Champion, 1963; Blamont and Barat, 1967; Rees, 1968).

In contrast to the discussion above and to the conclusions of other workers in the field, Manring and Bedinger (1968) and Layzer and Bedinger (1969) claim that the irregular appearance and rapid expansion of contaminant release trails is entirely due to the passage of the launch vehicle together with chemical heating of the release material by some unspecified exothermic reaction. This conclusion is based mainly on their observations of the difference in appearance between a trail formed by the residual chemicals on the down-leg of a rocket flight and that formed on the up-leg from the same rocket. However other experimenters using a number of different chemicals and release mechanisms, and with various photographic systems observing both up-trails and down-trails do not support these claims.

3.4 SUMMARY OF OBSERVATIONS AND A POSSIBLE MODEL OF IRREGULAR WINDS

As indicated in Chapter II vertical motion in the atmosphere can be affected by buoyancy forces. In the lower thermosphere where the mean temperature increases with height, the vertical motion of a parcel of air is inhibited and hence any irregular motion should have a limited vertical extent.

Structure functions computed for the height range 80 to 100 km from wind profiles determined by the contaminant release technique all show similar behaviour; for height differences between 1 and 5 km the structure functions have the form of a power law with an exponent of about 1.4. A maximum value for the structure function usually occurs near a vertical separation of 6 km. Because of the inhibiting effect of buoyancy forces at these altitudes it is unrealistic to propose that vertical structure with scales of this order (a few kilometres) is due to turbulence. Rather these scales are probably the source of energy for smaller scales. Care should be exercised in drawing any conclusions from the value of the exponent (1.4) in the power law for the structure function. It is interesting to note that a profile consisting of a single sinusoidal wave would give similar characteristics to the observed structure functions, in particular a power law variation with exponent 2 and a maximum determined by the vertical wavelength. The observations of Greenhow and Neufeld (1959b) and Roper (1966) of vertical structure using the radio-meteor technique are consistent with the conclusion that vertical scales of the order of the scale height are due to some form of "semi-organised" wind field such as internal gravity waves or a non-linear tidal regime.

Vertical scales less than one kilometre appear to be part of a different type of motion (Blamont, 1963 and Blamont and de Jager, 1961). It is feasible that buoyancy forces could cause stratification into layers with a thickness of the order of one kilometre (vertical motion being possible within the layers). This concept is consistent with observations of grenade glow clouds by Rofe (1961) and Rees (1969) which show that motion is confined to layers varying in thickness from 500 metres at 90 km to 2 km at 110 km. Motion within these layers is apparently turbulent in nature since the diffusion rate is compatible with this hypothesis.

Structure functions computed for horizontal separations follow the power law

$$D(\xi) \propto \xi^{2/3}$$

at least up to separations of a few kilometres. This result has been found by the radio-meteor method (Roper, 1966) for separations up to 3.5 km and by Justus (1967) using chemical clouds. Evidence that this law is obeyed at much larger horizontal separations is provided by the treatment of Elford and Roper (1967) of the auto-correlation function of Greenhow and Neufeld (1960). However this evidence must be regarded with reservation in view of the discussion on the maximum observable scale in §3.2.2. Observations of two simultaneous vapour trails separated by large horizontal distances (e.g. Justus and Roper, 1968) also indicate that large scale horizontal structure can exist. It appears in general that the

horizontal motion with scales up to many tens of kilometres is characteristic of an inertial turbulent regime even though buoyancy effects severely restrict vertical motion.

The diffusion rate of grenade glow clouds and chemical trails is generally much greater than molecular diffusion up to heights of 120 km. This high diffusion rate is considered to be due to turbulent diffusion in an inertial subrange, although as indicated in Table 3.1 some difficulties still remain in the interpretation of the early time behaviour of a contaminant release.

A possible model of the irregular structure in the mesosphere and lower thermosphere is a turbulent dissipation mechanism involving a horizontal, inertial cascade of energy through highly anisotropic eddies. Such a form of turbulence may be similar to the two-dimensional turbulence discussed by Kraichnan (1967) for conditions when the forcing function is of limited spectral width. Turbulent layers may be due to instabilities in the tidal wind field (Lindzen, 1968) or to superadiabatic conditions in gravity wave propagation (Hodges, 1967).

The apparent cessation of turbulence at the "turbopause" at heights of 105 km to 110 km is most probably due to the very rapid increase in the time constant of the Kolmogorov microscale at this level (Rees et al., 1970). The efficiency of molecular transport increases rapidly above 110 km and near 120 km the contribution by turbulence is insignificant even though the absolute value of turbulent diffusion may be as large as the value at the turbopause.

Author(s)	Resolution	Initial	Mid-Time	Late-Time
Blamont & Barat (1967)	High < 5 m	$r^2 \propto t$	$r^2 \propto t^3$	-
Blamont & Barat (1968)	High < 50 m	$r^2 \propto t$ (> 8 sec)	$r^2 \propto t^5$ (< 100)	$r^2 \propto t^2$ or $\propto t^3$
Rees et al., (1969)	High < 50 m	Indeterminate	$r^2 \propto t^3$	? trail too broken
Justus (1966)	Low > 200 m	?	$r^2 \propto t^3$ (> 100 sec)	
Justus (1969)	Inter-globular distance		$d^2 \propto t$ or $d^2 \propto t^3$	

TABLE 3.1: Diffusion laws found below 110 km. Initial time behaviour applies up to about 30 secs, mid-time behaviour 30 - 100 secs, and late-time behaviour > 100 secs. The distinction is usually apparent in a distinct change of slope in the growth curve.

All apparent irregularities in the spatial and temporal structure of the wind field are not due to turbulence. High order modes of the tidal wind field (Lindzen, 1967) and internal gravity waves (Hines, 1960) also contribute to the irregular structure. However, as pointed out in Chapter II, there is no technique which can uniquely indentify the various contributions to the irregular motion. The most promising line of investigation appears to be in observations of a passive scalar. Waves are not capable of transporting a passive scalar whereas turbulence is an extremely efficient method of transport.

While a turbulent dissipation mechanism will be the ultimate sink for much of the wave energy in the mesosphere and lower thermosphere, the transition between turbulent behaviour and wave-like behaviour is not distinct. Energy can flow between the two types of motion by non-linear effects; turbulence can grow at the expense of the energy in waves by wave-breaking phenomena while some turbulent energy can be transformed into waves in stratified region. Stewart (1969) and Bretherton (1969) have recently discussed many interesting ideas concerned with the possible distinction between turbulence and waves in stratified fluids and which may be applicable to some of the observations in the lower thermosphere.

CHAPTER IV

THE REFLECTION OF RADIO WAVES FROM METEOR TRAILS

4.1 INTRODUCTION

In order to appreciate the usefulness and limitations of meteor trails as sensors of atmospheric motion, a brief outline of the formation of the trail and of the reflection process is required. The discussion presented in this chapter is a somewhat oversimplified view of trail formation and radio wave reflection processes based on the classical physical theory of meteors (McKinley, 1961). In the light of new observational data the classical theory has been questioned during the past few years, however this theory is adequate for a discussion of meteor trails as wind sensors. A summary of the processes of formation and decay of the meteor trail is given in §4.2. A more detailed presentation is given by McKinley (1961).

In any real case the distribution of ionisation and light along the meteor trail is not uniform but increases as the meteoroid descends through the atmosphere reaching a maximum near the end of the life of the meteoroid. Furthermore the meteoroid may fragment and produce discontinuities in the light and ionisation profiles. These effects are not of major importance in the determination of the velocity of the incoming meteoroid and the location of the point of closest approach.

4.2 THE FORMATION AND DECAY OF THE TRAIL

As a meteoroid enters the earth's atmosphere collisions with air molecules decrease its forward momentum. The collision processes produce heating of the meteoroid and when the temperature is raised sufficiently atoms of the meteoroid are vapourised from the surface of the parent body. The ablated atoms move with the velocity of the meteoroid and hence have kinetic energies ranging from a few tens to some hundreds of electron volts. These energies are large compared with the ionisation potentials of the meteor and air atoms and subsequent collisions between the two produce a self-luminous ionised column whose initial diameter is about 1 metre at a height of 100 km.

The decay of the ionised trail is due to a combination of diffusion, recombination and attachment. In most cases ambipolar diffusion is the most important factor. The duration of the radio echo depends on the wavelength of the incident radiation as well as the mechanism of dissipation of the ionisation.

For the Adelaide Radio Meteor System the minimum detectable meteor has a line density of the order of 10^{12} electrons/metre and most echos observed in the present survey have durations of less than a second.

4.3 SCATTERING OF RADIO WAVES BY METEOR TRAILS

A number of workers have treated the problem of radio reflection by ionised meteor trails (Herlofson (1951); Kaiser and Closs (1952); Eshleman (1955); Lebedinec and Sosnova (1968)). The reflection coefficient

have been deduced by formally reducing the problem to an equivalent electrostatic situation (Kaiser and Closs, 1952; Lebedinec and Sosnova, 1968). The main parameters which determine the magnitude of the reflection coefficients are the electron line density and the polarisation of the incident wave.

Confusion has existed in radio meteor theory regarding the phase conventions used by various authors. If the wave transmitted from the aerial is written in the form

$$A_t = F_t\, e^{i\omega t} = F_t\, e^{i\phi},$$

the phase angle, $\phi (= \omega t)$, rotates in an anti-clockwise direction on a phase-amplitude diagram. This is the common convention in electrical engineering but opposite to that used in most text-books on optics (e.g. Born and Wolf, 1964) which write the wave in the form

$$A = Ue^{-i\omega t}$$

and define the phase angle as increasing in the clockwise direction. Because phase comparisons are a major concern in a CW system it is most important that a consistent method of phase measurement is used. The electrical engineering convention is used in the following discussion.

4.3.1 Stationary Trail

Consider a meteoroid trajectory as in Figure 4.1 where P represents the point of closest approach of the meteoroid to the observing site, O. Let s be the distance from the specular point, P, on the trail (usually termed the t_o point) to the point M, measured positively in the

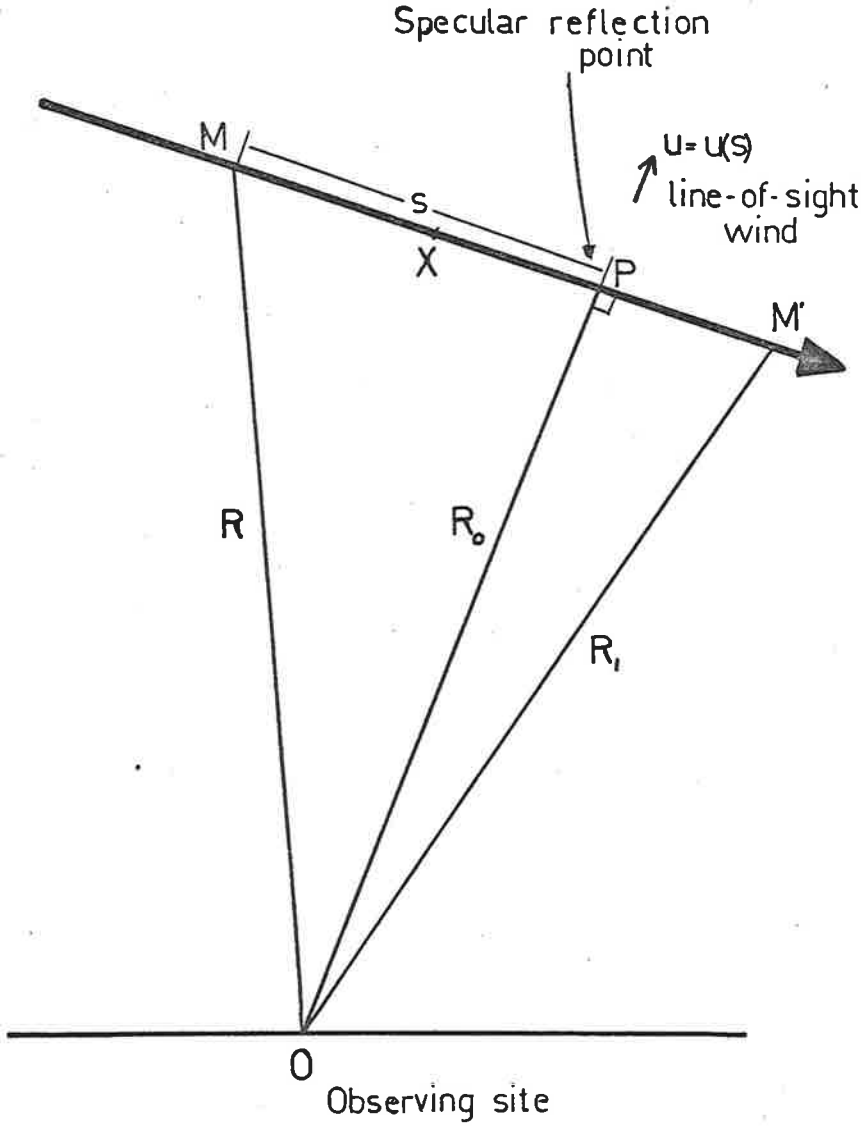

Figure 4.1: The geometry of a meteoroid path relative to an observing site.

direction of motion of the meteoroid. The wave received from an element ds of the trail at the point M travels a total distance 2R and its phase on reception is $\omega t - 4\pi R/\lambda - \beta$ where β is the phase retardation on reflection, ω is the frequency of the wave and λ is the wavelength. Thus the amplitude of the wave at the receiver can be written as

$$dA_r = \frac{A_T G \lambda \sqrt{2\rho}}{4\pi R^2} g(s) \exp i(\omega t - 4\pi R/\lambda - \beta) ds \qquad 4.1$$

where $g(s)$ = reflection coefficient for the point M; G = gain of receiving antenna; ρ = input resistance of the receiver; A_T = amplitude of the transmitted wave. Thus when the meteoroid has reached the point M, (a distance s_1 along the trail) the amplitude of the signal reflected by the meteor trail (Kaiser, 1955) is

$$A_R = \frac{A_T G \lambda \sqrt{2\rho}}{4\pi R^2} \int_{-\infty}^{s_1} g \exp i(\omega t - \frac{4\pi R}{\lambda} - \beta) ds \qquad 4.2$$

where the lower limit of the integral has been taken as $-\infty$ since as $s \to -\infty$, $dA_r \to 0$.

Assuming that the reflection coefficient varies only slowly along the trail in the vicinity of the point P and using the approximation $R = R_o + \frac{s^2}{2R_o}$ then expression 4.2 can be written as

$$A_R = F_R e^{i\psi}(C - iS) \qquad 4.3$$

where

$$C = \int_{-\infty}^{x_1} \cos \frac{\pi x^2}{2} dx, \quad S = \int_{-\infty}^{x_1} \sin \frac{\pi x^2}{2} dx$$

$$x = \frac{2s}{\sqrt{R_o \lambda}} \quad ; \quad F_R = \frac{A_T G \lambda \sqrt{2\rho}}{4\pi R_o^2} \cdot \frac{\sqrt{R_o \lambda}}{2} g$$

$$\psi = \omega t - \frac{4\pi}{\lambda} R_o - \beta \ .$$

If the optics convention had been used we would have arrived at the expression

$$A_r = F_r \, e^{i\phi}(C + iS) \qquad 4.4$$

This point has not been made clear in the past (e.g. McKinley (1961); Kaiser (1955)) and can lead to confusion in interpretation of records obtained in the case where a reference signal (for example a ground wave) is combined with the signal reflected from the meteor.

In a CW system the transmitter and receiver are usually separated by a short distance D, ($D \ll R$), just large enough to reduce the level of the ground wave below the overload point of the receivers. Then there is an additional field, $F_d \exp i(\omega t - \frac{2\pi D}{\lambda})$, present at the receiving aerial. Adding the two field vectors and averaging over one radio-frequency cycle we arrive at the following expression for the power received from the trail up to the point M_1

$$P_{R+d} = F_R^2 \left[C^2 + S^2\right] + F_d^2 + 2F_R F_d \left[C \cos\psi - S \sin\psi\right] \qquad 4.5$$

where $\psi = 2\pi\left[2R_o - D\right]/\lambda$ is the phase advance of the skywave with respect to the ground wave at the instant of closest approach.

4.3.2 Trail in Presence of a Wind

The discussion in §4.3.1 relies on the assumption that all segments of the trail retain their original positions in space after formation, that is the path differences to each segment of the trail remain constant. Kaiser (1955) has treated the problem where the path differences vary with time due to the motion of the trail in a wind.

Martyn (1953), Clemmow et al. (1955) and Kato (1959) have shown that a cylindrical irregularity of ionisation (such as a meteor trail) will move with the velocity of the neutral air below 120 km.

If there is a line-of-sight wind, u, at the specular reflection point then the power received from the meteor trail is:

$$P_{R+d} = F_R^2 |C^2 + S^2| + F_d^2 + 2F_R F_d |C(\nabla) \cos(\psi - \theta) - S(\nabla) \sin(\psi - \theta)|, \text{ (Kaiser, 1955)} \qquad 4.6$$

where

$$u = u_o + du/dx = u_o + u'$$

$$\delta = 2u'R_o/v \ .$$

The variable ∇ is a measure of distance along the actual trail as distinct from the distance s measured along the undisturbed meteoroid trajectory and is given by

$$\nabla = \frac{2 - \delta}{|R_o \lambda (1 - \delta)|^{\frac{1}{2}}} \; v \; t - \left| \frac{2u_o R_o}{v^2 (2 - \delta)} \right| \qquad 4.7$$

The angle θ is a measure of the extra phase shift introduced by the wind and is given by

$$\theta = \frac{2\pi}{\lambda} \left| u_o t \frac{(2 - \delta)}{(1 - \delta)} - \frac{\delta^2 v^2 t^2}{4(1 - \delta) R_o} - \frac{R_o}{(1 - \delta)} - \frac{u_o^2}{v^2} \right| . \qquad 4.8$$

The variation in phase due to the terms containing θ in (4.6) gives rise to a doppler beat of frequency $f = \frac{d\theta}{dt} / 2\pi$ which can be interpreted as due to an apparent velocity u of the trail with respect to the transmitter-receiver system. Thus

$$u = \frac{d\theta}{dt} \frac{\lambda}{4\pi} = \frac{u_o(2 - \delta)}{2(1 - \delta)} - \frac{\delta^2 v^2 t}{4(1 - \delta)R_o} \quad \text{(Kaiser, 1955).} \qquad 4.9$$

When there is no wind shear ($\delta = 0$), $u = u_o$ and hence the recorded velocity $u = \frac{d\theta}{dt} \frac{\lambda}{4\pi}$ is equal to the actual line-of-sight component of the wind.

The form of the signal received from a meteor trail in a wind field with a typical line-of-sight velocity of 50 m/sec and a shear of 20 m/sec/km is shown in Figure 4.2 for the case where the sky wave at the time of closest approach (the t_o point) leads the ground wave by 90^o i.e. $\psi = \pi/2$. The rapid variation in signal level before (and after) the t_o point is usually termed the "whistle" owing to the audible descending tone generated when the output of a receiver is connected to a loudspeaker. The post t_o whistle is usually difficult to detect owing to the obscuring effect of the doppler waveform.

The wind shear u^1 can be determined by measuring the velocities u_1 and u_2 at times t_1 and t_2 respectively and since, in general, $\delta \ll 1$ then from expression 4.9,

$$u^{-2} = - \frac{u_1 - u_2}{R_o(t_1 - t_2)} \qquad 4.10$$

Thus it appears possible to determine the wind shear at a single station by measuring the doppler frequency. Müller (1968) has used this technique in a survey conducted at Sheffield during the I.Q.S.Y. However the inability to determine the orientation of the trail limits knowledge of the form

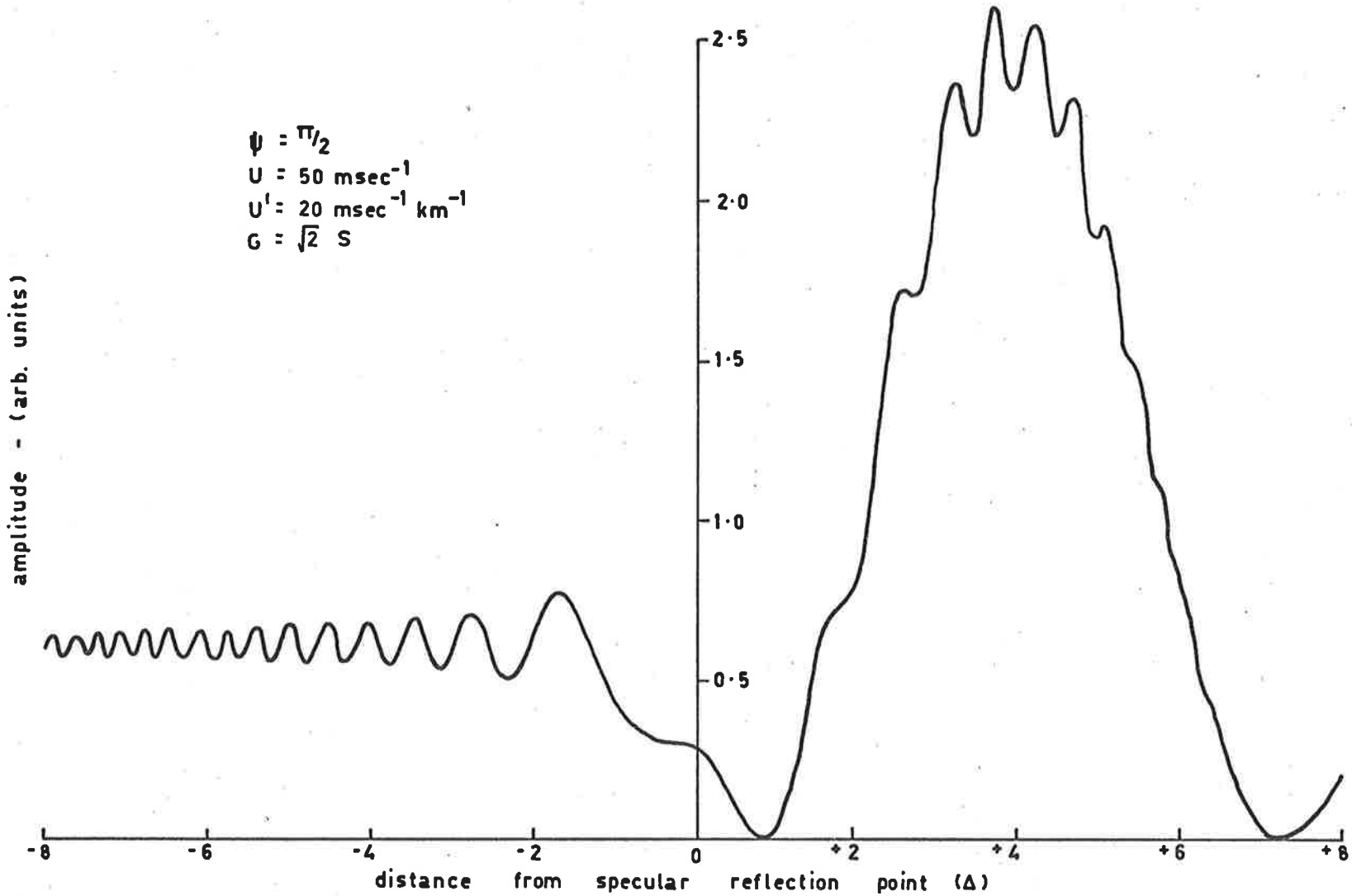

Figure 4.2: Theoretical amplitude - time curves of meteor echoes based on diffraction theory. The signal strength is plotted against the argument Δ of the Fresnel integrals and which is directly proportional to time.

of the trail shear. In particular shears can only be measured over a limited distance along the trail. Despite these limitations useful statistical data can be collected as has been shown in §3.2.1.

4.4 THE EFFECT OF A WIND ON THE MEASUREMENT OF RELATIVE POSITIONS OF t_o POINTS AND THE VELOCITY OF THE METEOROID

In order to determine the flight path of an incoming meteoroid using a multi-station system, measurements must be made of the velocity of the incoming meteoroid and the times at which the various specular reflection points are reached. These times are the t_o points for the echoes received at each receiving site. For convenience during the appearance of an echo at any one of these sites time is usually referred to the t_o point as origin.

In the absence of a wind the meteor trail lies along the flight path of the meteoroid and hence the positions (in time) of the diffraction pattern maxima and minima can be related directly to distance along the flight path. The velocity of the meteoroid can be determined from the time of occurrence of the maxima and minima of the amplitude fluctuations prior to the t_o point.

When a wind moves the meteor trail after formation, the diffraction pattern is displaced in time by an amount $\frac{2u_o R}{v^2(2 - \delta)}$ (Kaiser, 1955) (the symbols have the same meaning as in §4.3.2) and the time between the diffraction maxima and minima correspond to an apparent velocity

$$v_a = \tfrac{1}{2} v(2 - \delta)(1 - \delta)^{-\frac{1}{2}} .$$

For a typical case ($u' = \pm 10$ m sec^{-1} km^{-1}, $v = 40$ km sec^{-1}, $R_o = 200$ km) differences of approximately 5% in determination of the position of t_o point and 1% in determination of the velocity can occur. Measurement of the shear enables corrections to be made.

4.5 SUMMARY

In this chapter a brief introduction has been given to the process of reflection of a radio wave from a meteor trail. The discussion has been biased in considering only the form of the diffraction signal since this is the main observational requirement of the system.

Before the meteoroid velocity can be calculated from an observed diffraction signal, a knowledge of the phase of the sky wave relative to the ground wave is required. Mainstone (1960) has developed a technique for this, utilising the phase information contained in the doppler beat.

When the trail is fully formed the segment of the trail about the specular reflection point is responsible for most of the reflected power. This segment is effectively the first Fresnel zone and for the present system is of the order of 700 metres in length. The reflection points are simply the geometrical mid-points of the first Fresnel zone. In the presence of a wind shear the reflection points will also move along the trail. These two effects impose a limit on the minimum useful separation of reflection points.

CHAPTER V

THE ADELAIDE RADIO-METEOR SYSTEM

5.1 SYSTEM DEVELOPMENT

The basic principles on which the present system is based have been described by Robertson, Liddy and Elford (1953) in connection with the first prototype system for measuring meteor drifts. A network of remote receiving sites was added to the system in 1959 (Weiss and Elford, 1963; Roper, 1962; Nilsson, 1963) and this network has been further extended and improved in the years 1967-1969. At present the system consists of two transmitters (continuous wave and pulse) installed in the Department of Physics at Adelaide, a receiving and recording station at St. Kilda (23 km. north of Adelaide) and four remote receiving sites each equipped with a telemetry link to St. Kilda.

The radio-meteor system is used for the following studies:

(i) Measurement of the rate of drift of meteor trails to determine diurnal and seasonal variations in the motion of the atmosphere between 75 and 105 km.

(ii) Measurement of the relative motion of three or more segments of an individual meteor trail in order to investigate small scale motion of the atmosphere.

(iii) Routine measurement of the orbits of individual sporadic and shower meteors down to radio magnitude + 8.

(iv) A study of the distribution of ionisation along meteor trails.

The work described in this thesis relates to project (ii). The basic data required are:

(i) the relative drift velocity of three or more segments of a single meteor trail;

(ii) the relative separation of these segments along the trail and in height;

(iii) the absolute height of any one of these segments.

Observations at a single site only enable the determination of the following:

(a) the velocity of the incoming meteoroid,

(b) the position of the reflection point (range and direction),

(c) the radial component of the drift velocity of the reflection point,

(d) the variation in the strength of the reflected signal.

With this information only project (i) above can be carried out in full, however a limited amount of information regarding project (iv) can also be obtained. The other studies above all depend on a knowledge of the flight paths of the individual meteoroids. This requires at least two additional receiving sites.

5.2 MEASUREMENT TECHNIQUE

The scattering of radio waves from a meteor trail has been discussed in Chapter IV. The geometry of the ray paths for a suitably orientated

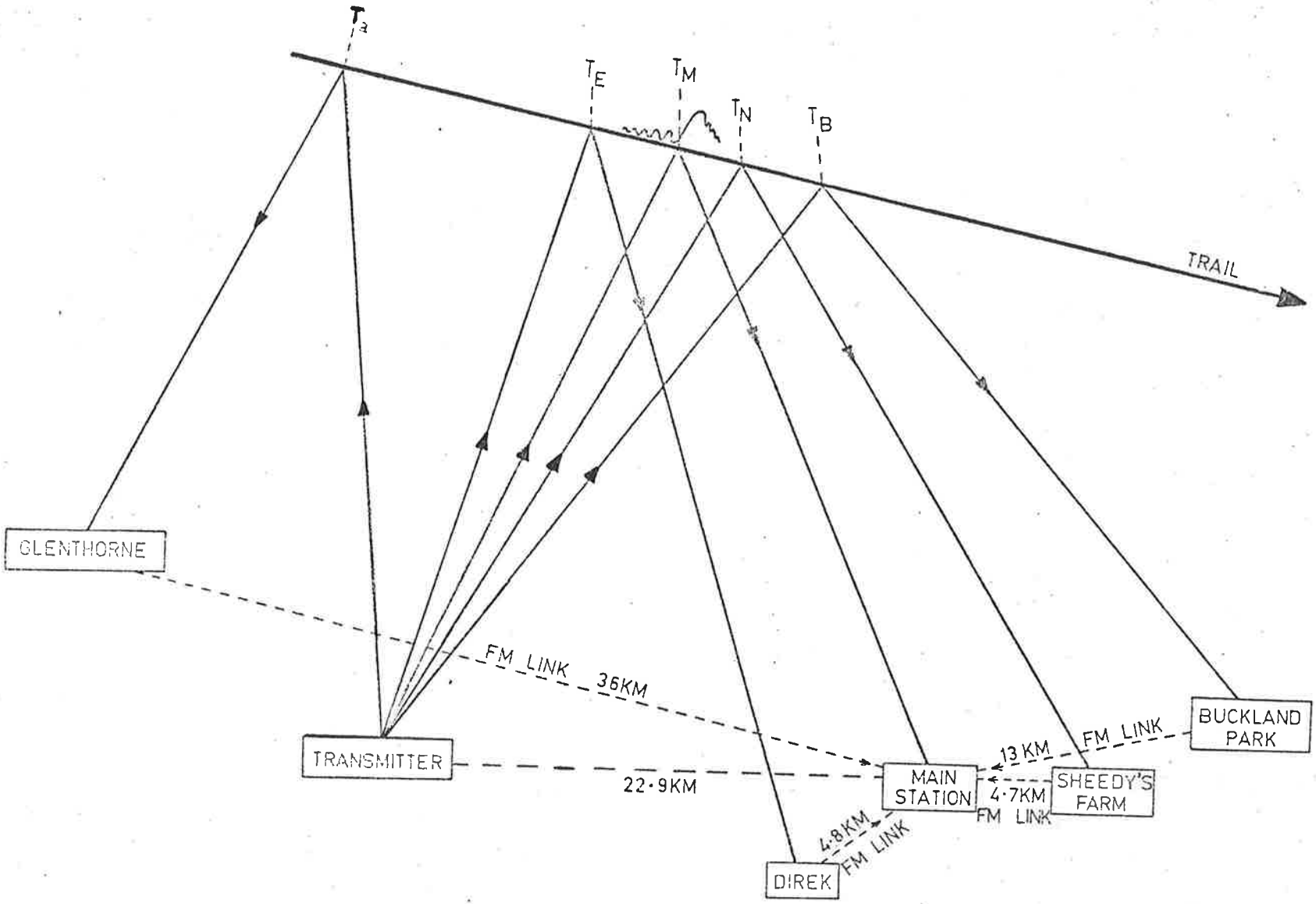

Figure 5.1: Schematic diagram (not to scale) of the site locations and geometry of the Adelaide Radio Meteor System. The times T_a, T_E, T_M, T_N, T_B refer to the times when the meteoroid passes the specular reflection points for each site.

trail that produces echoes at all of the receiving stations is shown in Figure 5.1. To locate a trail in space the position of the reflection observed from the St. Kilda station (see § 5.2.1) is combined with the times of commencement of the specular echoes from the other stations (see § 5.2.2).

5.2.1 Location of one Reflection Point and the Determination of the Line-of-Sight Wind

The direction of arrival of the reflected wave at the St. Kilda receiving station is found by comparing the phase of the sky-wave at five close-spaced receiving aerials. The layout of the antenna system at St. Kilda is shown in Figure 5.2. The antennae are orientated so that the ground-wave always presents a wave front parallel to the antennae which are half-wave dipoles mounted one quarter-wave above ground level. The directions OE and ON define the positive axes of a cartesian coordinate system and the direction cosines of the sky wave are determined relative to these axes. An analysis of phase diagrams for each aerial shows that the four possible measurements of relative phase are sufficient to determine unambiguously the direction of arrival of the sky-wave.

The range of the reflection point from the St. Kilda receiving site is determined by measuring the time difference between

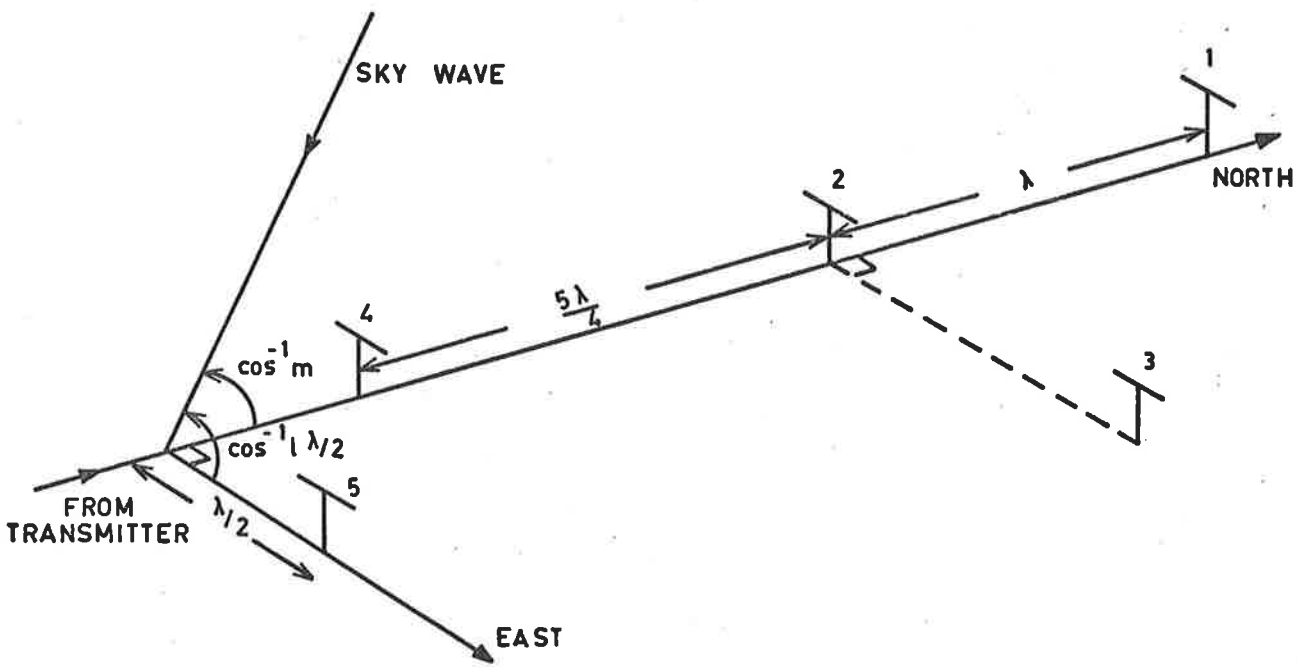

LAYOUT OF DIRECTION FINDING AERIALS AT ST. KILDA.

Figure 5.2: The layout of the antennae used for determining the direction of arrival of the sky wave. The transmitter is 23 km to the south.

the arrival of a ground-wave pulse and the associated sky-wave pulse, making an appropriate correction for the separation of the transmitting and receiving sites.

The drift of the trail is obtained from the measurement of the phase shift of the sky-wave relative to the phase of the ground wave as described in §4.3.2. The sense of trail drift (towards or away from the receivers) is determined by using a periodic (50 Hz) saw-tooth phase modulation of the transmitted continuous wave. The phase is retarded by 90° in 80 μsec and is then restored to zero in 20 msec. Normally this phase modulation produces no receiver output since conventional half-wave diode detectors are used. The slow advance of phase is virtually synchronous in the ground and skywaves at the receiving sites, but the rapid retardation in the ground wave reaches the receivers about one millisecond (for a typical range of 150 km) before the phase retardation in the sky-wave. Thus "sense spikes" at 20 msec intervals and approximately 1 msec in duration are produced on the doppler beat waveform. These "spikes" delineate a phantom trace shifted in phase by 90° with respect to the main waveform. The sense of the shift (leading or lagging) depends on whether the trail is advancing or receding from the receiving site.

5.2.2 Orientation of the Meteoroid Flight Path and the Separation of Reflection Points

Consideration of the reflection process as a diffraction problem as in §4.3 indicates that as long as a meteor trail remains straight then a unique specular reflection point exists for each receiving station. The times t_G, t_E, t_M, t_N, t_B shown on Figure 5.1 refer to the times at which the meteoroid passes the specular reflection point for each receiving site. These times are determined from an analysis of the diffraction signals at the commencement of the respective echoes. The velocity of the incoming meteoroid is found from the frequency-time relationships of the diffraction signals. Thus the spatial separations of the appropriate reflection points are readily calculated by combining the meteoroid velocity with the known time differences $t_G - t_E$, $t_G - t_M$, etc. The direction cosines of the meteoroid trajectory are determined by triangulation using the geometry of the observing system and the separation of the reflection points along the trail.

When the transmitting and receiving sites are separated then the condition for specular reflection is that the bisector of the angle between the incident and reflected wave is normal to the trail. Provided that this angle is small then the normal to the trail can be assumed to bisect the transmitter-receiver baseline. Using this "mid-point" approximation it can be shown that the maximum separation of any two reflection points on the trail is half of the distance between the respective receiving sites. Thus with the present multi-station system shown in Figure 5.3 the maximum possible separation along the trail is about 20 km. Although it

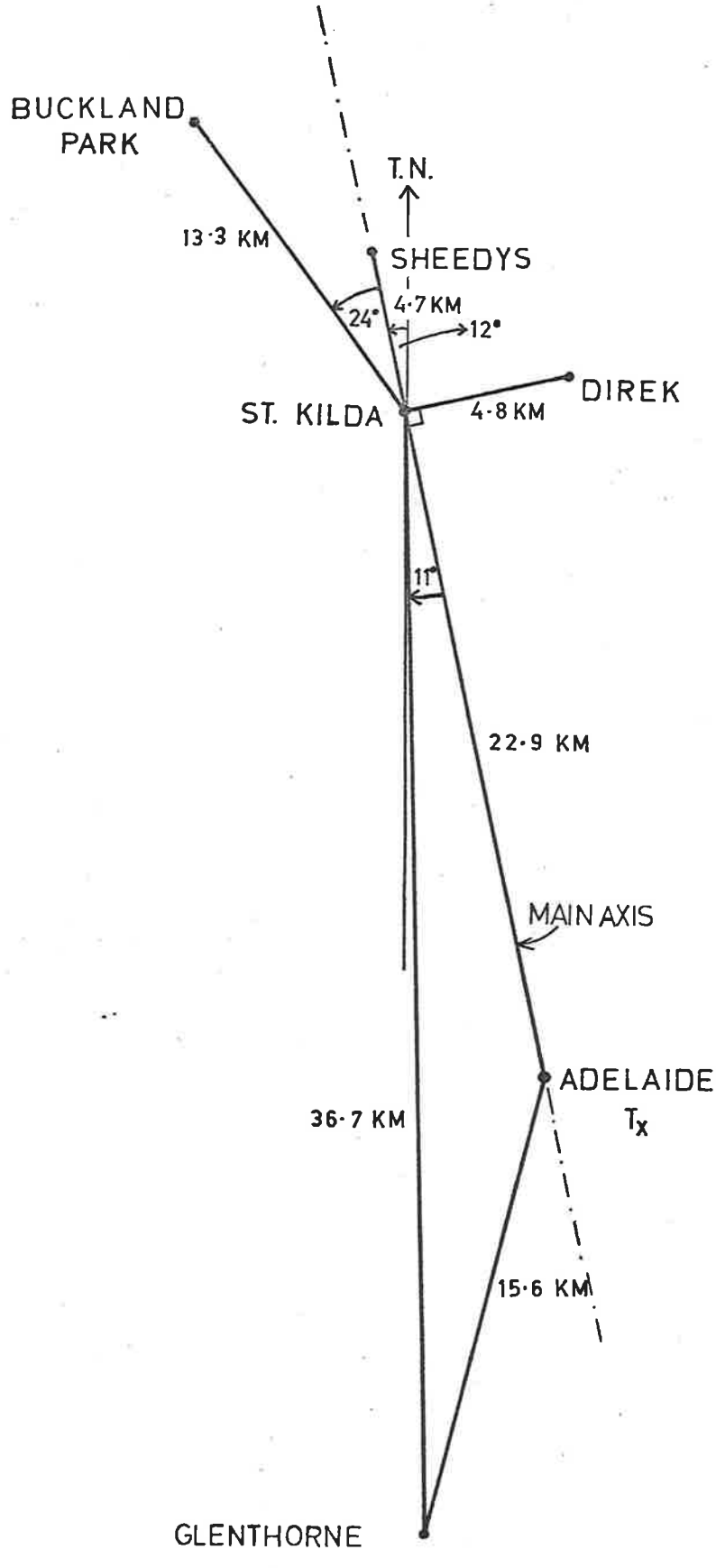

Figure 5.3: Plan of Transmitting and Receiving sites.

is useful to assume that the reflection occurs at a particular point it must be realised that most of the reflected power is returned from a short segment of the trail, of the order of one Fresnel zone in length, centred on the specular reflection point. At 27 MHz and for a typical range of 150 km, the length of this segment is approximately 0.7 km. It is this distance that determines the minimum usable separation of any two reflection points on a straight trail. However once the trail has been slightly deformed, trail lengths of about 50 metres can produce usable reflections and it is uncertain whether 700 metres represents an absolute lower limit to the separation.

5.3 DESCRIPTION OF EQUIPMENT

5.3.1 Main Transmitters

The CW transmitter operates on a frequency of 26.773 MHz and the pulse transmitter on a frequency of 27.540 MHz. Each transmitter feeds a simple half-wave dipole mounted one quarter-wave above the flat metal roof of one of the buildings of the Department of Physics at Adelaide. Block diagrams of each transmitter are given in Figure 5.4. Further details are given by Roper (1965).

The output of the CW transmitter is phase modulated by retarding the phase of the signal from the crystal oscillator (743.7 kHz) with a 50 Hz saw-tooth waveform to give a maximum deviation of 2.5°. Since the output frequency of the transmitter is 36 times that of the crystal oscillator the phase deviation in the output waveform is 90°. The useful power output is 1500 watts.

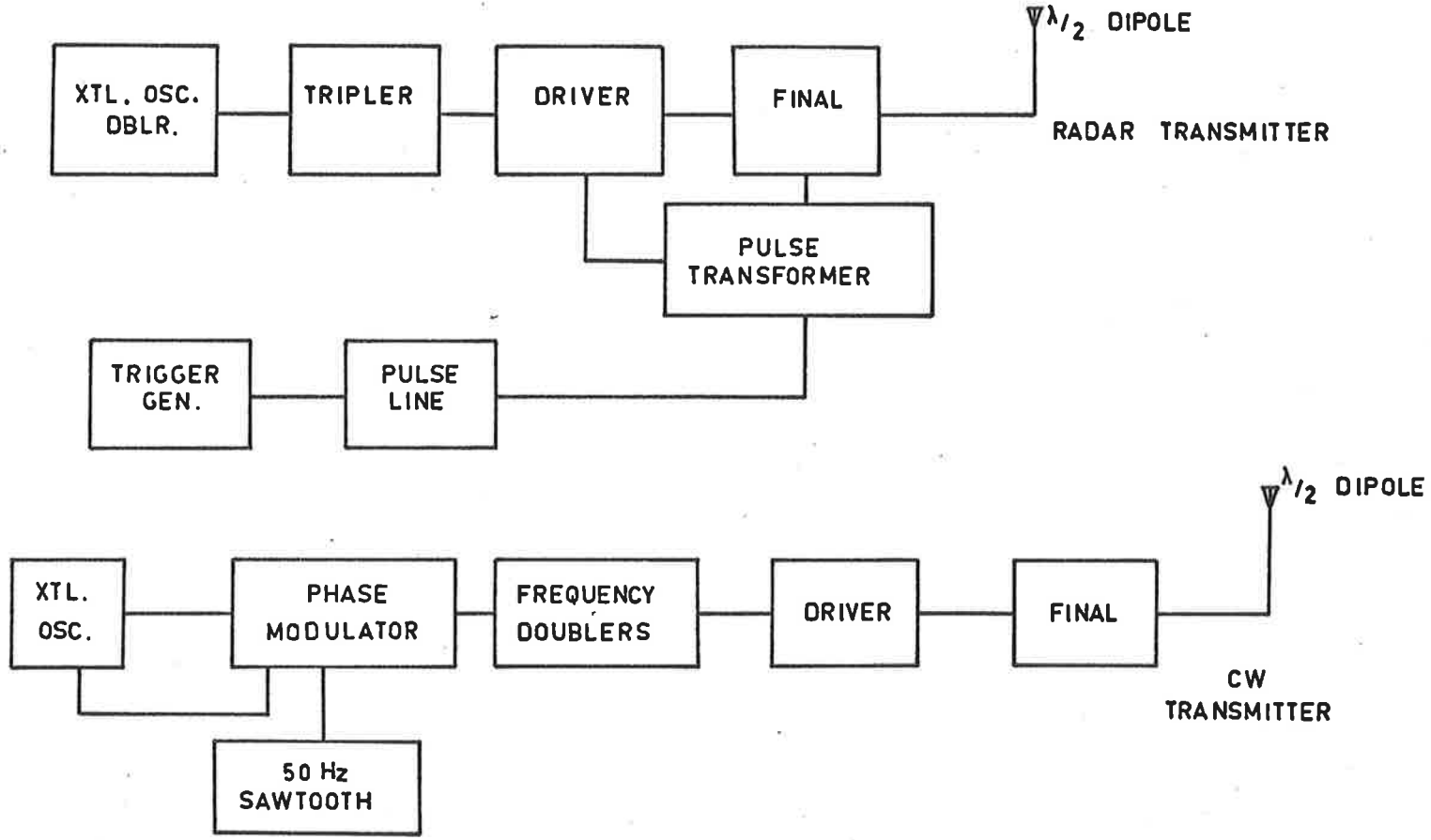

Figure 5.4: Block diagram of the radar and CW transmitters.

The driver and final stages of the pulse transmitter are modulated with a line type pulser that generates 8 μsec pulses at a repetition rate of 200 sec^{-1}. The pulse transmitter delivers pulses with a peak power of 6.5×10^4 watts to the aerial.

5.3.2 27 MHz Receivers

For optimum operation the receivers used should have noise figures of 3db or better so that galactic noise is the limiting factor in the detection of signals. It is also necessary that the receivers should handle the large dynamic range of signals, typically more than 30db. The bandwidth of the receivers should also be sufficient to permit the "sense spikes" to be detected without gross distortion of shapes.

The receivers in use at the main receiving site have noise figures better than 2db, an overall bandwidth ± 4.0 kHz at the 3db points and have a linear response up to an input of 30 μV with a smooth overload up to 55 μV input. The receivers at each of the remote stations were supplied by a contractor to the author's specifications. In the interests of reliability these receivers are of all solid-state construction. The receiver bandwidth is ± 3.0 kHz set by a mechanical filter, the noise figure lies between 2.8db - 3.4db. The linearity of these outstation receivers was not as good as those at the main station, overload occurs at 25 μV input despite modifications to the I.F. stages.

For a typical receiver bandwidth of ± 3 kHz the galactic background noise power at 27 MHz is approximately 3×10^{-15} watts. For the Adelaide Radio Meteor System the total power collected by a half-wave

dipole one quarter-wave above ground from a trail with an electron line density of q electrons m^{-1} is given by $P_R \doteq 6 \times 10^{-40} q^2$ watts.

This is the total power available to beat with the ground wave to produce the body doppler. However at any instant prior to the meteoroid passing the specular reflection point the power is much less than this as can be seen by inspection of Figure 4.2. For a meteor trail with a line density of 10^{13} electrons/m, $P_R = 6 \times 10^{-14}$ watts and it is only when the meteoroid has reached the sixth or seventh Fresnel zone that the power reflected from the trail is twice the background noise. Thus a trail with a line density of 10^{13} electrons/m represents a lower limit to the detection of the diffraction pattern.

5.3.3 The Outstations and Telemetry Links

A block diagram of the equipment installed at each outstation is shown in Figure 5.5. The 27 MHz receiving aerial is a half-wave dipole mounted one quarter wavelength above ground level and is connected to a low noise superheterodyne receiver. In order to calibrate the system gain automatically, a signal of a known voltage (10 μV) from a crystal controlled oscillator (26.773 MHz) is applied to the input terminals of the receiver once per hour.

When no meteor echo is present the output from the detector of the 27 MHz receiver is a D.C. voltage (approximately 1 volt) representing the amplitude of the ground wave. In order to transmit this information back to the main recording station an audio frequency subcarrier is generated by chopping this voltage level to ground potential.

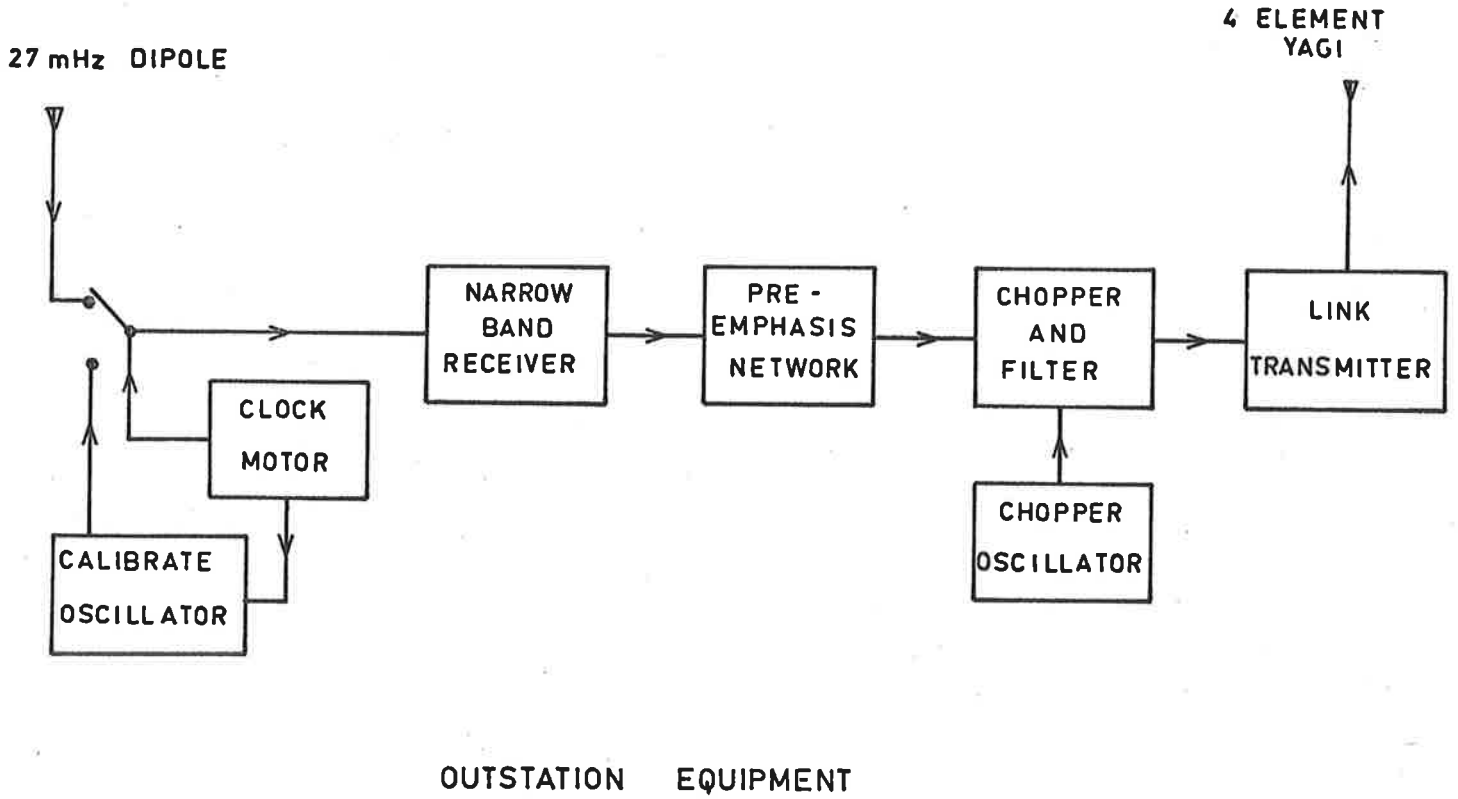

Figure 5.5: Block diagram of the equipment installed at each outstation.

After passing the chopped signal through a simple band-pass filter the sub-carrier is used to frequency modulate the telemetry transmitter. For a meteor line density of 10^{13} electrons/metre the diffraction signal represents an effective modulation of the sub-carrier of some 2% - 3%.

Because of the small deviation (± 5 kHz) now allowed in the 160 MHz band, the telemetry receiver noise is sufficiently large to represent an equivalent modulation of the sub-carrier of about 2%. If the signal to noise ratio is not to be degraded by the noise generated in the telemetry link, the diffraction signal should be amplified prior to transmission. Because of the dynamic range involved in the signals at the output of the receiver, the diffraction signal (commonly termed "the whistle") is amplified by a frequency selective network which boosts frequencies between 30 Hz and 600 Hz (the components of the "whistle"). The filter network used is shown in Figure 5.6 together with the amplitude response.

Each of the four outstations is completely self-contained and runs unattended except for routine maintenance and calibration. The actual method of housing an individual outstation varies with the site. The two closest outstations (Sheedys and Direk) are enclosed in the same steel tanks buried in the ground as were used in a previous survey (Roper, 1962). However improvements have been made to each for further protection against the weather and vandalism. All aerial connections are now encased in epoxy-resin and all other connections are fully enclosed (Figure 5.7). In an attempt to reduce the temperature variation within the tanks a false lid painted gloss white has been added.

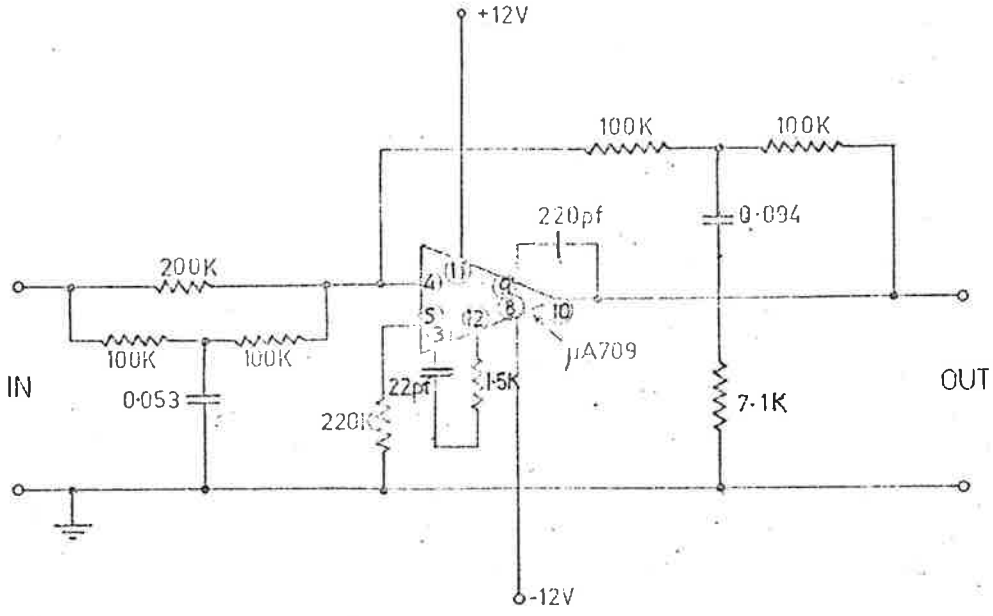

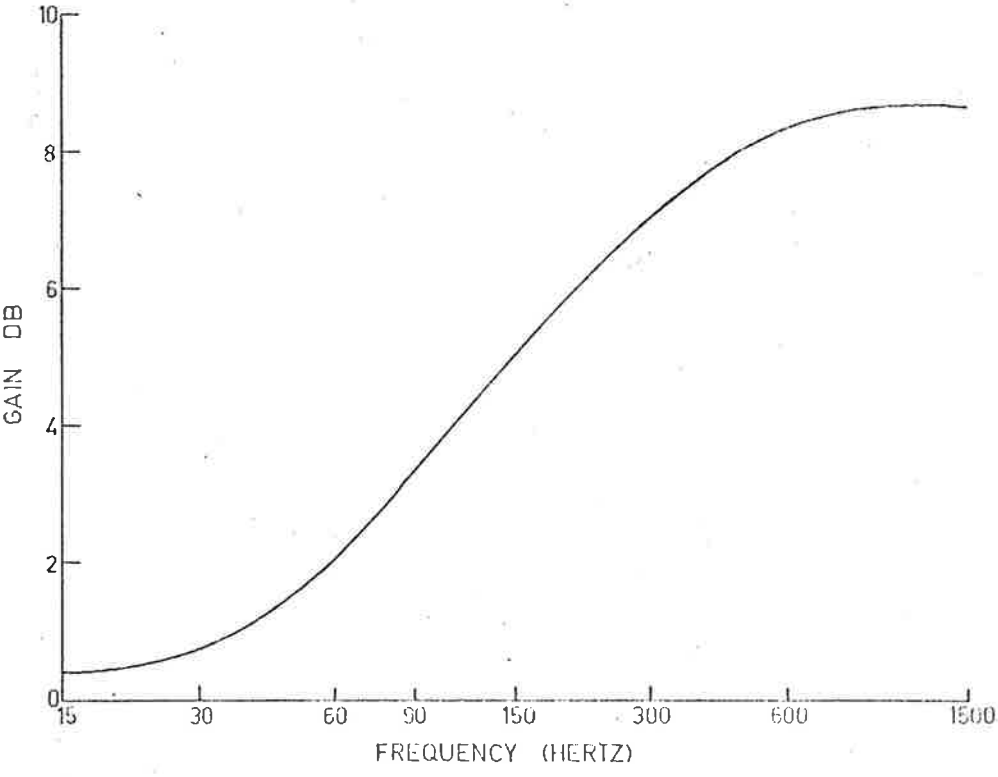

Figure 5.6: Filter (and response function) used to boost the whistle waveform before transmission over the telemetry link.

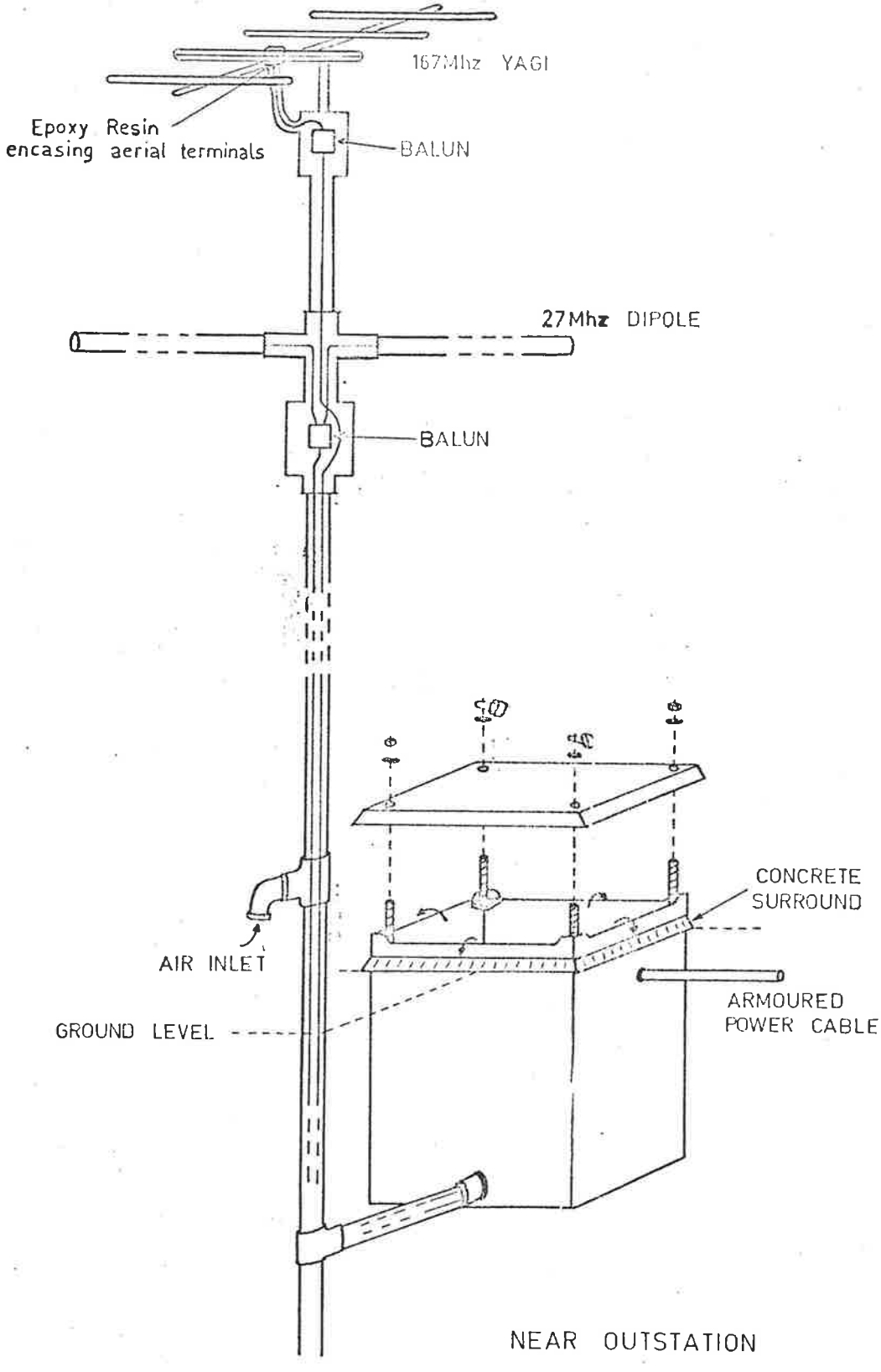

Figure 5.7: Schematic diagram of the method of construction at the Direk and Sheedys outstation sites.

The medium and long distance outstations (Buckland Park and Glenthorne) are not subject to the same threat of vandalism as the others and hence different methods of housing the equipment were adopted. At Buckland Park the aerial cables are brought into the main hut used for other experiments in progress at this site, whereas at Glenthorne the equipment is housed under the link transmitting tower itself.

Commercial FM transmitters and receivers are used in the telemetry system. Modifications have been made to both units to suit the requirements of the meteor system. The audio stages of both the transmitters and receivers have been modified to obtain a uniform frequency response up to 4.2 kHz, hence improving the overall linearity of the system. The final RF stage of the transmitters has been modified to allow continuous operation at 5 - 10 watts output power.

Four element Yagi antennae are used for telemetry. The front to side rejection ratio of these aerials is 36db. Because the link paths for Sheedys and Direk are at right angles this enables a common frequency of 167.02 MHz to be used at these stations. The signal strength of the undesired signal is sufficiently small that the limiter in the FM receiver only operates for the much stronger desired signal. The other pair of outstations, Buckland Park and Glenthorne share the 162.34 MHz frequency allocation. However because these stations are approximately on the same line (see Figure 5.3) the necessary attenuation of the unwanted signal is accomplished by using different polarisations for the two link paths as well as relying upon the front to back rejection ratio of the receiving antenna.

Voice communication is also possible between each outstation and the main recording station using a mobile VHF radio-telephone. The state of each telemetry link is monitored by displaying the strength of the received FM signal (the signal level at the first limiter) on panel mounted meters at the main station.

The main parameters of the telemetry system are given in Table 5.1 below.

Telemetry Link	Frequency (MHz)	Polarisation	Sub-Carrier Frequency (kHz)	Height of Tx Aerial Above Ground (Feet)
Buckland Park	162.34	Horizontal	2.0	35
Sheedys	167.02	Horizontal	2.0	10
Direk	167.02	Horizontal	3.5	10
Glenthorne	162,34	Vertical	3.5	35

TABLE 5.1 PARAMETERS OF TELEMETRY SYSTEM

5.3.4 Recording

At the main station (St. Kilda) the signals telemetred from the outstations are fed through band pass filters (± 600 Hz at the 3db points) centred on the particular sub-carrier frequency for the link concerned. These band pass filters improve the signal to noise ratio at the output of the telemetry receivers. The output of one of the 27 MHz receivers at the main station is also chopped and filtered.

Hence at this stage information from the five receiving sites is carried on five separate sub-carriers as follows:

2 kHz, Sheedys and Buckland Park

3.5 kHz, St. Kilda, Direk and Glenthorne.

Three independent display systems are used to record the data o: 35 mm film. One display system (the mean wind recording system) is used to record the direction of arrival and range of the echo received at the St. Kilda site. This display is used for routine wind measurements which do not require signals from any other receiving site. The other two display systems (the wind shear and velocity displays) are required to record the echo waveforms received at each receiving site.

The mean wind and wind shear recording systems use a slow speed camera (0.38 ins/sec) as only the low frequency (0.5 Hz - 20 Hz), large amplitude doppler beat waveforms need be recorded. However the high frequency (30 Hz - 300 Hz), small amplitude, generally shorter duration "whistle" waveform requires a higher camera speed. In order to use the available film efficiently the "whistle" waveforms from all receiving sites are recorded using a high speed (1.9 ins/sec) camera. Figure 5.8 illustrates how the five sub-carriers are distributed to the velocity and shear recording equipment via the channel distribution unit. This diagram also shows the manner in which the mean wind recording equipment is operated.

The film drive mechanism of each of the cameras is coupled to the motor through a magnetic clutch. The delay between activating

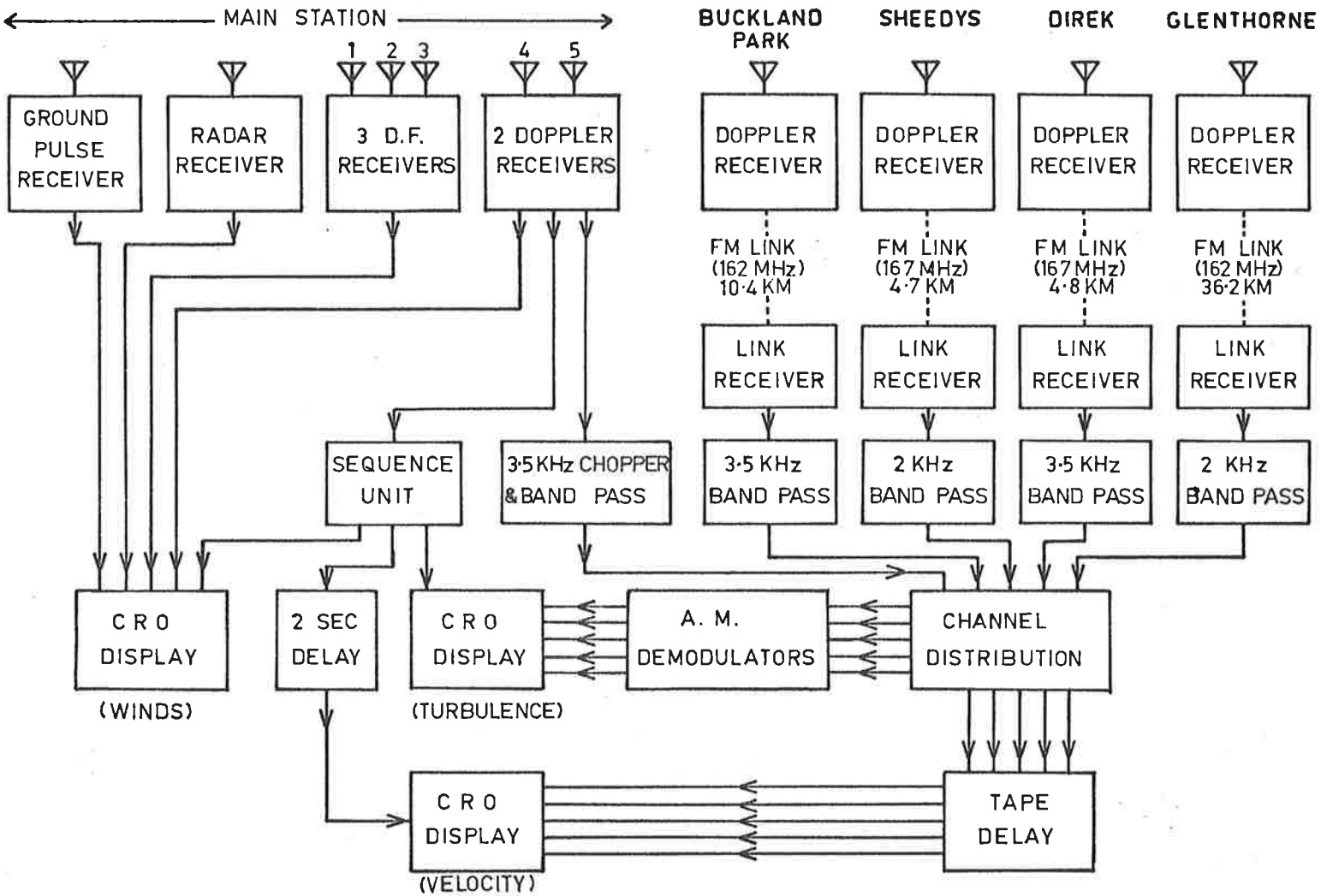

FIG. 5·8 BLOCK DIAGRAM OF MAIN RECEIVING STATION

the clutch and the film reaching constant speed is 20 m sec. These clutches are only operated when the 'sequence unit' shown in Figure 5.8 senses that the output of one of the receivers associated with the mean wind equipment varies about its mean level by more than a preset amount. The 'clutch pulse' generated by this event is used to start the recording sequence in each of the display systems.

To assist in the correlation of the films obtained from the three cameras a six digit counter is installed in each display. Whenever a recording sequence is initiated all counters are incremented and subsequently illuminated by an electronic flash to record the number on the film. A clock face may also be illuminated so that the time of occurrence of the recorded signal is known.

(i) Wind Shear Recording Equipment

The signals from the channel distribution unit are amplified before being demodulated and filtered to remove the sub-carrier component. The demodulator used is a balanced ring type with excellent linearity over the output range 0 - 20 V. The low pass filter used has an upper cut-off frequency of 1 kHz to allow the "sense spikes" of approximately 1 m sec duration to be recorded.

The outputs from the demodulator unit consist of DC levels representing the ground wave amplitude at the outstations plus the signal due to any meteor echo which might be present. These voltages are monitored on five panel

mounted meters and are applied to the vertical deflection plates of three double beam Telefunken oscilliscope tubes by DC amplifiers. These amplifiers are basically differential pairs with constant current sources in the emitter circuit; variation of the amount of current feedback between the two halves of the circuit controls the gain.

While every attempt has been made to preserve a reasonable degree of linearity in the system, regular overall amplitude calibrations are performed to determine any departures from the ideal linear case. Corrections are applied when necessary in the final data reduction. With the advent of modern fast computing methods regular calibration can overcome most of the difficulties associated with non-linear equipment. The system has not been calibrated for phase as a whole, but the phase variations in each item of equipment have been checked to ensure that gross phase delays do not occur over the frequency range of interest.

The recording sequence initiated when a 'clutch pulse' is detected is as follows;

(a) the oscilliscope tubes are brightened and the camera clutch is engaged,

(b) the recording continues for a predetermined time which can be adjusted between the limits 0.5 sec to 10 sec

(c) after the recording interval the six digit counter is incremented, the clutch disengaged and the electronic flash illuminates the counter,

(d) the clock face is illuminated by another electronic flash and the oscilliscope tubes darkened ready for the next echo.

The normal recording interval is about 1.5 secs, however occasionally longer intervals are used when long enduring echoes are to be recorded.

(ii) Velocity Recording

Normally the recording sequence described in the previous section is initiated by the large amplitude body doppler signal from a meteor (or interference, e.g. from aircraft) because the preset level referred to in the above is normally chosen to be 20% - 50% of the mean signal. Since the post t_o diffraction signal is normally obscured by the doppler waveform (see §4.3), it is necessary to record the diffraction waveform (whistle) occurring before the t_o point. This could be done either by running the film continuously, an uneconomic procedure, or else by using some form of memory device and record only the pre- t_o "whistle". In the present system a tape loop in a multi-channel tape recorder is used as a temporary storage medium.

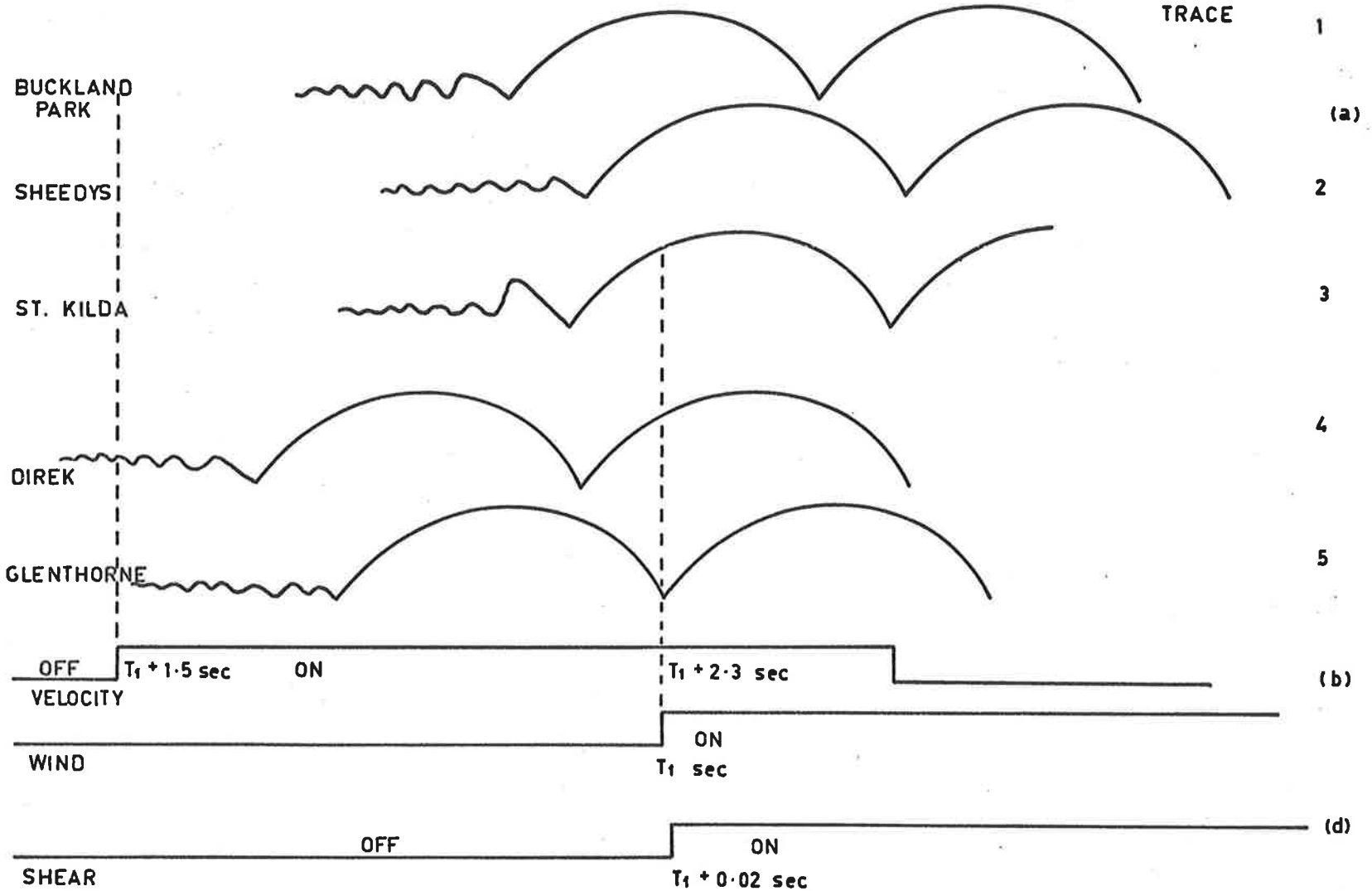

FIG. 5·9 TIMING DIAGRAM FOR RECORDING EQUIPMENT. THE SEQUENCES IN (c) AND (d) OCCUR IN REAL TIME WITH RESPECT TO (a), SEQUENCE (b) IS DELAYED BY 1·5 SEC WITH RESPECT TO (a).

Information from the five receiving sites is continuously recorded on the tape loop which moves at 30 ins/sec. The length of the loop is such that the delay between recording and subsequent playback is 2.3 seconds. A timing diagram which shows the order of events is given in Figure 5.9. When the mean wind equipment is triggered at time t_1 then the recording sequence for the velocity camera is initiated at t_1 + 1.5 secs. Thus recording of the whistle has already begun 0.6 secs before the signal which initiated the whole sequence is recorded at t_1 + 2.3 sec.

A block diagram of the tape delay system is shown in Figure 5.10. The outputs from each of the four telemetry receivers plus the chopped and filtered version of the output from the main station receiver are first demodulated with a standard diode ring network and then filtered with an active low pass network (1 kHz cut off frequency) followed by a notch filter centred on the sub-carrier frequency. The demodulated signals, whose frequencies range from 0.1 Hz to 600 Hz, each control the frequency of an oscillator (mean frequency 10 kHz). The linearity of these oscillators is excellent over the large frequency range used (5 kHz to 20 kHz) The signals from each channel (now in frequency modulated form) are recorded on five tracks equally spaced across the one inch magnetic tape used. The magnetic heads have been

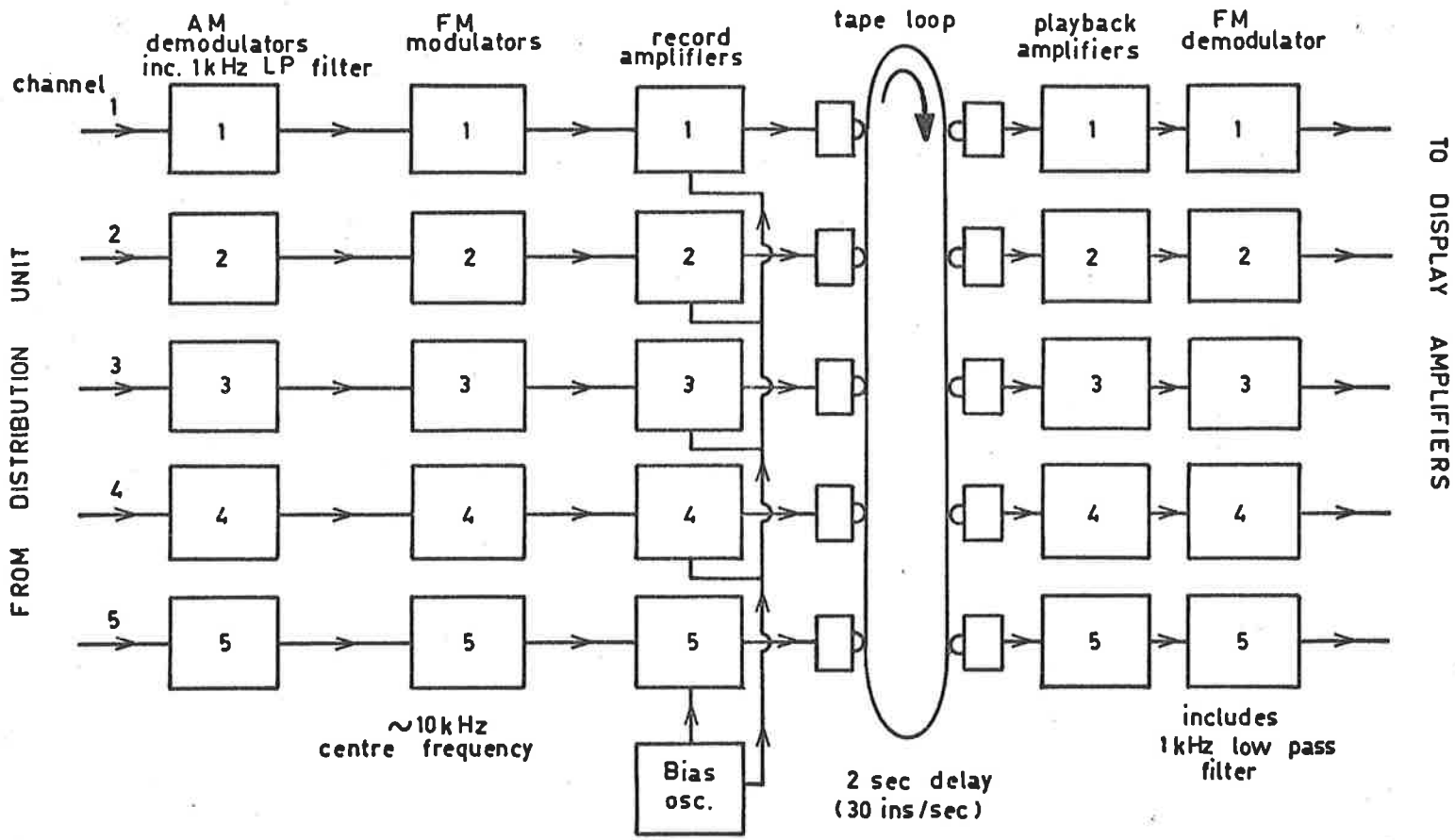

Figure 5.10: Block diagram of the tape delay system used in recording the whistle waveforms.

aligned so that the timing errors (< 200 μsec) between the two most widely separated tracks are much smaller than the timing accuracy required in the measurements (± 2 m sec).

On replay the modulated signals are amplified by conventional playback amplifiers and fed into a zero-crossing detector. The width of the pulses at the output of this detector is set to half of the period of the undeviated carrier. The position of these pulses in time depends on the original modulating signal. The pulse train is passed through a low pass active filter with a 1 kHz cut-off frequency. The output from this filter is of the same form as the original signal at the input to the voltage controlled oscillator. The signals are finally displayed on three oscilliscope tubes.

The Shackman camera used for this display has been modified to give a film speed of 1.9 ins/sec. In all other respects this camera is identical to those used in the wind shear and mean wind recording systems. The recording sequence is slightly different to the wind shear sequence because of the delay due to the tape loop. The 'clutch pulse' causes illumination of the clock face during the 1.5 sec delay period before the oscilliscope tubes are brightened and the camera clutch engaged.

The purpose of the tape delay unit is to act merely as a temporary store for the signals which originally appeared at the output of the 27 MHz receivers; thus the signal to noise ratio at the display stage ideally should be as good as the signal to noise ratio at the input to any of the receivers. In the case of the receiver at the main station this is essentially achieved; however the signal to noise ratio for the other stations is degraded by the link telemetry system. For the remote stations, reasonable records of the "whistle" are possible for trails above a limiting electron line density of about 5×10^{13} electrons/metre.

The main frequencies of interest with the velocity recording equipment are between about 20 Hz and 150 Hz.* Over this frequency range the equipment has a linear amplitude response to within 5%; the phase variation over this frequency range is less than 20^{o}. The dynamic range is restricted and only covers some 16 db so that clipping of the later parts of the whistle waveform can occur for the larger echoes.

---

*The upper limit is set by the method of data reduction. A maximum of nine full cycles of the whistle are used in the determination of the velocity of the meteoroid.

(iii) Mean Wind Recording

Signals from the three principal direction finding aerials (numbered 1, 2, 3 in Figure 5.2) are switched asymetrically between two receivers. Their outputs are displayed on a double beam oscilliscope tube and hence appear as "light" and "dark" traces on the film. The supplementary direction finding aerials 4 and 5 are connected to the two doppler receivers and the outputs displayed on another double beam oscilliscope tube as shown in the block diagram (Figure 5.8). One of these doppler receivers is also used to sense the occurrence of a meteor echo as described earlier.

The range of the reflection point is recorded using a conventional intensity modulated A-scan display. A wide band receiver (150 kHz) is connected to a sixth dipole and its output intensity modulates another oscilliscope tube in the display. The time base and range marker generator is triggered by the output of an additional wide band receiver connected to a horizontal three element Yagi array beamed on Adelaide. This ensures that the timebase is always triggered on the ground wave pulse even when the sky wave amplitude (as received on a dipole) exceeds the groundwave level.

The recording sequence is almost identical to that used in the wind shear recording equipment. For a short interval towards the end of the sequence the input to the display is switched to ground. This enables corrections for trace alignment to be made during film reading as well as indicating any changes in signal levels.

5.4 FILM RECORDS

The film records from the velocity display (a), the shear display (b) and mean wind display (c) are shown in Figure 5.11. The traces (reading from top to bottom) in Figure 5.11(a) and (b) are Buckland Park, Sheedys, St. Kilda, Direk, Spare (normally St. Kilda repeated) and Glenthorne. The whistle patterns of Figure 5.11(a) show that this echo was received in the order Direk, St. Kilda, Sheedys, Buckland Park. The time scale is indicated by the sense spikes which are quite evident particularly during the doppler beat waveforms. These spikes (0.02 sec apart) have been considerably distorted (unfortunately) by the various filter networks used in the link telemetry and tape recording process.

The record of Fig. 5.11(b) shows the presence of wind shear. The initial whistle does not appear, since it precedes the main echo which triggers the camera. The line of sight drifts are (from top to bottom)

- 88 metres/sec at Buckland Park
- 85 metres/sec at Sheedys
- 90 metres/sec at St. Kilda
- 93 metres/sec at Direk
- metres/sec at Glenthorne (no echo present).

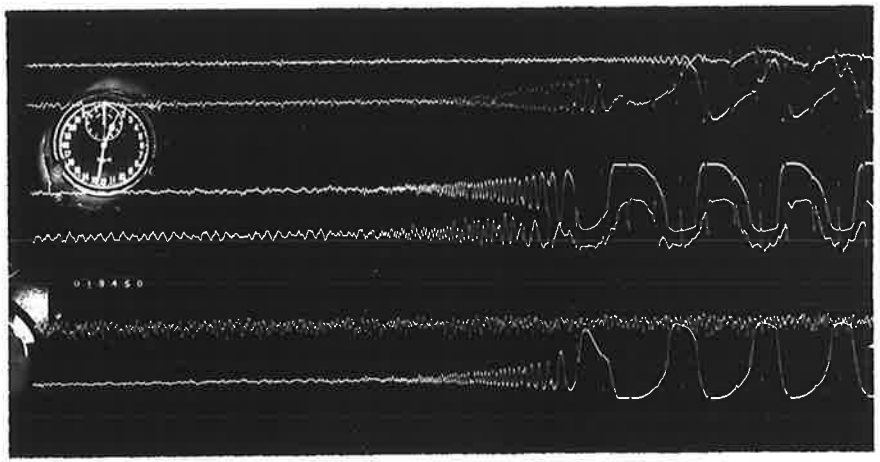

a

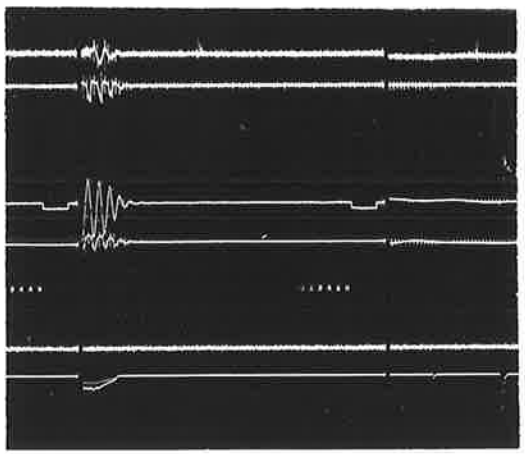

b

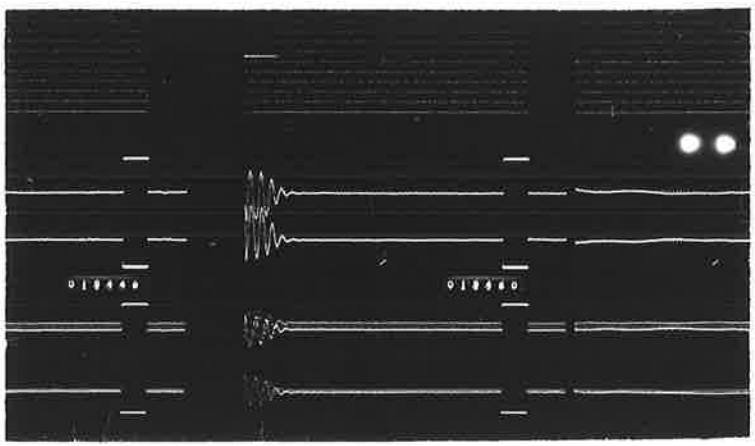

c

Figure 5.11: Films from; (a) velocity display showing whistles, (b) mean wind display showing doppler waveforms at each outstation, (c) wind display.

The lower trace shows the variation in the amplitude of the echo received by the radar receiver.

Before the meteor velocity and separation distances can be determined from Fig. 5.11(a), a knowledge of the range and direction cosines of at least one reflection point are required. This information is contained in Fig. 5.11(c), the echo received on the main station (St. Kilda) equipment. The upper trace is a conventional radar scan, the equispaced dotted horizontal lines being range markers (20 km intervals). The slant range at 150 km is clearly visible. The next two traces are the outputs of the two "doppler" receivers. The "sense spikes" on the trace caused by the phase modulation of the transmitter are plainly visible. Since the wave traced out by these spikes lags the doppler beat, the trail drift is towards the observer. The lowest four traces show the relative phase at the three D.F. aerials. These three aerials are switched asymmetrically between two receivers, the upper brighter trace and the lower lighter trace are both derived from the same aerial (aerial 2 in Fig. 5.2). The presence of this extra trace simplifies film reading and helps correct for any small mis-alignment of the camera and oscilliscope in the display.

Local time is recorded by the clock in the orbit display and also separate clocks in each of the other displays. Individual echoes are correlated by means of the electronically flashed counters.

5.5 SUMMARY OF SYSTEM PARAMETERS

For ease of reference a complete set of specifications for the Adelaide Radio-Meteor System is given below:

Location: $34^{\circ}\ 43'$ S, $138^{\circ}\ 35'$ E

Main Transmitters

(a) C.W.

Frequency: 26.773 MHz
Power at antenna: 1500 watts
Modulation: phase - retarded linearly by 90° in 80 μsec and restored to zero in 20 msec
Antenna: half-wave dipole, $\lambda/4$ above ground

(b) Pulse

Frequency: 27.540 MHz
Power at antenna: 65×10^3 watts
Pulse width: 8 μsec
Repetition rate: 200 sec^{-1}
Antenna: half-wave dipole, $\lambda/4$ above ground

Main Receiving Station

Receiver Bandwidth: Doppler and DF - 7 kHz
Noise figure: < 2 db
Dynamic range: 34 db
Receiver Bandwidth (Radar): 150 kHz
Antenna: half-wave dipoles, $\lambda/4$ above ground

Outstations

(4 off)

27 MHz Receiver Bandwidth: 6 kHz
Noise figure: < 3 db
Antenna: half-wave dipole, $\lambda/4$ above ground

Telemetry Links

(4 off)

Frequency: 167.02 MHz
or 162.34 MHz

Power: 15 watts max

Deviation: 5 kHz

Sub-carriers: 2 kHz and 3.5 kHz

Antenna: four element Yagis.

The system accepts meteor echoes from all azimuths and from elevations within 60° of the zenith. For details of meteor rate and system accuracy see later (Chapter VI).

CHAPTER VI

METHODS OF DATA REDUCTION

6.1 FILM READING

The large number of echoes recorded by a radio-meteor system presents a problem in data handling which can only be solved satisfactorily with the aid of a large digital computer. All of the information obtained by the Adelaide Radio-Meteor System is recorded on film and hence must be digitised. If the film is to be read and the data punched onto cards within a reasonable time some form of semi-automatic facility is required. The wind and shear films were read on a specially designed film-reader (Stone, 1966) which converted the information on the film to digital form and punched this information on computer cards. The velocity films required better resolution and were read on a Telereader at the Weapons Research Establishment, Salisbury. Temporal calibration of the records was possible using the "sense spikes" which appear on all of the film records. These spikes are locked to the mains frequency so that, on the average, five spikes are equivalent to 100 msec.

The selection of suitable records for reduction and subsequent detailed film-reading were long and tedious tasks. The overall sequence of operations, all involving time measurement only, is described below:

(i) The films from the mean wind display were read in the standard manner to produce the line-of-sight component of the wind and

direction cosines of the reflection point. In order for an echo to be acceptable at least one cycle of doppler beat had to be present so that the phase differences could be read uniquely.

(ii) The films from the velocity display were read if there was a usable whistle from at least three stations, and the wind film had been read for that echo. A note was taken of any other usable echoes for which there was no wind information.

(iii) The shear film was read for the line-of-sight motion at all the reflection points.

(iv) Those echoes which had been noted in stage (ii) as having usable whistles were re-read for wind information where practicable.

Quite early in the digitising stage it was realised that the reasons for neglecting an echo at stage (i) above severely restricted the number of echoes that could be read in stage (ii). Short duration echoes were often excluded at stage (i) even though whistle waveforms were readable. Because of a variable signal to noise ratio in the telemetry system a severe selection effect was also placed on the usable echo rate. At least four cycles of the diffraction waveform at three receiving sites were required for the echo to be considered acceptable and hence many small amplitude echoes had to be rejected.

6.2 DETERMINATION OF REFLECTION POINT SEPARATION

As discussed in § 4.4 the velocity of the incoming meteoroid may be determined from the diffraction waveform. In the case of a CW system the analysis is made more complicated by the presence of a ground wave vector which remains stationary while the skywave vector rotates slowly due to the presence of a wind. The phase angle of the reflected skywave relative to the direct ground wave can vary greatly over the diffraction pattern depending as it does on the rate of drift of the trail. However this variation in phase angle can be found from the Doppler beat between the ground wave and the skywave and hence can be extrapolated back into the diffraction waveform as described by Mainstone (1960

The diffraction waveforms observed prior to the specular reflection point would be expected to follow theoretical predictions reasonably closely since distortion of the trail by wind shear and diffusion are only small effects at this early stage in the life of the trail. The velocity of the meteor is found by determining the one to one correspondence between points on the echo waveform and on the theoretical Cornu spiral. In practice only the maxima and minima of the signal are used since these points are most easily identified in the presence of noise. With the notation of equation 4.3 the position of a particular point on the Cornu spiral is defined by the value of x, x being negative prior to the t_o point. To determine the value of x for a particular diffraction maximum or minimum it is only necessary to know the order of the Fresnel zone corresponding to that point (by counting the number of maxima or

minima between the point and the t_o point) and the value of the phase angle, ψ, over the spiral.

Provided that the phase of the skywave at the t_o point, ψ_o, is known then a plot of the set of points (x_i, T_i), where T_i is the time of occurrence of a particular maxima or minima, should lie along a straight line the slope of which is proportional to the velocity of the meteoroid and the intercept T_o is the time at which the specular reflection point is reached.

The method of analysis used on the records obtained is based on that proposed by Nilsson (1962). An estimate of the value of ψ_o is made by inspection of the record. This value is used as a datum in calculating the expected position, x, of the various maxima and minima (allowing for the varying phase of the skywave due to the wind). If ψ_o is in error then the best fit curve to the value of x against time of occurrence T is no longer a straight line but a curve which approaches a straight line for large values of x. Figure 6.1 illustrates this for one particular echo.

Inspection of equation (4.6) indicates that the positions of the first few maxima and minima on the theoretical spiral are very sensitive to the value of ψ_o used, whereas, as can be seen in Figure 6.1, little change occurs for later maxima and minima. This fact suggests an iterative procedure to determine the best value of ψ_o. A computer program has been devised which compares the slope of the best fit straight line to the first three data points with the best fit straight line to

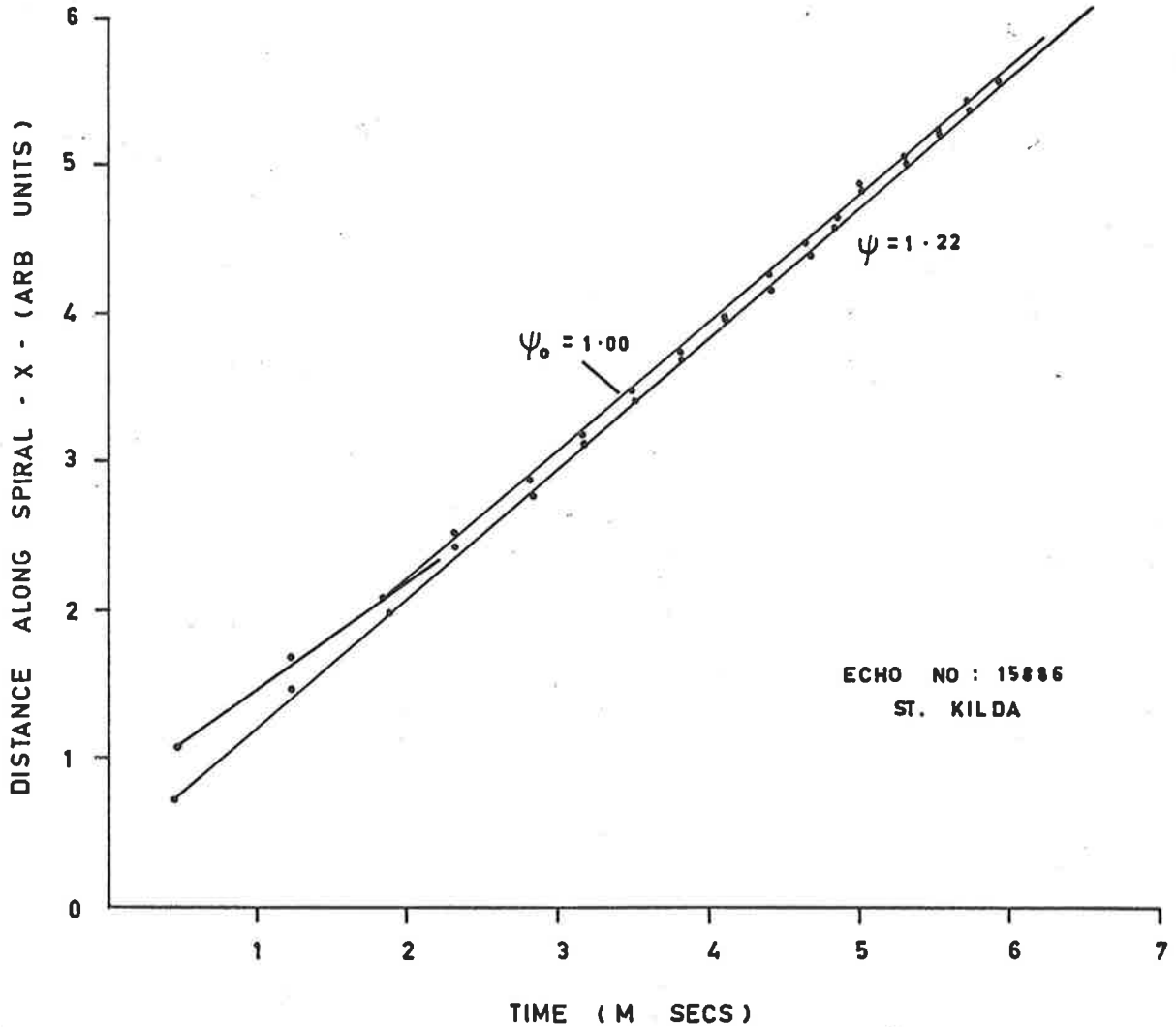

Figure 6.1: The time of occurrence of a maximum or minimum of the diffraction pattern for echo number 15886 plotted against position on the theoretical Cornu spiral for two estimates of ψ_o.

the remaining points. The estimate of ψ_o is then varied in discrete steps until the two slopes agree to within specified error limits. This value of ψ_o is accepted as the best estimate. The corresponding slope, V, of the best fit straight line to all the data points is used as a measure of the meteoroid velocity for the particular outstation record concerned, while the corresponding intercept T_o locates the position of the specular reflection point in time.

If the discrepancy between the slopes computed for each of the outstation records (normally four) is larger than 10% of the mean then the data for that particular meteor echo is considered of doubtful reliability. Often such discrepancies are due to excessive amounts of scatter in the positions of the first few data points. A mean slope for a particular echo is determined by weighting the slope determined for each record by the number of diffraction maxima and minima used. The velocity of the incoming meteoroid can then be determined from this mean slope since the range of one reflection point is known. Time differences between the specular reflection points for the various receiving sites are determined using one particular "sense spike" as a time reference.

The separation of the reflection points along the trail is given by,

$$S_i = v(t_i - t_3), \; i = 1,2,4,5$$

where v is the velocity of the meteoroid and the t_i are the times of arrival of the meteor at each reflection point using the time of arrival at St. Kilda, t_3, as a reference. These reflection point spacings depend

on the ground geometry and the direction cosines of the trail. The direction cosines of the trail can be determined using the solutions given by Nilsson (1964) for three reflection points. Usually four reflection points were used and the extra redundancy enabled a "best fit" set of trail direction cosines to be determined by allowing the mean velocity and values of t_i to be varied within prescribed limits.

A combination of the velocity of the meteoroid and the direction cosines of the trail make it possible to determine the elements of the orbit of the meteoroid. In fact this method is being used to determine southern hemisphere meteor streams using the data collected in the current survey.

6.3 DATA STATISTICS

The reliability of the wind and shear measurements made with a radio meteor system can only be assessed if the distribution of meteors in height and time is known. Any changes or variations in either of these distributions may influence the accuracy of the results.

Because of the large amount of time required for data reduction the equipment in Chapter V has only been operated for five to seven days each month. The multi-station equipment was operated from December 1968 to June 1969 and again in October 1969, although the mean wind equipment in its present form has been in regular monthly operation since June 1966.

Some 22,000 feet of film was exposed during the multi-station survey. About 60% of this film was used in the fast recording camera of the velocity display system (described in § 5.3.4). The total number of meteor echoes recorded over the main period of interest was about 50,000 of which approximately 17,000 were useful for wind measurements. Table 6.1 shows the percentage of echoes rejected for the categories listed. Only about 1400 echoes were useful for shear determination, the main limitation being the requirement of usable diffraction waveforms.

Type of Echo	Percentage Rejected
Decay too rapid	34
Distorted waveform	17
Amplitude too small	10
Doppler frequency too small	4
Inconsistent phase	1
Range inderterminable	1
Amplitude too big	1

TABLE 6.1: PERCENTAGE OF ECHOES REJECTED FOR WIND MEASUREMENT. DATA SAMPLE USED CONTAINED 2520 ECHOES

Because of the difference in numbers, the statistics for the mean wind determination will be presented separately from those relating to shear determination. Table 6.2 shows the total number of useful echoes recorded on each of the days in the period December 1968 to October 1969. The rates given do not represent the true influx of meteoroids since no

Month	Dates	No. on Each Day							
Dec. 1968	10 - 16th	90	246	226	243	323	239	169	
Jan. 1969	20th - 25th	188	429	407	250	330	254		
Feb.	10th - 17th	289	300	355	448	504	452	342	333
Mar.	18th - 23rd	439	287	408	471	601	434		
Apr.	14th - 19th	218	459	359	195	406	343		
May	12th - 18th	336	323	410	364	294	241	262	
June	8th - 14th	389	298	398	484	473	432	465	
July	20th - 26th	181	557	561	569	516	688	269	
Aug.	10th - 16th	138	619	627	569	570	674	219	
Sept.	15th - 22nd	205	271	144	192	88	262	184	237
Oct.	5th - 9th	203	481	340	394	362			
	15th - 19th	167	749	782	771	655			

TABLE 6.2: THE NUMBER OF USABLE METEORS RECORDED ON EACH DAY OF OPERATION OVER THE PERIOD DECEMBER 1968 TO OCTOBER 1969

allowance is made for variations in the sensitivity of the system. In particular during some days severe forms of interference were encountered which substantially depressed the number of useful records.

The diurnal variation in meteor rate is plotted in Figure 6.2 which shows the total number of usable echoes recorded during a given hour of local time for the period December 1968 to June 1969. The total number of hours during which the equipment was operating is also shown. The ratio of the maximum at 0600 hours local time to the minimum at 1800 hours local time is about 6. This diurnal variation in meteor rate is due to the passage of the earth through the background of sporadic meteors. The diurnal variation in the rate of meteors used in wind shear determination is also shown in Figure 6.2. The number of multi-station echoes has been multiplied by ten before being plotted so that a comparison can easily be made between the two curves. The difference in the shape of the two curves is due to the influence of interference on the multi-station equipment.

Two types of interference were encountered, local man-made impulsive interference and interference due to ionospheric effects. The impulsive form of interference caused the main receiving equipment to trigger randomly and during the recording cycle which followed the diffraction waveforms from genuine echoes were often lost. The worst forms of interference weredue to the presence of signals from an illegal transmitter operating in Indonesia and also to ground backscatter of some CW transmitter power via the ionosphere. Because of the long range involved

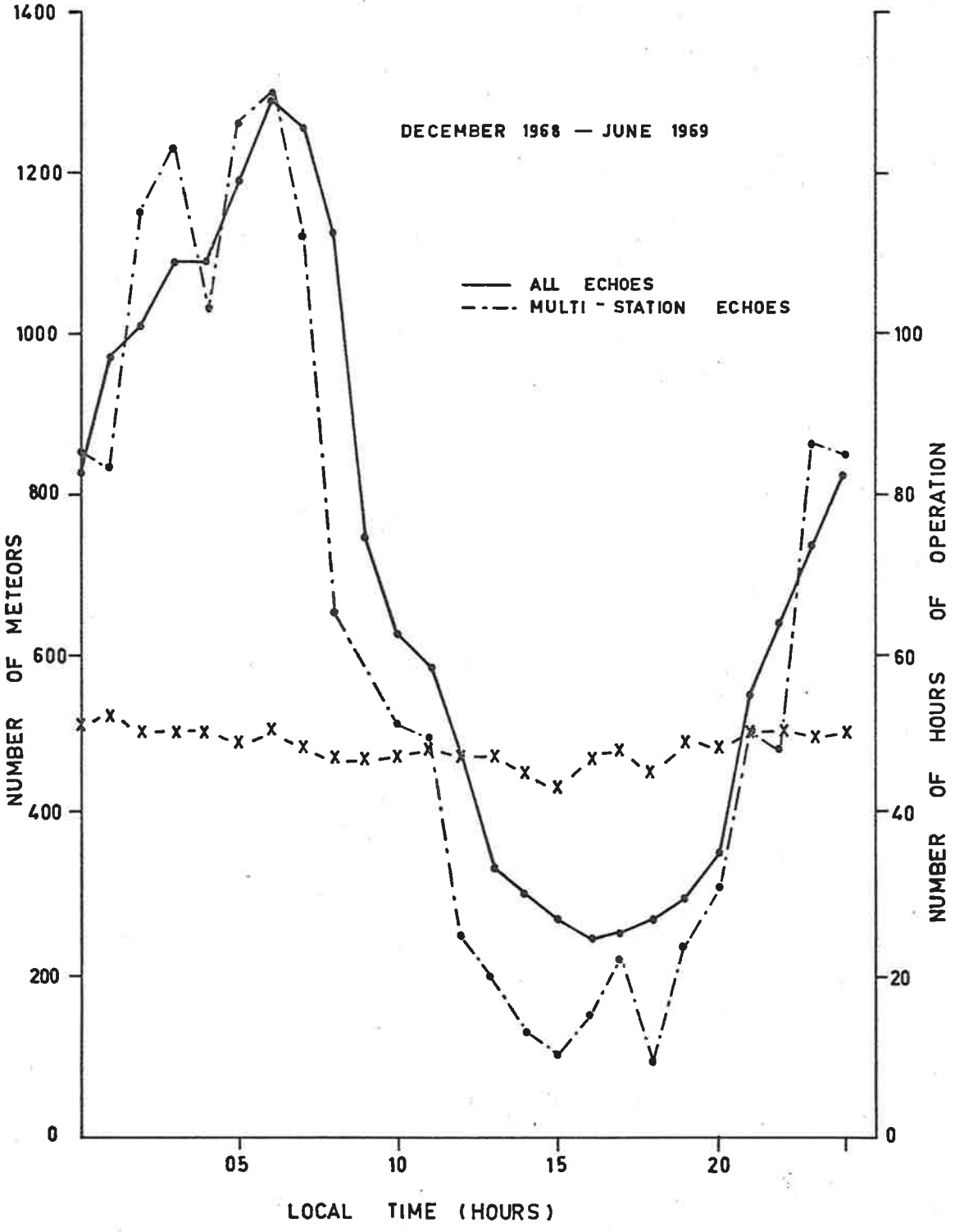

Figure 6.2: The diurnal variation in meteor rate for all echoes, and for multi-station echoes. The crosses show the number of hours of operation of the equipment for each hour of local time.

in this latter case the "sense spikes" for the return signal were quite wide (5 - 10 msec) and of significant amplitude (10-20%) compared with the ground wave signal strength. When such a signal was present together with a reflected signal from a meteor trail considerable confusion could result particularly for the whistle waveform. This backscatter phenomena has occurred in the past near the maximum of the solar sunspot cycle*.

The variation in height of the reflection points for the usable meteors recorded over the interval December 1968 to June 1969 is shown in Figure 6.3. The mean height for these meteors (a total of 17150) is 89.3 km compared with the mean height of 90.2 km for all meteors recorded over the period 1966-1968. The distribution in height of the meteors used for wind shear determination is slightly different and is shown in Figure 6.4, the mean height being 92 km. The slight difference in the height distributions probably reflects the selection effects in the data reduction process which tends to emphasise the number of over-dense echoes. The latter type of echo is of longer duration and thus more likely than an under-dense echo to have the required number of cycles in the diffraction waveform. Thus the distribution of echoes from the multi-station network would tend to be shifted to greater altitudes reflecting the larger number of over-dense meteors.

6.4 DETERMINATION OF THE MEAN WIND

The basic data available from the St. Kilda receiving site for a single meteor echo is;

---

* The Adelaide Radio-Meteor System was inoperative from 1955-1958 due mainly to this effect.

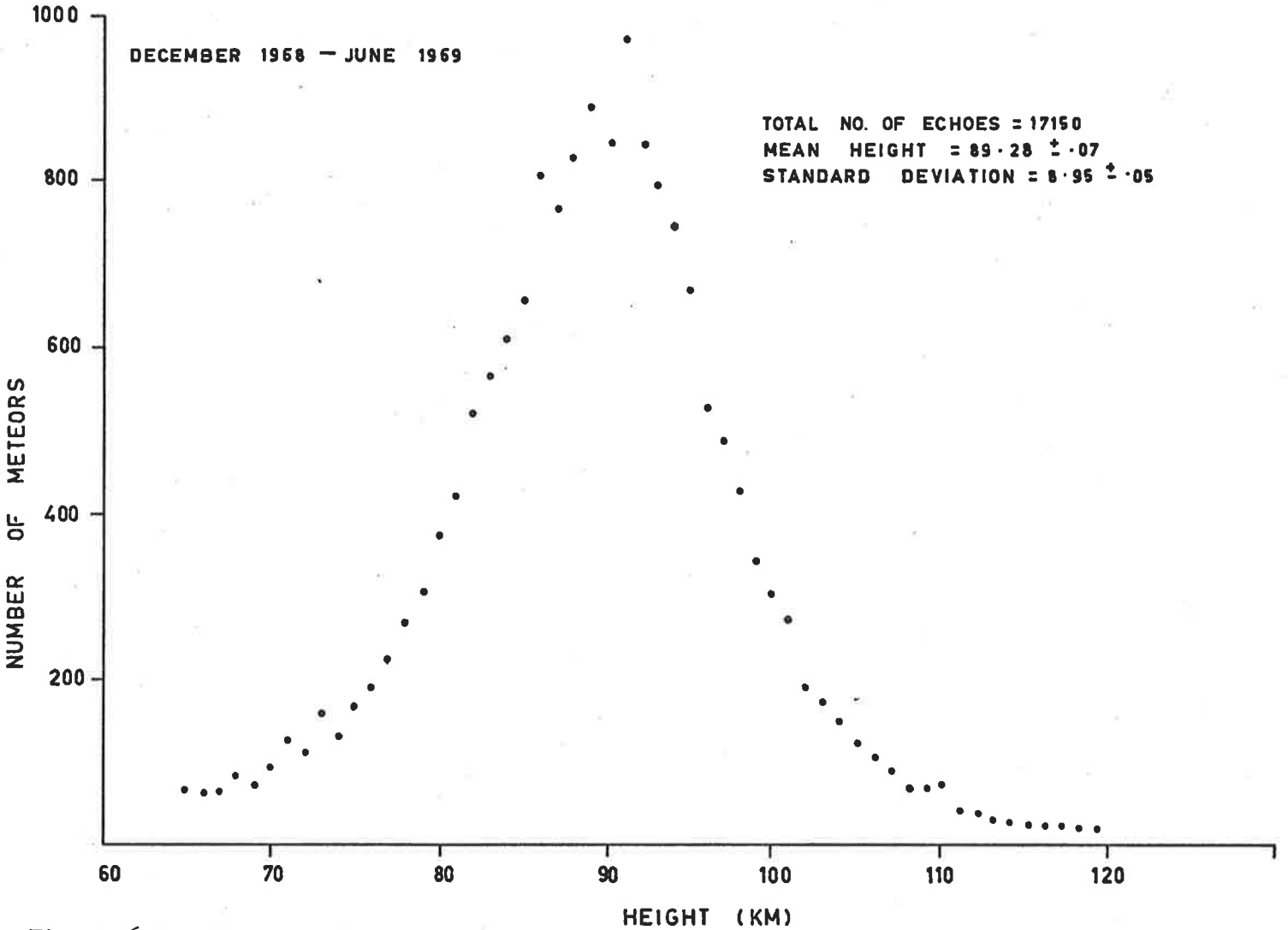

Figure 6.3: The distribution in height of all usable echoes recorded during the interval December 1968 to June 1969.

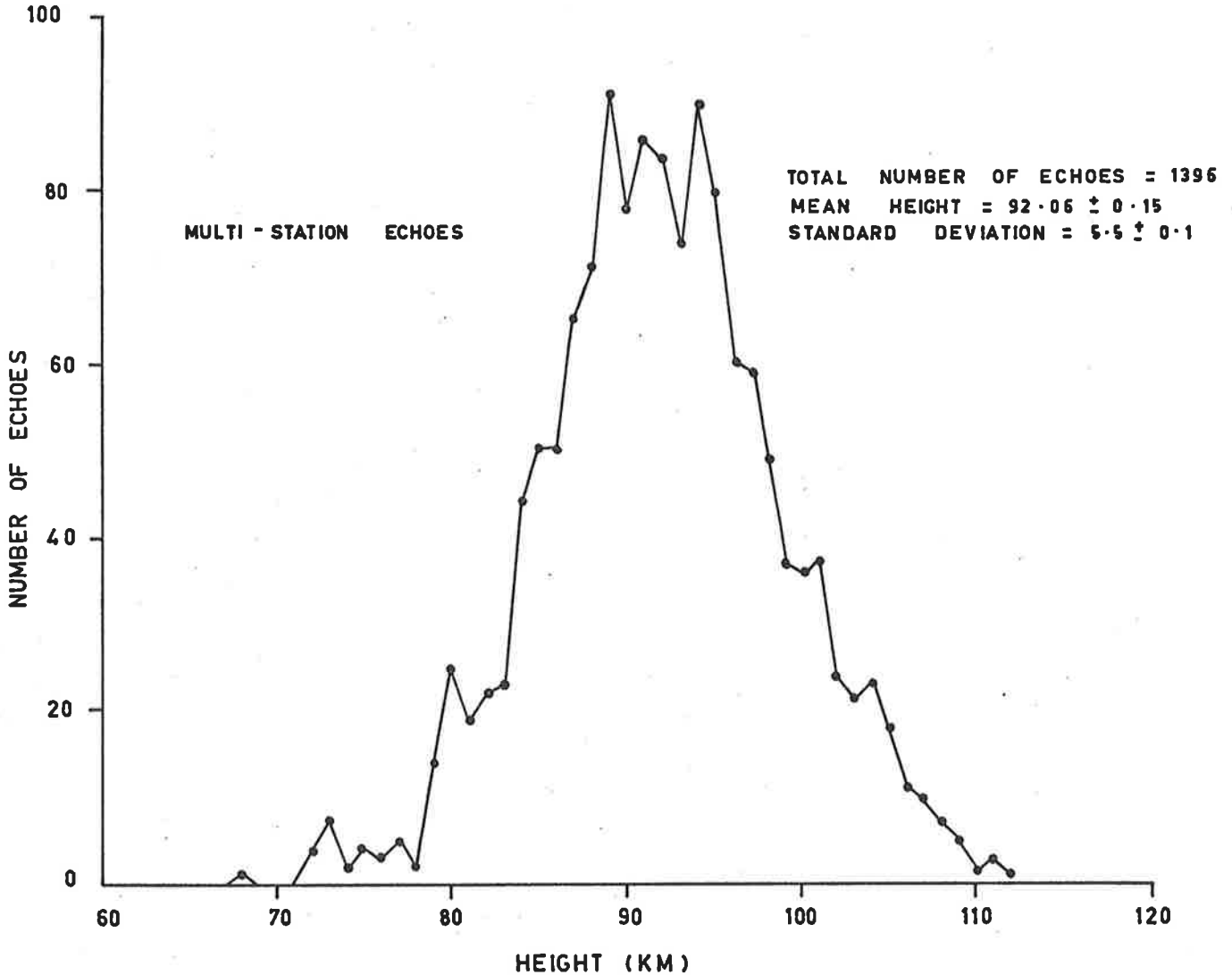

Figure 6.4: The distribution in height of echoes used in the measurement of wind shear.

(i) The direction cosines (l, m, n) of the specular reflection point (error ± 0.02)

(ii) the height of the reflection point (± 2 km)

(iii) the line-of-sight component of the trail drift (± 3%)

(iv) the time (local civil) when the echo was recorded (to the nearest 15 mins).

The horizontal wind at a particular height and time can be determined, in principle, if two line-of-sight velocities are measured simultaneously at the point concerned. This is rarely possible with the large beam-width used in the Adelaide system; the ideal can only be approached at times of very high meteor rate. The usual method of analysis is to find a "best fit" model to represent the data using a least-squares method developed by Groves (1959). A model wind $V_T(z, t)$ is expressed in terms of zonal, meridional and vertical components, (U, V, W) respectively such that

$$V_T = U\underline{i} + V\underline{j} + W\underline{k}$$

where $U = U(z, t, a_{1,n_1})$

$V = V(z, t, a_{2,n_2})$

$W = W(z, t, a_{3,n_3})$

with the a_{k,n_k} ($k = 1,2,3$; $n_k = 1,2, \ldots N_k$) being the parameters of the model. Usually a polynomial variation in height with a periodic variation in time is allowed. For a typical model consisting of N_k harmonics of a fundamental frequency ω with polynomial variations of degree A_{n_k} in each component, the wind components U, V, W have the form

$$U(z, t) = U_o + \sum_{n=1}^{N_k} U_n \cos \{n\omega(t - \xi_n)\}$$

where

$$U_o = \sum_{j=0}^{A_o} u_{o,j} S^j$$

$$U_n = [u_n^2(z) + u_n^{*2}(z)]^{\frac{1}{2}}$$

$$= \left[\left(\sum_{j=0}^{A_n} u_{n,j} S^j\right)^2 + \left(\sum_{j=0}^{A_n} u^*_{n,j} S^j\right)^2\right]$$

$$\xi_n(z) = - \arctan (u_n(z)/u_n^*(z))$$

and where S is a normalised height for the height range z_{min} to z_{max} and is defined as

$$S = (2z - (z_{max} + z_{min}))/(z_{max} - z_{min}).$$

Similar expressions can be written for the components V and W in terms of V_n, η_n and W_n,ζ_n respectively. The fundamental frequency is usually chosen as $2\pi/24$ hours^{-1} and the N_k are usually chosen to be 3, giving 24, 12 and 8 hour periodic components. This choice of N_k can be justified either on the basis of tidal theory or by inspection of periodograms obtained previously (see Chapter VII).

The order of the polynomials used in the model is determined using the following criteria:

(i) The coefficients a_{k,n_k} associated with high order terms in the polynomials should be significant compared with their standard deviations.

(ii) The vertical wind should be no greater than 20 to 30 $msec^{-1}$ since independent observations have indicated that the vertical wind, in general, is small (usually less than 10 $msec^{-1}$).

(iii) The amplitude of the 8 hour tidal components should be small compared to the amplitude of the 24 hour and 12 hour periodic components since previous observations have shown that the amplitude of the 8 hour component is about a tenth of the 24 hour component.

In general the lowest order polynomial variation which adequately represents the data is used. If a polynomial of too high an order is specified the fitting process can become unstable in regions (in either height or time) where there are relatively few echoes. Second or third order polynomials for the zonal and meridional components are normally suitable while first order polynomials are generally used for the vertical component.

Doyle (1968) has shown that a minimum of about 100 meteor echoes distributed throughout the day provide sufficient data to give a stable model for the height range between 80 and 100 km. Even in the presence of a four hour break in the data the amplitude and phase of the 12 hour component remained stable.

6.5 DETERMINATION OF THE IRREGULAR VELOCITY FIELD

The irregular wind field is generally calculated from the total wind field by eliminating the mean wind. The mean wind, in the case of interest, should include all fluctuations with periods greater than

about six hours. Usually the model wind computed for one day as described in the previous section is adequate. However it is sometimes necessary to combine data for several days to improve the reliability of the model.

The initial step in the analysis is to calculate the height of each reflection point on a particular meteor trail using the St. Kilda reflection point height as a reference. As the direction cosines of the trail and the separation of the reflection points along it are known, the height differentials can be readily calculated with an accuracy of about ± 50 metres. The mean wind velocity corresponding to each reflection point can then be calculated from the model. The mean line-of-sight wind component at each reflection point is then calculated and subtracted from the measured line-of-sight wind to give the value of the irregular component.

The structure function (mean square velocity differences for a given separation) has been used as a description of the irregular wind and is found from the following expression

$$D(\xi) = \frac{\sum_{i=1}^{N}(u(r_i + \xi) - u(r_i))^2}{N}$$

where $u(r_i + \xi)$ and $u(r_i)$ are the line-of-sight turbulent velocities measured at two reflection points separated by the distance ξ, and N is the number of observations with this value of ξ. In practice the observations were divided into groups of separation interval as follows; all observed separations less than 100 metres form one group, all with separations between 100 metres and 300 metres belong to the next group,

and so on. Estimates of the variance for each value of D are made since this varies with the number of observations, N. If N is less than about six the value of D for that particular separation is usually ignored because of the uncertainty associated with the mean for such a sma sample.

Some justification for using separations of 100 metres has to be presented since in §4.5 it was pointed out that the size of the reflecting region itself was about 700 metres. However the assumption used to obtain this estimate is that the trail does not depart significantly from linearity over the length of the first Fresnel zone. If the trail is distorted focusing effects occur and segments of the trail of only a few wavelengths in length can give rise to echoes with amplitudes very nearly equal to that from the original first Fresnel zone. Greenhow and Neufeld (1959a) have demonstrated that this effect places a lower limit on the separation of discrete echoes of some 50 - 60 metres. Another factor which can influence the measurement of reflection point separation is the movement of the reflection point along the trail in the presence of wind shear. Using the information given in §4.3.2 with typical values of wind shear (10 m/sec/km) and mean wind speed (30 m/sec) then it can be seen that the reflection point would move about 150 metres in the time necessary to trace out the Doppler cycle needed for the wind measurement.

The limitations discussed above are most important when the separation between reflection points is small. In particular for separations less than about 500 metres the measurements of mean square velocity difference are not generally reliable. This point is discussed further in Chapter VIII where the structure functions are considered in detail.

CHAPTER VII

OBSERVATIONS OF THE PREVAILING AND TIDAL WINDS DURING 1968 - 1969

7.1 INTRODUCTION

This chapter describes the prevailing and tidal winds measured with the radio meteor system during the period November 1967 to October 1969. Results for the period June 1966 to November 1967 have been described by Doyle (1968). The measurements of wind shear presented in the following chapter require the elimination of the 'mean wind' from the data, hence it is natural to discuss this 'mean wind' (the prevailing and tidal components) at this stage. The author was responsible for data collection and analysis over the whole of the interval. The day to day variability in the wind measurements will not be discussed in detail since the variations found are similar to those described by Doyle (1968). Because of the longer period over which data has been collected more emphasis will be given to seasonal variations.

The data for each of the 137 days on which the equipment was operating was analysed separately using the Groves method of analysis described in §6.2. A total of 99 days proved suitable for reliable wind determinations, the minimum number of meteor echoes on any one of these days was 163 and the maximum number 702. The 38 days rejected usually had gaps in the data coverage because of equipment malfunction or severe inter-

ference which prevented successful reading of echoes. Methods of analysing these broken days are still being investigated.

Throughout the discussion of the results the vector convention is used to describe the wind components; the wind is defined to be towards the direction specified. Thus when the wind vector is resolved into its geographic components, a positive wind amplitude refers to a component directed towards the east or north for a zonal or meridional component respectively. The phase of a tidal component is defined as the local time of maximum positive velocity and is expressed in hours after local midnight.

7.2 THE PREVAILING WIND

In an earlier investigation of the wind pattern, Doyle (1968) found much variability in the day to day winds measured over the period June 1966 to November 1967. Most of the variations appeared to be due to fluctuations in the relative strengths of the periodic components (24 hour, 12 hour and 8 hour). However longer period oscillations with quasi-periods of the order of two days were also found in the data; there was also evidence of shorter period variations. Similar variations have been found in the data for December 1967 to November 1969* but are not discussed here.

Because of the variability of the wind discussed above the prevailing wind determined for a single day may not be a true measure of the

---

* More recent data (up to May 1970) is only available for a few days owing to delays in film reading.

mean or prevailing wind at that time of year. However by averaging over groups of three months of data centred on the solstices and equinoxes a reliable measure of the prevailing wind can be obtained. If data for more days (at least six) in each month were available** less severe averaging might be possible. The seasonal averages at 90 km are given in Table 7.1 for each season since Winter 1966. The number of days used in computing the mean prevailing wind is given in column 2. Columns 3 and 4 give the zonal (eastwards) and meridional (northwards) components respectively of the wind. The close similarity between the seasons for different years indicates that sufficient averaging has been done to eliminate the random component from the data.

In general at these heights the magnitude of the zonal wind component is larger than the magnitude of the meridional component, this is to be expected from other measurements and the various wind models that have been developed (see Groves (1969) for the most recent model for the height range 60 to 130 km). The current measurements, showing a consistent reproducibility from year to year, strongly support the model of Groves (1969) for the latitude 35°. Height-season cross-sections for the zonal and meridional wind components are shown in Figures 7.1 and 7.2 respectively. The data is presented at four kilometre height intervals. The intrusion of the winter westward winds above about 95 km is evident with

---

** Data is only available for about three days per month during 1968 and about six days per month during 1969.

Season	No. of Days	Zonal Eastwards	Meridional Northwards
Winter, 1966*	9	16	- 9
Spring, 1966*	38	10	- 6
Summer, 1966*	25	33	19
Autumn, 1967*	24	30	5
Winter, 1967*	18	9	- 8
Spring, 1967*	11	12	7
Summer, 1967	11	22	12
Autumn, 1968	10	36	7
Winter, 1968	10	19	- 12
Spring, 1968	9	7	17
Summer, 1968	14	33	5
Autumn, 1969	15	21	9
Winter, 1969	17	26	- 6
Spring, 1969	18	2	- 1

TABLE 7.1: THE SEASONAL VARIATION IN THE PREVAILING WIND AT 90 km AT ADELAIDE. THE DATA MARKED * IS FROM DOYLE (1968).

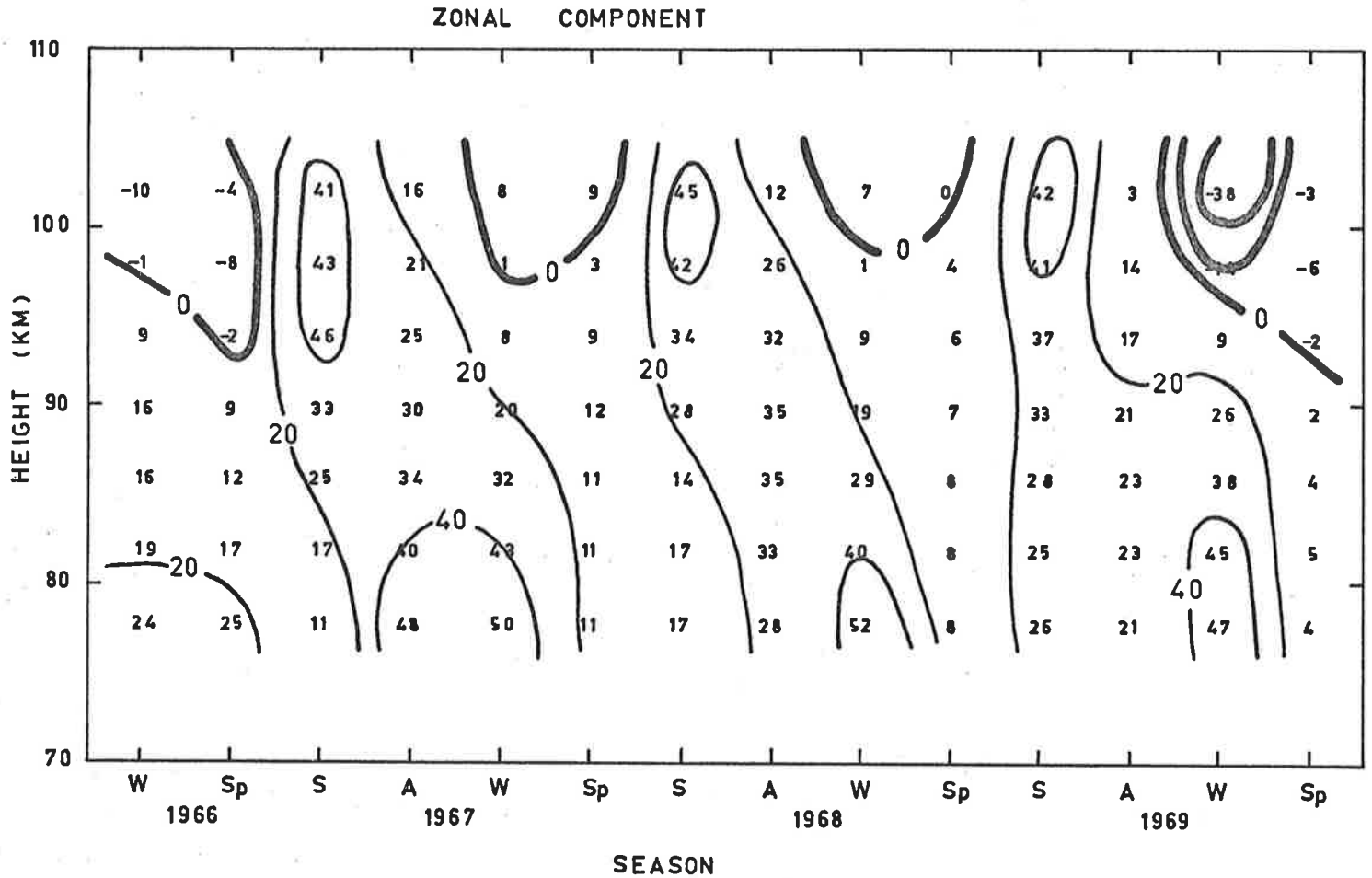

Figure 7.1: The mean zonal component of the prevailing wind for various seasons from 1966 to 1969.

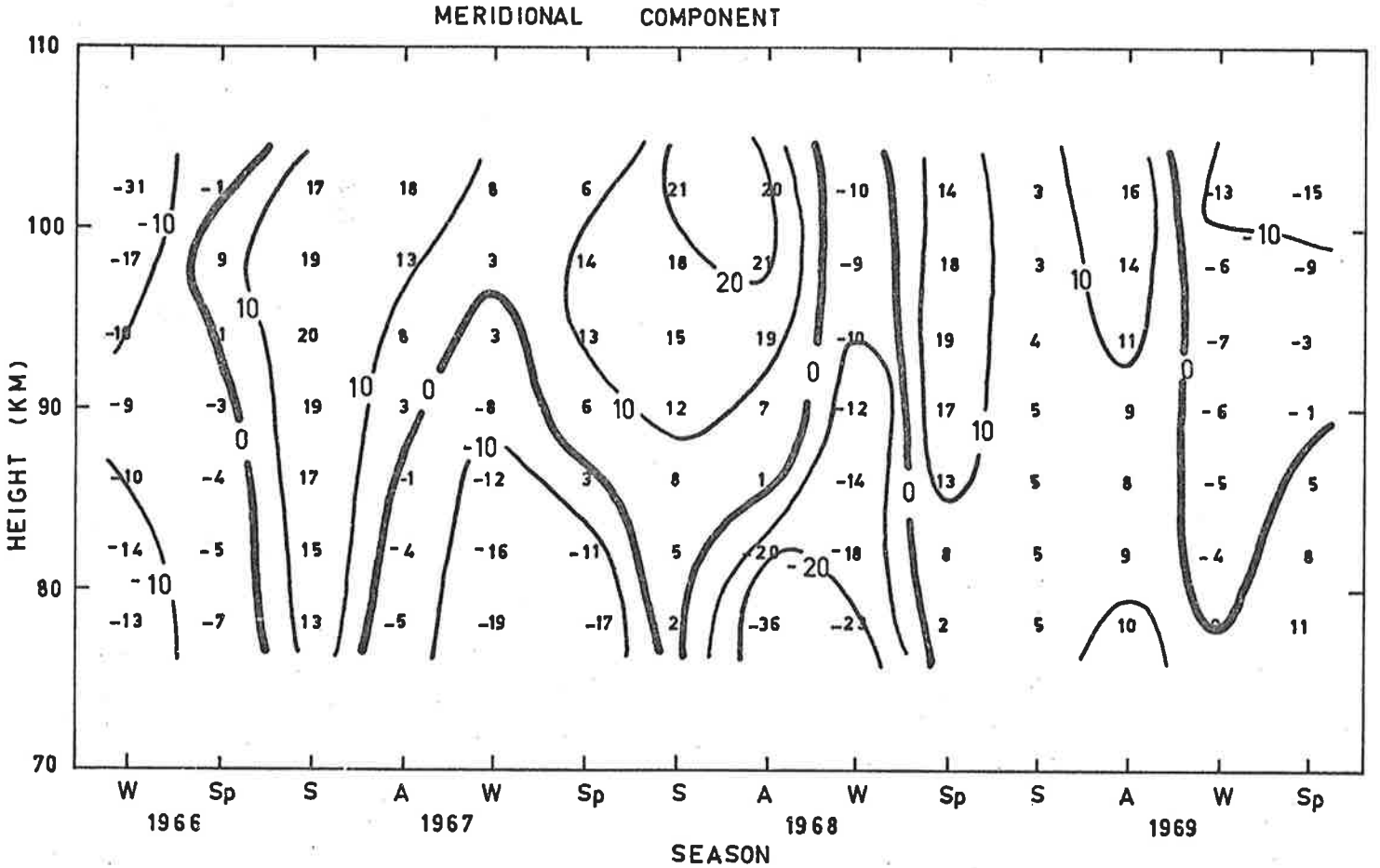

Figure 7.2: The mean meridional component of the prevailing wind for various seasons from 1966 to 1969.

the deep penetration in 1969 being of considerable interest. Below 95 km it appears that the variation in the zonal winds is predominantly due to the monsoonal circulation in the mesosphere with maximum velocities around 60 - 65 km. The meridional pattern is characterised by a flow directed away from the pole (northwards) during the summer and poleward during the winter.

7.3 PERIODOGRAM ANALYSIS

The use of periodograms in time series analysis has not been very widespread. Most of the criticism of the technique has been centred around its use when strict preiodicity is not present in the data. In such a situation periodogram analysis produces a spectral density estimate with irregular fluctuations of large amplitude. Increasing the length of the original time series does not reduce the magnitude of these fluctuations. However it is possible to improve the stability of the spectral estimates by averaging over adjacent frequencies (Jones, 1965). This procedure can also improve the spectrum by reducing the effect of the side-lobes due to the sampling 'window'. The practice of estimating the spectral density by taking the Fourier transform of the weighted autocorrelation function (Blackman and Tukey, 1959) is an equivalent procedure. Since the development of the "fast Fourier transform" algorithm by Cooley and Tukey (1965) considerable interest has been re-established in a modified form of periodogram analysis where the data itself is smoothed initially.

The raw data obtained from the Adelaide radio-meteor system is not in the form of a distinct time series so that normal methods of periodogram analysis cannot be applied immediately. However the method of analysis developed by Groves (1959) is well suited to determine the amplitude and phase for any frequency ω, and can be used to determine a periodogram as described below.

The model fitted to each wind component u_i for each frequency ω by the method of least squares has the form

$$u_i(z, t) = u_{o_i} + u_{1_i} \cos(\omega t - \omega\xi_{1_i}), \quad i = 1,2,3$$

where u_{o_i}, u_{1_i}, ξ_{1_i} have the same form as in §6.2. The normalised height, S, is computed for the height range 75 to 110 km. By trial and error the following criteria were established for the order of the polynomials for each wind component used in the analysis: (i) prevailing and periodic zonal components - quadratic; (ii) prevailing and periodic meridional components - cubic; (iii) vertical component - constant with height but a linear variation in time.

As data is available for five to ten days each month the resolution possible in the periodogram is 0.2 - 0.1 cycles/day. Amplitudes and phases of periodic components were calculated for the frequency range 0.5 cycles/day to 4 cycles/day (periods 48 hour to 6 hour) with a resolution of at least 0.2 cycles/day. To emphasise the fact that the method of analysis used is somewhat different from the usual periodogram

analysis the results are presented in terms of the amplitude, A of the vector which best fits the data at the particular period, τ, of interest thus

$$A(\tau) = \sqrt{u_1^2(\tau) + u_2^2(\tau) + u_3^2(\tau)}.$$

The results of this form of analysis for the month of August 1966 are shown in Figure 7.3 for heights of 81, 91 and 101 km. The data for this particular month were collected over an interval of 20 days, the total number of meteors being 5108. The resolution generally used (0.1 cycles/day) can be improved in this case because of the longer data span. In particular the resolution around the main frequencies of interest (1 cycle/day and 2.0 cycle/day) is extended to 0.05 cycles/day*. The main effect on the appearance of the periodogram can easily be seen in Figure 7.3 where the solid line connects the points at intervals of 0.05 cycles/day, the extra points do not alter the random character of some of the peaks. At 81 km the predominant feature is the strength of the 24 hour periodic component, no other peak can be regarded as significant. At 91 km the strength of the 24 hour component has decreased and at 101 km has disappeared into the background noise. The apparent decay of this 24 hour component with increasing height is in direct contrast with the expected variation from tidal theory and, if real, could mean that a significant amount of tidal energy was being dissipated near 100 km at this time.

---

* The limited computing time available did not permit full resolution over the whole frequency range.

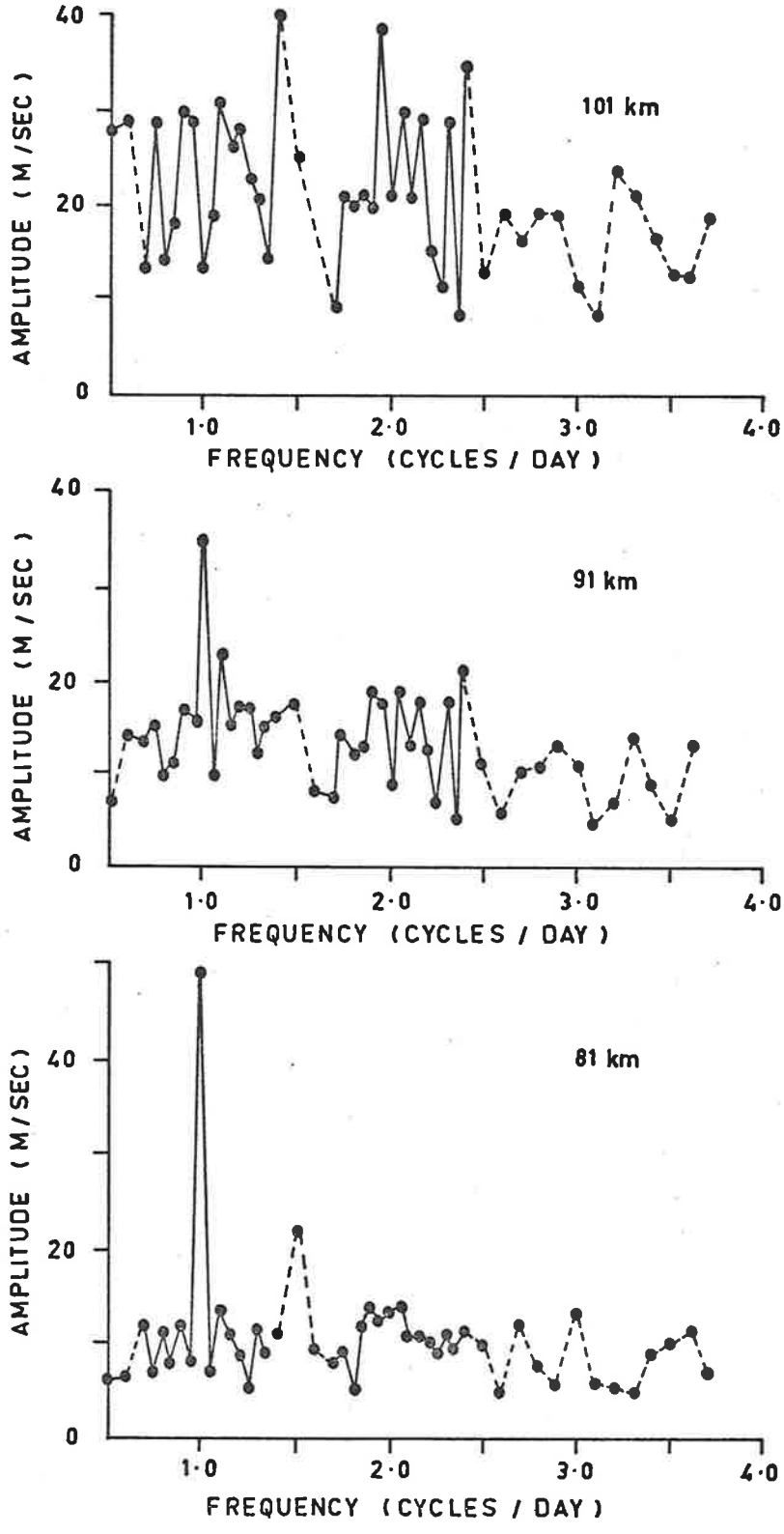

Figure 7.3: The periodograms for August 1966 for the three altitudes, 81 km, 91 km and 101 km.

In the absence of a reliable statistical technique for deciding the significance of individual peaks on the periodogram, a simple non-parametric procedure has been adopted. Separate periodograms computed with odd and even numbered meteor echoes respectively have been compared around the apparent peak at a frequency of 1 cycle/day (complete periodograms were not computed owing to the large amount of computer time required*). Figure 7.4 shows the relevant portions of the three periodograms. The line drawn on these graphs is for all of the data (as in Figure 7.3) and it can be seen that the points for the odd and even numbered meteors respectively would not significantly change the appearance of the peak at any height. Moreover it appears that the differences in amplitude between the three points at a given frequency are of the same order as the fluctuations between adjacent frequencies in the periodograms shown in Figure 7.3 and hence indicates the reliability of the spectral estimates. The decline in the importance of the diurnal tide with increasing height for this month is thus considered to be real and significant.

The variation with height of the diurnal tide shown in Figure 7.3 for August 1966 may not be typical. The periodograms obtained for August 1969, Figure 7.5, show quite different behaviour, the amplitude of the diurnal component increases with height and a significant semi-diurnal component is present. This variability of the tidal component is discussed further in the following section.

---

* The time to produce a full periodogram on the CDC 6400 is about 26 mins.

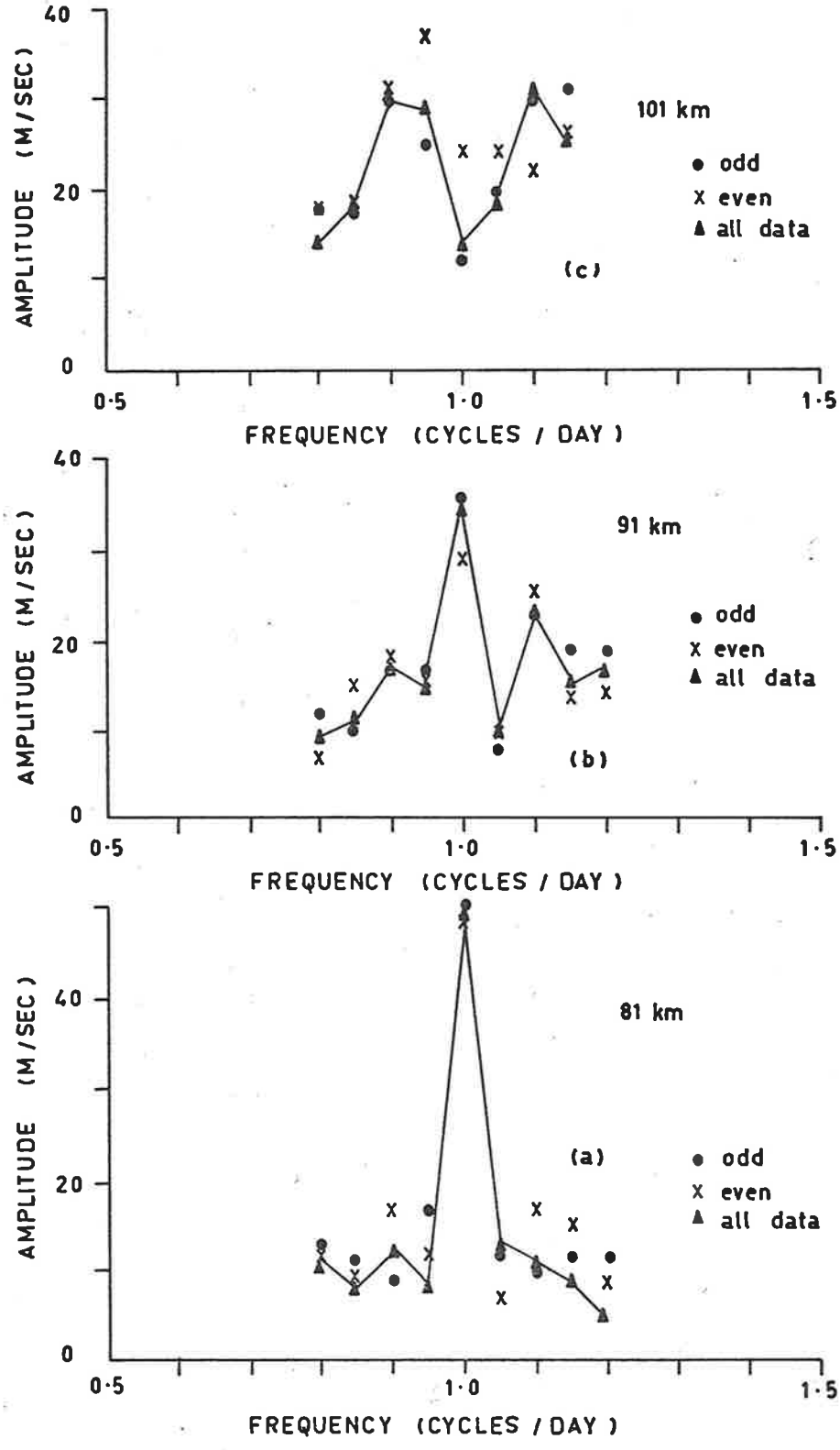

Figure 7.4: Part of the periodogram for August 1966 around the frequency 1.0 cycle/day for three selections of data; all echoes, odd numbered echoes, even numbered echoes.

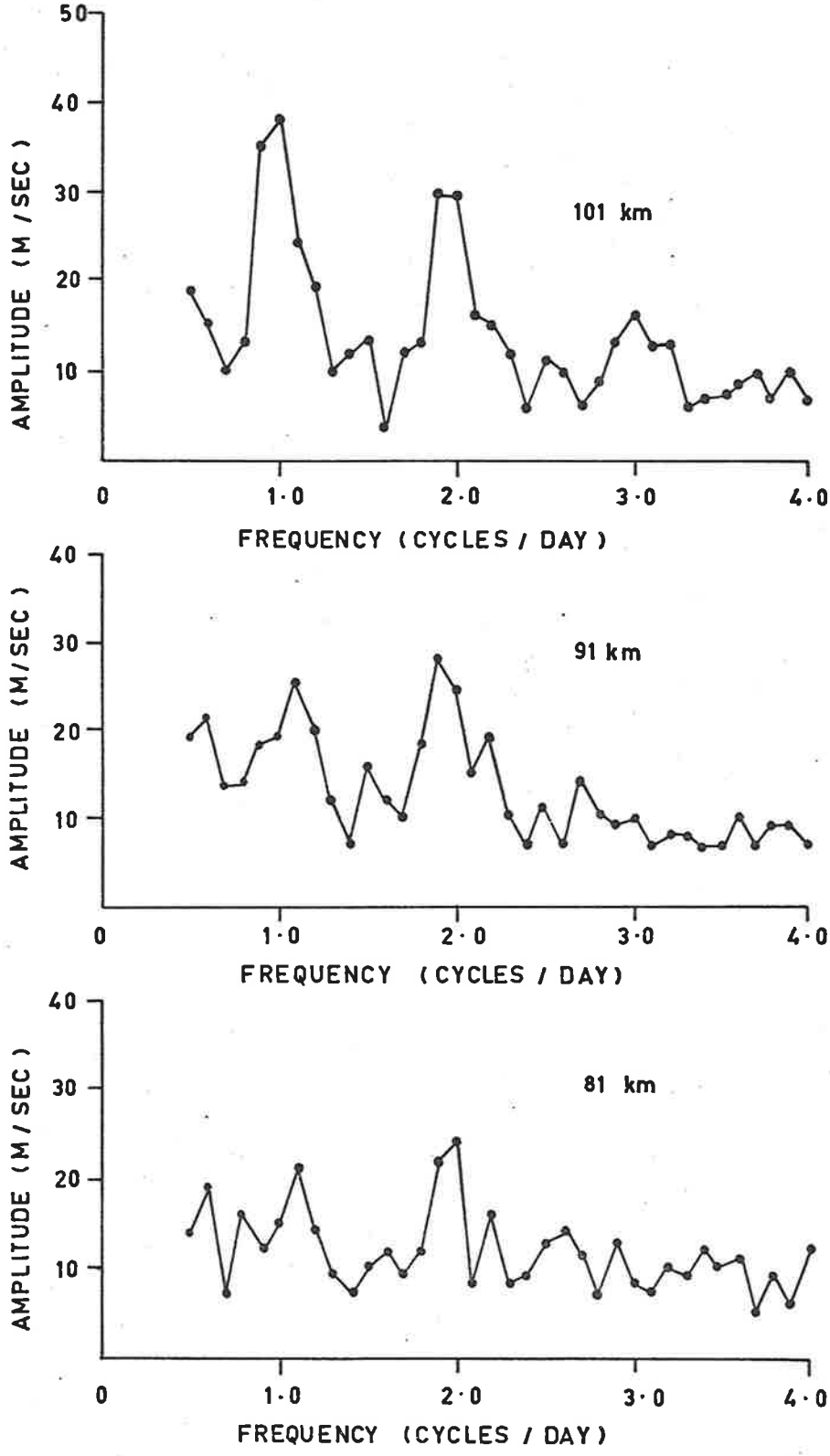

Figure 7.5: The periodograms for August 1969 for the three altitudes, 81 km, 91 km and 101 km.

7.4 TIDAL WINDS

The importance of the atmospheric tides in the wind field of the upper atmosphere has long been recognised and indeed the measurements of tidal winds deduced from radio meteor observations have greatly stimulated theoretical interest. Sufficient data on both the diurnal and semidiurnal tides near 90 km has become available that much experimental effort is now directed in determining the variability in the tidal components. In particular, the recent measurements of Doyle (1968) and Spizzichino (1969) are of interest in this regard.

Spizzichino finds that at Garchy (47°N) the semidiurnal tide is a stable regular oscillation which is well described by theory. In contrast, the diurnal tide is smaller in amplitude, very irregular, and does not fit the relatively simple theoretical model. Doyle (at Adelaide, 35°S) has found that both the diurnal and semidiurnal tides show large fluctuations in amplitude and phase, with the semidiurnal tide generally having the smallest amplitude. She found that similar fluctuations occurred in both tidal components with occassional phase and amplitude jumps with season, particularly near the equinoxes. For 20% of the data the sense of rotation of both tidal components was opposite to that from tidal theory.

In view of the fluctuations observed in the Adelaide results it was decided to make a new attempt to obtain statistically reliable estimates of the tidal components with more recent data. The method of averaging the observations is described first together with an investigation of

the statistical reliability of the mean values found. A comparison of the observational data with theoretical predictions is made in §7.4.2.

7.4.1 The Data

Because the number of days per month for which data is available is small (3 - 4 on average) the data is combined into the three 'Lloyd' seasons (and the whole year) defined as follows:

Name	Symbol	Months Included
December solstitial	D	November to February
June solstitial	J	May to August
Equinoctial	E	March, April, September, October
Yearly	Y	All Data

Probably the best method of presenting the individual amplitude and phases from the Groves harmonic analysis is to use the harmonic dial described by Chapman and Bartels (1940) and strongly advocated by Haurwitz (1964). The individual points on such a plot can scatter widely around the mean and hence it is important to decide whether the mean amplitude and phase computed from a given number of data points, m, has any physical significance. A simple statistical parameter which can be used to assess the reliability of a mean amplitude $\bar{A}$ is the radius of the probable-error circle r_p.

The probability P that the computed mean amplitude $\bar{A}$ could have arisen from the analysis of randomly distributed data is exp $(- q^2)$ where

$$q^2 = m(1 + 1.45\ m\ r_p^{\,2}/(\bar{A})^2)^{-1}$$

Chapman (1951) has suggested that a determination may be considered satisfactory if $\bar{A} \geq 3\ r_p$. It is apparent that when m is small care must be exercised in using mean values.

The amplitude and phase of the diurnal zonal and meridional wind components are shown in Table 7.2 for three heights 80 km, 90 km and 100 km. The observations are combined as shown in the first column of the table. The second column gives the number, N, of days used in each determination. The third and fourth columns give the amplitude $\bar{A}$ and the radius r_p of the probable error circle. In the fifth column the time of the maximum positive wind is shown. Columns 3, 4 and 5 apply to the zonal component while 6, 7 and 8 apply to the meridional. Table 7.3 gives the results of a similar analysis carried out for the semidiurnal wind components. The time of the maximum wind refers to the local time of the first maximum.

Figures 7.6 and 7.7 show the individual data points plotted on harmonic dials for the diurnal and semidiurnal components at 90 km only. Before applying the statistical test for reliability it is necessary to determine whether the points are normally distributed. The probable-error in an individual point (r^*) is $m^{\frac{1}{2}}$ as great as the probable-error in the mean, and if a circle of radius r^* is drawn with the mean as centre then for a normal distribution half of the points should lie outside this circle. This criterion is met for the distributions shown in Figures 7.6 and 7.7 as can be seen using the data in Tables 7.2 and 7.3. The results for altitudes 80 km and 100 km also satisfied the criterion.

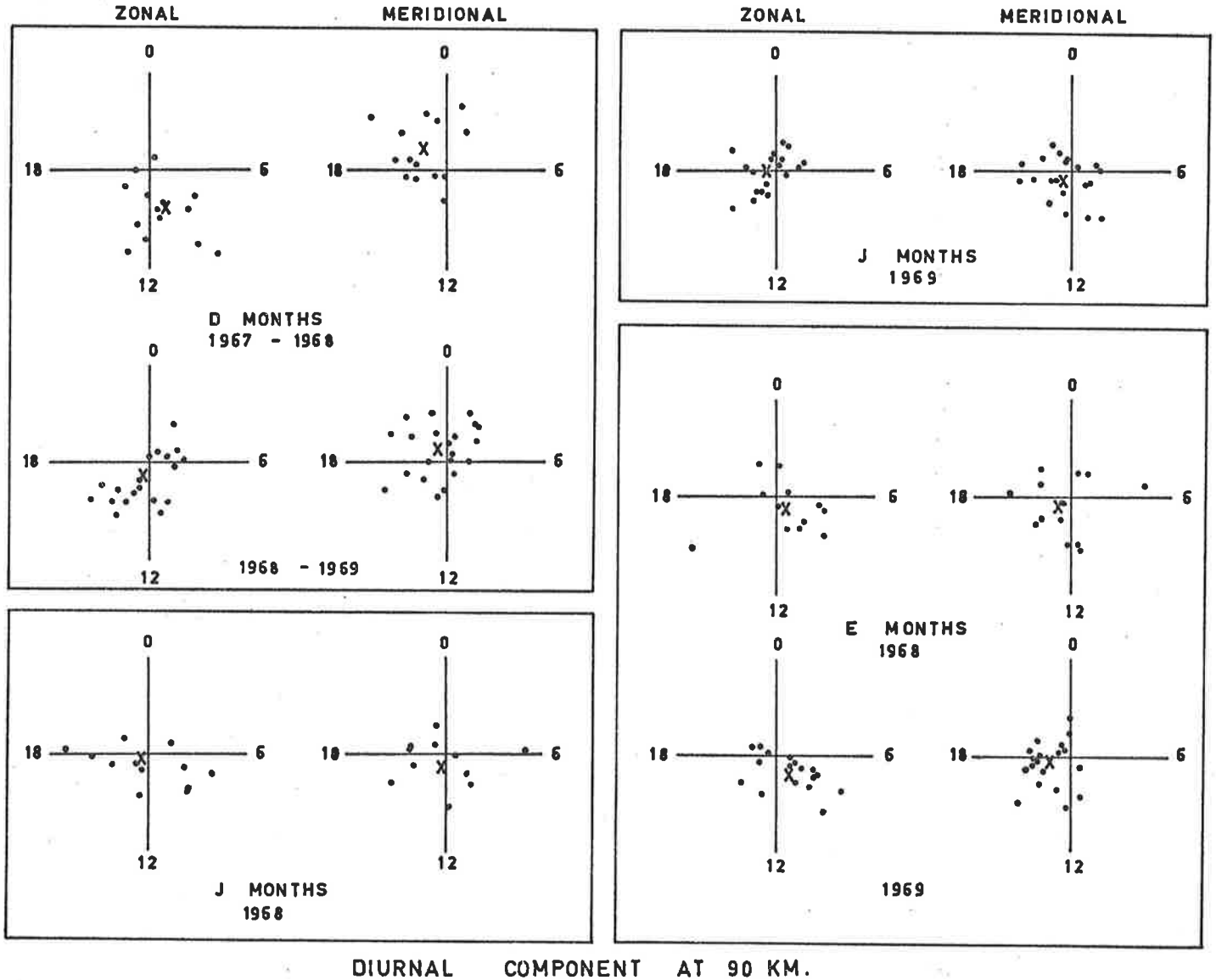

Figure 7.6: Harmonic dials for the diurnal wind component at 90 kms. The mean for each Lloyd season is shown by the cross.

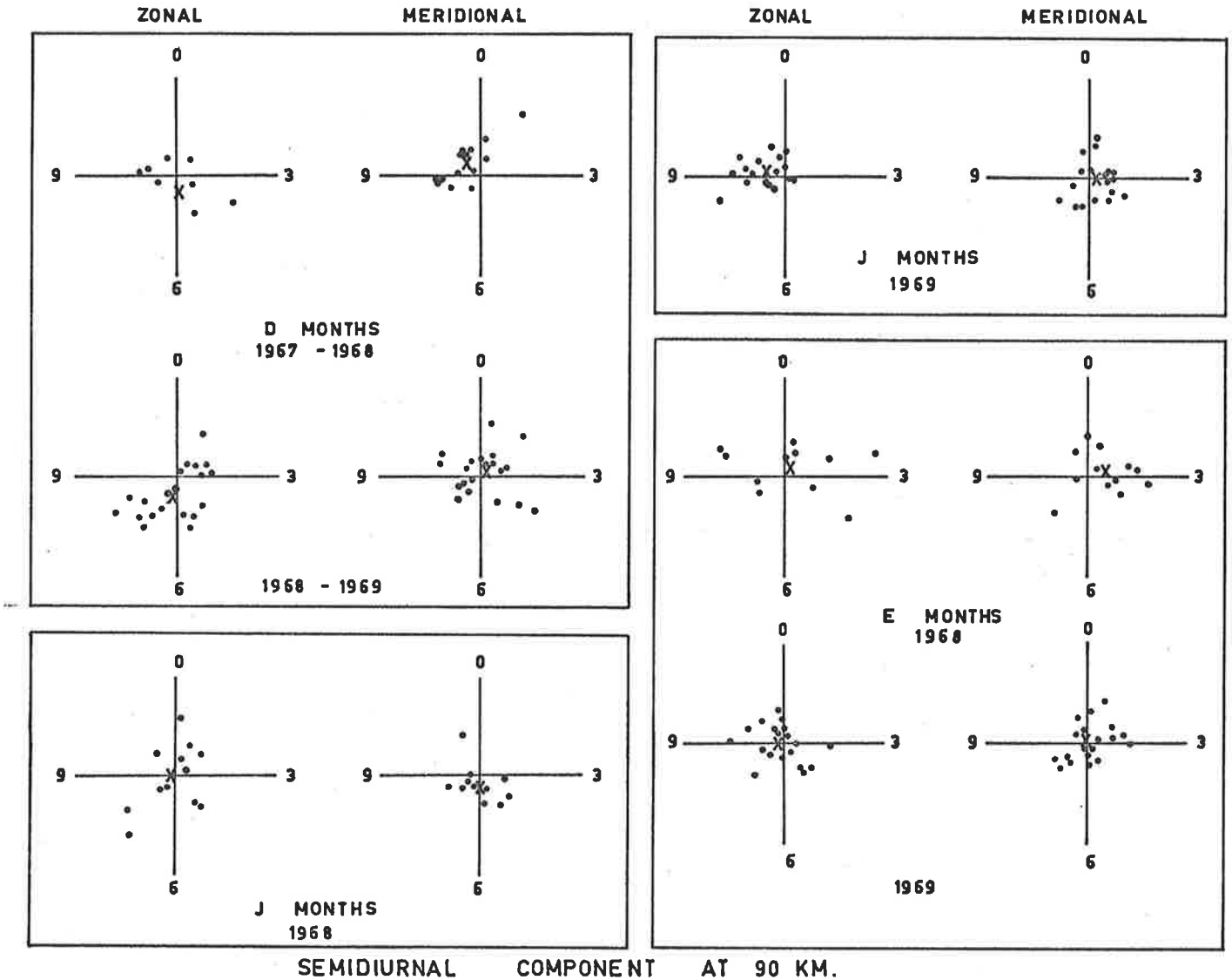

Figure 7.7: Harmonic dials for the semidiurnal wind component at 90 kms. The mean for each Lloyd season is shown by the cross.

DIURNAL SOLAR TIDE

		Zonal			Meridional			
	N	Amplitude (m/sec)	r_p	Phase (hours)	Amplitude (m/sec)	r_p	Phase (hours)	
D, 1968	14	14.2	9.3	14.7	15.9	7.9	20.6	80 kms
J, 1968	12	25.9	12.1	18.5	8.1	7.3	14.6	
E, 1968	13	8.8	11.5	9.1	11.2	9.0	12.1	
Year, 1968	39	10.4	6.9	16.1	6.4	5.0	16.7	
D, 1969	21	17.5	7.8	13.9	5.2	6.0	22.9	
J, 1969	20	25.6	4.9	16.8	8.3	4.0	17.2	
E, 1969	19	21.3	4.5	12.3	14.1	4.1	19.8	
Year, 1969	60	18.7	3.7	14.6	8.2	2.9	19.4	
D, 1968	14	30.7	6.7	10.7	22.0	6.4	21.1	90 kms
J, 1968	12	6.1	8.0	12.9	6.0	7.3	12.5	
E, 1968	13	14.9	5.8	9.1	9.0	7.2	14.8	
Year, 1968	39	17.1	4.4	10.4	7.9	4.4	18.8	
D, 1969	21	13.8	5.0	12.1	11.0	5.0	22.8	
J, 1969	20	5.8	3.6	14.4	6.9	4.5	15.4	
E, 1969	19	16.6	4.3	9.7	17.8	4.2	16.7	
Year, 1969	60	9.0	2.7	11.6	8.3	2.9	18.1	
D, 1968	14	33.5	10.8	9.5	19.1	10.8	20.9	100 kms
J, 1968	12	16.9	11.8	8.7	9.8	12.5	6.4	
E, 1968	13	9.7	14.8	9.3	5.2	14.8	11.1	
Year, 1968	39	20.4	7.5	9.3	3.1	7.5	22.0	
D, 1969	21	13.4	7.8	16.0	20.1	7.8	23.4	
J, 1969	20	9.5	8.0	0.2	6.6	6.7	12.9	
E, 1969	19	11.8	8.2	4.7	9.6	6.5	18.3	
Year, 1969	60	2.1	4.8	23.3	6.9	4.2	21.1	

Table 7.2: THE DIURNAL SOLAR TIDE DETERMINED AT ADELAIDE FOR THREE HEIGHTS, 80 km, 90 km and 100 km.

SEMIDIURNAL SOLAR TIDE

		Zonal			Meridional			
	N	Amplitude (m/sec)	r_p	Phase (hours)	Amplitude (m/sec)	r_p	Phase (hours)	
D, 1968	14	24.9	7.9	6.4	14.2	6.0	10.0	80 kms
J, 1968	12	5.2	10.4	6.1	5.4	4.5	9.5	
E, 1968	13	26.1	10.5	2.6	15.4	9.7	2.1	
Year, 1968	39	10.8	6.2	4.8	5.3	4.4	11.5	
D, 1968	21	7.6	6.9	3.5	6 4	4.6	1.9	
J, 1969	20	0.6	4.0	5.7	2.9	4.0	3.0	
E, 1969	19	1.9	4.6	2.4	0.9	3.3	6.9	
Year, 1969	60	3.3	3.1	3.4	2.9	2.4	2.4	
D, 1968	14	10.7	4.1	5.6	14.2	4.9	10.5	90 kms
J, 1968	12	1.7	6.9	10.5	6.4	4.5	6.0	
E, 1968	13	8.0	7.9	1.7	14.4	5.4	2.4	
Year, 1968	39	4.2	3.8	10.8	3.2	3.1	0.6	
D, 1969	21	2.5	3.7	5.0	5.4	4.1	1.4	
J, 1969	20	12.8	3.1	9.4	6.3	3.6	3.3	
E, 1969	19	3.2	3.9	9.0	2.5	3.7	1.5	
Year, 1969	60	4.7	2.2	21.1	4.2	2.2	2.3	
D, 1968	14	13.3	11.2	11.3	23.9	7.9	11.5	100 kms
J, 1968	12	12.8	11.4	10.6	16.7	8.3	5.6	
E, 1968	13	21.8	15.5	8.9	16.7	9.0	1.9	
Year, 1968	39	13.6	7.5	10.9	7.2	5.6	1.0	
D, 1969	21	4.4	6.0	6.9	7.5	6.0	13.5	
J, 1969	20	17.3	6.3	8.2	11.7	7.2	3.1	
E, 1969	19	16.2	4.6	8.5	7.0	5.2	0.1	
Year, 1969	60	12.0	3.3	8.2	9.2	3.7	2.0	

Table 7.3: THE SEMIDIURNAL SOLAR TIDE DETERMINED AT ADELAIDE FOR 80 km, 90 km, 100 km FOR 1968 - 1969. N IS THE NUMBER OF INDIVIDUAL DETERMINATIONS FOR EACH SEASON.

If the determination of a particular harmonic component is considered to be satisfactory when $\bar{A} \geq 3\, r_p$ then many of the determinations in Tables 7.2 and 7.3 are unreliable. In general the diurnal tide, with a larger amplitude, is better determined than the semidiurnal tide but this is certainly not the case for all heights and all seasons.

When the data for 1968 and 1969 are combined and the seasonal means again determined, the semidiurnal tide is still not well determined at 80 and 90 km while the diurnal tide is not well determined at 100 km. The results of this averaging process are shown in Tables 7.4 and 7.5 for the diurnal and semidiurnal components respectively. The value of P in these tables is the probability of obtaining the mean value $\bar{A}$ purely by chance. To enable the seasonal variations to be easily visualised the means for 80 km from tables 7.4 and 7.5 have been plotted on harmonic dials in Figures 7.8 and 7.9. The mean for all data are marked with a cross on these diagrams.

The day to day variations in the amplitude and phase of the 24 and 12 hour periodic components discussed earlier is the basic reason why many of the mean values determined above are statistically unreliable. By combining all of the data available at Adelaide into Lloyd seasons it is hoped that reliable estimates can be made for all tidal components (this analysis is in its initial stage).

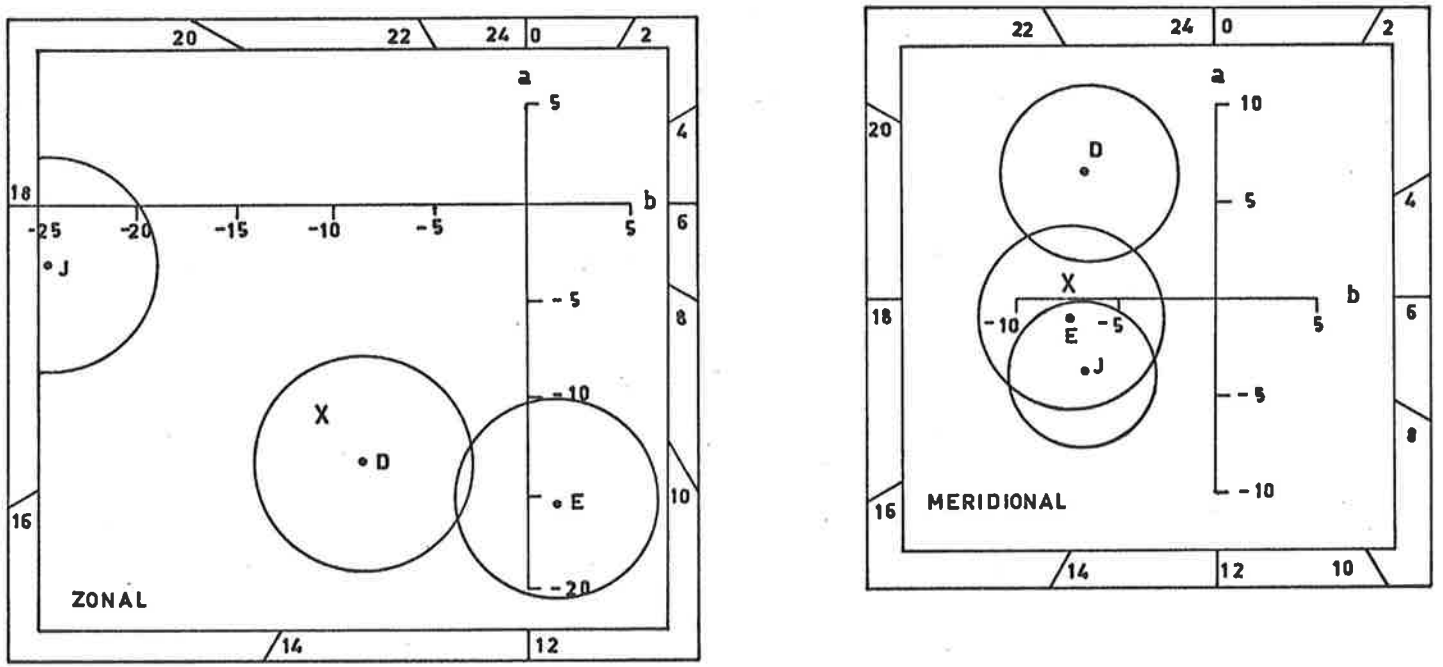

Figure 7.8: The mean seasonal zonal and meridional diurnal wind components (1968-1969) at 80 kms. The probable error circle for each measurement is shown. The cross gives the mean for all the data.

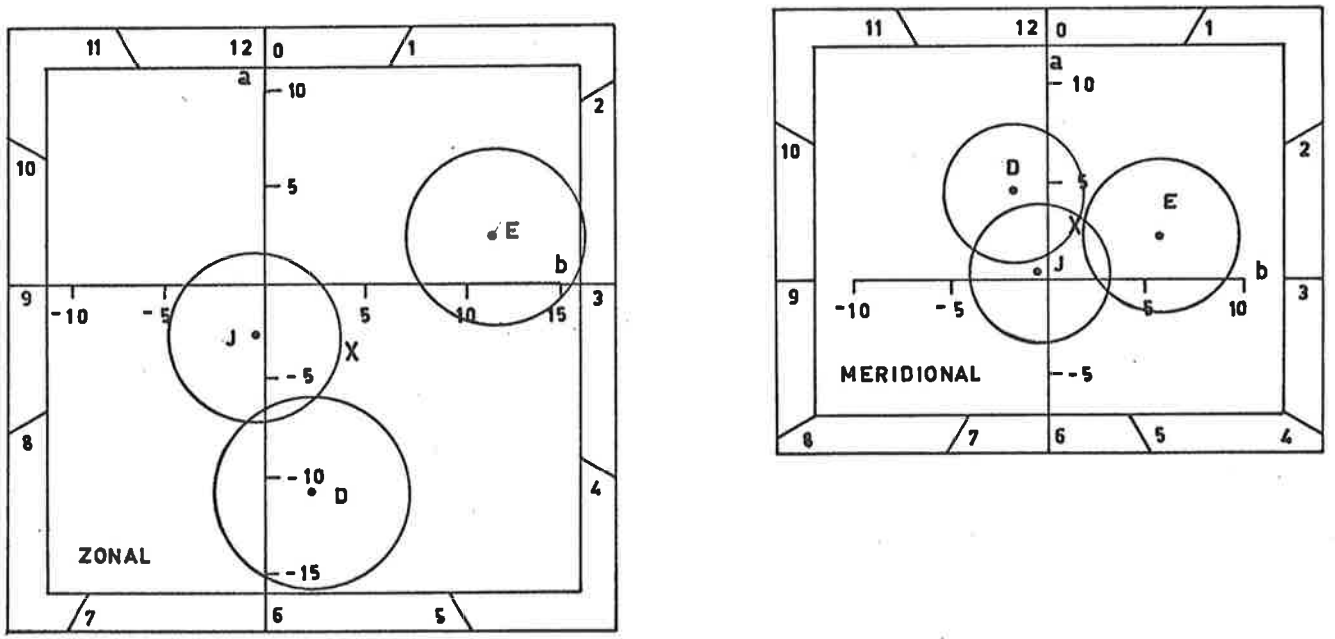

Figure 7.9: The mean seasonal zonal and meridional semidiurnal wind components (1968-1969) at 80 kms. The mean for all the data is shown by the cross.

		Zonal				Meridional			
80 km	N	Amplitude (m/sec)	r_p	Phase (hours)	P	Amplitude (m/sec)	r_p	Phase (hours)	P
D Months	35	16.1	6.0	14.2	1.3×10^{-2}	9.4	4.8	21.0	8.7×10^{-2}
J Months	32	25.1	5.6	17.2	6.2×10^{-5}	7.8	3.8	16.2	7.0×10^{-2}
E Months	32	15.3	5.5	11.6	1.0×10^{-2}	7.6	4.7	17.6	0.18
All	99	15.2	3.5	15.0	1.0×10^{-5}	7.1	2.6	18.5	7.6×10^{-3}
90 km									
D Months	35	20.2	4.2	11.2	1.7×10^{-5}	15.0	4.1	21.8	6.5×10^{-4}
J Months	32	4.5	3.8	16.4	0.38	6.1	3.9	14.4	0.20
E Months	32	15.9	3.5	9.4	5.0×10^{-5}	13.9	4.0	16.2	1.0×10^{-3}
All	99	12.1	2.4	11.0	3.6×10^{-7}	8.1	2.4	18.4	6.6×10^{-4}
100 km									
D Months	35	14.8	6.9	11.7	5.6×10^{-2}	18.8	6.4	22.4	6.2×10^{-3}
J Months	32	5.5	6.9	4.7	0.65	5.2	6.4	9.9	0.64
E Months	32	9.1	7.6	6.3	0.38	5.5	7.1	16.8	0.67
All	99	6.9	4.2	8.9	0.16	5.4	3.9	21.3	0.27

Table 7.4: THE DIURNAL TIDE COMPUTED FOR ALL DATA COLLECTED DURING 1968 AND 1969 AT ADELAIDE.

		Zonal				Meridional			
80 km	N	Amplitude (m/sec)	r_p	Phase (hours)	P	Amplitude (m/sec)	r_p	Phase (hours)	P
D Months	35	11.1	5.4	5.6	6.7×10^{-2}	5.1	3.9	11.4	0.31
J Months	32	2.3	4.6	6.1	0.84	0.5	3.1	11.3	0.98
E Months	32	11.8	5.4	2.6	5.0×10^{-2}	5.9	4.6	2.3	0.34
All	99	5.9	3.0	4.4	$7.4 \quad 10^{-2}$	2.8	2.3	0.8	0.36
90 km									
D Months	35	5.7	4.2	5.5	8.1×10^{-2}	6.7	3.3	23.5	7.1×10^{-2}
J Months	32	8.6	3.5	9.5	2.5×10^{-2}	4.9	2.7	4.3	0.12
E Months	32	2.2	4.1	0.6	0.78	7.2	3.3	2.3	5.0×10^{-2}
All	99	2.0	2.1	8.5	0.53	3.5	1.9	1.7	0.10
100 km									
D Months	35	4.1	5.8	10.3	0.71	14.4	5.1	0.6	8.8×10^{-3}
J Months	32	13.1	5.9	8.9	4.7×10^{-2}	10.7	5.6	4.2	9.7×10^{-2}
E Months	32	18.4	6.9	8.7	1.4×10^{-2}	9.8	4.9	1.2	7.9×10^{-2}
All	99	11.2	3.6	8.9	1.9×10^{-3}	8.1	3.1	1.6	1.0×10^{-2}

TABLE 7.5: THE SEMIDIURNAL TIDE COMPUTED FOR ALL DATA COLLECTED DURING 1968 AND 1969 AT ADELAIDE.

7.4.2 Comparison with Theory

Some aspects of the theory of tides as pertaining to latitude 35°S and the height range 70 to 110 km will be briefly discussed before comparison with the observational results described in the previous section. Lindzen and Chapman (1969) have given an excellent review of the theory of atmospheric tides. The main methods of excitation of the solar tides are due to the absorption of solar energy by water vapour and ozone. Surface temperature variations are considered relatively unimportant and give rise to local effects in the tidal variations restricted mainly to the troposphere.

In the case of the solar semidiurnal tide the most important mode is the (2,2) which associated with long vertical wavelengths ($\sim$ 150 km); this mode responds to the excitation due to ozone heating. However the (2,2) mode is trapped below the mesopause so that with a slight change in the distribution of ozone the (2,4) mode may make an important contribution to the wind field above 80 km. At 35° latitude the amplitude of the semidiurnal wind is predicted to be about 10 m/sec at 80 km increasing to about 40 m/sec at 100 km with a phase lag of about 2 hours between these levels.

No particular mode of the solar diurnal tide responds efficiently to the excitation function and hence a number of modes are important in determining the total wind field. Slight variations in the excitation functions (both water vapour and ozone heating) can change the type and number of significant modes in the wind field. Evanescent modes,

particularly the (1, - 1) mode, are important near the regions of excitation but contribute little to the diurnal oscillation at upper levels (unless local heat sources of sufficient strength exist). Most other modes propagate freely and are not trapped below the mesopause so that equatorwards of about 40° the diurnal tide is much greater than the semidiurnal tide. The refraction effects of the background temperature structure are important for the short wavelength modes and hence above 30 km the diurnal tide can be quite variable. Typical amplitudes expected are 30 m/sec at 80 km and 100 m/sec at 100 km with a phase lead of about 7 hours between these levels.

The main fact of interest from the observational data is that the amplitudes of both the diurnal and semidiurnal tides are smaller than theory predicts for the latitude and height. In particular the amplitude of the diurnal tide, which would be expected to increase with height, in fact decreases for all seasons. The semidiurnal tide, on the other hand, generally increases with height as is expected but is much more variable than theory would predict.

For the diurnal component the maximum wind towards the north follows the maximum wind towards the east by about six hours as would be expected from theoretical considerations. However the semidiurnal component is less reliably determined and does not show the expected phase lag of three hours between northward and eastward wind components. The variation of phase with height is also irregular.

The above facts imply that more than one mode is present in both the diurnal and semidiurnal tidal components. It is interesting to speculate that the variability of the semidiurnal tide may be due to the fluctuating importance of the (2,4) mode, while in the case of the diurnal tide the larger number of short wavelength modes may vary in relative importance. Lindzen (1968a) has shown that small changes in the background temperature profile have an important influence on the relative strength of the various propagating diurnal modes. Variations in the distribution of ozone are certainly observed and hence variations in the importance of the (2,4) mode might be expected. Speculations such as these can only be checked if simultaneous observations are made at a number of locations.

Seasonal variations in the mean winds and temperature below 80 km are expected to cause changes in the phase of the diurnal and semidiurnal waves arriving in the region 80 - 100 km. The observations of the diurnal tide show little seasonal variation in amplitude (below 100 km), and a small phase variation as can be seen from Figure 7.8. The variation with season of the semidiurnal tide is not clearly defined but it would be interesting to consider the effects of seasonal variations in the distribution of ozone (the main exciting function).

CHAPTER VIII

MEASUREMENTS OF WIND SHEAR IN THE LOWER THERMOSPHERE

8.1 INTRODUCTION

As indicated in Chapter VI measurements of wind shear were made with the multi-station radio meteor system over the period December 1968 to June 1969. The distribution of echoes in height and time is given in the aforementioned chapter as are the methods of data reduction. The wind shear data is presented in the form of structure functions computed as described in §6.5.

As the orientation of each meteor trail with respect to the observing stations is known it is possible to compute the horizontal and vertical components of the reflection point separation. Thus structure functions are computed for horizontal separations (increments of 200 metres) and vertical separations (increments of 100 metres). However it should be remembered that a slight amount of coupling will occur between these functions, and is more serious for the vertical function due to the inclination of the meteor trails to a horizontal plane (about 30° on average). Even if the separation is not complete it is still useful to present the data in the form of horizontal and vertical measurements of wind shear in view of the stabilising nature of the background temperature variation. It should be noted that this has not been particularly successful in the past because of the limited spatial separation of reflection points along the trail.

The approach in the discussion of the results in §8.4 will not be to presuppose any particular structure but rather to attempt to show some relationship between the observed structure functions and various theoretical predictions. A brief discussion of the statistical properties of wind shear measurements in the lower atmosphere is given in the following section. The present results indicate that the same considerations are applicable to conditions in the lower thermosphere.

8.2 STATISTICAL WIND SHEAR RELATIONSHIPS

Essenwanger (1963) has shown empirically that wind shear $\overline{\Delta u}$ is related to the shear interval ξ by a power law as follows:

$$\overline{\Delta u} = a_o \xi^{a_1} \qquad 8.1$$

and with the standard deviation $\sigma_{\Delta u}$ given by

$$\sigma_{\Delta u} = c\xi^{a_1} + A_o \qquad 8.2$$

and

$$= A_o + A_1 \overline{\Delta u} \, . \qquad 8.3$$

The quantities a_o, c, A_o and A_1 are the various coefficients or constants associated with the power law with exponent a_1. In a later publication Essenwanger (1966) linked his results to statistical theory and showed that the exponent a_1 had the value $\frac{1}{2}$ for mean shear due to the persistence (meso-scale structure) in the wind profile. Extreme values of shear appear to be independent of any particular statistical distribution and the exponent tends towards 1/3 implying that the structure may be that of

isotropic turbulence. The precise value of the exponent depends on the particular meteorological conditions in existence at the time of the measurements.

The power law behaviour of the mean wind shear with vertical separation (exponent 0.5) has been confirmed by the balloon observations of Armandariz and Rider (1966). It is also possible that the wind shear measurements of Weinstein et al. (1966) may also follow the power law behaviour (Essenwanger, 1967).

The relations given in 8.1 and 8.2 may be related to the structure functions discussed in Chapter II. In particular for an inertial subrange of turbulence the transverse structure function has the form

$$D_{tt}(\xi) = \frac{4}{3} a(\varepsilon\xi)^{2/3}$$

Thus it is apparent (Essenwanger, 1969) that the relations $a_1 = 1/3$ and $a_o = \sqrt{\frac{4}{3}}\, a \cdot \varepsilon^{1/3}$ should hold for conditions of extreme shear.

8.3 THE OBSERVATIONS

The basic measurements for five months* of the survey are presented as structure functions for vertical and horizontal separations in Figures 8.1 - 8.5 where the logarithm of the squares of the velocity differences has been plotted against the logarithm of the horizontal and vertical separations respectively (the structure functions for October 1969 are

---

* As noted earlier in Chapter VI wind shear data for April and May 1969 are not yet available owing to delays in reading the velocity films beyond the author's control.

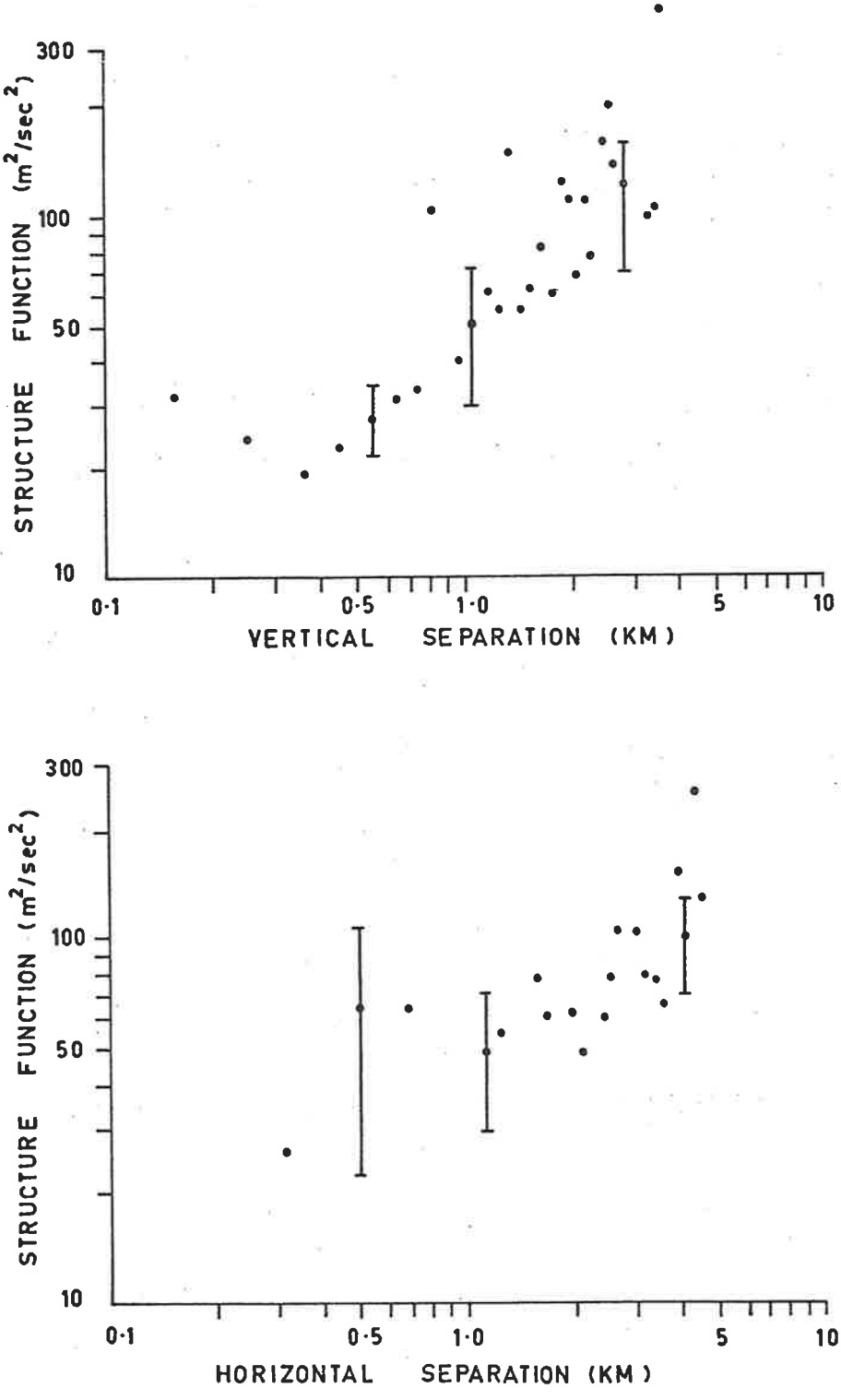

Figure 8.1: Structure functions for December, 1968, (158 meteors).

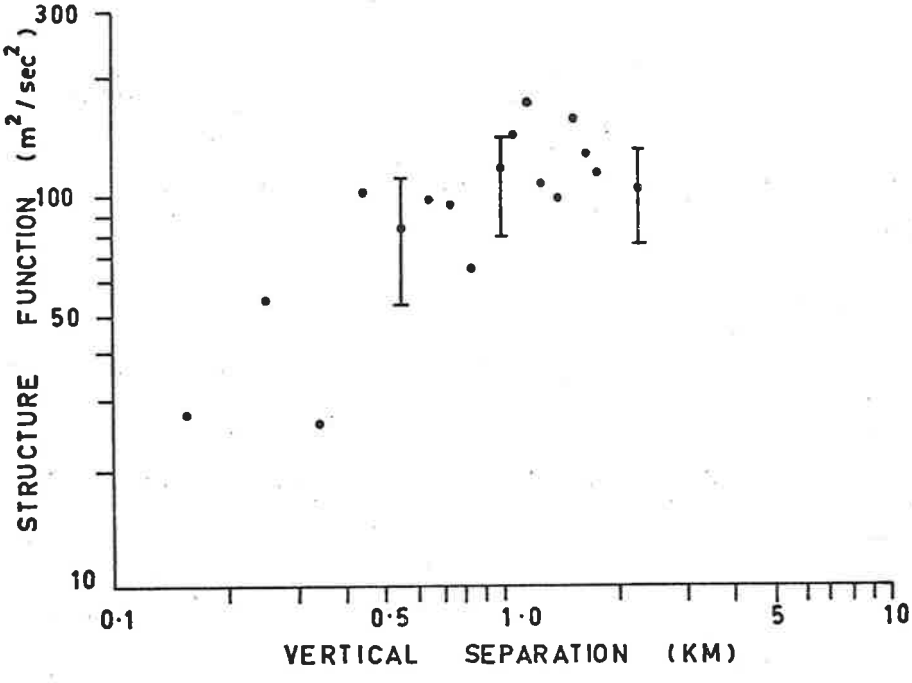

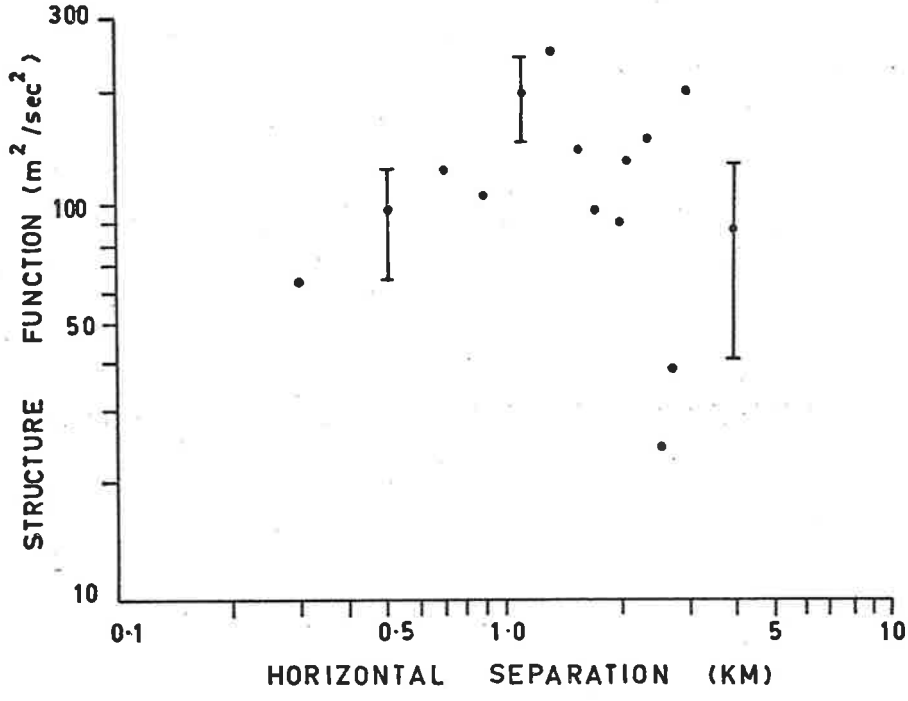

Figure 8.2: Structure functions for January, 1969 (58 meteors).

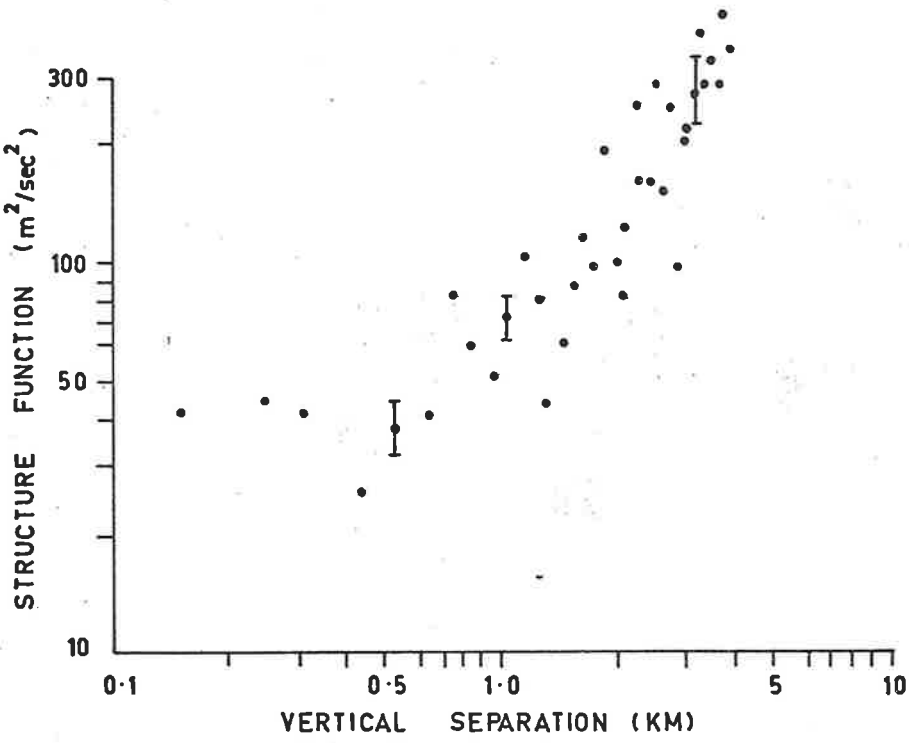

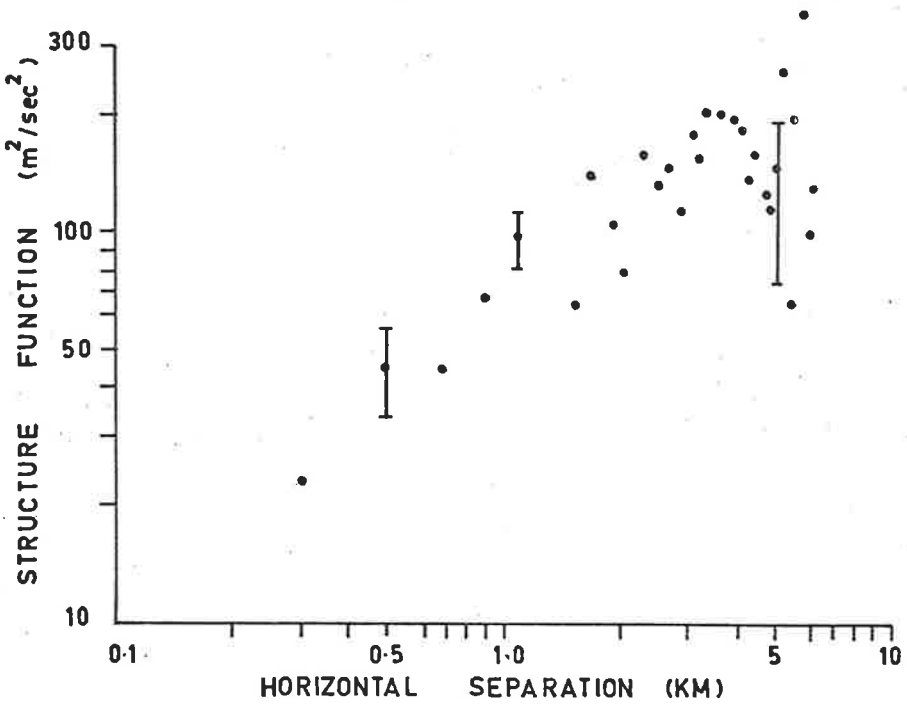

Figure 8.3: Structure functions for February, 1969 (366 meteors).

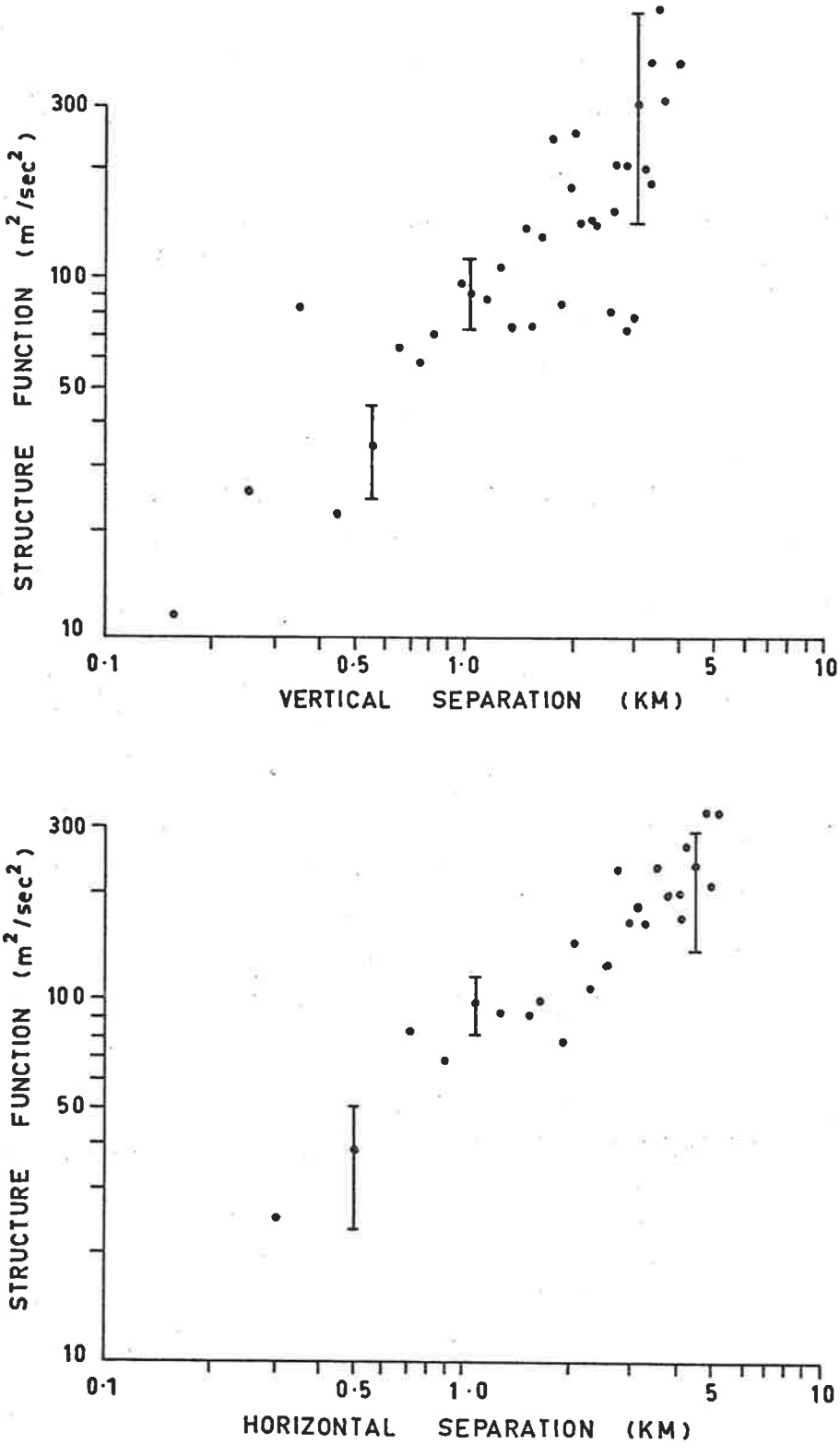

Figure 8.4: Structure functions for March, 1969 (269 meteors).

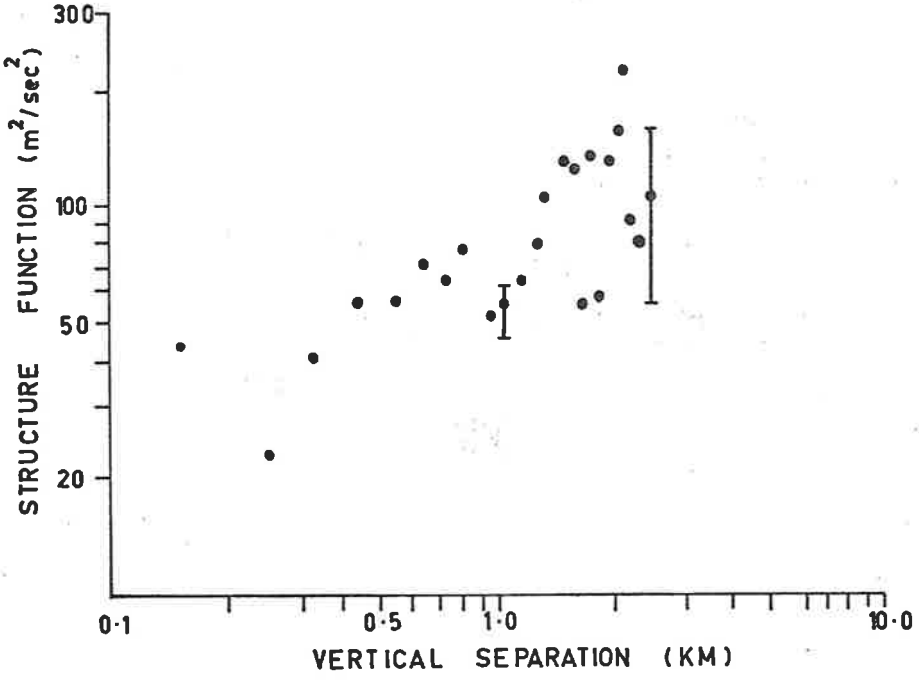

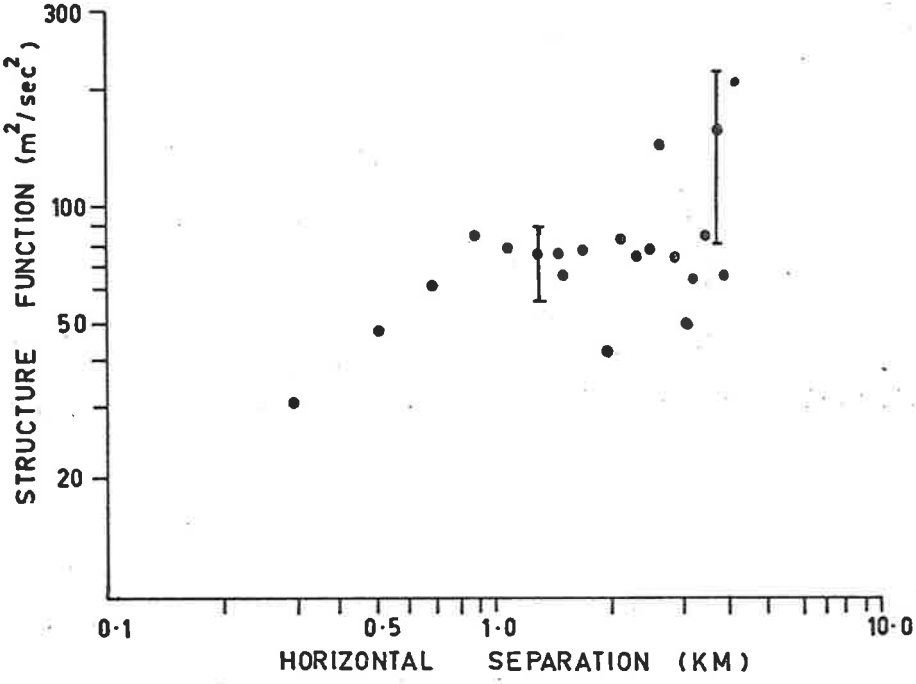

Figure 8.5: Structure functions for June, 1969 (266 meteors).

presented separately in the following chapter). The error bars shown for a few points (small separation, separation $\sim$ 1 km, and large separation) are simply the standard error in the mean square velocity difference for the particular separation concerned. In general the mean square velocity difference increases more rapidly with vertical than with horizontal separations. The amount of scatter in some of these plots makes it difficult for an objective decision to be made as to the closeness of fit to a particular expected curve.

Any discussion of these plots must be tempered by consideration of the following factors:

(i) At separations less than about 300 metres anomalous velocity differentials are prevalent due to the inaccuracy associated with separation measurement brought about by the phenomenon of reflection point motion, and also due to the inherent inaccuracy in measuring the original line-of-sight-velocities.

(ii) Reliable estimates of the mean square velocity difference are only obtained when the number of differences is large. As shown later at least ten velocity differences are required to obtain a significant value. In general the total number of multi-station echoes in each month has to exceed 70 (yielding about 400 velocity differences) in order to obtain a set of reliable mean square velocity differences.

(iii) Due to the non-uniform echo rate (outlined in Chapter VI) the measurements for a given month are biased towards the high rate hours centred around 0500 local time.

In order to make some objective comparisons between the horizontal and vertical structure functions and also between the observations for various months a power law of the form $\overline{\Delta u^2} = kx^{\Delta}$, where k and Δ are the constants to be determined, is fitted to the data by the method of least squares. In view of the factors discussed in the previous paragraph a weighting factor was introduced for each data point as follows. Each mean square velocity difference was weighted by a factor $w_i = n_i/\sigma_i$ where n_i is the number of differences at that separation and σ_i is the standard deviation. The appearance of the factor n_i is in an attempt to allow directly for variations in the number of differences whereas σ_i allows for the accuracy in the determination in the classical manner.

Other parameters which have been determined from the irregular velocity field are shown in Table 8.1. Column 1 gives the number of meteor trails recorded during the month, while column 2 gives the total number of reflection points recorded (a maximum of five points on each trail). $\bar{V}$ is the root mean square velocity of all the line-of-sight velocities measured during a given month. T_{max} and T_{rms} refer to the motion of reflection points along the trail. Because the wind shear on an individual trail can be measured it is possible to determine the speeds of each reflection point as it moves along the trail using the formula given in §4.3.2. The maximum value (in km/sec) found for each month is entered under the heading T_{max}. The root mean square speed measured for each month is entered under the heading T_{rms}. This motion of the

Month	N_T	N_R	$\bar{V}$ (m/sec)	$\overline{\frac{\Delta V}{\Delta h}}$ (sec^{-1})	T_{max} (km/sec)	T_{rms} (km/sec)
December, 1968	158	780	26	0.0081	+ 3.1	0.4
January, 1969	58	288	36	0.019	- 2.5	0.5
February, 1969	365	1131	31	0.0075	- 4.4	0.4
March, 1969	269	509	29	0.011	+ 4.3	0.5
April						
May						
June, 1969	266	1328	27	0.0092	+ 2.9	0.4
October, 1969	213	1045	27	0.011	- 4.7	0.4
All data	1330	6632	29	0.0096	6.4	0.4

TABLE 8.1: PARAMETERS OF THE IRREGULAR WIND FIELD AS DETERMINED FOR EACH MONTH OF THE SURVEY. THE SYMBOLS ARE EXPLAINED IN THE TEXT

reflection point can greatly affect measurements of diffusion (Brown, private communication). $\overline{\Delta V/\Delta h}$ is the rms value of the wind shear measured for each trail.

The results presented in Table 8.1 are very similar to the earlier measurements of Roper (1962) obtained during 1961. The present observations do not show any definite variations with season or height, in particular evidence for a maximum shear near the equinoxes is not apparent. This null result is in contrast with the results of Roper (1962) but will not be discussed further. It is worth noting that the present results (with the exception of January, 1969) are statistically more reliable than those of Roper.

The various constants associated with the best fit power laws to the spatial, vertical and horizontal structure functions respectively are given in Table 8.2. Standard errors for each parameter are given in the table, any differences in the parameters greater than about twice the standard error are considered significant.

Since little variation between different months is apparent all the data has been combined to produce the spatial structure function shown in Figure 8.6 and the vertical and horizontal structure functions shown in Figure 8.7. The relevant parameters have also been added to Tables 8.1 and 8.2. This combined data simply serves to confirm the lack of variation between different months.

Month	N	Spatial		Vertical		Horizontal	
		k	Exponent	k	Exponent	k	Exponent
December, 1968	158	24.7 ± 0.3	.77 ± .16	36.2 ± .3	.76 ± .09	44.2 ± .3	.70 ± .15
January, 1969	58	101 ± 1	.46 ± .07	95.3 ± .6	.70 ± .14	105 ± 1	.53 ± .19
February, 1969	385	54.0 ± 0.1	.56 ± .05	62.8 ± .2	.69 ± .08	66.5 ± .2	.56 ± .06
March, 1969	269	56.0 ± .1	.73 ± .04	71.4 ± .2	.83 ± .07	71.9 ± .2	.57 ± .06
April, 1969							
May, 1969							
June, 1969	266	53.6 ± .2	.46 ± .07	62.7 ± .3	.46 ± .09	62.6 ± .3	.11 ± .09
October, 1969	213	59.1 ± .2	.62 ± .08	74.4 ± .3	.72 ± .11	75.9 ± .2	.46 ± .06
All data	1330	57.5 ± .1	.60 ± .04	77.3 ± .1	.64 ± .03	73.7 ± .1	.46 ± .03

TABLE 8.2: PARAMETERS OF THE WEIGHTED BEST FIT POWER LAWS TO THE STRUCTURE FUNCTIONS FOR EACH MONTH. THE ERRORS SHOWN ARE THE STANDARD ERRORS FOR EACH PARAMETER.

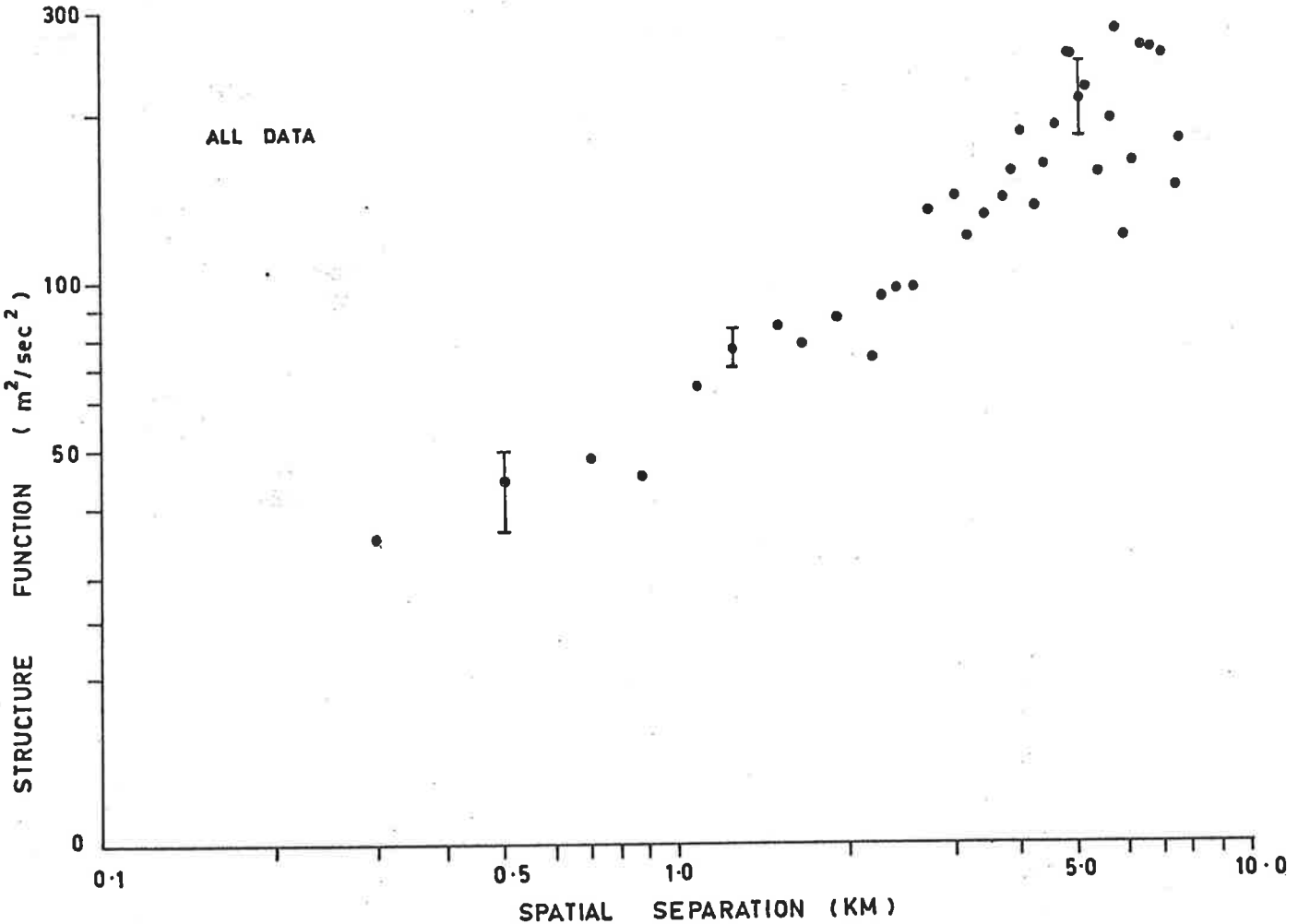

Figure 8.6: Spatial structure function for all data 1968 - 1969 (1330 meteors).

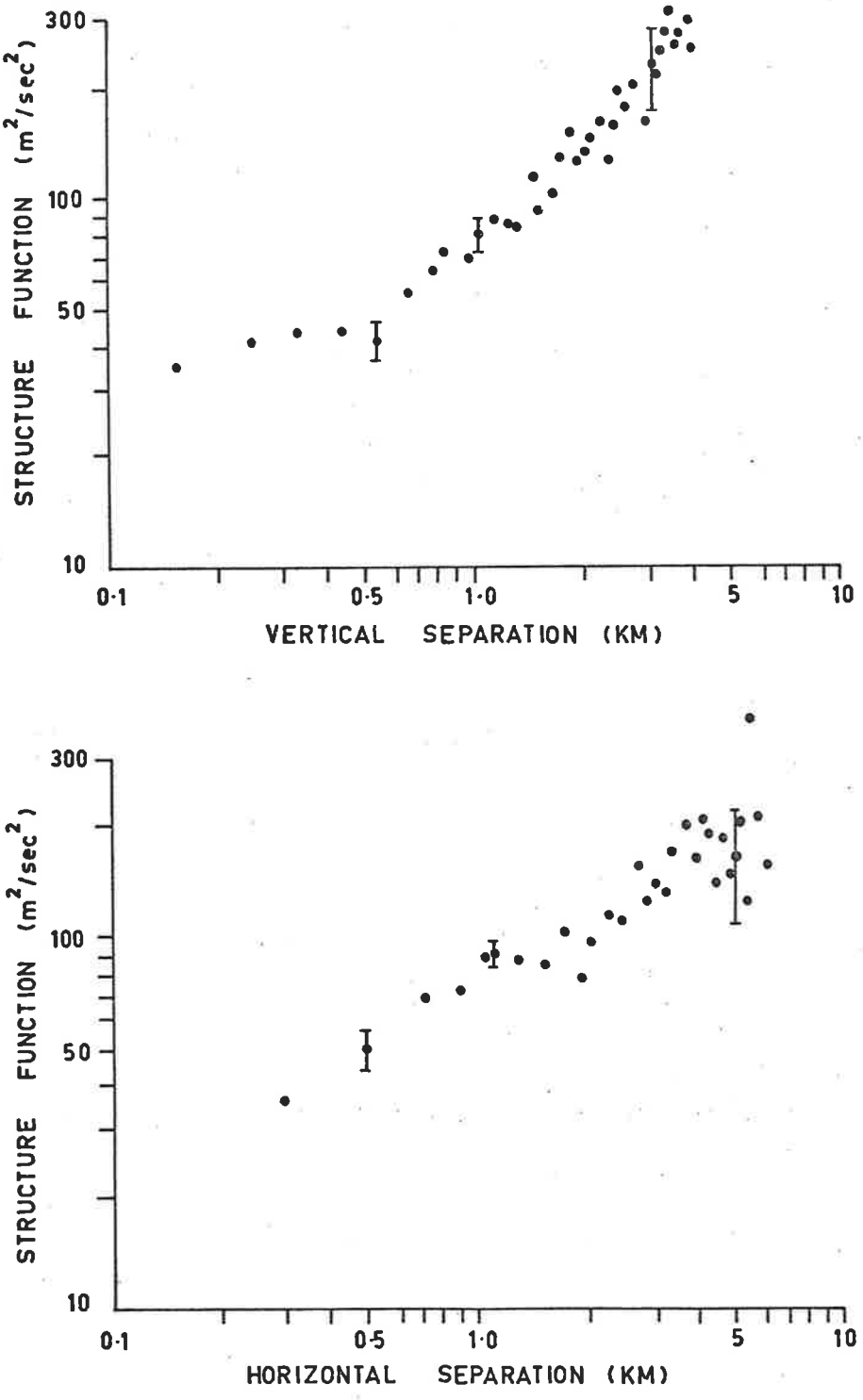

Figure 8.7: Structure functions for all data 1968 - 1969 (1330 meteors).

8.4 COMPARISON WITH PREVIOUS OBSERVATIONS AT ADELAIDE

Previous observations made with a three station radio meteor system during 1961 have been described by Roper (1962) and (1966). The main observational difference in the present work is the addition of two extra out-stations which, when coupled with greater overall sensitivity of the system, increases the number of velocity difference determinations that can be made in a given time interval. With four reflection points there are six velocity differences and with five points the number is ten. Thus the reliability of mean square velocity differences is improved, particularly for separations greater than about 2.0 km. Differences can be obtained up to a maximum separation of about 5.5 km compared with 2.5 km in the 1961 survey.

In order to make some quantitative assessment of the reliability of values of D (the mean square velocity difference) when the number of velocity differences is small (particularly near the maximum separation) for both the results of the present (1969) survey and the 1961 survey the 1969 data was treated in the following manner. Data for only the three close-spaced receiving sites as used in the 1961 survey (St. Kilda, Direk and Sheedys) were selected and structure functions computed. It was found that some of these new structure functions differed from the functions computed using all available stations. In particular the greater uncertainty in the values of D for separations of the order of 2 km tended to give larger values for the exponent in the best fit power law. At least 10 velocity differences appeared necessary for a stable value of D. This

criterion was only met for separations less than about 2.0 km for most months of the 1961 survey whereas for the 1969 survey this criterion is met up to a separation of about 5.5 km for all months except January 1969.

The considerations above have the greatest effect on the vertical structure functions computed for the 1961 survey. The exponent of 1.4 found in the 1961 survey (max vertical separation of 1.5 km) is not found in the 1969 survey (max vertical separation of 3.0 km), the exponent in the latter case being always less than 1.0. This discrepancy is probably due to the unreliable values of D determined for the 1961 survey for vertical separations greater than 1.2 km. It has been found that a weighted least squares fit on some of the 1961 data would reduce the value of the exponent slightly. The structure functions determined from chemical release trails, as discussed in §3.3.1, often have exponents close to 1.4 which appears compatible with the results of the 1961 survey. However large variations can occur in the structure functions computed for different heights as shown by Rees et al. (1970) and hence the present results are still compatible with the analysis of chemical trails.

One further feature of the scatter in values of D as it affects the 1961 results is worthy of mention. The mean square velocity differences for the spatial separations in the 1961 survey were interpreted directly as being due to an inertial sub-range of a turbulent field since a power law of the form $D \propto \xi^{2/3}$ fitted the data reasonably well. Zimmerman (1969) questioned this interpretation because of an apparent difference in slope for small separations (less than 0.8 km). However it has been

pointed out earlier in this chapter that the velocity differences for separations less than 0.5 km are very unreliable. The measurements of velocity differences for small separations often fluctuate wildly when the basic data are split into, say, even and odd numbered echoes whereas for separations greater than about 0.5 km the measurements are relatively stable. It has since been demonstrated that the main variations for separations less than 0.5 km are due to the inherent inaccuracies in the measurement of the individual line-of-sight velocities.

8.5 DISCUSSION OF PRESENT OBSERVATIONS

Unambiguous evidence for the existence of a turbulent velocity field is not available from the observations. The radio meteor technique cannot be used in the same way as an array of sensors might be used in the troposphere and hence it is difficult to separate completely the effects of horizontal and vertical structure. The separation that has been attempted for the data indicates a disting difference between the vertical and horizontal structure. In every case in Table 8.2 the exponent in the best fit power law is larger for the vertical structure function than for the horizontal structure function although the differences for some months are not statistically significant.

If the wind shear measurements were due to 'white noise' an exponent $a_1 = 0$ (see §8.2) would be expected (Essenwanger and Billions, 1965). Only the horizontal structure function for June 1969 would be explained by this argument. A linear trend for wind shears would yield an exponent of 2 for the structure functions and hence can be excluded.

As discussed earlier in §8.2 mean shears which contain meso-scale structure as well as turbulence would give structure functions with exponents of about 1.0. Weinstein et al. (1966) have shown that the meso-scale structure observed in vertical wind profiles above the tropopause can be explained by the effect of internal gravity waves. Further, the results of Phillips (1968) show that structure functions with exponents of 1.0 can be expected for a spectrum of internal gravity waves for conditions that apply in the present case. The vertical structure functions determined by the radio meteor system have exponents near 0.8 and thus are in reasonable agreement with this idea.

The horizontal structure functions have exponents near 0.6 and thus indicate the possibility of being due to an inertial sub-range of turbulence. Thus the model of small scale wind structure proposed in §3.4 holds for the present observations. However more observations are needed before a definite statement as to the existence of an inertial turbulent regime out to separations of about 10 km can be made.

If it is assumed that the results for horizontal displacements are due entirely to turbulence then the constants k in Table 8.2 can be used to determine values of the dissipation rate as shown in §8.2. Values thus obtained ($\sim$ 0.01 watts/kg) are not incompatible with the results of Justus (1966). The seasonal variation of the dissipation rate found by Roper (1966) (maximum near the equinoxes) is not substantiated although the period covered by the present data is not sufficient to justify a definite statement.

The energy for the small scale motion observed probably comes from the diurnal tide since, as discussed in Chapter VII, much of the energy in the diurnal tide is lost in the lower thermosphere.

CHAPTER IX

A DIRECT COMPARISON OF WIND AND SHEAR MEASUREMENTS MADE WITH RADIO-METEOR AND CHEMILUMINESCENT TRAIL TECHNIQUES

9.1 DETAILS OF THE EXPERIMENT

A joint experiment to measure neutral winds, ion drifts and temperature in the upper atmosphere was conducted during October 1969 by the Department of Physics, University College, London; Max-Planck-Institut für Physik und Astrophysik, Munich; and the Weapons Research Establishment, Salisbury, S.A. Two Skylark rockets (designated SL 861 and SL 862) were launched from Woomera during twilight at 0446 C.S.T., 16th October, 1969 and 1915 C.S.T., 17th October, 1969. The Radiophysics Group of the Department of Physics, University of Adelaide participated in this experiment by making ground-based radio observations of the neutral wind and ion drifts over the launch period and for a few days before and after the launchings.

Details of the rocket experiments are as follows:

(i) 5 kg of trimethyaluminium (TMA) was released as a trail between 85 and 150 km in the shadow region of the vehicle trajectory. This trail was photographed at three sites using F24 cameras and also a series of high resolution plates were taken by the Baker-Nunn camera situated at the Island Lagoon tracking station.

(ii) Four high explosive (HEX) standard 1 lb grenades were released in the TMA trail. The velocity of the shock wave produced by them gave the temperature of the ambient atmosphere (Rosenberg, 1964).

(iii) Standard aluminium loaded 1 lb grenades were released at intervals between 150 km and 240 km altitude in sunlight. Aluminium monoxide (AlO) is produced which resonantly scatters sunlight (Johnson, 1965). From time sequenced photographs of the AlO clouds, the diffusion coefficient and neutral winds may be determined (Manring et al., 1961). Spectral observations of the band structure of the resonant radiation enable the temperature to be determined (Authier et al., 1962).

(iv) Two special grenades each containing 3 kgm of a barium, copper oxide mixture were released at 180 km and 218 km respectively. The mixture undergoes an exothermic reaction which vaporises the excess barium producing a cloud of neutral and ionised atoms. Neutral and ion winds can be determined by time sequence photographs of the neutral and ionised barium clouds (Haerendel et al., 1967).

The multi-station radio-meteor system described in Chapter V was used to determine the prevailing, periodic and irregular winds in the height range 75 to 110 km, while the Buckland Park aerial system described by Briggs et al. (1969) was used to measure ionospheric drifts in the D, E and F regions when possible. Observations with the radio-meteor system which is about 450 km south-east of Woomera were made on the dates shown in Table 9.1.

Dates	Mean Wind	Multi-station	Comments
5-10-69	Yes (after 1000)	Yes (after 1800)	Multi-station data not yet available
6-10-69	Yes	Yes	
7-10-69	Yes	Yes	
8-10-69	Yes	Yes	
9-10-69	Yes (to 1700)	Yes (to 1400)	Transmitter failure
15-10-69	Yes (after 1200)	Yes (after 1800)	Commenced 1200
16-10-69	Yes	Yes	Launch at 0446
17-10-69	Yes	Yes	Launch at 1915; film mechanism
18-10-69	Yes	Yes	jammed on shear camera (2300-1530)
19-10-69	Yes	Yes (to 2100)	Concluded 2340

TABLE 9.1: DATES ON WHICH METEOR EQUIPMENT WAS OPERATED DURING OCTOBER 1969

The discussion which follows will be concerned mainly with a direct comparison between the winds determined by the radio-meteor method and those determined by tracking the TMA trail. This comparison can be useful in the interpretation of both types of wind measurement. Also the observations of turbulent phenomena on the TMA trail give a basis for interpreting the horizontal structure functions determined from the multi-station observations of wind shear.

9.2 WIND PROFILES

9.2.1 TMA Release Observations

The motion of the TMA trail and grenade glow clouds were measured relative to the star background. Records from three camera sites were used covering a period of up to 200 seconds after release. Easily identifiable points on the trail were used as primary tracers of the motion determined by direct triangulation. Motion of the smooth portions of the trail was determined by using the best fit lines-of-sight from the three camera sites. The error in the measured wind velocity was about 10 m/sec between 100 and 200 km and increased to 20 - 25 m/sec near the limits of observation about 90 and 220 km*.

The wind profiles for the morning and evening launches are shown in Figures 9.1 and 9.2. These profiles show the rather typical nature of the wind profiles found at these altitudes; a large scale

---

* This analysis was performed by Dr. D. Rees at University College, London

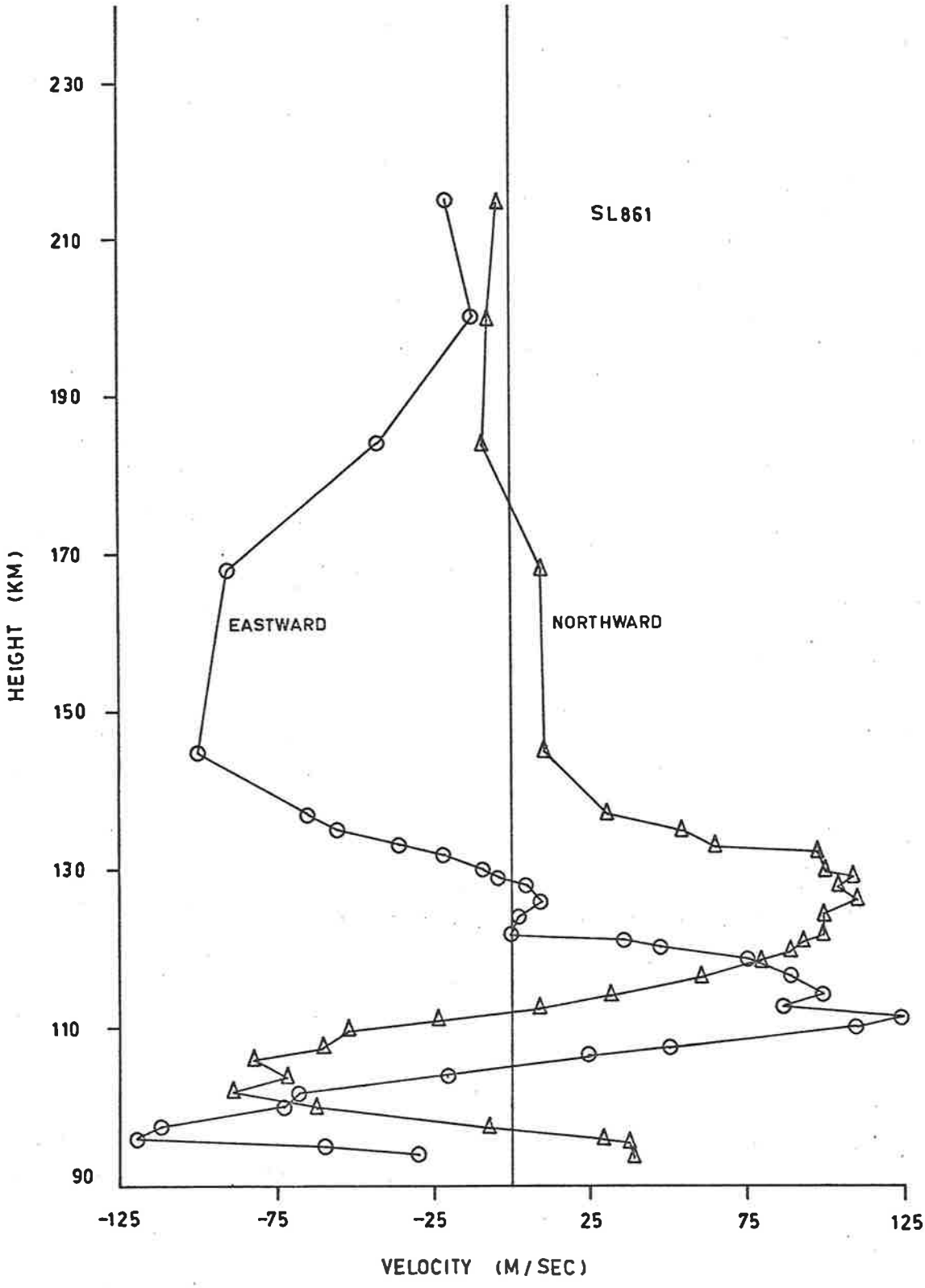

Figure 9.1: Wind profile measured by the contaminant release technique at 0446, 16th October 1969.

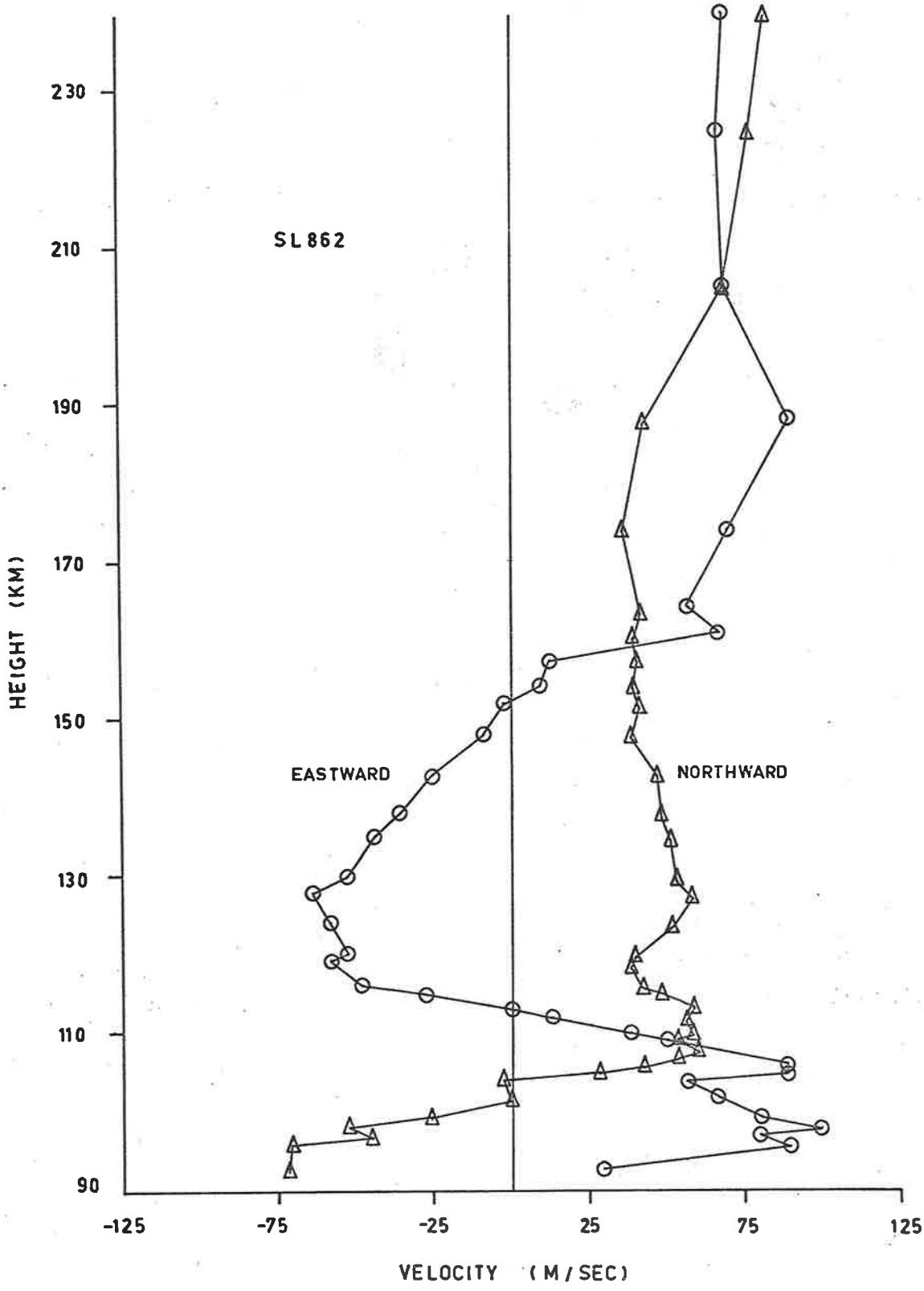

Figure 9.2: Wind profile measured by the contaminant release technique at 1915, 17th October, 1969.

wave-like structure on which is superposed smaller scale irregular structure for heights below 120 km and a relatively uniform wind above this height. The altitude scale in Figures 9.1 and 9.2 can also be expressed in scale height units above 80 km, defined by

$$S = \int_{80}^{h} \frac{1}{H}\, dh$$

where H is the (local) scale height. This scale is convenient for estimation of vertical wavelength by auto-correlation techniques since it allows for the variation in density with height. The auto-correlation and cross-correlation functions (calculated over height interval 94 km to 130 km) for the morning and evening profiles are shown in Figure 9.3 (Lloyd, 1970, private communication). As the value of shift for which the correlation has fallen to zero can be taken as one-quarter of the dominant wavelength it can be seen that the behaviour of the eastward and northward components for each sounding are similar but the wavelength of the evening profile (7 scale heights or about 49 km) is considerably greater than the morning value (4 scale heights or about 28 km). The cross-correlation functions for each sounding show that the northward wind component was in advance of the eastward wind component by about a quarter wavelength. This helical behaviour progressing anti-clockwise with altitude is to be expected for tidal winds; the wavelength found in the morning profile ($\sim$ 28 km) is compatible with the diurnal (1,1) mode while the wavelength found in the evening profile ($\sim$ 49 km) is

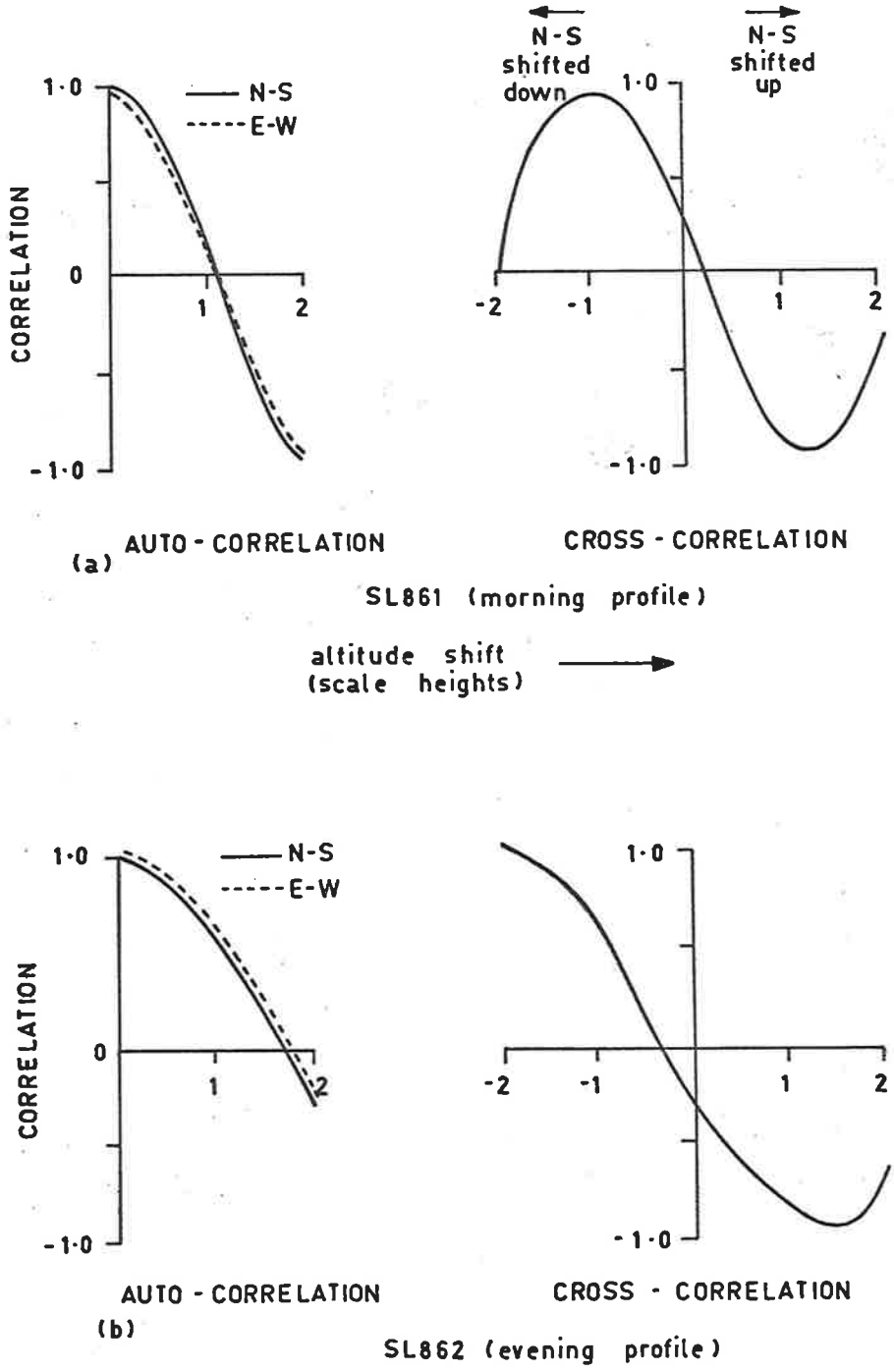

Figure 9.3: Correlation functions determined from
(a) the profile of 16th October (morning)
(b) the profile of 17th October (evening)

	Date				
Local Time	15	16	17	18	19
00		47	44	46	63
01		55	47	63	58
02		50	54	62	44
03		43	51	49	39
04		50	41	44	26
05		51	10	66	32
07		42	28	48	28
08		28	36	12	41
09		32	45	28	22
10		26	29	29	18
11		29	37	18	25
12	17	22	30	23	34
13	15	17	18	20	24
14	9	10	15	16	22
15	3	9	15	18	16
16	9	10	20	12	10
17	6	5	12	7	11
18	8	18	21	8	14
19	8	12	34	11	20
20	13	13	21	10	12
21	16	19	23	16	23
22	30	22	31	37	28
23	31	35	58	40	
Totals:	165	721	752	739	641
	Total for period:				3018

TABLE 9.2: DISTRIBUTION OF ECHOES IN TIME; PERIOD 15-10-69 TO 19-10-69 (ALL HEIGHTS). EQUIPMENT WAS NOT OPERATING WHERE BLANKS APPEAR

compatible with the semi-diurnal (2,2) mode but obviously unique identification with a particular tidal mode is impossible from single station data.

9.2.2 The Radio-Meteor Observations

Over the period from 1200, 15/10/69 until 2245, 19/10/69 the radio-meteor system recorded 3018 usable meteor echoes distributed in time as shown in Table 9.2. Unusually large usable echo rates were achieved near the times of each rocket launch by the simple expedient of recording continuously for about an hour centred on each launch time. By bypassing the sequence unit (see §5.3.4) in this manner many small short duration echoes which would normally not have been detected early enough were able to be read. The frequency of occurrence of meteors in height is shown in Figure 9.4; the mean height 89.1 km is slightly lower than the mean for all echoes 1966 - 1968, 90.2 km.

Two methods of analysis were used in conjunction with the raw meteor data. A model analysis (GROVES) was used* as described in §6.4 for each day and in particular for the two periods 1200 15/10/69 to 1200 16/10/69, and 1200 17/10/69 to 1200 18/10/69 the results of this analysis, presented as contours on a height-time diagram, are shown in Figures 9.5 to 9.8 for the zonal and meridional wind components respectively The variation allowed within the restrictions of the model are evident; information outside the height range 75 to 105 km has not been used because

---

* A justification (in part) for using a model with mean, 24 hr, 12 hr and 8 hr components is presented later.

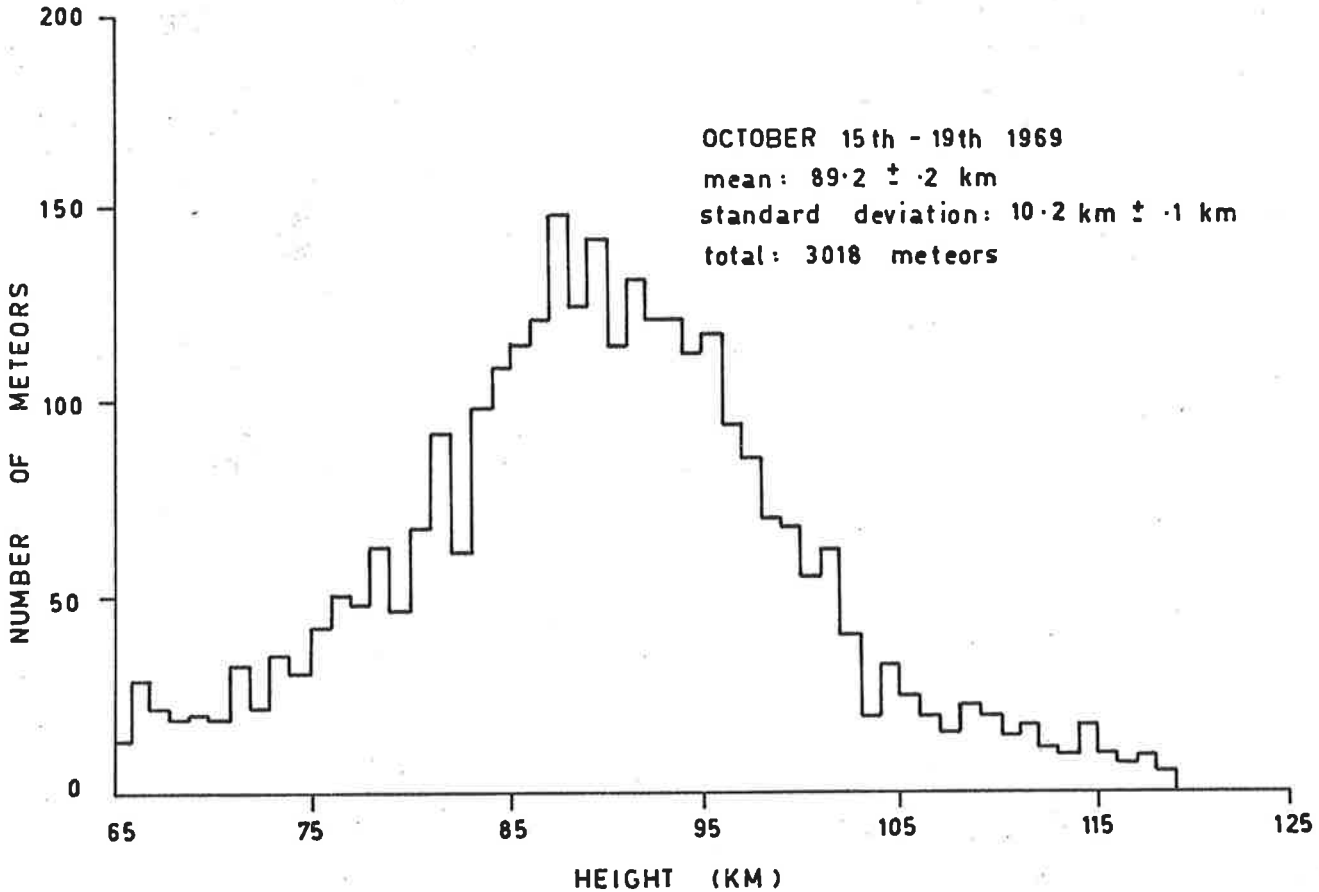

Figure 9.4: Distribution in height of all usable meteors recorded during the interval October 15th - 19th, 1969.

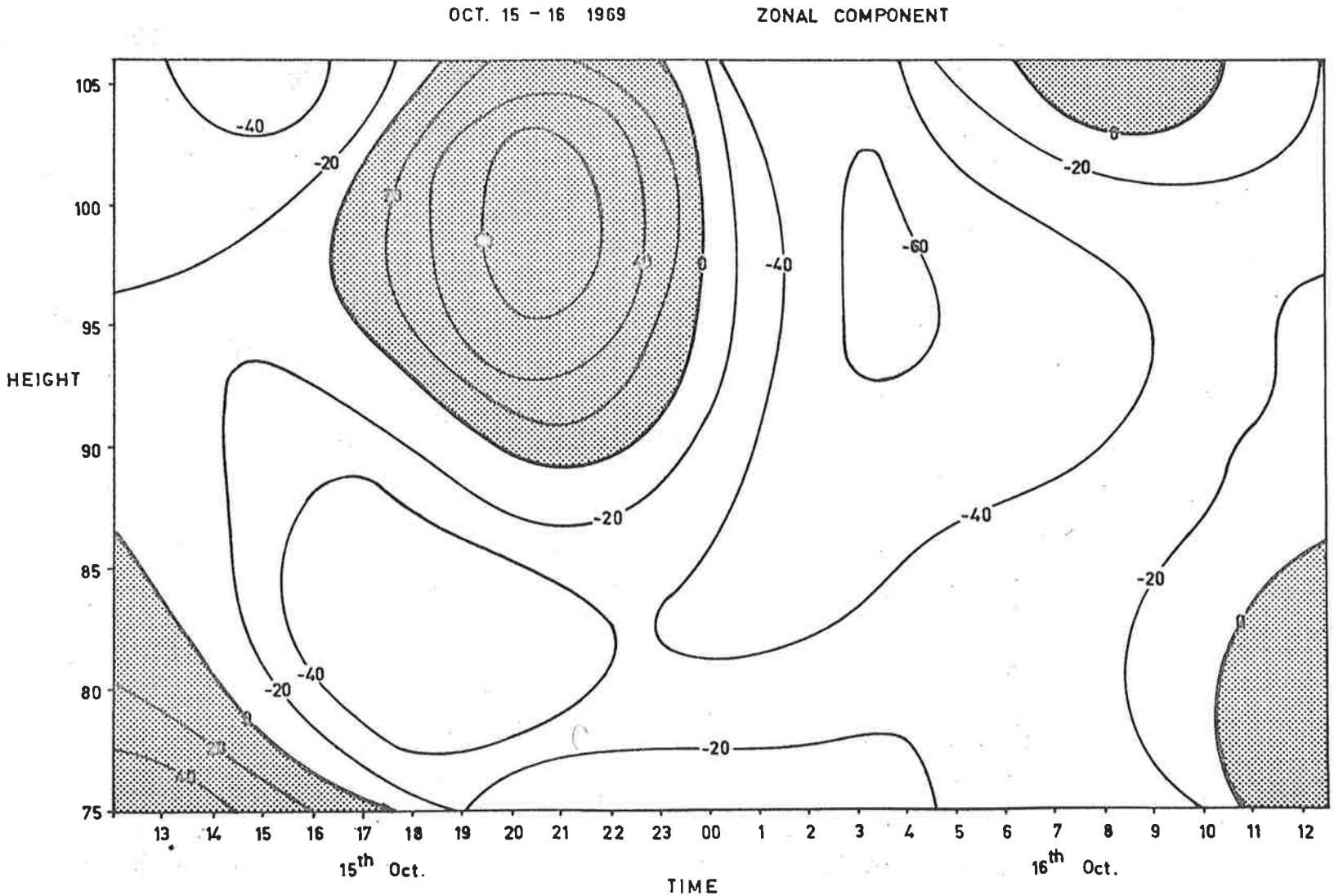

Figure 9.5: Contours of the zonal wind component determined by the radio-meteor technique for the 15th and 16th October, 1969.

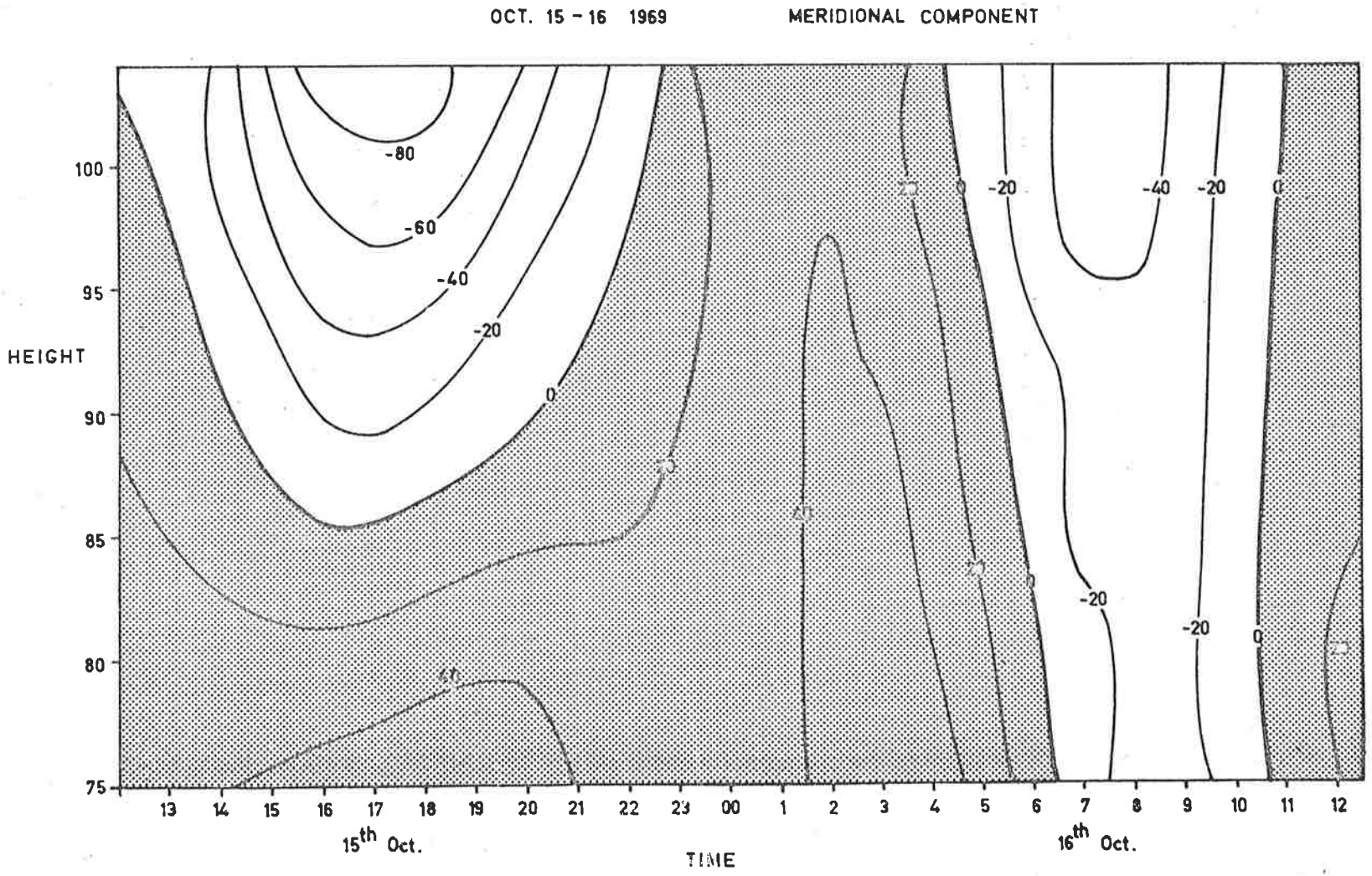

Figure 9.6: Contours of the meridional wind component determined by the radio-meteor technique for the 15th and 16th October, 1969.

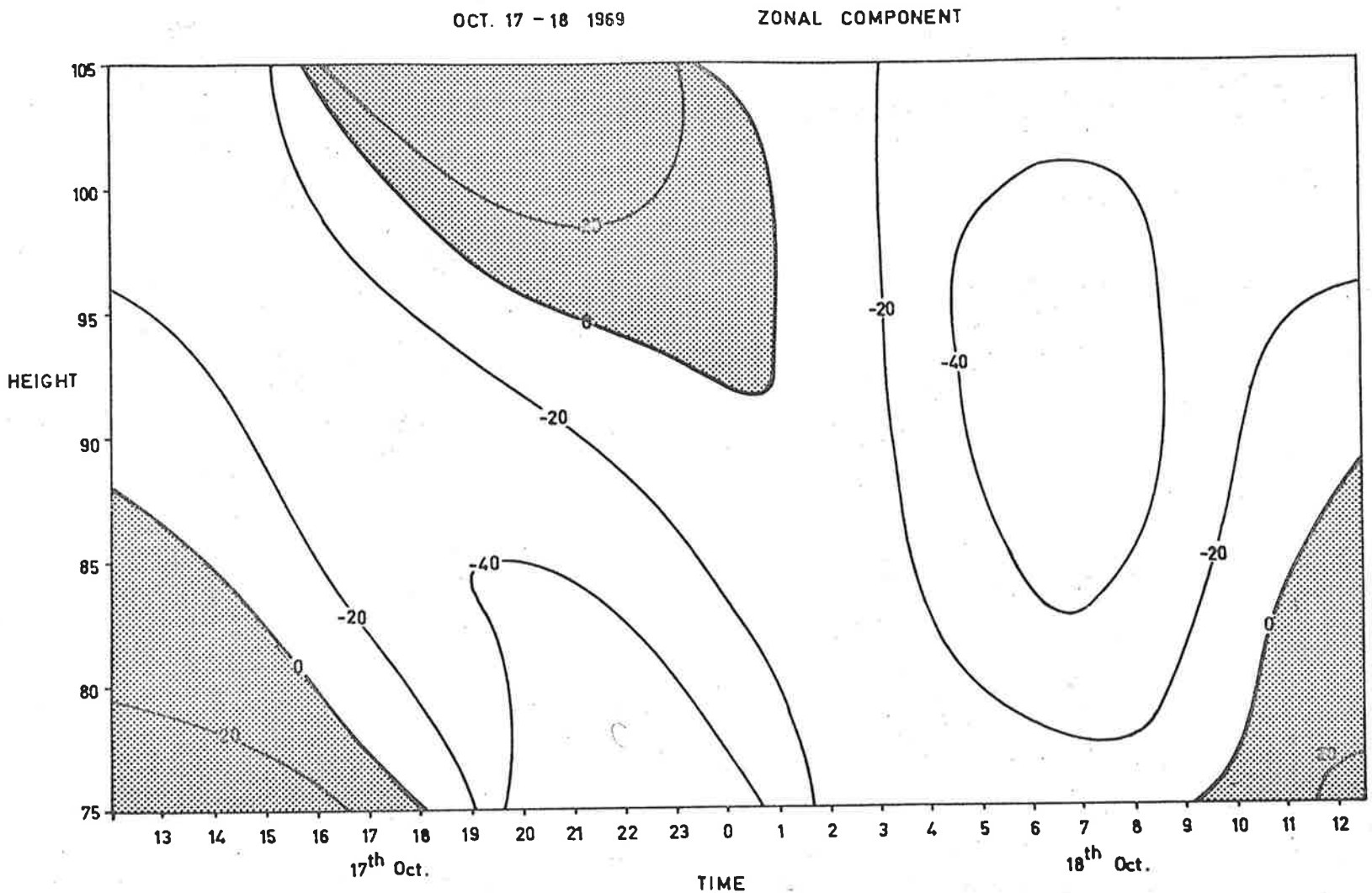

Figure 9.7: Contours of the zonal wind component determined by the radio-meteor technique for the 17th and 18th October, 1969.

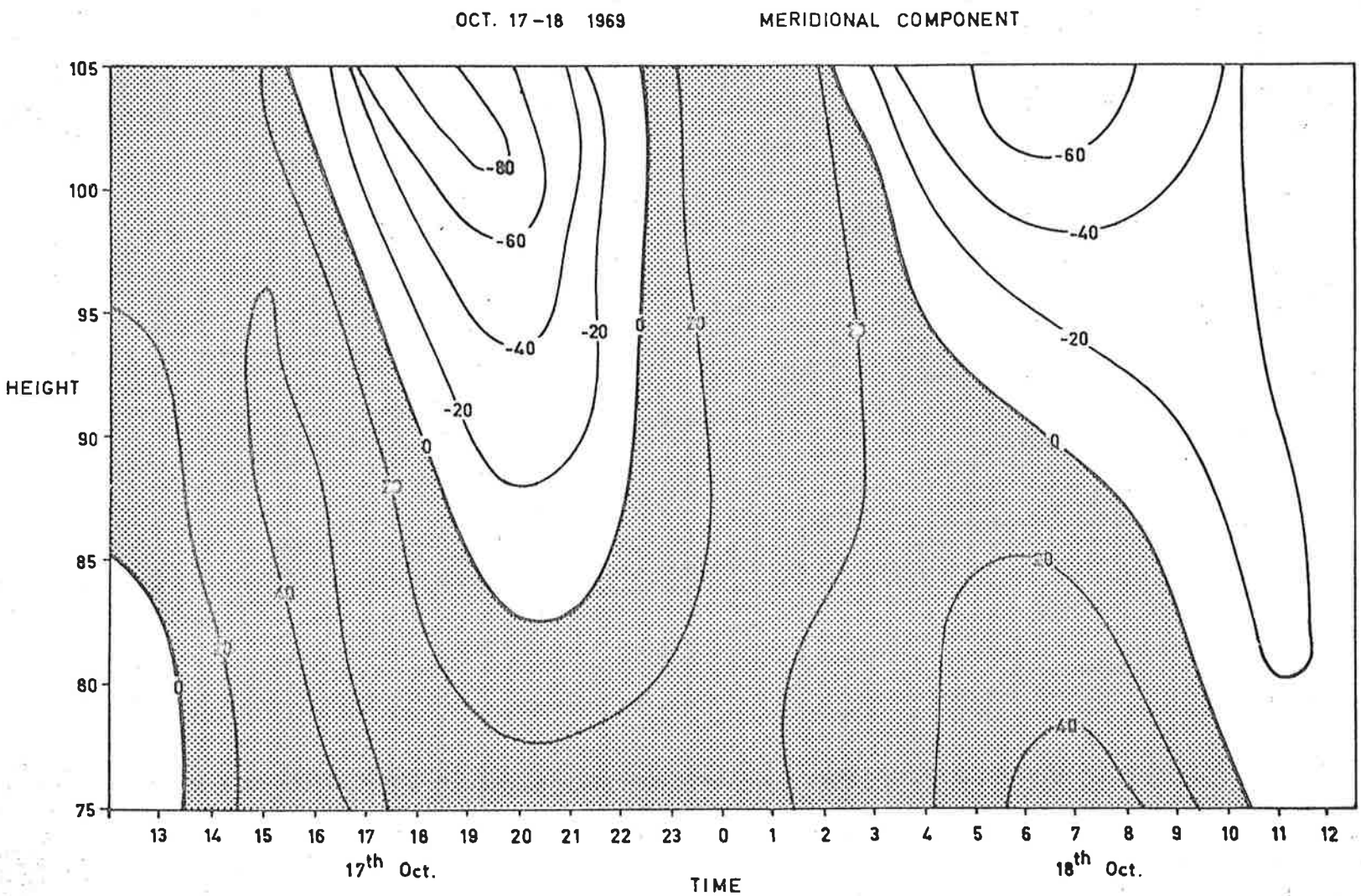

Figure 9.8: Contours of the meridional wind component determined by the radio-meteor technique for the 17th and 18th October, 1969.

of the uncertainty in the model at these extremes of the height range. The other method of analysis used is a modified form of the GROVES analysis: no time variation is allowed (TIGA). Using meteors recorded over a period of about an hour centred on the launch time of each rocket and distributed in time and height as shown in Table 9.2, wind profiles as shown in Figures 9.9 and 9.10 are obtained. The large number of echoes (65) recorded during the period of the morning launch (SL 861) permitted much height variability in the model for this time. The agreement between these profiles and the lower wind determinations from the chemical trail results also shown on these diagrams is quite reasonable considering the separation between the two measurements. Further comments regarding comparison of these profiles will be found in §9.4.

A test of the consistency of the two wind measurements (meteor and chemical trail) was to project the horizontal wind vector measured by the chemical trail at a given height along the line-of-sight for all meteors within 2 km of that height. Figure 9.11 shows the measured line-of-sight velocity plotted against the value expected from the chemical trail measurements from SL 861 and SL 862. The negative correlation apparent on the diagrams is due to the opposite sign convention used for the two measurements. The line-of-sight velocity for a meteor trail moving away from the observer is given a negative sign whereas the chemical trail results have the more normal vector convention - positive away from the origin. The correlation coefficients found are - 0.54 for the morning profile (SL 861) and - 0.59 for the evening profile

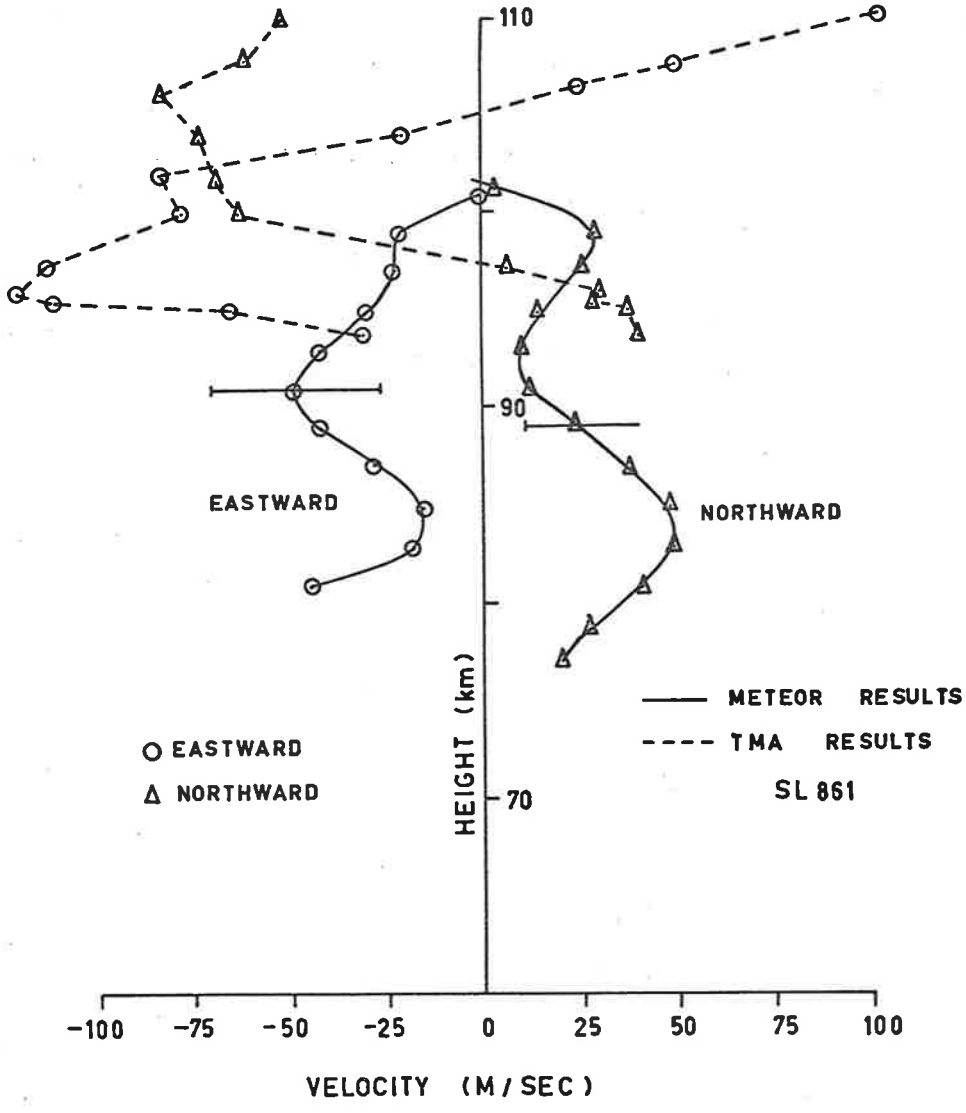

Figure 9.9: The wind profiles determined by the radio meteor system for the interval 0430 - 0515, October 16th. Portion of the wind profile from SL 861 is shown for comparison.

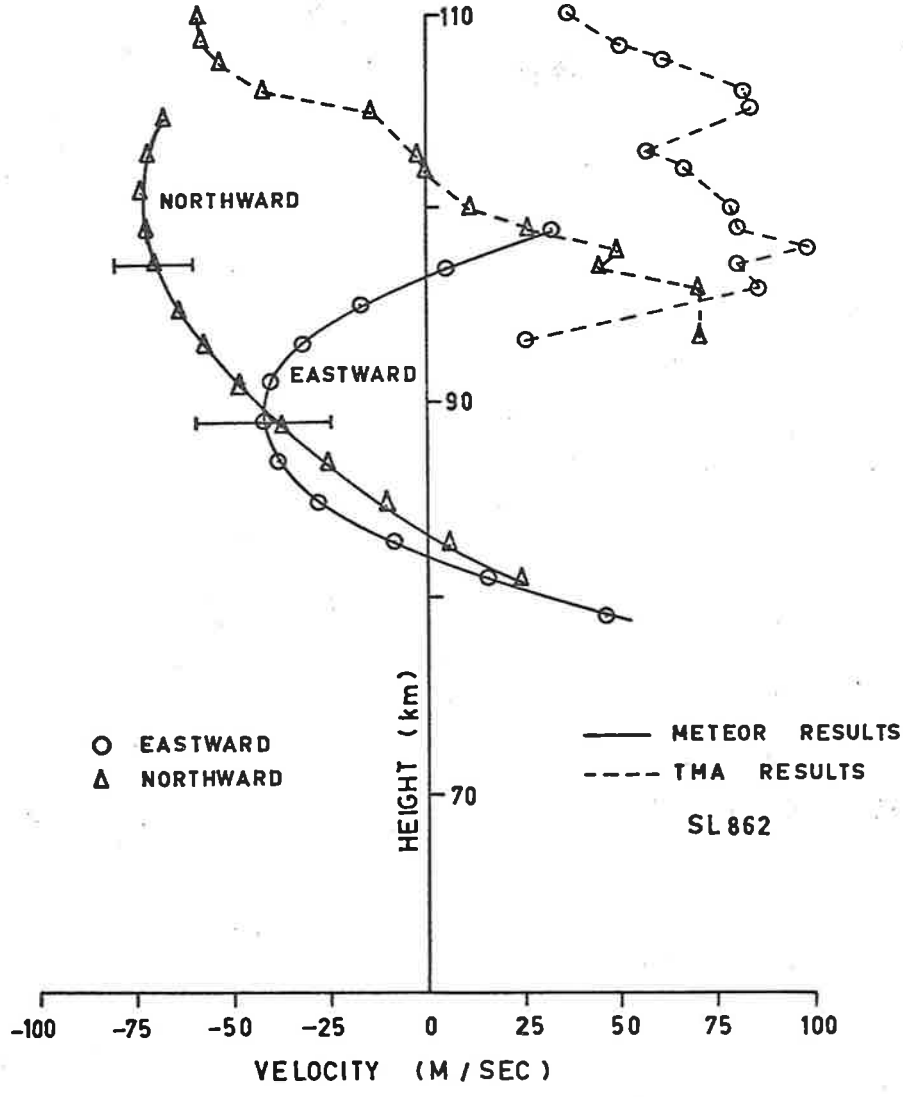

Figure 9.10: The wind profiles determined by the radio meteor system for the interval 1830 - 2000, October 17th. Portion of the wind profile from SL 862 is shown for comparison.

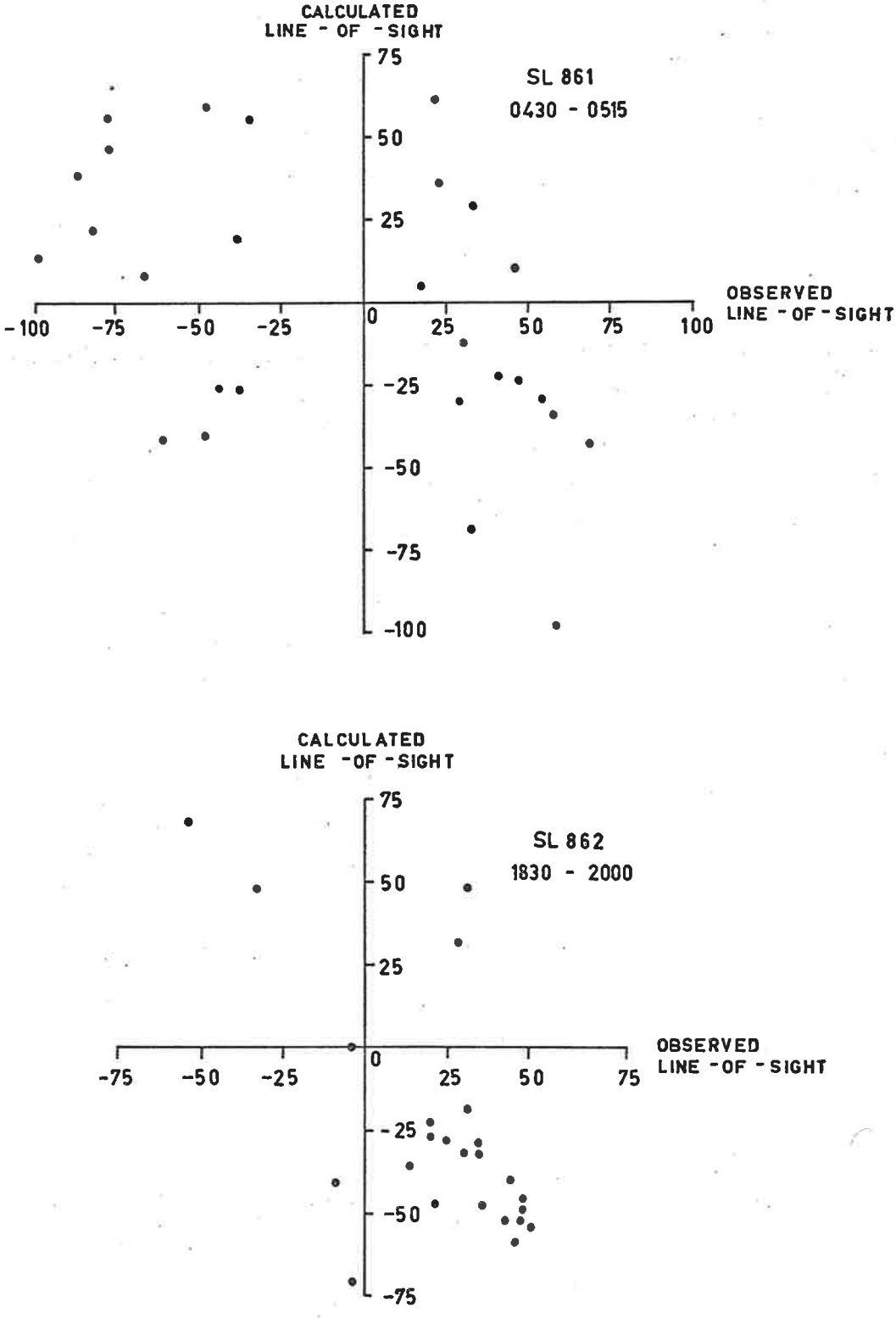

Figure 9.11: Expected line-of-sight velocity from the chemical trail observations plotted against the observed line-of-sight meteor velocity for the two periods, 0430 - 0515, 16th October 1969 and 1830 - 200, 17th October, 1969.

(SL 862) both coefficients being significant at the 0.1% confidence level.

A number of possibilities exist for the relatively low correlation found. The separation of 450 km between the launch site and the observing point is of course a major point. The meteor echoes recorded come from within a radius of about 150 km of the receiving site at St. Kilda. The distribution of the direction cosines for all echoes recorded for the morning (SL 861) profile is shown in Figure 9.12. The concentration of echoes to the south is to be expected because of the position of the radiants for the sporadic meteors at this time. The separation between the two wind measurements can therefore be as much as 600 km at which distance only the gross features of the wind profiles could be expected to be similar. The strong shears evident from the chemical trail wind profiles are probably responsible for much of the scatter on the plots since meteors over a 2 km interval were used in a comparison with each chemical trail wind determination.

By plotting the wind profiles in the form of hodographs, which allow comparison of the total wind vector determined by both techniques at a given height, a better idea of the differences between the meteor wind profiles and chemical trail profiles can be gained. In Figure 9.13 (the morning profile) the main point to note is the difference in amplitude of the two wind vectors. This difference may be ascribed to the failure of the model analysis to follow very rapid wind shears and is discussed further in §9.4. The main difference in the two profiles

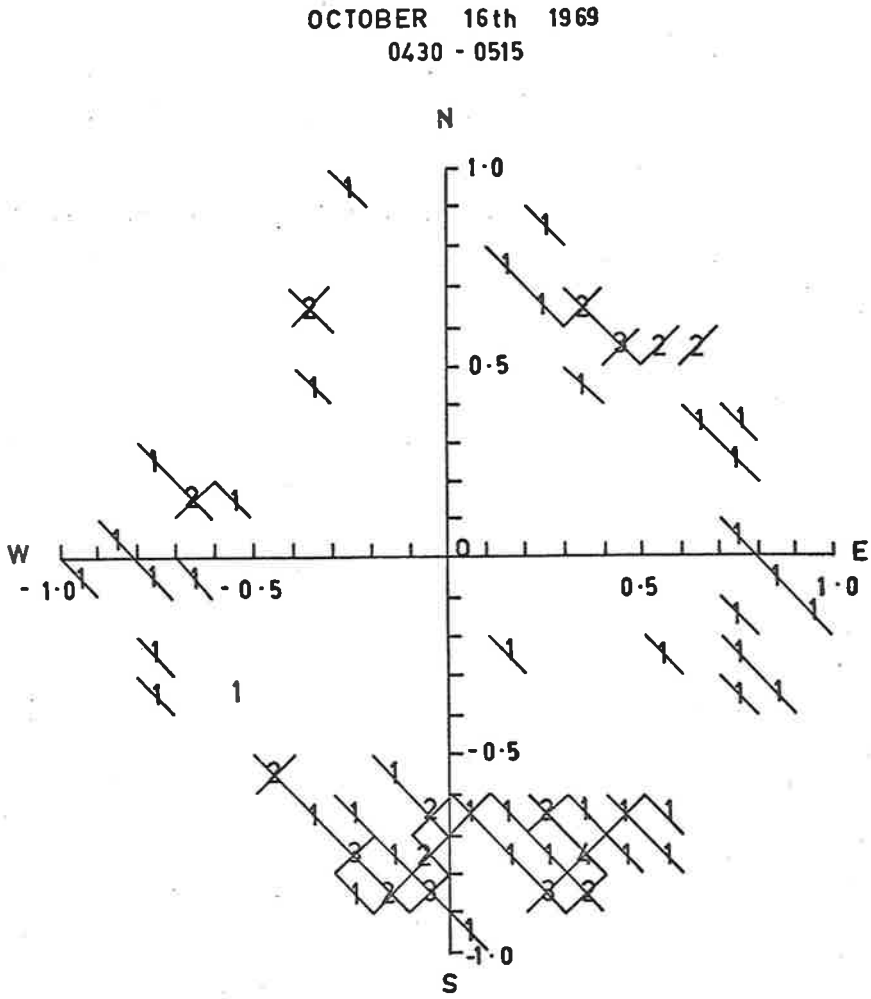

Figure 9.12: Distribution of the direction cosines of meteors recorded in the interval 0430 - 0515, 16th October, 1969.

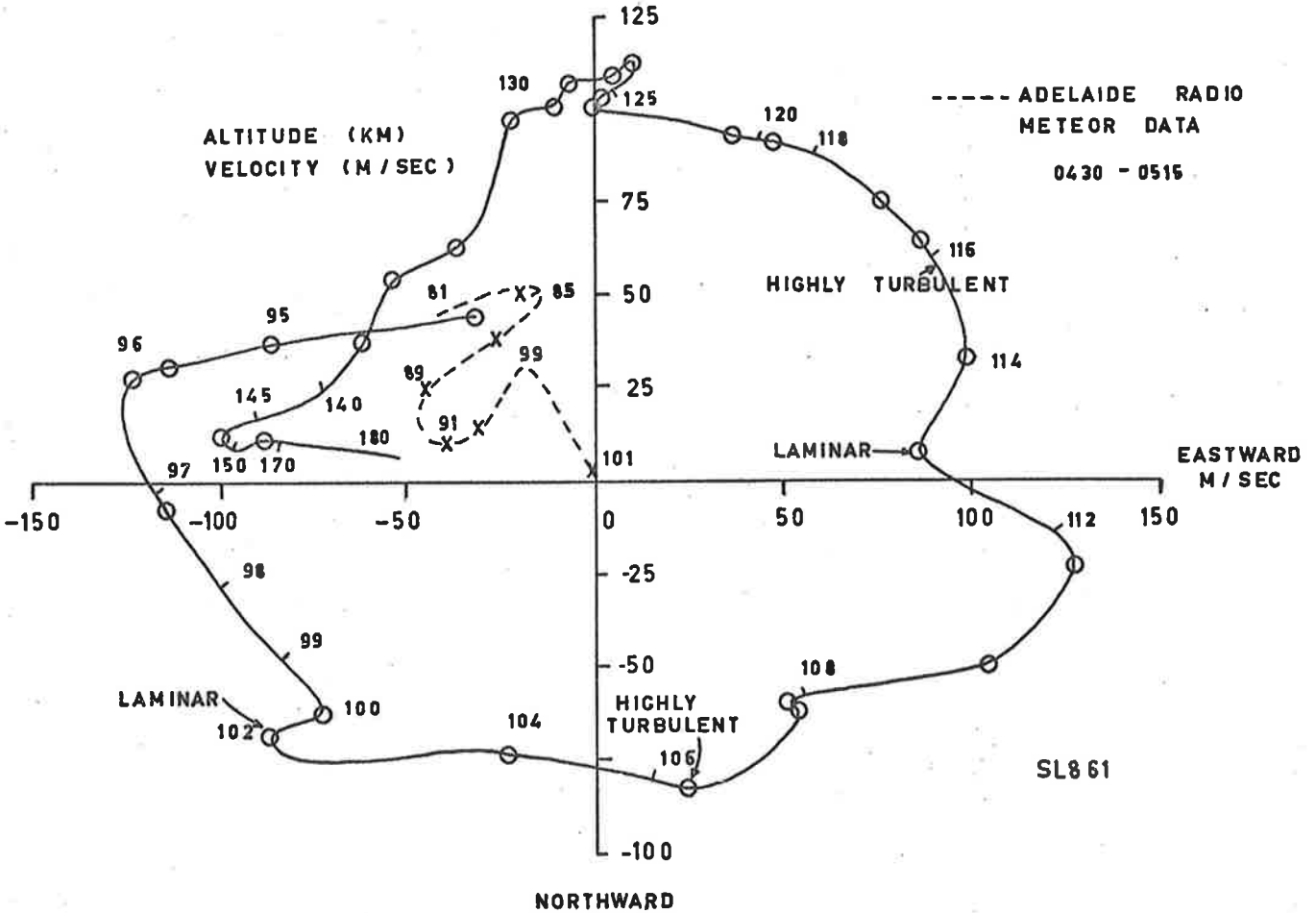

Figure 9.13: Hodograph of wind determined on 16th October, 1969. The numbers marked on the profile refer to the height of the measurement. The full line gives the results from the contaminant release measurements while the dashed line is for the results from the radiometeor analysis.

shown in Figure 9.14 (the evening profile) is the 90° lag of the meteor wind profile. It should also be noted that the meteor wind profile in Figure 9.13 can also be considered to lag the chemical trail profile. A phase lag of the order of 90^{0} between the tides at Adelaide and Woomera would not be expected from tidal theory alone and no satisfactory explanation exists for the apparent differences.

In order to check the validity of the GROVES model used in the determination of the wind profiles discussed earlier a periodogram analysis as described in §7.3 was performed on all of the radio meteor data for October 1969. The results of this analysis for the heights 81 km, 91 km and 101 km are shown in Figure 9.15. The periodograms in this diagram are oversampled, the actual resolution is only about 0.2 cycles/day. The peaks at periods of 24 hour and 12 hour (1 cycle/day and 2 cycles/day) are significant and indicate that the GROVES model of a prevailing component plus 24 hour, 12 hour and 8 hour components is applicable for this data. Variation of the parameters of the model associated with the eight hour periodic component makes little change in the resultant wind profile.

9.3 WIND SHEAR AND TURBULENCE MEASUREMENTS

Both of the TMA trails developed an extensive irregular (turbulent) region below 110 km about 30 secs after release. Two frames from the Baker-Nunn (f/1, 50 cm focal length) of the SL 862 trail show this development reasonably well. The first frame (Figure 9.16) is taken 30 secs after the commencement of trail release. The grenade bursts within the trail are clearly visible at the upper levels while lower down the trail appears

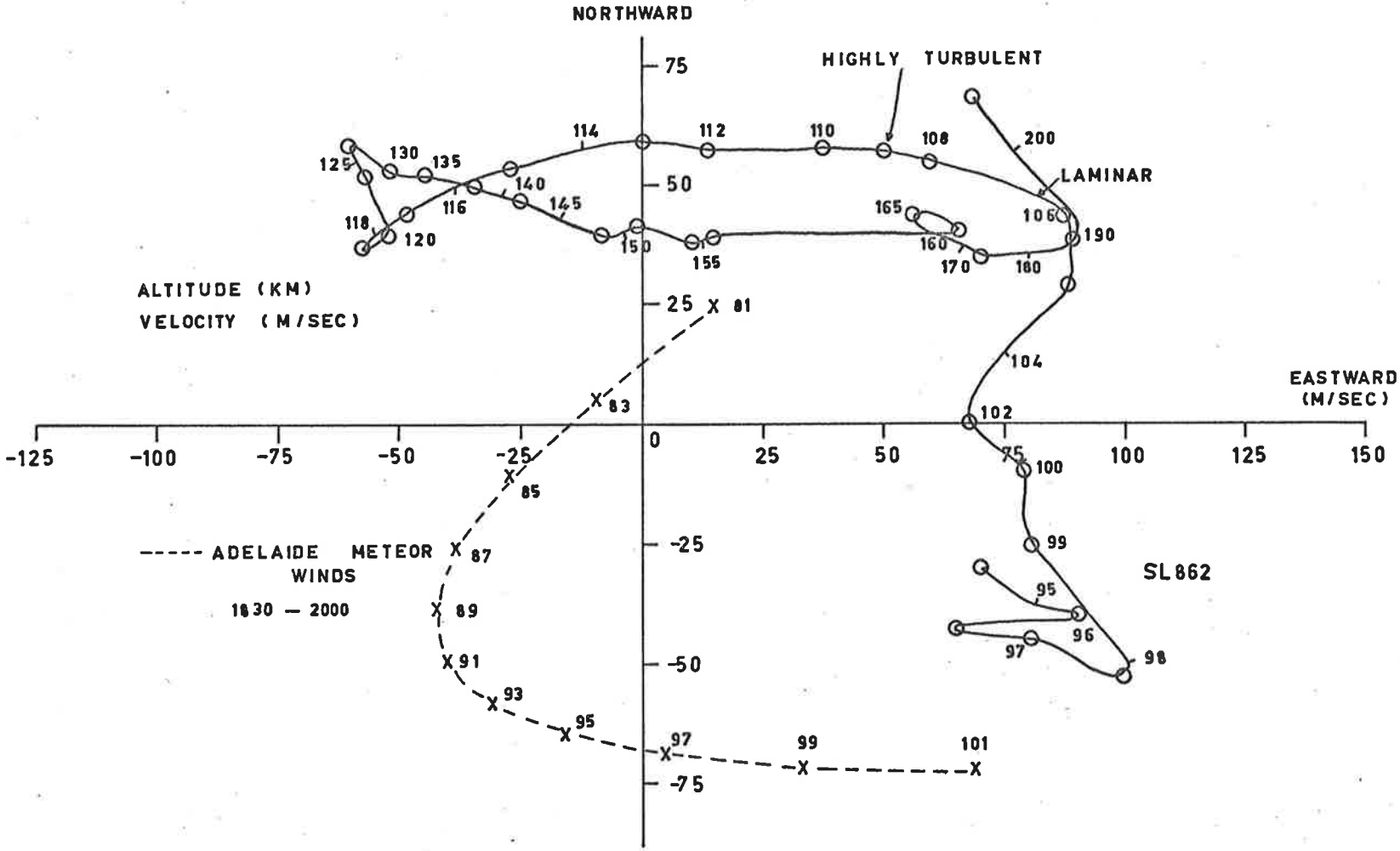

Figure 9.14: Hodograph for the wind determined on October 17th, 1969. The full line is for the contaminant release observations, while the dashed line is for the results from the radio-meteor analysis.

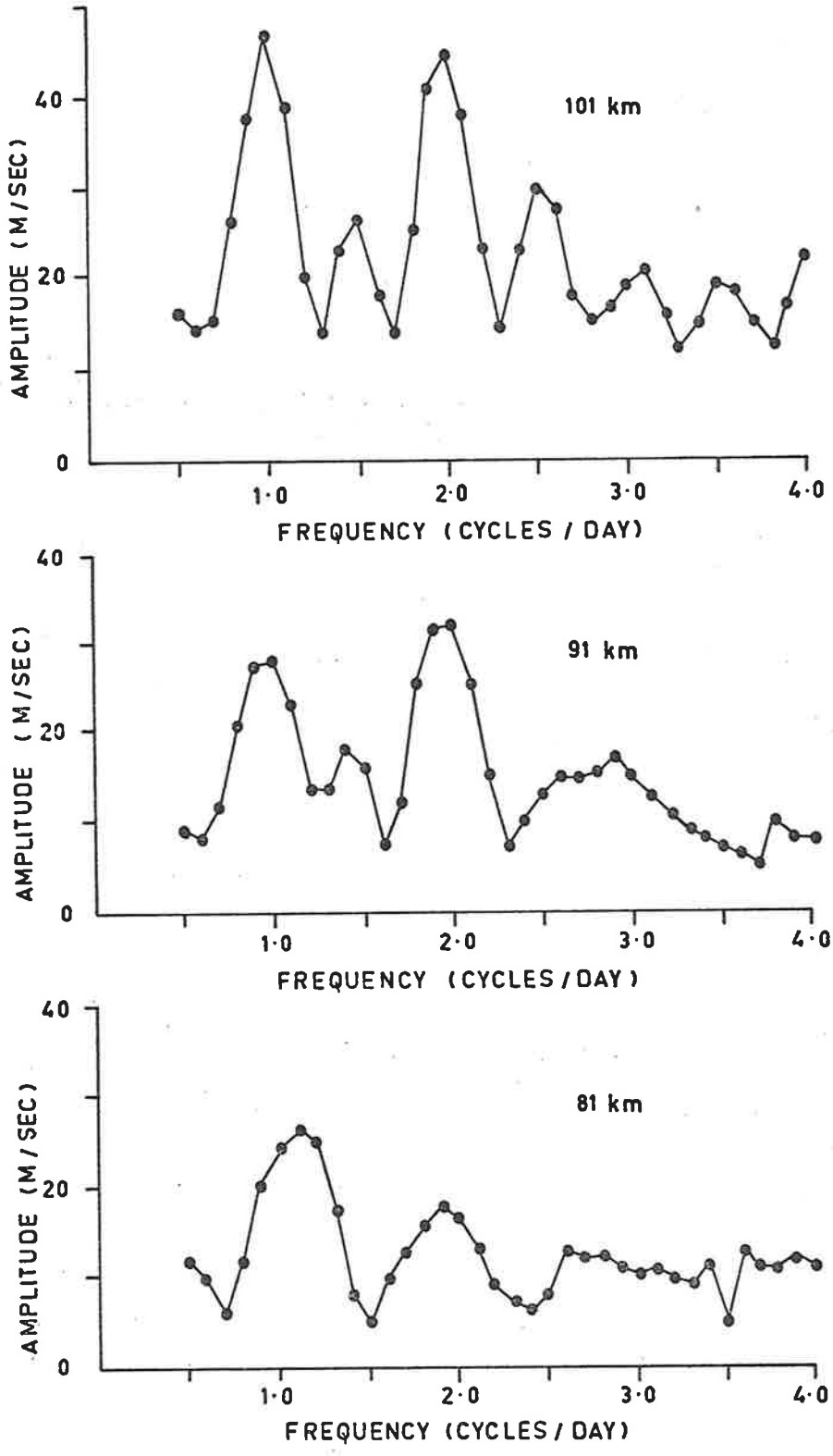

Figure 9.15: Periodograms computed for heights 81, 91 and 101 km for October 1969.

Figure 9.16: The TMA trail from SL862 photographed 30 seconds after release.

Figure 9.17: The TMA trail from SL862 photographed 40 seconds after release.

reasonably "smooth". However in Figure 9.17 taken 40 secs after release, the lower portion of the trail has become very chaotic without any association with a grenade burst.

The breakdown from a "smooth" appearance to "turbulent" is a dramatic change and easily recognisable by visual inspection of the original photographs. The delay in onset of turbulence is clearly shown in Figure 9.18 which shows isodensitrace scans of a portion of the trail from SL 861. The transition between "rough" and "smooth" in the region near 110 km is easily seen in the upper diagram. When the lower portion of the trail has broken up it can be seen that "blobs" in the trail can be smaller than the trail diameter at earlier times. Thus it appears that the criterion for the commencement of turbulence is not necessarily that the trail must grow to the size of the smallest eddy. Rees et al. (1970) observed a similar phenomena with two trails released in May 1968 and they proposed that the delay in the onset of turbulence is a measure of the time constant of the Kolmogonov microscale. Figures 9.19 and 9.20 taken from Rees et al. (1970) illustrate the delay in onset of turbulence very clearly. The latter diagram shows that although the trail at 108 km remains laminar, the growth rate of the trail at this point is much faster than could be produced by molecular diffusion alone.

Figure 9.21, plotted from information provided by Lloyd (1970), shows the best estimates of the time of onset of turbulence at various altitudes for the SL 861 trail. The occurrence of alternate laminar and turbulent regions is quite interesting and has been observed previously by other

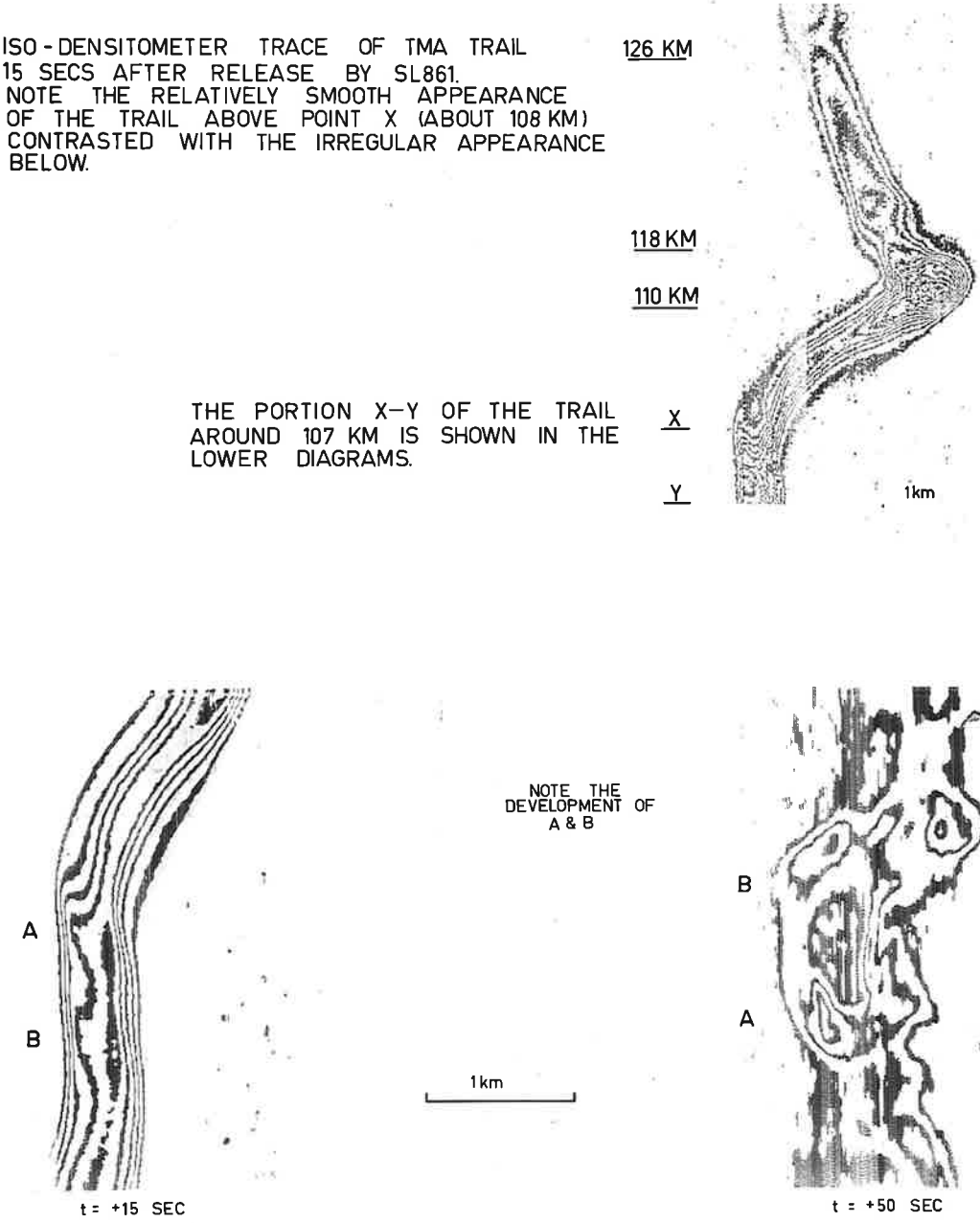

NOTE THAT THE SCALE OF THE EDDIES AT +50 SEC IS GREATER THAN THE DIAMETER OF THE TRAIL AT +15 SEC. (THE "DOT" NODE ON THE +50 SEC MONTAGE WAS INOPERATIVE.)

Figure 9.18: Isondensitrace scans of part of the trail from the SL861 release showing the breakdown from "smooth" to "rough" appearance.

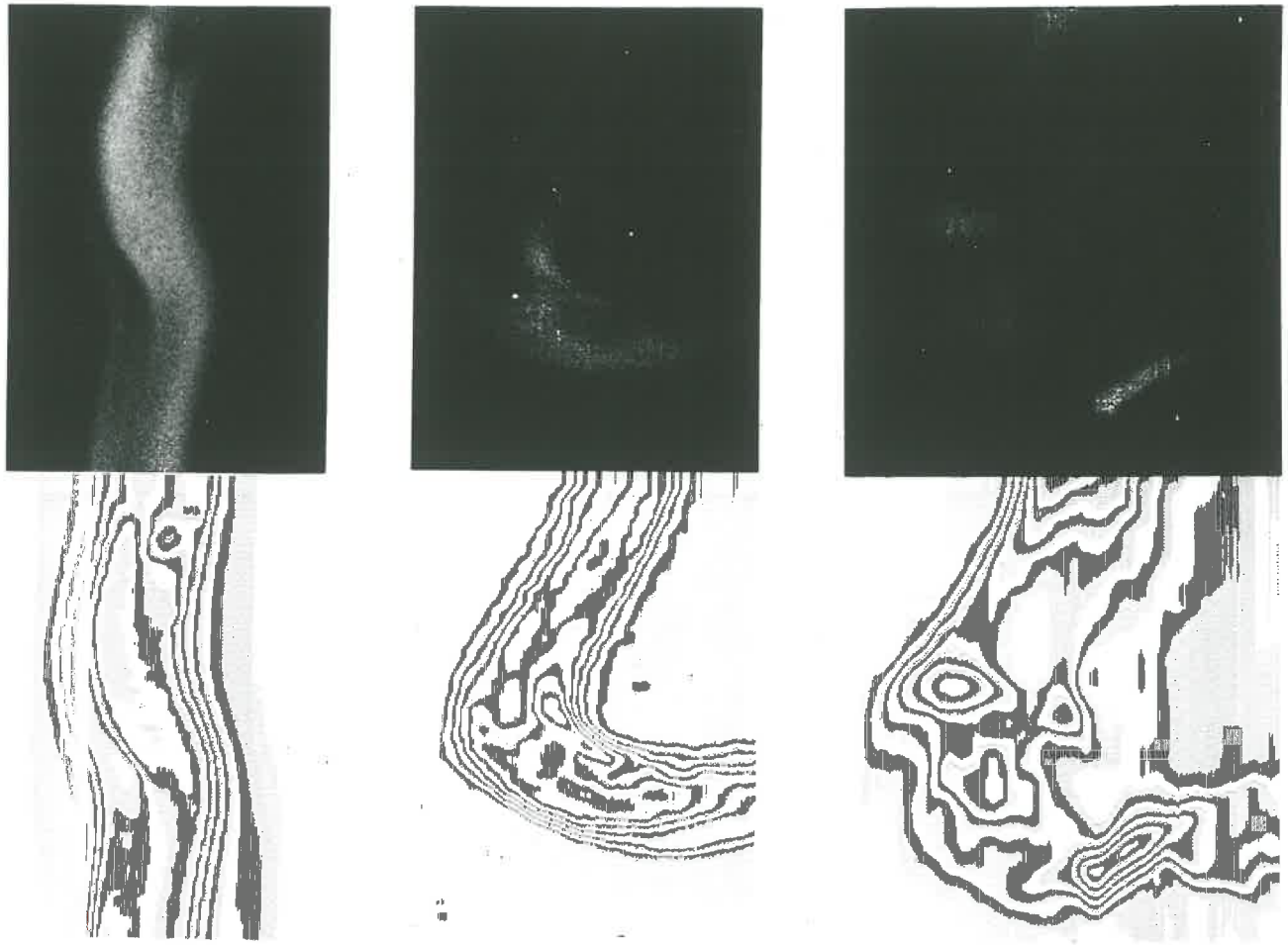

Figure 9.19: Montage of portion of TMA trail released at 0609, 31st May, 1968 (after Rees et al., 1970).

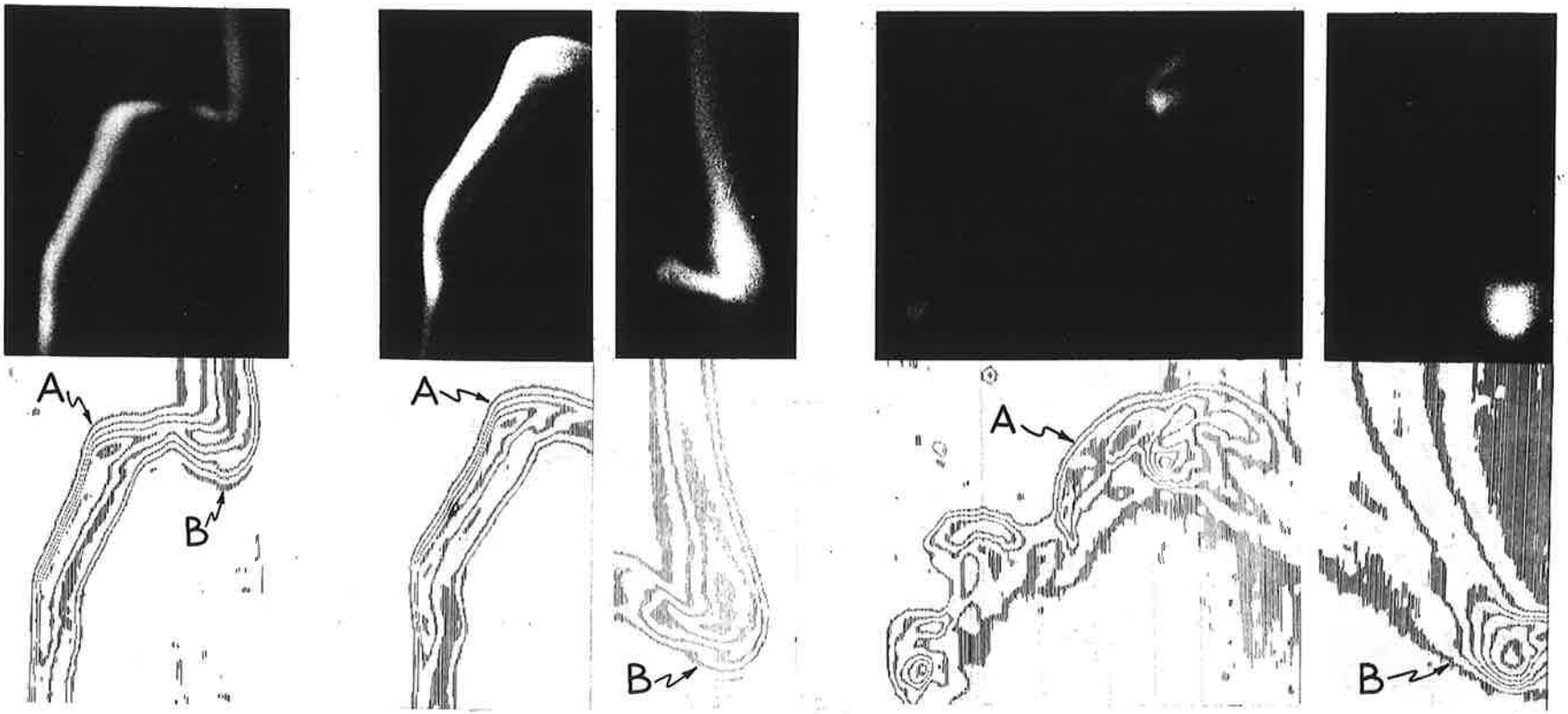

Figure 9.20: Montage of portion of TMA trail released at 1819, 31st May, 1968 (after Rees et al., 1970).

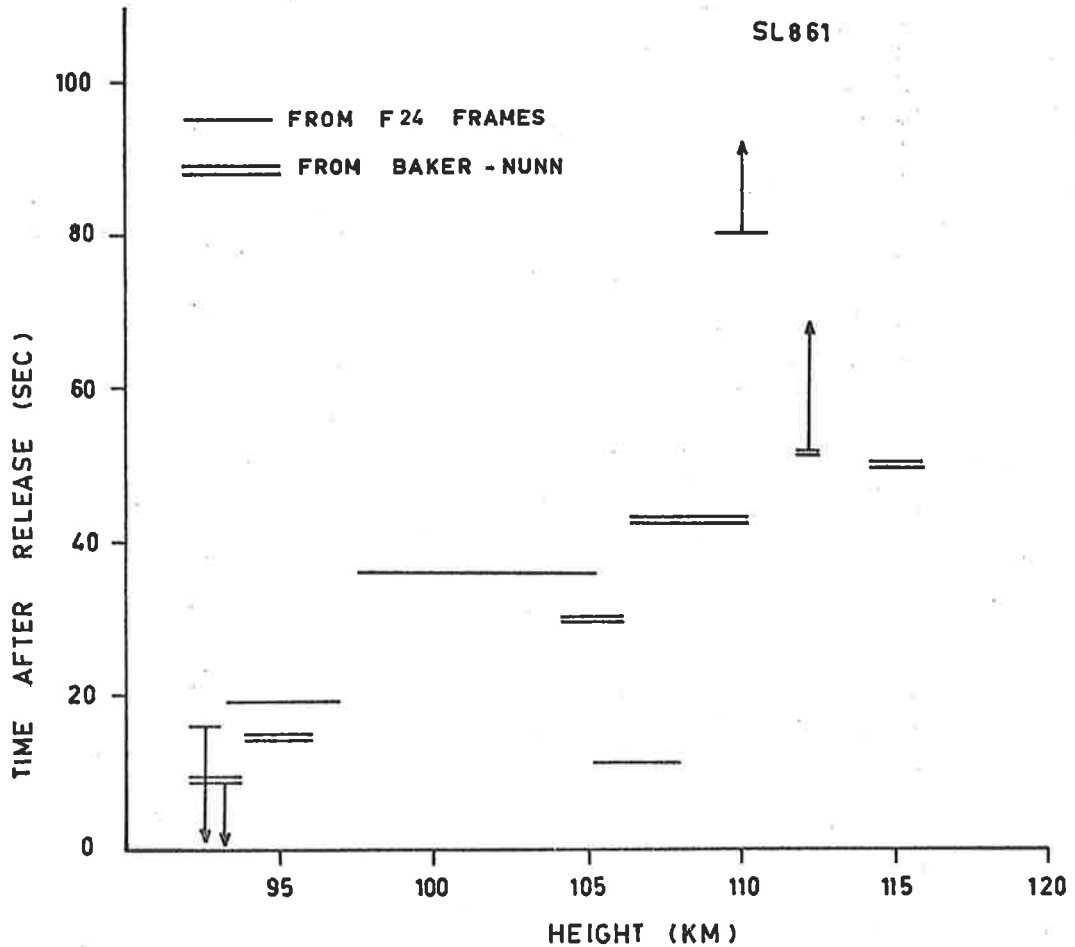

Figure 9.21: Estimates of the delay in onset of turbulence at various altitudes for the morning profile (16th October).

workers (Blamont and Barat, 1967; Shafi Ahmad, 1969). Both Baker-Nunn and F24 (f/2.9, 200 mm focal length) photographs were examined, the two sets of values for the delay are plotted on the diagram. Care must be exercised in interpreting the photographs since the explosion of grenades at 113 and 118.5 km represents a large perturbation; a turbulent region near 115 km separated from the grenade bursts by laminar regions is apparent on the photographs. The times of onset as determined are not incompatible with the hypothesis of the time constant of the Kolmogorov microscale.

It would be expected intuitively that turbulence would be most likely to occur either at a velocity maxima where breakdown of a gravity wave might be expected to occur or else at regions of maximum wind shear. However there appears to be no correlation between the onset of turbulence and either wind speed or shear as can be seen by inspection of the hodographs (Figures 9.13 and 9.14). Unfortunately no measurements of the temperature structure over the region of interest are available so that it is impossible to state whether small scale temperature inhomogeneities could explain the occurrence of turbulence.

In order to examine the wind structure at larger scales the vertical wind shears are presented in the form of structure functions as defined earlier (§2.2). Provided that the structure function is computed over at least the correlation distance in the wind profiles (∿ 1 scale height) then a reasonable measure of the wind shear is obtained. There is a

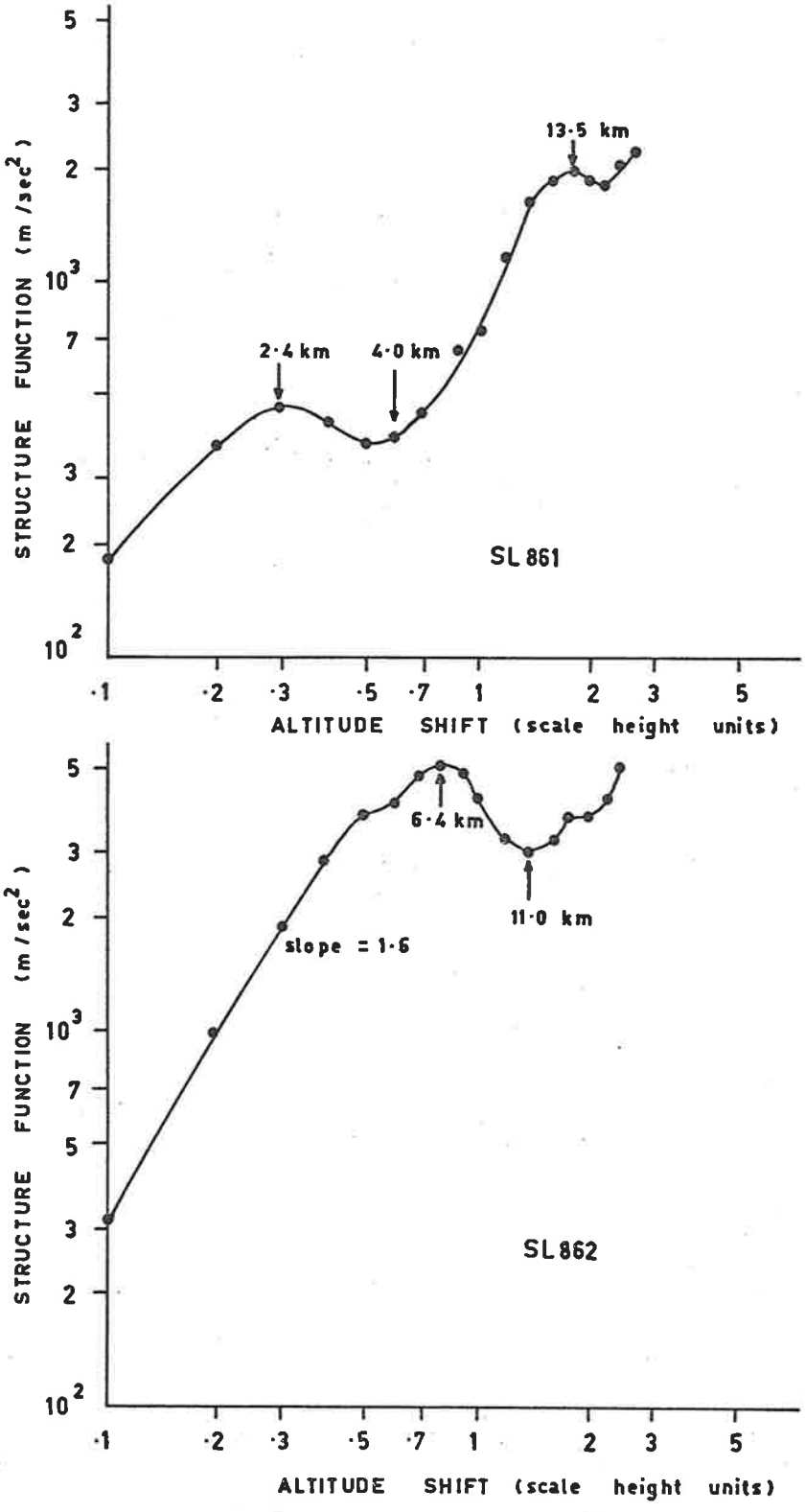

Figure 9.22: Structure function at 110 km computed for the two wind profiles determined from the chemical releases.

considerable difference between the structure functions at 110 km computed for the morning and evening wind profiles as can be seen in Figure 9.22. The differences may be due to a differing spectrum of internal gravity waves being present on the two occasions.

The measurements of wind shear made with the multi-station radio meteor equipment are presented in the form of structure functions in Figure 9.23 for vertical and horizontal separations respectively. The method of obtaining these functions has been discussed in Chapter VIII. The difference in slope of the best fit straight lines is readily apparent by eye with the vertical slope being the greater. Using the weighted least squares fitting method described in the previous chapter the slopes of the best fit straight lines are 0.8 ± 0.1 for the vertical structure function and 0.5 ± 0.1 for the horizontal structure function. Neither of these slopes can be taken as proving the existence of an inertial sub-range of turbulence for which a slope of 2/3 is expected, however the difference between the slopes is statistically significant and must reflect a differing structure. Following the discussion in §8.2 the vertical structure function can be interpreted as being due to the mean shear whereas the horizontal structure function may be due to extreme values of shear and even to turbulence.

Because of the known existance of turbulence at 90 km from photographs of the contaminant release trails it is interesting to assume that the horizontal structure function found by the radio-meteor technique is due to an inertial sub-range of turbulence. It is then possible to

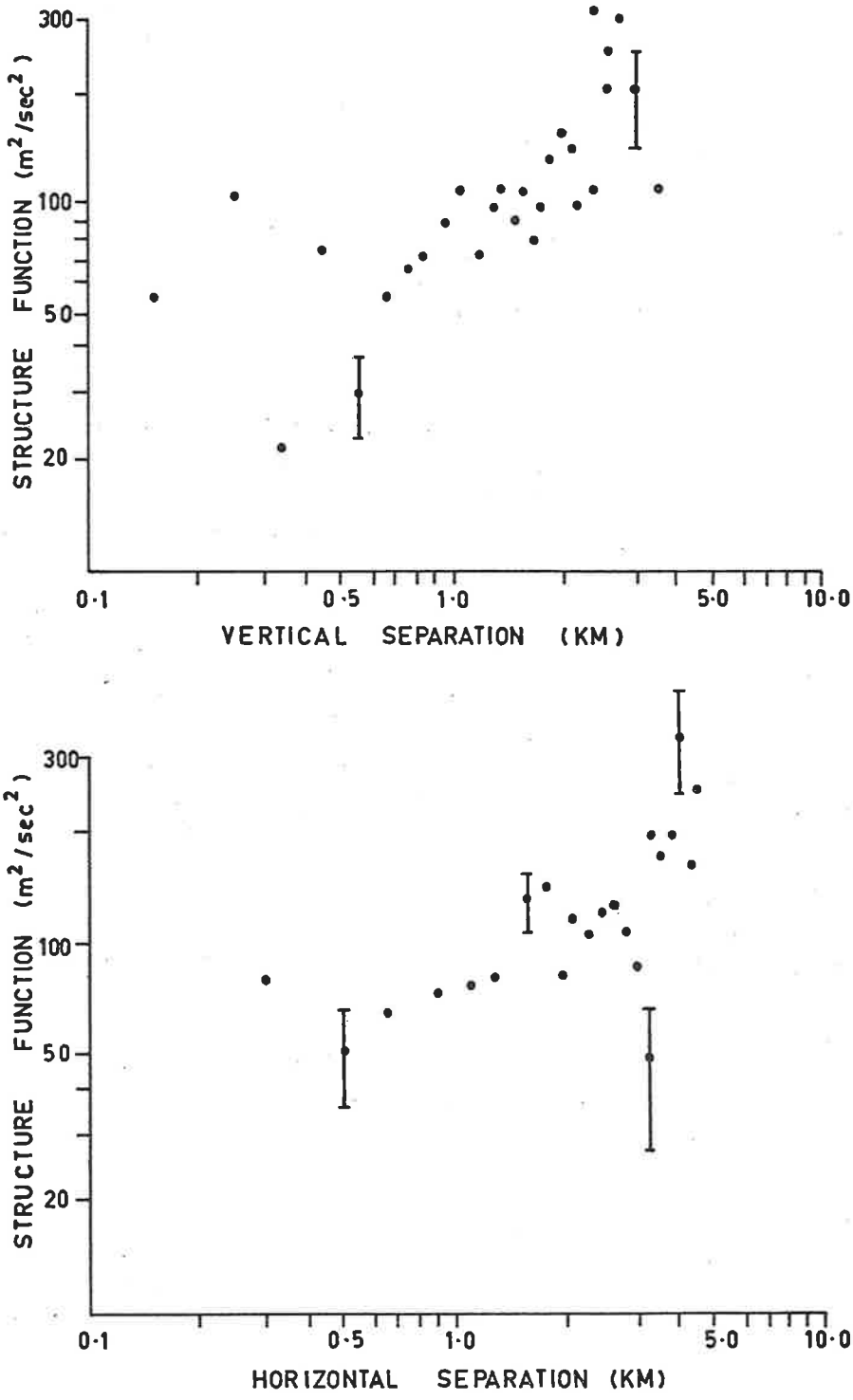

Figure 9.23: Structure functions for October, 1969 (213 meteors).

deduce some parameters of the turbulent field which can be compared with parameters determined from the contaminant releases. The only parameter which can be determined directly from the radio-meteor observations is the rate of dissipation of turbulent energy ε, which is considered to be the value at the mean height of the meteors, 92 km, its value is 0.045 watt/kg. The parameter most readily measured from the contaminant release trails is the time of onset of turbulence which from Figure 9.21 has the value of about 15 secs at 92 km. Rees et al. (1970) have proposed that the time constant of the Kolmogorov microscale, which has the value

$$t^* = (\nu/\varepsilon)^{\frac{1}{2}} ,$$

is the parameter associated with trail break up (ν is the kinematic viscosity). The kinematic viscosity is determined from the viscosity μ and density ρ of the U.S. Standard Atmosphere Supplements, 1966 and has the value 7.7 m^2/sec at 92 km. Using the value $t^* = 15$ secs deduced above, Rees et al. found the value $\varepsilon = 0.03$ watt/kg. This is very similar to the value found from the radio-meteor studies and is consistent with the value obtained by Justus (1967b).

9.4 SUMMARY AND CONCLUSIONS

Simultaneous wind measurements made with a radio-meteor system and contaminant release trails have shown differences which are probably due to the separation of the two measurements (400 - 500 km). The large wind shears measured with the contaminant trails have not been detected with the radio-meteor system. This difference is most probably due to the

methods of analysis used with the radio-meteor data. A comparison of the line-of-sight velocity from individual meteors with the wind velocity determined from the contaminant releases gives quite good agreement (correlation coefficients greater than 0.5). Thus the form of smoothing used on the radio-meteor data must be considered in more detail.

The method of analysis developed by GROVES appears to be an excellent method for determining the prevailing and periodic components of the wind field (for which it was designed), however the application of a time-independent (TIGA) model appears uncertain. Very rapid variations in wind with height, as for example during the time of the morning chemical release , cannot be followed successfully with the model (TIGA) analysis. This failure derives from two sources, the time interval necessary to obtain enough meteors for a stable model and the distribution of echoes in height. Rapid variations in wind velocity in a region of few meteors usually lead to instability in the model. No satisfactory alternative analysis has been found although simple averaging over 5 km height intervals may be adequate for some purposes (e.g. comparison with D region partial reflection drift measurements).

Photographs of both chemical trails (morning and evening) reveal the existence of extensive areas of turbulence below 110 km. The structure functions determined by the radio-meteor system indicate the possible existence of turbulence at least for horizontal displacements. The rate of dissipation of turbulent energy (4.5×10^{-2} watts/kgm) that can be determined is not inconsistent with previous measurements. The source

for this turbulent energy is unknown although the failure of the tidal components (as deduced from the periodogram analysis) to increase with altitude indicates that some of the tidal energy must either be dissipated in the region or be converted into other forms of motion.

Many of these areas of discrepancy can only be checked by repeating the experiment again preferably with a radio-meteor system at the same site or at least with two successive chemical trails about an hour apart so that some measure of temporal changes in the wind field can be determined.

CHAPTER X

ROCKET MEASUREMENTS OF WIND AND DENSITY IN THE MESOSPHERE AND STRATOSPHERE

10.1 INTRODUCTION

This chapter is independent of the rest of this thesis and is concerned with methods of data reduction associated with a meteorological rocket programme. Since 1962 the Weapons Research Establishment, Salisbury, S.A. has been engaged in measuring meteorological parameters in the stratosphere and mesosphere (40 - 90 km). The most common measurements available are wind profiles obtained by tracking some falling object with an accurate radar (details of the measurement are given in the following section).

Because the maximum height for which the wind can be measured by the rocket technique lies within the height range covered by the Adelaide radio meteor system direct comparison of the two measurements is possible. Rofe, Elford and Doyle (1966) have shown that excellent agreement is possible between the mean zonal winds determined by the two methods. Thus it was natural to attempt to extend this comparison to the small scale wind structure. However it was found that knowledge of the errors involved in the wind profiles was limited at that time (1966) and hence methods of determining these errors were investigated first. This study showed that the errors in the wind profiles above about 60 km were too large to permit

determination of any structure with scales of 2 km or less and hence no comparisons with the meteor results were possible.

The error analysis which had been developed proved to be very easy to incorporate into the standard data analysis procedure and since 1967 has been part of the routine data reduction. As far as is known the method of determining the radar error described in this chapter has not been used elsewhere.

10.2 EXPERIMENTAL METHODS

Two methods are used to determine the winds and density (or temperature). One method is to eject a metallised sphere (2 metre diameter) from a rocket near apogee and track the sensor with an accurate radar. The other method uses an active rocketsonde package attached to a metallised parachute which again is tracked with an accurate radar.

The sphere is released from a two-stage solid propellant rocket near apogee (approximately 115 km) and is then inflated to a pressure of about 0.2 millibar by 70 gm of iso-pentane. The inflated sphere accelerates essentially in a free fall condition until about 95 km where the drag retardation becomes measureable (2 m/sec/sec). Maximum sphere velocity of 640 m/sec is reached near 85 km and maximum drag deceleration of 25 m/sec/sec occurs near 75 km. An FPS16 radar is normally used to track the sphere during its descent and hence enables the velocity and acceleration of the sphere to be determined.

The rocketsonde package, which contains sensors to measure the temperature and pressure of the atmosphere is released from a much smaller rocket near 75 km. The rocketsonde is attached to a metallised parachute which is also tracked with an FPS16 radar. The maximum velocity of the parachute is about 200 m/sec.

10.3 DATA ANALYSIS

The FPS16 radar provides positional data of range, azimuth and elevation at 40 points per second (the primary data). A linear discrete smoothing technique is used to provide a secondary set of data at 2 points per second with any points in the primary data deviating from the mean by more than three standard deviations being ignored. This secondary data is also converted to a Cartesian coordinate system with an origin at the launch site.

The velocity and acceleration of the falling object are determined from this secondary data using the method originally proposed by Engler (1965). Because the vertical component of velocity of the object gradually decreases with decreasing height a decision must be made whether to use a constant height interval with a variable number of data points or a fixed number of points and a variable height range. It is generally argued that in order to preserve detailed structure at lower heights a fixed number of points should be used. The velocity of the sphere or parachute is found by applying a sliding linear fit to 31 data points from the secondary tape; the slope of the best fit line is taken as the

velocity for the midpoint of that group of points. A further linear fit is made over 7 velocity points to determine the acceleration.

The atmospheric density is found from the velocity and acceleration using the following expression (applicable only to a fully inflated sphere) derived from the equation of motion.

$$\rho = \frac{m(g - \ddot{x}_3 - 2(\underline{\omega} \times \underline{v})_3)}{\frac{1}{2}C_D A|\underline{u}|(\dot{x}_3 - W_3) + gV} \qquad 10.1$$

where: $2(\underline{\omega} \times \underline{v})_3$ is the component of the Coriolis acceleration in the vertical direction;

$|\underline{u}|$ is the velocity of the sphere relative to the wind;

C_D is the drag coefficient of the sphere;

A and V are respectively the area of cross-section and volume of the sphere;

g is acceleration due to gravity;

m is mass of sphere;

$\ddot{x}_3, \dot{x}_3$ are the vertical acceleration and velocity of the sphere;

W_3 is vertical wind component.

The east-west and north-south components of the wind can be determined from the relation,

$$W_i = \dot{x}_i - \frac{\dot{x}_3(\ddot{x}_i + C_i - B_i)}{\ddot{x}_3 + C_3 - B_3} \quad i = 1,2 \qquad 10.2$$

where: $\dot{x}_i$ are the components of the velocity of the sphere;

C_i, C_3 are the components of Coriolis acceleration;

B_i, B_3 are the buoyancy terms.

The addition of the Coriolis term can be important at the higher altitudes (> 80 km) while the buoyancy term may be important at lower altitudes (below 35 km).

In the case of the parachute the horizontal wind components are found using the relation

$$W_i = \dot{x}_i - \frac{\dot{x}_3 \ddot{x}_i}{\ddot{x}_3 - g}, \quad i = 1,2 \qquad 10.3$$

The error introduced by neglecting Coriolis and buoyancy effects is only a few per cent.

For each falling sphere sounding the atmospheric density is calculated for heights from near 95 km (where the deceleration first becomes measurable) to 45 km (where the sphere first starts to deflate) while the horizontal wind components are calculated for heights from 85 km down to 30 km. Winds are deduced from the parachute observations over the height range 65 km to 30 km.

10.4 ERRORS IN MEASUREMENT

10.4.1 Errors in Wind. I. Mean Radar Errors

For the purposes of error prediction, expression (10.3) is sufficiently accurate for both the sphere and parachute observations. By applying an elementary theorem of statistics to equation 10.3 and neglecting

second order terms the variance in the wind components is found to be

$$\sigma^2_{W_i} = \left[\frac{1}{(\Delta t)^2 \sum_{j=1}^{31} P_j^2} + \frac{\dot{x}_3^2}{\sum_{k=1}^{31} P_j^2 \sum_{k=1}^{7} P_k^2 (\Delta t)^4 g^2} \right] \sigma_{x_i}^2 \quad i = 1,2 \qquad 10.4$$

where: Δt is time interval between data points (0.5 sec),

$P_j = j - 16$, results from the linear fit of 15 seconds of position coordinates,

$P_k = k - 4$, results from the linear fit to 3 seconds of velocity determinates,

$\sigma_{x_i}^2$ are variance of the position coordinates x_i.

Substituting for the various constants, expression 10.4 becomes

$$\sigma^2_{W_i} = (1.6129 \times 10^{-3} + 11.996 \times 10^{-7} \dot{x}_3^2) \sigma^2_{x_i}, \quad i = 1,2 . \qquad 10.5$$

The first term depends on the length of the smoothing interval (in time) and the second term includes the effect of smoothing the velocities, and the fall velocity itself. The second term dominates over most of the height range because of the high values of fall velocity ($\sim$ 200 m/sec). To calculate the actual errors in the wind it simply remains to determine the variance in the position coordinates.

Two FPS16 radars are in use at Woomera, one radar (R38) is only a few kilometres to the north east of the launch site while the other (R39) is about 200 km to the west of the launch site. By comparing the positions of various targets determined by these radars and by ballistic cameras

Evans and Evans (1963) have been able to estimate the error in the two radars (both systematic and random). These errors are shown in Table 10.1 and represent values averaged over a number of target flight paths and radar bandwidth settings. Slight differences in the errors for the two radars are apparent with R39 being the less accurate.

Station	ERRORS IN FPS16 RADARS					
	Range (feet)		Elevation (mils)		Azimuth (mils)	
	Bias	Random	Bias	Random	Bias	Random
R38	- 5	11	0.06	0.33	0.06	0.26
R39	1	11	0.09	0.40	0.23	0.34

TABLE 10.1: Errors in FPS16 Radars at Two Stations at Woomera

These mean errors can be used in equation 10.5 to determine the errors in a wind profile. Using the two radars to track a falling sphere two independent zonal wind profiles can be determined as shown in Figure 10.1. The two wind profiles are consistent below 55 km whereas above this height many differences are observed. The variance computed from expression (10.5) is shown for a few points on the curves. It appears that the variances (particularly for the R39 profile) are greater than necessary to explain the discrepancy between the two profiles. It is possible that the mean radar errors used may not be the best estimates possible for the particular trajectory concerned. Evans (1963) has shown that considerable variation in the radar error can be expected depending on the position of the object and the bandwidth of the radar servomechanism used.

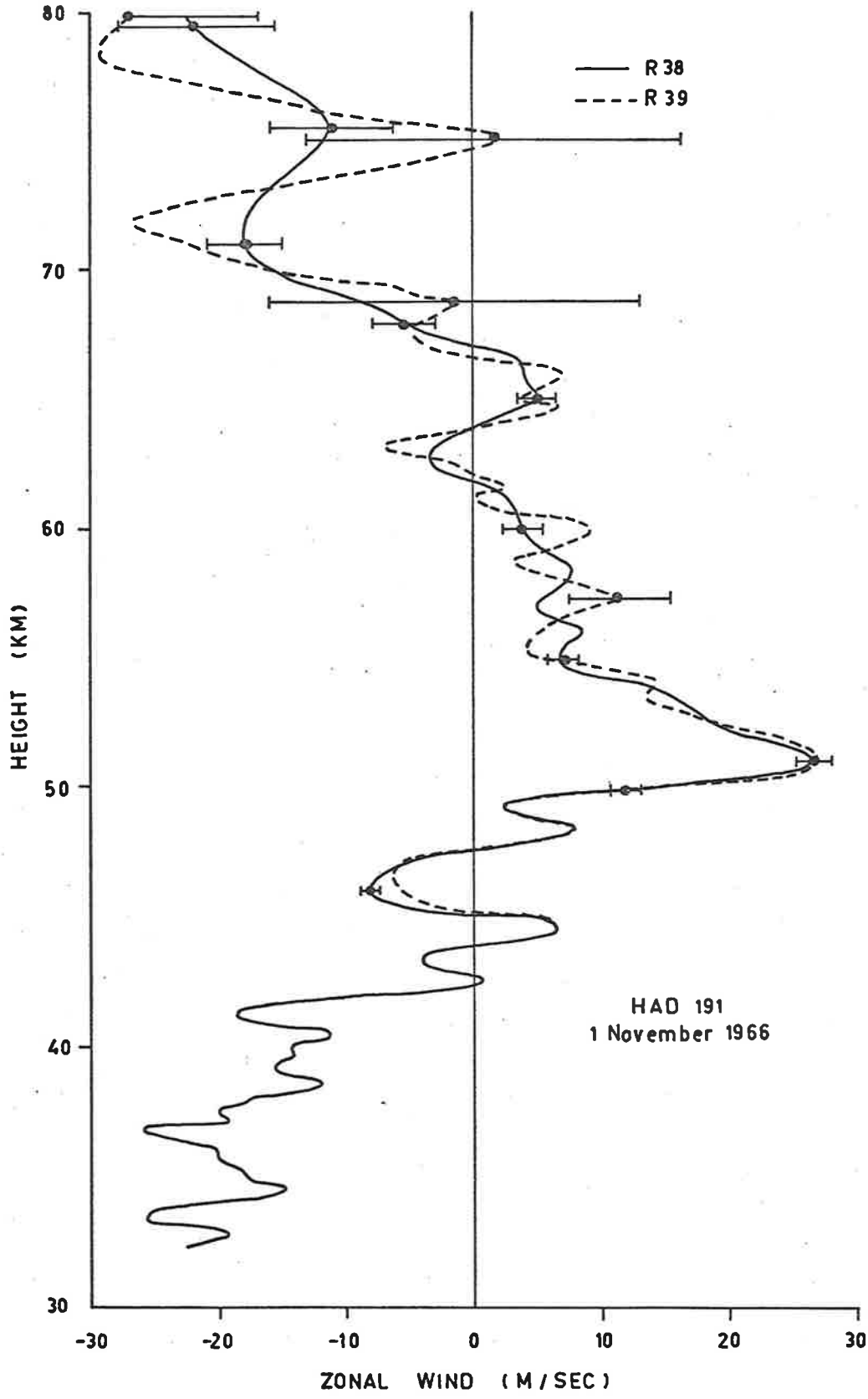

Figure 10.1: The zonal wind component measured with the falling sphere technique. The error bars are measured of the variance for each profile.

10.4.2 Errors in Wind. II. Individual Radar Errors

In view of the discussion in §10.4.1 above an alternative method of estimating the radar error was adopted so that the errors associated with each sounding could be determined more reliably. The basic assumption is that the secondary position data (as described in §10.3) can be considered to be composed of some analytic function describing the position of the object with time together with super-imposed noise. The terms in the Fourier series which describes the analytic function should converge while the terms describing the noise should diverge and hence separation of the noise from the data should be possible.

Thus the technique used to estimate the radar error is to fit a truncated Fourier series to the coordinate data and then estimate the variance by comparing the truncated fit with the original data. The number of terms (m) required in the expansion is decided by the nature of the function. To improve the convergence of the terms describing the motion it is necessary to remove the discontinuities at the beginning and end of the function (and its first derivative) describing the motion of the falling object. This is done simply by removing a linear trend from the observations and representing the remainder as a pure sine series. The order of magnitude of the Fourier terms under such conditions varies as m^{-3} which is a satisfactory degree of convergence (Lanczos, 1957).

If there are n data points R_i at times t_i then, after subtraction of a linear trend, a set of normalised values g_i can be found where

$$g_i = R_i - \left[R_1 + \frac{(R_n - R_1)(t_i - t_1)}{(t_n - t_1)}\right] \quad i = 1,2, \ldots n \qquad 10.6$$

The Fourier series representation of g_i is then

$$g(t) = \sum_{k=1}^{\infty} b_k \sin\left[\frac{k\pi(t - t_1)}{t_n - t_1}\right] \qquad 10.7$$

where the Fourier coefficients b_k are given by the condition that at the data points the function shall give the normalised values, thus

$$b_k = \frac{2}{(n - 1)} \sum_{j=1}^{n-2} g_{j+1} \sin\left[\frac{k\pi j}{n - 1}\right], \quad k = 1,2, \ldots n - 2 \qquad 10.8$$

Truncation of the series at term m is normally done such that $m/n \leqslant \frac{1}{2}$. Thus the truncated series representation of the normalised data is

$$\bar{g}(t) = \sum_{k=1}^{m} b_k \sin \frac{k\pi(t - t_1)}{t_n - t_1} \qquad 10.9$$

A measure of the precision of the fit of the function is the standard deviation of the residuals,

$$\sigma = \sqrt{\frac{\sum_{i=1}^{n} (g_i - \bar{g}(t_i))^2}{n - 1}} \qquad 10.10$$

and this is used as an estimate of the random errors in the observations.

Evans (1963) has shown that a similar Fourier series technique produces estimates of the random errors which agree well with estimates made from comparison of ballistic camera tracking and radar tracking of aircraft.

The random error in the wind profiles from each sounding is estimated using the radar errors deduced from the truncated Fourier series

fit. By consideration of a number of profiles deduced from sphere soundings it has been established that the vertical structure with scales less than 1 - 2 km can only be reliably investigated for heights below 55 km. The wind profiles shown in Figure 10.1 indicate this limit quite well.

Because of the slower rate of fall of the parachute system the random errors in the wind profiles obtained by tracking this device are correspondingly smaller than those obtained with the sphere. Figure 10.2 demonstrates this for a zonal wind profile obtained by tracking a parachute with the more accurate radar, R38.

10.4.3 Error in Density

An expression for the coefficient of variance in density can be found from equation 10.1,

$$\left(\frac{\sigma_\beta}{\rho}\right)^2 = \left(\frac{\sigma_{C_D}}{C_D}\right)^2 + \left(\frac{2\sigma_{\ddot{x}_3}}{\dot{x}_3}\right)^2 + \left(\frac{\sigma_{\ddot{x}_3}}{\ddot{x}_3}\right)^2 + \left(\frac{2\sigma_{W_3}}{\dot{x}_3}\right)^2 \qquad 10.11$$

where all second order terms have been neglected and where

σ_ρ is the standard deviation in density;

σ_{C_D} is the standard deviation in the drag coefficient;

$\sigma_{\dot{x}_3}$ and $\sigma_{\ddot{x}_3}$ are the standard deviations in the vertical velocity and acceleration respectively;

σ_{W_3} is standard deviation in the vertical wind.

The first term in the above expression, $\left(\frac{\sigma_{C_D}}{C_D}\right)^2$ is due to the experimental error in the determination of the drag coefficient for given

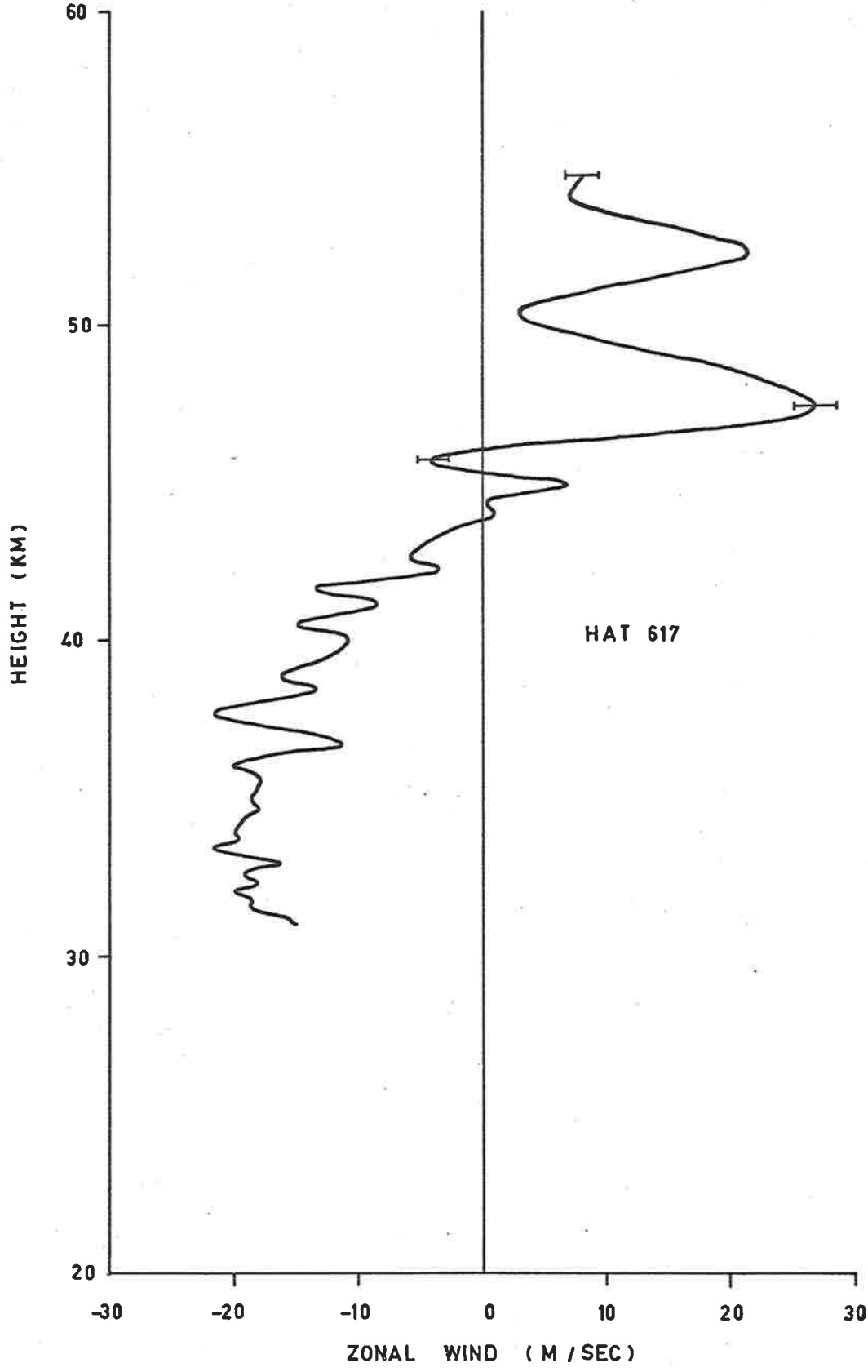

Figure 10.2: The zonal wind component measured with a parachute. Only the trajectory from radar R38 has been used.

Reynolds and Mach numbers and hence also includes the error in the determination of the Reynolds and Mach numbers for a given sphere motion and position. The error in the drag coefficients can be estimated from the published data while the Reynolds and Mach number errors can be determined from the sphere trajectory. Above 60 km this term dominates the expression 10.11. The second and third terms,

$$\left(\frac{2\sigma_{\dot{x}_3}}{\dot{x}_3}\right)^2 \quad \text{and} \quad \left(\frac{\sigma_{\ddot{x}_3}}{g}\right)^2,$$

are due to the radar error and can be calculated in the manner described in §10.4.1. The final term

$$\left(\frac{2\sigma_{w_3}}{\dot{x}_3}\right)^2$$

is usually negligible in magnitude since the vertical wind is small (less than 5 m/sec).

Figure 10.3 shows a typical variation of the percentage error in density with height. Since the error in the drag coefficient is dominant over much of the height range little difference in the density error is found for other soundings. Below about 45 km the radar error begins to be important and is particularly noticeable in the case of the radar at R39. For this site the elevation angle of the object has become small hence introducing a larger error in position.

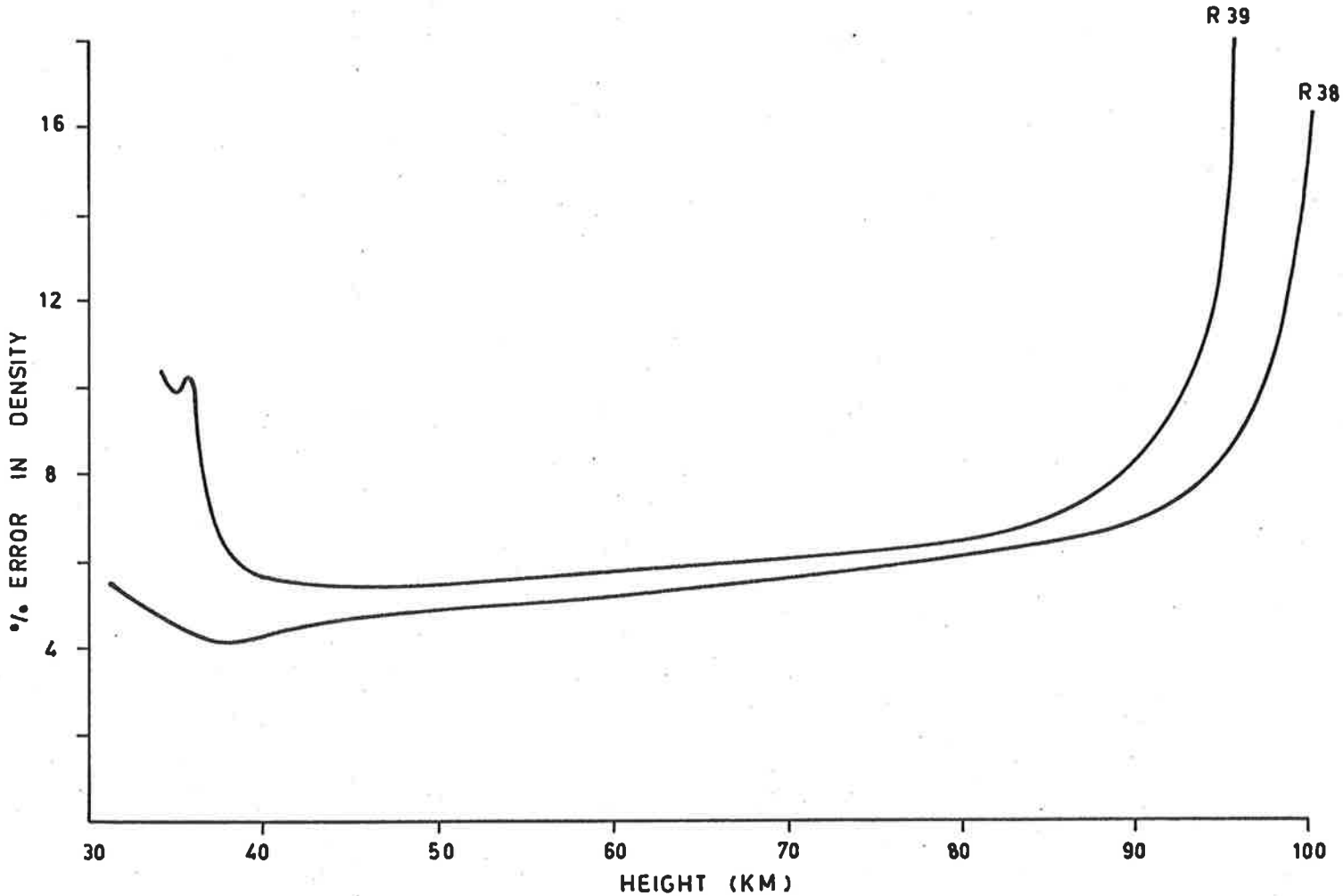

Figure 10.3: The percentage error in density calculated for the falling sphere released 1st Nov. 1966. The two curves are for the two radars R38 and R39.

10.5 OTHER METHODS FOR DETERMINING THE ERRORS

Luers and Engler (1967) have evaluated the error in the wind profile and also the distortion due to the method of data analysis by a different technique. The method uses a model atmosphere with a sinusoidal wind, the relevant equations of motion are solved for the position of a hypothetical object "falling" through the model. The position data is then treated as actual data (applying typical radar errors) and a new wind profile produced which can be compared with the original model profile.

The advantage of this technique is that an estimate of the optimum method of smoothing can be found together with possible correction factors. In practice the wind field is not sinusoidal and any spatial periodicities are unknown prior to data reduction, hence the optimum reduction method cannot be decided beforehand. Again trial and error methods have to be employed.

The simple method of error analysis described in §10.4 is of more immediate use particularly in view of the large amount of data already in existence.

10.6 CONCLUSIONS

At heights above about 60 km the wind profiles measured by radar tracking of falling spheres and parachutes cannot be used to determine wind structure with scales of 2 - 3 km or less unless more accurate radars than the FPS16 type are used. Below 60 km where the variance in the wind determination is generally less than 5 m/sec it is possible to determine the wind shear over 1 km intervals with a reasonable degree of confidence.

The method of determining the radar error discussed in §10.4.2 is quite general and appears to be a convenient method of estimating the error from the data itself. The radar errors found for various trajectories (both falling sphere and parachute) are consistent with other determinations. However when the single to noise ratio for the radar echo is low for some reason, for example a partially deflated sphere at large range, then the Fourier results seem to be more reliable.

The data analysis system, with accompanying error analysis, described in this chapter has been part of the normal reduction procedure since mid 1967.

CHAPTER XI

CONCLUSIONS AND FUTURE WORK

This thesis has been concerned with an experimental investigation of small scale wind structure in the mesosphere and lower thermosphere. The relationship between these winds and the prevailing, and tidal winds has been stressed, particularly through the use of radio-meteor observations. The results presented in this thesis cover a larger range of scales than has previously been the case.

A detailed comparison of the winds determined with chemiluminescent trails, and radio-meteor drifts during October, 1969, is the first comparative experiment of this type.

The possibility of measuring wind shears with the falling sphere technique has been examined and shown to be limited by observational errors to heights below 60 km.

11.1 SMALL SCALE WIND MEASUREMENTS

A review of the literature in the field of the irregular, small scale wind structure in the mesosphere and lower thermosphere has revealed that although a large amount of observational material is available the resolution, either spatial or temporal, is usually insufficient to enable an unequivocable description to be given either in terms of internal gravity waves or turbulence.

The Adelaide Radio-Meteor System in its present form has been shown to give reliable measurements of wind shear for reflection point separations between 0.5 km and 5.5 km, this latter separation is considerably larger than had been possible previously. It appears that the structure function is the best method of presenting the results of this type of observation. Power laws are found adequate to represent the structure functions for vertical and horizontal separations. The exponents for the vertical structure functions for the radio-meteor data are in close agreement with the value found by other workers for meso-scale structure in vertical wind profiles and which can be explained in terms of inertial oscillations. On the other hand the exponents for the horizontal structure functions for the radio-meteor data are close to the value expected for an inertial sub-range of turbulence.

The horizontal structure function determined for October, 1969 gives a measure of the turbulent dissipation rate which is in excellent agreement with the value that can be deduced from the time of onset of turbulence in two TMA trails released at Woomera during the observing interval. An investigation of the irregular appearance of these trails shows that the turbulence cannot be associated with any features on the wind profiles and at the present time no satisfactory explanation of the cause of the turbulence has been found.

It is apparent that the types of observation discussed in this thesis do not permit an accurate assessment of the relative importance of internal gravity waves in the wind field of the lower thermosphere. Unless internal

gravity waves can be traced from some specific source up to the levels where observations are made and theoretical predictions checked, the existence or otherwise of these waves in the lower thermosphere must remain an open question.

The energy necessary for the structure (both small-scale and meso-scale) observed in the wind field can be provided adequately by the dissipation of tidal energy (particularly the diurnal component). On the assumption that the horizontal structure functions are due to a turbulent regime, a value of about 0.01 watts/kg is a reasonable estimate of the rate of dissipation of energy near 90 km and hence could represent the amount of heating due to the dissipation of tidal energy. As the mass of atmosphere in a column of unit area above 90 km is roughly 7 gm/m^2, the heating effect due to the dissipation of turbulent energy is approximately 0.07 m watts/m^2, which is almost two orders of magnitude less than the solar energy absorbed near this height ($\sim$ 30 m watts/m^2).

11.2 THE PREVAILING AND TIDAL WINDS

11.2.1 General

The observations of the mean seasonal prevailing wind over the height range 75 - 105 km presented in Chapter VII are compatible with the wind model proposed by Groves (1969). However there are significant year to year differences, particularly for the winter meridional wind pattern, and these suggest that the heat sources and sinks outlined in Chapter I are not stationary. Unfortunately no comparable series of measurements exist at these heights at other latitudes in the southern

hemisphere so that it is impossible to determine whether the variations observed are representative of conditions over the whole hemisphere. Isolated comparisons of the radio-meteor winds with meteorological rocket observations from Woomera (heights up to about 75 km) indicate general agreement in spite of the 5^{o} latitudinal difference, and a combination of all existing rocket observations and radio-meteor observations should lead to a better understanding of the wind flow in the mesosphere.

The observations of the tidal wind components point out quite definitely that both the diurnal and semidiurnal tides are more variable than present theory will admit. The irregularity of the tides at these altitudes might be due to variation in the background conditions which can cause refractive effects and can also alter the heights at which dissipative effects are important. However as Lindzen (1968) has shown introduction of dissipative effects into the tidal equations merely alters the amplitude of the tidal components and, as might be expected, the phase changes are relatively unimportant. Further work, both observational and theoretical, is necessary before the effect and possible causes of the tidal variations are to be understood.

Dissipation of diurnal tidal energy at heights near 100 km must be considered a strong possibility, since the amplitudes of the diurnal and semidiurnal wind components do not increase with height. Woodrum et al. (1969) have reached a similar conclusion from an analysis of rocket released chemical trails. In view of the fact that such a source of heating, which can vary seasonally, can modify the temperature structure above the mesopause at mid latitudes it is important that the variation of the tidal wind

components with height should be studied in greater detail.

The periodogram analysis, originally used by Roper (1966b), has been shown to give reliable determinations of tidal components. There is an absence of significant periodic components with periods less than eight hours, and hence this form of analysis is not suitable for examining the motion induced by internal gravity waves.

11.2.2 The October, 1969 Comparison

This experiment was the first, as far as is known, to compare the winds measured by the radio-meteor technique directly with the winds measured by the chemical release technique. However the separation o 450 km between the two measurements places some uncertainty in the conclusions that can be drawn since it is impossible to decide uniquely whether the differences in the observed wind profiles are due primarily to differences in the measurement techniques themselves or to the existance of some large scale horizontal eddy.

If the measurements of the diurnal and semidiurnal tide determined by the radio-meteor system are to be taken as reliable and roughly applicable to Woomera then it is reasonable to deduce that the winds observed by the contaminant release method are little influenced by the relatively small tidal motion ($\sim$ 20 m/sec). If this supposition is correct then the differences in the wind profiles must be explained either in terms of the influence of large scale horizontal eddies in the wind field, or differences in gravity wave activity at the two sites. However the difficulty which then arises is how to explain the spiral structure shown in the chemiluminescent wind hodographs. Although the

amplitude is much larger than expected the spiral character is consistent with tidal theory.

Yet another possibility is that the method of analysis used to obtain the radio-meteor wind profiles may not be adequate to follow reasonably rapid changes in wind speed with altitude. This is supported by the relatively high correlation between the wind velocity from individual meteors and the wind velocity determined by the chemical trail measurements It is not unreasonable to propose that the decrease in amplitude of the radio-meteor observations might be due to the above cause. However simple averaging of the radio-meteor winds over 5 km height intervals does not produce wind profiles which differ greatly from the results of the model analysis. New methods of analysis - particularly in relation to the variation of the wind with height - are under investigation.

The experiment is to be repeated sometime during February, 1971. It is hoped that an improved data reduction procedure for small amplitude meteor echoes will be in routine operation by this time so that the usable echo rate will be increased. Further, it would be an advantage to obtain measurements of the wind in separate quadrants at times of high meteor rate leading to a more detailed comparison with the wind profiles from the TMA release. Meanwhile an attempt is to be made to modify an existing transmitter at Woomera to produce 20 kW phase coherent pulses at 25 MHz in order to set up a low power meteor radar. Such a facility would be extremely valuable for the comparison.

11.3 WIND AND DENSITY MEASUREMENTS BY RADAR TRACKING OF SPHERES AND PARACHUTES

A small independent research project has served to determine estimates of the errors in the wind profiles measured by the radar tracking of falling spheres and parachutes. It appears that although mean winds can be determined up to about 85 km any investigation of vertical wind shears for scales less than 2 km is limited to heights below about 60 km by the errors in the wind profiles. It would be of considerable interest to make a statistical study of wind shear below 60 km using all the wind profiles now available from Woomera.

The method of estimating the errors in the tracking radar developed for this project may be useful in other areas of Geophysics where a signal of limited bandwidth exists in the presence of a large bandwidth background noise.

11.4 SUGGESTIONS FOR FUTURE WORK

11.4.1 Equipment Improvement

Provided that the ground wave signal is kept near its present level ($\sim$ 12 μV across 72 Ω), the meteor rate currently being achieved for single station work is quite acceptable for the determination of the prevailing and 24 hour and 12 hour periodic wind components on a day to day basis. The main limitation in the use of the system at the moment is the amount of time required to read the film records (at present data for some seven months is still to be read). Installation of an automatic data recording facility with the data written directly in binary form onto magnetic tape would certainly facilitate data handling.

An extremely useful addition to the system would be a device which discriminated against false echoes due to interference since, particularly during daylight hours, random triggering of the equipment often causes true meteor echoes to be lost. The possible use of a system developed for the Harvard Radio Meteor Project (Schnaffner, private communication) is being investigated. If all the available information, both CW and pulse, is used it should be possible to exploit many more small amplitude meteor echoes thus increasing the usable echo rate.

The multi-station equipment could be significantly improved by changes in the telemetry system. The present frequency allocations in the 160 MHz band have allowable bandwidths which severely restrict the signal to noise ratio for records from the remote sites. Allocations in the 420 MHz band, where a maximum deviation of 15 kHz is allowed (instead of 5 kHz as used at present), would be ideal. Determination of the range of the reflective point at each out-station site would be very useful because of the extra redundancy this would introduce in the determination of the direction cosines of the trail. With the improvements suggested the number of multi-station echoes should increase dramatically and should also allow the system to produce reliable results for separations much closer to the theoretical maximum of 14 km.

11.4.2 Future Experiments

The most important extension of the present work is co-operation with other workers using sounding rockets as part of a latitudinal survey of winds in the southern hemisphere. Many of the problems associated with interpretation of the tidal and prevailing winds need series of

observations at different latitudes. It is hoped that a meteor-radar network in the latitude belt 30° - 45°N currently being set up under the auspices of IUCSTP Working Group 10 will add significantly to a knowledge of the wind systems near 95 km. By operating the Adelaide Radio-Meteor System in conjunction with stations in the northern hemisphere, a study of possible differences between hemispheres could be carried out.

Periods of extended operation during the equinoctial months would enable a more detailed study of the change between the summer and winter circulations. Although observations from a single site are of limited use in investigating such a complex phenomenon, it is thought that a long series of observations can be used to supplement a meteorological rocket programme.

Further operation of the multi-station equipment should be contemplated particularly if the signal to noise ratio in the telemetry link can be improved. If the echo rate can be increased sufficiently then the irregular wind field can be better determined and may lead to routine measurements of the wind field in different parts of the observing volume.

If the temporal resolution for the radio-meteor system can be improved in the manner outlined above, then a combination of this technique with the chemiluminescent trail technique should be capable of resolving structures with scales of 1 km or less and quasi-periods of the order of 10 mins. With that type of observation the relationship between the various scales of motion should become clearer.

BIBLIOGRAPHY

1. Armendariz, M. and Rider, L. J., 1966, J. Appl. Meteorol., 5, 810

2. Authier, B., Blamont, J. E. and Carpentier, G., 1962, Compt. Rend. Acad. Sci., 255, 1974

3. Baker, D. M. and Davies, K., 1968, J. Geophys. Res., 73, 448

4. Bartman, F. J., Chaney, L. W., Jones, L. M. and Liu, V. C., 1956 J. Applied Phys., 27, 706

5. Batchelor, G. K., 1950, Quart. J. Roy. Met. Soc., 76, 183

6. Batchelor, G. K., 1953, "Theory of Homogeneous Turbulence" Cambridge University Press, London

7. Blackman, R. D. and Tukey, J. W., 1959, The 'Measurement of Power Spectra from the Point of View of Communications Engineering', Dover, New York

8. Blamont, J. E., 1963, Planet. Space Sci., 10, 89

9. Blamont, J. E. and Barat, J., 1967, Ann. de Géophys., 23, 173

10. Blamont, J. E. and Barat, J., 1968, Ann. de Géophys., 24, 375

11. Blamont, J. E., and de Jager, C., 1961, Ann. de Géophys., 17, 134

12. Blamont, J. E., Teitelbaum, H. and Barat, J., 1969, Ann. de Géophys., 24, 115

13. Bolgiano, R., Jr., 1959, J. Geophys. Res., 64, 2226

14. Bolgiano, R. Jr., 1962, J. Geophys. Res., 67, 3015

15. Booker, J. R. and Bretherton, F. P., 1967, J. Fluid Mech., 27, 513

16. Born, W. and Wolf, E., 1964, 'Principles of Optics', 2nd ed., Oxford, Pergamon Press

17. Bretherton, F. P., 1966, Quart. J. Roy. Met. Soc., 92, 466

18. Bretherton, F. P., 1969, Radio Sci., 4, 1279

19. Briggs, B. H., Elford, W. G., Felgate, D. G., Golley, M. G., Rossiter, D. E. and Smith, J. W., 1969, Nature, 223, 1321

20. Bull, G. V., 1964, Can. Aeronautics and Space J., 10, 238

21. Carru, H., Petit, M. and Waldteufel, P., 1967, C. R. Acad. Sci. Paris., 264 (B), 560

22. Chapman, S., 1951, Compendium of Meteorology, Boston

23. Chapman, S. and Bartels, J., 1940, Geomagnetism, Clarendon Press, Oxford

24. Charney, J. G., and Drazin, P. G., 1961, J. Geophys. Res., 66, 83

25. Clemmow, P. L., Johnson, M. A. and Weekes, K., 1955, Proc. Ionosphere Conf., (Phys. Soc. London), p136

26. Colegrove, F. D., Johnson, F. S. and Hanson, W. B., 1966, J. Geophys. Res., 71, 2227

27. Cooley, J. W. and Tukey, J. W., 1965, Math. of Comput., 19, 297

28. Coté, O., 1962, Geophysics Corporation of America Technical Report No. 62-12-N

29. Dickinson, R. E., 1969a, Space Sci. Rev., 7, 483

30. Dickinson, R. E. 1969b, Space Sci. Rev., 7, 515

31. Doyle, E. M., 1968, Ph.D. Thesis, University of Adelaide

32. Eckart, C., 1960, "Hydrodynamics of Oceans and Atmospheres", Pergamon Press, New York

33. Elford, W. G., 1959, Planet. Space Sci., 1, 94

34. Elford, W. G. and Roper, R. G., 1967, Space Research VII, 42

35. Engler, N. A., 1965, AFCRL-65-448, Contract Report

36. Eshleman, V. R., 1955, I.R.E. Trans., AP-3, 32

37. Essenwanger, O. M., 1963, Geofis. pura appl., 56, 216

38. Essenwanger, O. M., 1966, Arch. Met. Geoph. Biokl., A, 15, 50

39. Essenwanger, O. M., 1967, J. Appl. Meteorol., 6, 591

40. Essenwanger, O. M., and Billions, N. S., 1965, Pure and Applied Geophys., 60, 160

41. Essenwanger, O. M. and Reiter, E. R., 1969, Arch. Met. Geoph. Biokl., A, 18, 17

42. Evans, R. H., 1963, WRE Technical Note SAD113

43. Evans, H. H., and Evans, R. H., 1963, WRE Technical Note SAD109

44. Fedele, D., 1968, in 'Winds and Turbulence in Stratosphere, Mesosphere and Ionosphere', Ed. K. Rawer, North Holland, Amsterdam

45. Felgate, D. G., 1970, J. Atmosph. Terr. Phys., 32, 241

46. Fraser, G. J., 1965, J. Atmosph. Sci., 22, 217

47. Fraser, G. J., 1968, J. Atmosph. Terr. Phys., 30, 707

48. Freidman, J. P., 1966, J. Geophys. Res., 71, 1033

49. Gibson, M. M., 1962, Nature, 195, 1281

50. Gibson, M. M., 1963, J. Fluid Mech., 15, 161

51. Golley, M. G. and Rossiter, D. E., 1970, J. Atmosph. Terr. Phys., 32, 1215

52. Golomb, D. and MacLeod, M. A., 1966, J. Geophys. Res., 71, 2299

53. Grant, H. L., Stewart, R. W. and Moilliet, A., 1962, J. Fluid Mech., 12, 241

54. Greenhow, J. S., 1952a, J. Atmosph. Terr. Phys., 2, 282

55. Greenhow, J. S., 1952b, Proc. Phys. Soc., 65B, 169

56. Greenhow, J. S. and Neufeld, E. L., 1959a, J. Atmos. Terr. Phys., 16, 384

57. Greenhow, J. S. and Neufeld, E. L., 1959b, Proc. Phys. Soc., 74, 1

58. Greenhow, J. S. and Neufeld, E. L., 1960, Proc. Phys. Soc., 75, 228

59. Greenhow, J. S., and Neufeld, E. L., 1961, Quart. J. Roy. Met. Soc., 87, 472

60. Groves, G. V., 1959, J. Atmosph. Terr. Phys., 16, 344

61. Groves, G. V., 1960a, Nature, 187, 1001

62. Groves, G. V., 1960b, Space Res. 1, 144

63. Groves, G. V., 1969, J. British Interplanet.Soc., 22, 285

64. Haurwitz, B., 1964, WMO Technical Note No. 58

65. Haerendel, G., Lüst, R. and Rieger, E., 1967, Planet Space Sci., 15, 1

66. Herlofson, N., 1951, Ark. Fys., 3, 247

67. Hines, C. O., 1960, Can. J. Phys., 38, 1441

68. Hines, C. O., 1965, J. Geophys. Res., 70, 177

69. Hines, C. O., 1967, J. Geophys. Res., 72, 1877

70. Hines, C. O., and Reddy, C. A., 1967, J. Geophys. Res., 72, 1015

71. Hinze, J. O., 1959, "Turbulence", McGraw-Hill, New York

72. Hodges, R. R., 1967, J. Geophys. Res., 72, 3455

73. Hodges, R. R., 1969, J. Geophys. Res., 74, 4087

74. Houghton, D. D. and Jones, W. L., 1969, J. Computational Phys., 3, 339

75. Johnson, E. R., 1965, J. Geophys. Res., 70, 1275

76. Jones, R. H., 1965, Technometrics, 7, 531

77. Justus, C. G., 1966, J. Geophys. Res., 71, 3767

78. Justus, C. G., 1967a, J. Geophys. Res., 72, 1035

79. Justus, C. G., 1967b, J. Geophys. Res., 72, 1933

80. Justus C. G., 1968, J. Geophys. Res., 73, 455

81. Justus, C. G., 1969, J. Atmosph. Sci., 26, 1137

82. Justus, C. G., Edwards, H. D. and Fuller, R. N., 1964, Photogrammetric Eng., 30, 594

83. Kaiser, T. R., 1955, Spec. Supp. J. Atmosph. Terr. Phys., 2, 55

84. Kaiser, T. R. and Closs, R. L., 1952, Phil. Mag., 43, 1

85. Kato, S., 1959, Rep. Ionos. Space Res. Japan, 13, 62

86. Kent, G. S. and Wright, R. W. H., 1968, J. Atmosph. Terr. Phys., 30, 657

87. Kochanski, A., 1964, J. Geophys. Res. 69, 3651

88. Kolmogorov, A. N., 1941, Doklady Akad. Nauk. SSSR 30, 301

89. Kraichnan, R. H., 1967, Phys. Fluids, 10, 1417

90. Lamb, H., 1910, Proc. Roy. Soc. (Lond.)., A84, 551

91. Lanczos, C., 1957, 'Applied Analysis', Pitman, London

92. Landau, L. D. and Lifshitz, E. M., 1959, 'Fluid Mechanics', Addison-Wesley, N. Y.

93. Layzer, D. and Bedinger, J. F., 1969, Planet. Space Sci., 17, 1891

94. Lebedinec, V. N. and Sosnova, A. K., 1968, I.A.U. Symposium No. 33 "Physics and Dynamics of Meteors", Kresak and Millman (eds.) p27

95. Leovy, C., 1964, J. Atmosph. Sci., 21, 327

96. Leovy, C., 1969, Advances in Geophysics, 13, 191

97. Lin, C. C., 1960, Proc. Nat. Acad. Sci., 46, 566

98. Lindzen, R. S., 1967, Quart. J. Roy. Met. Soc., 93, 18

99. Lindzen, R. S., 1968, Proc. Roy. Soc., A, 303, 299

100. Lindzen, R. S., 1968b, Meteorological Monographs, 9, 37

101. Lindzen, R. S., 1969, J. Atmosph. Terr. Phys., 31, 449

102. Lindzen, R. S., and Chapman, S. C., 1969, Space Sci. Rev., 10, 1

103. Lloyd, K. H., and Sheppard, L. M., 1966, Aust. J. Phys., 19, 323

104. Lloyd, K. H., 1970, Private communication

105. Luers, J. and Engler, N., 1967, J. Appld. Met., 6, 816

106. Lumley, J. L., 1964, J. Atmosph. Sci., 21, 99

107. Lumley, J. L. and Panofsky, H. A., 1964, "The Structure of Atmospheric Turbulence", Wiley, New York

108. MacCready, P. B., 1962, J. Geophys. Res., 67, 1051

109. McKinley, D. W. R., 1961, "Meteor Science and Engineering", McGraw-Hill, N. Y.

110. Mainstone, J. S., 1960, Mon. Not. Roy. Astron. Soc., 120, 517

111. Manning, L. A., 1959, J. Geophys. Res., 64, 1415

112. Manning, L. A., Villard, O. G. and Peterson, V. M., 1950, Proc. I.R. 38, 877

113. Manring, E. R., Bedinger, J. F. and Knaflitch, H., 1961, Space Res. II, 1107

114. Manring, E. R. and Bedinger, J. F., 1968, Meteorological Monographs 9, 196

115. Martyn, D. F., 1950, Proc. Roy. Soc. (Lond.), A28, 216

116. Martyn, D. F., 1953, Phil. Trans. Roy. Soc., A246, 306

117. Midgley, J. E. and Liemohn, H. B., 1966, J. Geophys. Res., 71, 3729

118. Millman, P. M., 1959, J. Geophys. Res., 64, 2063

119. Monin, A. S., 1962, Izvestia Akad. Nauk. SSSR Geophys. Ser., 3, 397

120. Mowbray, D. E. and Rarity, B. S. H., 1967, J. Fluid Mech., 28 1

121. Müller, H. G., 1968, Planet. Space Sci., 16, 61

122. Murphy, C. H., Bull, C. V. and Edwards, H. D., 1966, J. Geophys. Res. 71, 4535

123. Newell, R. E. and Dickinson, R. E., 1967, Pure Appl. Geophys., 68, 162

124. Newell, R. E., 1968, Meteorological Monographs, 9, 98

125. Nilsson, C. S., 1962, Ph.D. Thesis, University of Adelaide

126. Nilsson, C. S., 1964, Aus. J. Phys., 17, 205

127. Panofsky, H. A. and Pasquill, F., 1963, Quart. J. Roy. Met. Soc., 89, 550

128. Pasquill, F., 1963, Weather, 18, 233

129. Pfeffer, R. L. and Zarichny, J., 1962, J. Atmosph. Sci., 19, 256

130. Pfeffer, R. L. and Zarichny, J., 1963, Geofis. Pura e Appl., 55, 175

131. Phillips, E., 1969, Planet. Space Sci., 17, 553

132. Phillips, O. M., 1968, J. Fluid Mech., 34, 407

133. Pierce, A. D., 1966, Radio Science, 1, 265

134. Pond, S., Stewart, R. W. and Burling, R. W., 1963, J. Atmosph. Sci., 20, 319

135. Pond, S., Smith, S. D., Hamblin, P. F. and Burling, R. W., 1966, J. Atmosph. Sci., 23, 376

136. Press, F. and Harkrider, D., 1962, J. Geophys. Res., 67 3889

137. Rayleigh, L., 1883, Lond. Math. Soc., XIV, 170

138. Rees, D., 1968, Space Res., VIII, 909

139. Rees, D., 1969, J. Brit. Interplanet. Soc., 22, 275

140. Rees, D., Roper, R. G., Lloyd, K. H. and Low, C. H., 1970 Phil. Trans. Roy Soc. (in press)

141. Revah, I., Spizzichino, A. and Taieb, C., 1963, Ann. de Géophys., 19, 43

142. Revah, I. and Spizzichino, A., 1964, Ann. de Géophys., 20, 248

143. Revah, I., 1969, Ann. de Géophys., 25, 1

144. Robertson, D. S., Liddy, D. T. and Elford, W. G., 1953, J. Atmosph. Terr. Phys., 4, 255

145. Rofe, B., 1961, WRE Tech. Memo SAD 125

146. Rofe, B., Elford, W. G. and Doyle, E. M., 1966, WRE Tech. Note PAD 116

147. Roper, R. G., 1962, Ph.D. Thesis, University of Adelaide

148. Roper, R. G., (Editor), 1965, Laboratory Report, Univ. of Adelaide, Physics Dept.,

149. Roper, R. G., 1966, J. Geophys. Res., 71, 5785

150. Roper, R. G., 1966b, J. Geophys. Res., 71, 5746

151. Rosenberg, N. W., 1964, J. Geophys. Res., 69, 1451

152. Rosenberg, N. W., 1968a, Space Res., VIII, 673

153. Rosenberg, N. W., 1968b, J. Atmosph. Terr. Phys., 30, 907

154. Rosenberg, N. W., Golomb, D. and Allen, Jr, E. F., 1963, J. Geophys. Res., 68, 5895

155. Rosenberg, N. W. and Justus, C. G., 1966, Radio Science 1, 149

156. Rossiter, D. E., 1970, Ph.D. Thesis, University of Adelaide

157. Row, R. V., 1966, J. Geophys. Res., 71, 343

158. Row, R. V., 1967, J. Geophys. Res., 72, 1599

159. Shafi Ahmad, M., 1969, Space Research IX, 354

160. Shur, G. N., 1962, Trudy Tsentral Aeor. Obs., 43, 79

161. Southworth, R., 1968, AFCRL Special Reports, No. 75, p 161

162. Spizzichino, A., Delcourt, J., Giraud, A. and Revah, I., 1965, Proc. I.E.E.E., 53, 1084

163. Spizzichino, A., 1968, in "Winds and Turbulence in the Upper Atmosphere" ed. K. Rawer, North-Holland, Amsterdam, p 201

164. Spizzichino, A., 1969, D.Sc. Thesis, AO-3685, Faculty of Science, Paris

165. Stewart, R. W., 1969, Radio Sci., 4, 1269

166. Stone, B. J., 1966, Laboratory Report, Physics Dept., Univ. of Adelaide

167. Stroud, W. G., Nordberg, W. and Walsh, J. R., 1956, J. Geophys. Res., 61, 45

168. Tchen, C. M., 1961, Advances in Geophysics, 6, 165

169. Theon, J. S., Nordberg, W., Katchen, L. B. and Howarth, J. J., 1967, J. Atmosph. Sci., 24, 428

170. Tolstoy, J., 1963, Revs. Mod. Phys., 35, 207

171. Townsend, A. A., 1966, J. Fluid Mech., 24, 307

172. Webb, W. L., Hubert, W. E., Miller, R. L. and Spurling, J. F., 1961, Bull. Am. Met. Soc., 42, 482

173. Weinstein, A. I., Reiter, E. R., Scoggins, J. R., 1966, J. Appl. Meteor., 5, 49

174. Weiss, A. A. and Elford, W. G., 1963, Proc. I.R.E. Aus., 24, 197

175. Weston, V. H., 1962, Can. J. Phys., 40, 446

176. Witt, G., 1962, Tellus, 4, 1

177. Woodrum, A. and Justus, C. G., 1968a, J. Geophys. Res., 73, 467

178. Woodrum, A., and Justus, C. G., 1968b, J. Geophys. Res., 73, 7535

179. Woodrum, A., Justus, C. G. and Roper, R. G., 1969, J. Geophys. Res., 74, 4099

180. Zadorina, F. K., Pokrovskii, G. B., Sidorov, V. V., Teptin, C. M. and Fakhrutdinova, A. M., 1967, Izv. Atmospheric and Oceanic Phys., 3, 1

181. Zimmerman, S. P., 1968, J. Geophys. Res., 73, 452

182. Zimmerman, S. P., 1969, AFCRL Environmental Research Papers, No. 300

183. Zimmerman, S. P. and Champion, K. S. W., 1963, J. Geophys. Res., 68, 3049